5. SITE 803[1]

Shipboard Scientific Party[2]

HOLE 803A

Date occupied: 28 January 1990

Date departed: 28 January 1990

Time on hole: 18 hr, 10 min

Position: 2°25.98′N, 160°32.40′E

Bottom felt (rig floor; m, drill-pipe measurement): 3421.5

Distance between rig floor and sea level (m): 11.80

Water depth (drill-pipe measurement from sea level, m): 3409.7

Total depth (rig floor; m): 3477.00

Penetration (m): 55.50

Number of cores (including cores with no recovery): 6

Total length of cored section (m): 55.50

Total core recovered (m): 57.99

Core recovery (%): 104.5

Oldest sediment cored:
　Depth (mbsf): 55.50
　Nature: nannofossil ooze
　Youngest age: Quaternary
　Oldest age: early Pliocene
　Measured velocity (km/s): 1.55

HOLE 803B

Date occupied: 28 January 1990

Date departed: 29 January 1990

Time on hole: 10 hr

Position: 2°25.98′N, 160°32.40′E

Bottom felt (rig floor; m, drill-pipe measurement): 3422.2

Distance between rig floor and sea level (m): 11.80

Water depth (drill-pipe measurement from sea level, m): 3410.4

Total depth (rig floor; m): 3483.50

Penetration (m): 61.30

Number of cores (including cores with no recovery): 7

Total length of cored section (m): 61.30

Total core recovered (m): 58.18

Core recovery (%): 94.9

Oldest sediment cored:
　Depth (mbsf): 61.30
　Nature: nannofossil ooze
　Youngest age: Quaternary
　Oldest age: Pliocene
　Measured velocity (km/s): 1.54

HOLE 803C

Date occupied: 29 January 1990

Date departed: 30 January 1990

Time on hole: 1 day, 9 hr, 15 min

Position: 2°25.98′N, 160°32.40′E

Bottom felt (rig floor; m, drill-pipe measurement): 3422.2

Distance between rig floor and sea level (m): 11.80

Water depth (drill-pipe measurement from sea level, m): 3410.4

Total depth (rig floor; m): 3659.70

Penetration (m): 237.50

Number of cores (including cores with no recovery): 23

Total length of cored section (m): 218.50

Total core recovered (m): 226.31

Core recovery (%): 103.6

Oldest sediment cored:
　Depth (mbsf): 218.50
　Nature: nannofossil ooze
　Youngest age: upper Pliocene
　Oldest age: middle/late Miocene
　Measured velocity (km/s): 1.62

HOLE 803D

Date occupied: 30 January 1990

Date departed: 6 February 1990

Time on hole: 7 days, 2 hr, 45 min

Position: 2°25.98′N, 160°32.46′E

Bottom felt (rig floor; m, drill-pipe measurement): 3424.0

Distance between rig floor and sea level (m): 11.80

Water depth (drill-pipe measurement from sea level, m): 3412.2

Total depth (rig floor; m): 4080.00

Penetration (m): 656.00

Number of cores (including cores with no recovery): 71

Total length of cored section (m): 656.00 (APC, 217.1; XCB, 394.9; RCB, 44)

Total core recovered (m): 494.96 (APC, 228.88; XCB, 248.47; RCB, 17.61)

Core recovery (%): 75.5 (APC, 105.4%; XCB, 62.9%; and RCB, 40.0%)

Oldest sediment cored:
　Depth (mbsf): 630.98
　Nature: claystone
　Youngest age: Quaternary
　Oldest age: Late Cretaceous
　Measured velocity (km/s): 1.87

Basement:
　Depth (mbsf): 630.98
　Nature: highly altered, fine grained, and pyroxene phyric pillow basalt
　Measured velocity (km/s): 4.18

Principal results: Site 803 (proposed Site OJP-4) is located near the equator on the northeastern margin of the Ontong Java Plateau (latitude 2°26.0'N, longitude 160°32.4'E) in 3410 m of water, roughly 400 km northeast of DSDP Site 289/586. Site 803 was occupied with three major objectives: (1) to serve as a deep-water anchor site on a Neogene depth transect designed to detect depth-related paleoceanographic signals; (2) to provide Paleogene and Cretaceous sediments for studies of pre-Neogene paleoceanography; and (3) to obtain basement rock for studies of the origin of the Ontong Java Plateau.

The site is located on a single-channel seismic (SCS) line acquired by the *Thomas Washington* during the ROUNDABOUT Cruise 11 "DANCER" survey. The site was positioned on the SCS line at 2205 hr UTC (Universal Time Coordinated) on 23 December 1989, between proposed Sites OJP-4 and OJP-4B.

Four holes were drilled at Site 803. Hole 803A, a dedicated hole, was cored with the advanced hydraulic piston corer to 55.5 m below seafloor (mbsf). Average recovery was 104%. Hole 803B was cored with the APC to 61.3 mbsf, at which point a core barrel became stuck and was left in the hole, which forced us in turn to abandon the hole. Average recovery was 95%. Hole 803C, after washing down 19 m, was cored with the APC to 237.5 mbsf; below this depth an APC rod parted during an 100,000-lb. overpull on Core 130-803C-24H, again forcing us to abandon a hole. Average recovery was 104%. We cored Hole 803D with the APC and the extended core barrel (XCB) to 612.0 mbsf; at this depth an 170,000-lb. overpull occurred that ended further XCB coring in the hole. After we dropped a free-fall funnel (FFF) in Hole 803D, it was successfully reentered using the slimline sonar reentry tool. We then cored Hole 803D with the rotary core barrel (RCB) to a total depth of 656.0 mbsf; this included 25.6 m of basement, of which 9.6 m was recovered. Average recovery at Hole 803D was 76%. The hole was successfully logged and a good suite of geophysical measurements was obtained.

The following lithostratigraphic units were recognized:

Unit I (0–563.7 mbsf): Pleistocene–upper Eocene nannofossil ooze and chalk to foraminifer nannofossil ooze and chalk, divisible into two subunits.

Subunit IA (0–217.1 mbsf): Pleistocene–middle Miocene nannofossil ooze to foraminifer nannofossil ooze. The ooze ranges in color from pale yellowish brown (at the top) through light gray to white. Bioturbation is ubiquitous. Faint color bands in various shades of green, purple, and red are common.

Subunit IB (217.1–563.7 mbsf): middle Miocene–upper Eocene nannofossil and foraminifer nannofossil chalk. Colors range from light gray to white. Bioturbation is common. Absent above 409 mbsf, color banding becomes more abundant, more intense, and more distinct downhole.

Unit II (563.7–621.8 mbsf): upper Eocene to middle Eocene nannofossil chalk with radiolarians, radiolarian nannofossil chalk, and nannofossil radiolarite. Sparse chert is present. Colors range from white to light brownish gray. Bioturbation is slight to heavy.

Unit III (621.8–626.3 mbsf): middle Eocene–lower Upper Cretaceous claystone and clayey siltstone, with minor nannofossil-bearing to radiolarian-rich intervals. Colors vary in intervals from brown to dark brown to very dark brown, with minor intervals of dark yellowish brown. Sharp contacts between colored intervals may represent significant unconformities. The discrepancy in the lower depth of Unit III and the upper depth of Unit IV is the result of using an "ODP-curated" depth for the base of Unit III and a "best guess" depth for basement based on drilling information.

Unit IV (630.4–656.0 mbsf): Cenomanian? or older tholeiitic basalts that are predominantly aphyric, fine grained, and nonvesicular. The basalts consist of multiple pillow lavas, which together make up a sequence roughly equivalent to one "subunit" at Site 807. Here at Site 803, the sequence was divided into nine subdivisions on the basis of interpillow limestones, suggesting nine flows distinctly separated in time. Average basalt recovery was 38%. Alteration varies from severe to mild, and small amounts of fresh glass are present.

Shipboard X-ray fluorescence (XRF) measurements indicate that the basalt units are chemically uniform and distinct from normal mid-ocean ridge basalt (MORB) (e.g., Zr/Nb = 14–17 vs. >30 for normal MORB). They are, however, quite similar to the basalt drilled at Site 289 on the Ontong Java Plateau, to the few analyzed basement lavas of Malaita (eastern Solomon Islands), and to the basalts drilled at Site 462 in the Nauru Basin (i.e., within the range of variation displayed by the flow and sill complex).

The severe alteration of the uppermost lava flow of Unit IV suggests the presence of a considerable hiatus between basaltic basement and Unit III. Moreover, the basal sediments of Unit III, which directly overlie basaltic basement, are not metalliferous. This situation also suggests that a significant hiatus may exist between the underlying basalt and the overlying basal sediments of Unit III. Additional hiatuses also may occur at overlying sharp color contacts in Unit III.

Despite the occurrence of dark-colored intervals in the siliciclastic sediments of Unit III, no evidence for the presence of black shales was detected. Because of the likelihood of significant hiatuses within the condensed section, however, their formation and deposition on the Ontong Java Plateau cannot be excluded.

The Cretaceous/Tertiary (K/T) boundary occurs near the top of Unit III. Remarkably, the entire K/T transition zone appears to have been preserved in Section 130-803D-68R-1. Initially restricted to the interval between 53 and 38 cm in Section 130-803D-68R-1 by nannofossil dating, the K/T boundary was finally placed at 45 cm in Section 130-803D-68R-1, based on the first appearance of *Thoracosphaera* at 46.5 cm in the section coupled with a peak in magnetic susceptibility at 45 cm in the section.

Above the K/T transition zone at the top of Unit III, a major hiatus occurs that encompasses most of the Paleocene and all of the lower Eocene. Sedimentation rates during the middle Eocene, about 7 m/m.y., almost doubled to 13 m/m.y. at 40 Ma, and increased to 25 m/m.y. at 35 Ma. In the late Oligocene, they dropped to below 10 m/m.y. but rose again dramatically during the Oligocene-Miocene transition, attaining 30 m/m.y. for a brief period just preceding the hiatus. Paleomagnetic analyses of the Oligocene sediments have resulted in a tentative magnetostratigraphy spanning Chrons 7 through 11. Preliminary analyses suggest a paleolatitude of 4.5°S for Site 803 during the Oligocene, which, in turn, suggests that the Ontong Java Plateau has been part of the Pacific Plate for the last 30 m.y.

A significant hiatus (or rather hiatus pair) occurred in the early Miocene within the interval from 22 to 15 Ma. Sedimentation rates in the middle Miocene are typically near 10 m/m.y. In the late Miocene, the rates abruptly increased, reaching a maximum near 30 m/m.y. between 6 and 8 Ma. After 5 Ma, sedimentation rates decreased rapidly, falling to near 10 m/m.y. in the late Pleistocene.

Pass-through cryogenic magnetometer measurements have yielded a virtually complete magnetostratigraphic sequence from 3.4 Ma to the present, including the Mammoth, Kaena, Olduvai, and Jaramillo subchrons. Sedimentation rates based on this magnetostratigraphy decreased from 15 to 10 m/m.y. at the base of the Olduvai Subchron (1.88 Ma), averaging 10 m/m.y. to the present. The cause of this drop in sedimentation rate is not obvious.

Hole 803D logging data, in conjunction with a detailed suite of physical property measurements obtained from the split cores, confirm the depth of the ooze-chalk transition and reveal the presence of local maxima and minima in velocity that correlate with chert horizons and radiolarian-rich zones deep in the section. The logs also provide important data for the generation of synthetic seismograms.

Results from interstitial water geochemistry at Site 803 suggest that, in contrast to Site 289, there is no evidence of nonconservative behavior of Mg, despite the presence of a noticeable ash layer. Calcium and magnesium depth gradients are larger, and the maximum dissolved strontium concentrations are higher at Site 803 than at Site 289.

BACKGROUND AND OBJECTIVES

Overview

The general background for all sites is contained in the "Introduction" chapter of this volume. Site 803 (proposed Site OJP-4), the first of the Leg 130 sites to be drilled on the Ontong Java Plateau, was scheduled as one of the deep-water sites for a depth transect of Neogene sediments along the equator. The transect was designed for the study of paleoceanographic events of global significance. The pelagic sediment cover of the plateau is uniquely suited for such studies. The maximum thickness of

the cover is more than 1200 m; moreover, it occurs below the crest of the plateau in water depths greater than 2200 m. The water depth at the site (near the lysocline) promised a large carbonate dissolution signal, as reflected in the various sediment properties.

We anticipated that the section would be reasonably complete, despite the loss from carbonate dissolution, at least above the Eocene. This site also was planned for drilling to basement, and our hope was to recover Paleogene and Cretaceous sediments, as well as basement rock, for pre-Neogene paleoceanography and for studies on the origin of the Ontong Java Plateau. Within the upper portion of the section, we drilled multiple holes to provide material for concurrent detailed studies and to provide for overlap between cores.

We reached basement after penetrating 630 m of sediment. The proportional decrease in thickness of sediment that occurs with increasing depth of the seafloor varies between the different sediment layers, as can be seen on the seismic profiles (see "Introduction" chapter, this volume). The linkage of paleoceanographic events to acoustic stratigraphy will allow three-dimensional mapping as well as correlation into distant sediment sections throughout the Pacific basin.

Background

The Ontong Java Plateau (see Fig. 1, "Introduction" chapter, this volume) is a broad, shallow, mid-ocean submarine plateau in the western equatorial Pacific. Its shallowest regions lie above 2000 m, and its flanks reach depths in excess of 4500 m. With an area of 1.5 million km², it is the largest of the "classic" Pacific plateaus. The plateau has a crustal thickness on the order of 40 km, yet it is in isostatic equilibrium, apparently maintaining its depth over much of its history. Crustal seismic velocities are in the range of oceanic crust (Hussong et al., 1979).

The Ontong Java Plateau has long been the focus of paleoceanographic studies based on conventional coring and on seismic profiling. Leg 130 is the fourth drilling expedition to sample the sediment cover here: four Deep Sea Drilling Project (DSDP) sites were drilled earlier on the plateau. Three sites were rotary drilled, with Site 64 spot cored during Leg 7 (Winterer, Riedel, et al., 1971) and Sites 288 and 289 continuously cored during Leg 30 (Andrews, Packham, et al., 1975). Site 289, which was drilled in a water depth of 2206 m, ended at 1271 mbsf in tholeiitic basalt overlain by Aptian sediments. Sediment thickness at Site 289 was 1262 m, of which the lowermost 293 m were mid-Cretaceous to upper Eocene radiolarian-bearing limestones, nannofossil foraminifer chalks, and nodular cherts. The upper 969 m consisted of upper Eocene to Pleistocene nannofossil foraminifer chalks and oozes, with a continuous section down to the lower Oligocene. Semilithified chalk was first encountered near 250 mbsf, in the upper Miocene part of the section. Site 586, drilled on Leg 89 next to Site 289, was piston-cored to 305 mbsf, the lowermost upper Miocene (Moberly, Schlanger, et al., 1986), and recovered a complete section of well-preserved nannofossil ooze.

Objectives

Site 803, roughly 400 km northeast of DSDP Sites 289/586 on the northeastern margin of the Ontong Java Plateau, was planned as the first of the four Leg 130 sites that constitute a Neogene depth transect (Sites 803–806; Fig. 1). This transect, complementary to similar ODP transects elsewhere along the equator, was designed to allow detection of depth-related paleoceanographic signals. The sediments sampled along the transect would have been produced in the same surface-water conditions and thus in the same pelagic rain; any differences in accumulation and preservation could be attributed to depth effects. The depth sampled at Site 803 (Fig. 1), near the lysocline

(around the 3400 m), is that at which dissolution gradients are most pronounced, so that saturation fluctuations should leave a maximum imprint in physical properties (Johnson et al., 1977). In turn, this imprint should be detectable in the acoustic stratigraphy (Berger and Mayer, 1978; Mayer et al., 1986).

With regard to Paleogene and Cretaceous sediments, ocean-wide coverage leaves much to be desired. Recovery has been much less comprehensive than in the Neogene. Substantial hiatuses exacerbate this situation. Major hiatuses were encountered in Upper Cretaceous to Paleogene sediments previously drilled at DSDP Sites 288 and 289, lowering expectations for finding complete sequences. However, many of the unconformities at Site 288 do not correlate with those at Site 289 (or the shallower, spot-cored Site 64), implying that they represent local events of limited areal extent (Andrews, Packham, et al., 1975). There was some hope, therefore, that drilling at Site 803 would recover key sections missed earlier. There was also the expectation that we would find clues to the extent of Cretaceous anoxic events in the South Pacific and to the original basement depth of the Ontong Java Plateau and subsequent bathymetric change. Although we assigned a low probability of success to the goal of recovering a well-preserved Cretaceous/Tertiary boundary and despite the presence of a foreshortened section, the K/T boundary was indeed recovered at this site.

We planned to sample basement at Site 803 for dating purposes and petrologic analyses. Basement previously had been drilled at Site 289, recovering basalt samples of varying texture from several meters of penetration. Recently, a $^{40}Ar/^{39}Ar$ date of 113 Ma was obtained on one sample of this basalt (R. Duncan, pers. comm., 1990). With a second basement sample from Site 803, and a third from Site 807, the nature and origin of the Ontong Java Plateau could be determined on a much sounder basis.

The criteria used to select Site 803 included the avoidance of erosion (i.e., reflection hyperbolae or channel structures), displacement or disruption in the sediment column, faulting, and such seismic anomalies as the strongly reverberant mid-section reflectors (MSRs) that commonly occur throughout the area (see Mayer et al., this volume). Site 803 is located in 3410 m of water, about one mile west of a small MSR (Fig. 2). The thickness of the sedimentary section at the site is 0.65 s (two-way traveltime [twt]), approximately 60% of that at Sites 289/586. The section is well stratified and appears to include most of the Neogene seismic reflection horizons that had been previously mapped on the Ontong Java Plateau.

OPERATIONS

Guam to Site 803

The *JOIDES Resolution* left Guam at 0215 hr (UTC) on 23 January 1990 and steamed toward Site 803 (proposed Site OJP-4), 1180 nmi southeast of Guam. The magnetometer was streamed at 0255 hr. The first leg of the transit covered 932 nmi to proposed Site OJP-5 (future Site 807) at an average speed of 11.4 kt. Seas were moderate at 5–9 ft, with winds gusting 28–40 kt and side currents running at 3 kt. A 42-nmi seismic survey was run at 8 kt over the OJP-5 site, and a 239-nmi seismic survey was run at 8 kt to Site 803 (OJP-4) (see "Underway Geophysics" chapter, this volume). The entire transit to the first site covered 1213 nmi in 120 hr at an average speed of 10.1 kt.

Site 803

A 19-nmi, pre-site seismic survey was run over the site area under optimal global positioning system (GPS) windows. The first beacon was dropped at 0120 hr on 28 January 1990 over proposed Site OJP-4A. A second beacon was dropped at 0126 hr to mark proposed Site OJP-4.
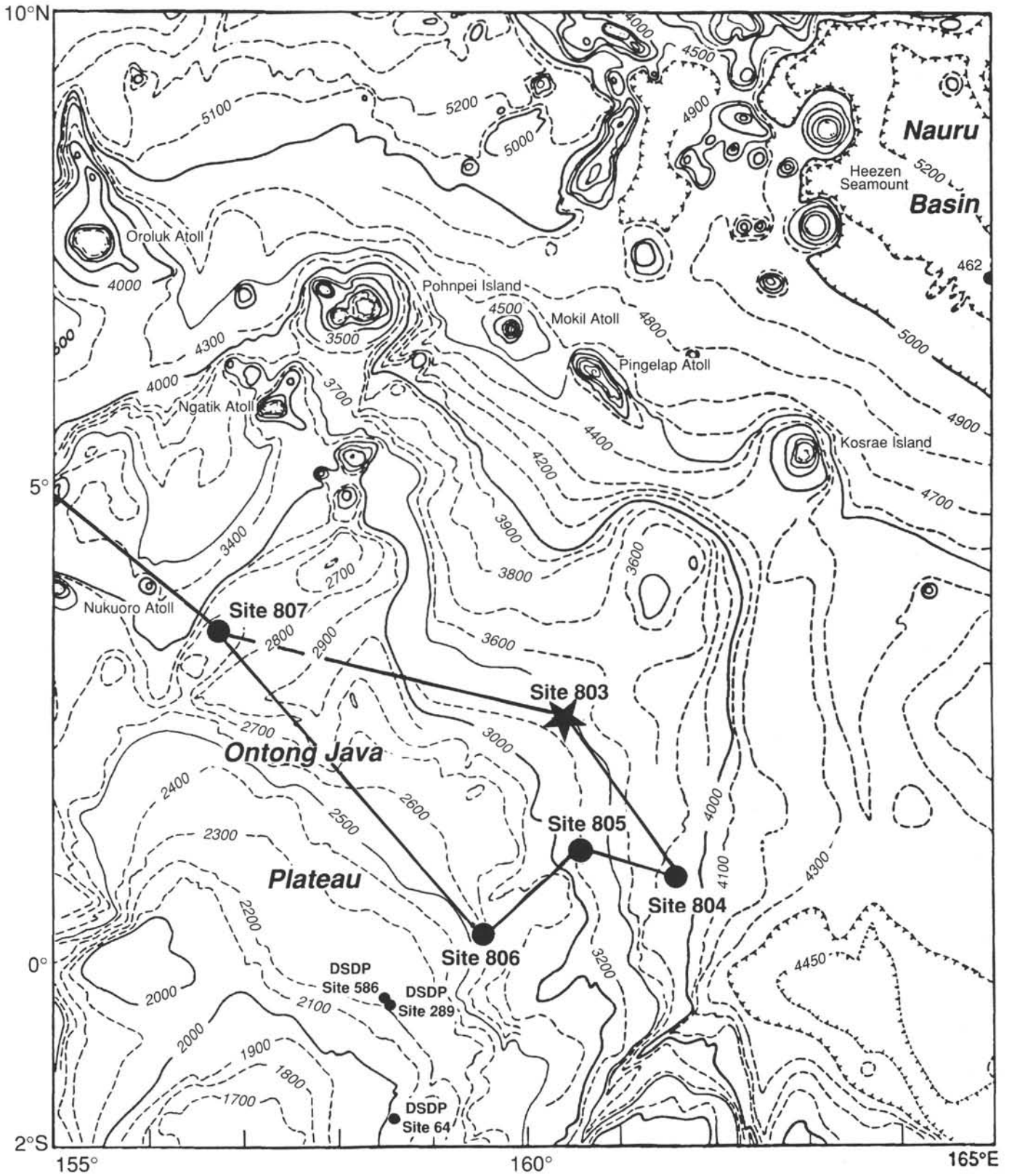
Figure 1. Bathymetry in meters of the northwestern part of the Ontong Java Plateau (after Mammerickx and Smith, 1985). The location of the Leg 130 sites together with those from DSDP Legs 7, 30, and 89 are shown for reference. Contour interval is 100 m.
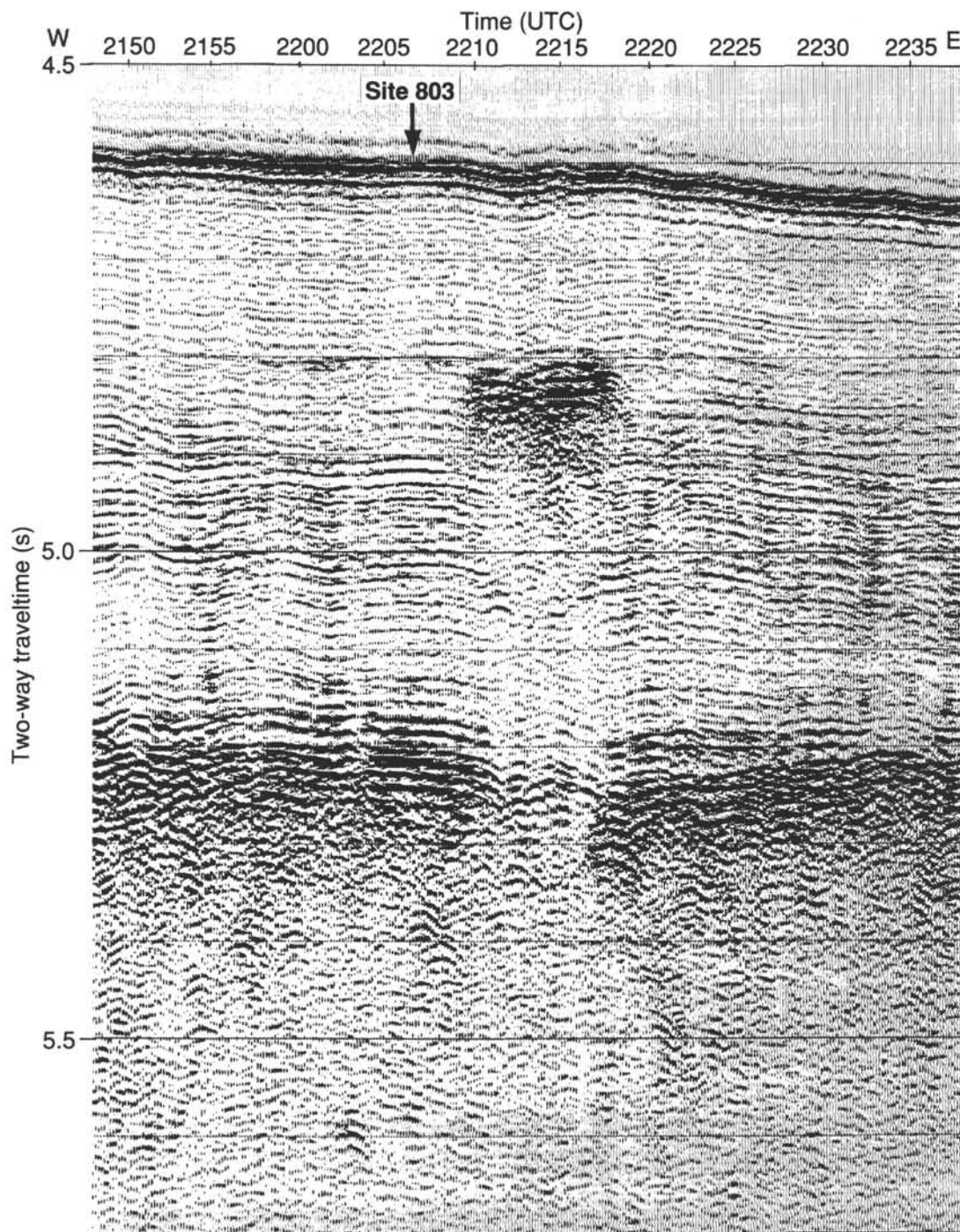
Figure 2. Site survey reflection profile from ROUNDABOUT Cruise 11 made across Site 803 (see Mayer et al., this volume).

Hole 803A

The ship was positioned 100 m east of the second beacon, and Hole 803A was spudded at 1300 hr on 28 January 1990 at 2°25.98′N and 160°32.40′E in 3409.7 m of water.

Cores 130-803A-1H through -6H were taken from 0 to 55.5 mbsf with 55.5 m of sediment cored and 57.99 m recovered (104.49% recovery; see Table 1). Orientation surveys were taken during Cores 130-803A-3H through -6H, but the orientation sleeve broke during the surveys, and the orientation data are questionable. The new, stronger APC piston-rod assembly was

tested in this hole and was used throughout Leg 130. The hole was terminated per program after Core 130-803A-6H. The pipe was pulled out of the hole and the bit cleared the seafloor at 1930 hr on 28 January 1990, ending Hole 803A.

Hole 803B

The ship was offset 20 m east of Hole 803A, and Hole 803B was spudded at 2050 hr on 28 January 1990 in 3410.4 m of water. Cores 130-803B-1H through -7H were taken from 0 to 61.3 mbsf with 61.3 m of sediment cored and 58.18 m recovered (94.91% recovery; see Table 1). Orientation surveys were taken

Table 1. Coring summary, Site 803.

Core no.	Date (1990)	Time (UTC)	Depth (mbsf)	Cored (m)	Recovered (m)	Recovery (%)
130-803A-						
1H	Jan. 28	1325	0–8.0	8.0	8.04	100.0
2H	28	1430	8.0–17.5	9.5	9.90	104.0
3H	28	1545	17.5–27.0	9.5	10.05	105.8
4H	28	1645	27.0–36.5	9.5	10.02	105.5
5H	28	1745	36.5–46.0	9.5	9.89	104.0
6H	28	1845	46.0–55.5	9.5	10.09	106.2
Coring totals				55.5	57.99	104.5
130-803B-						
1H	28	2115	0–4.3	4.3	4.36	101.0
2H	28	2200	4.3–13.8	9.5	9.89	104.0
3H	28	2300	13.8–23.3	9.5	9.82	103.0
4H	29	0015	23.3–32.8	9.5	9.85	103.0
5H	29	0115	32.8–42.3	9.5	10.06	105.9
6H	29	0215	42.3–51.8	9.5	6.85	72.1
7H	29	0315	51.8–61.3	9.5	7.35	77.3
Coring totals				61.3	58.18	94.9
130-803C-						
1H	29	1300	19.0–28.5	9.5	9.80	103.0
2H	29	1350	28.5–38.0	9.5	9.56	100.0
3H	29	1450	38.0–47.5	9.5	9.88	104.0
4H	29	1610	47.5–57.0	9.5	9.92	104.0
5H	29	1705	57.0–66.5	9.5	9.92	104.0
6H	29	1800	66.5–76.0	9.5	9.30	97.9
7H	29	1920	76.0–85.5	9.5	10.13	106.6
8H	29	2030	85.5–95.0	9.5	10.10	106.3
9H	29	2130	95.0–104.5	9.5	9.79	103.0
10H	29	2230	104.5–114.0	9.5	10.03	105.6
11H	29	2315	114.0–123.5	9.5	10.04	105.7
12H	30	0110	123.5–133.0	9.5	9.74	102.0
13H	30	0210	133.0–142.5	9.5	10.07	106.0
14H	30	0310	142.5–152.0	9.5	9.38	98.7
15H	30	0400	152.0–161.5	9.5	9.77	103.0
16H	30	0445	161.5–171.0	9.5	10.15	106.8
17H	30	0530	171.0–180.5	9.5	10.03	105.6
18H	30	0630	180.5–190.0	9.5	10.13	106.6
19H	30	0730	190.0–199.5	9.5	9.83	103.0
20H	30	0930	199.5–209.0	9.5	10.14	106.7
21H	30	1030	209.0–218.5	9.5	9.83	103.0
22H	30	1120	218.5–228.0	9.5	8.81	92.7
23H	30	1205	228.0–237.5	9.5	9.96	105.0
Coring totals				218.5	226.31	103.6
130-803D-						
1H	30	1700	0–2.5	2.5	2.53	101.0
2H	30	1830	2.5–12.0	9.5	9.94	104.0
3H	30	1940	12.0–21.5	9.5	9.84	103.0
4H	30	2100	21.5–31.0	9.5	10.01	105.3
5H	30	2155	31.0–40.5	9.5	9.92	104.0
6H	30	2300	40.5–46.1	5.6	9.87	176.0
7H	31	0000	46.1–55.6	9.5	9.98	105.0
8H	31	0100	55.6–65.1	9.5	9.93	104.0
9H	31	0215	65.1–74.6	9.5	9.82	103.0
10H	31	0315	74.6–84.1	9.5	9.86	104.0
11H	31	0400	84.1–93.6	9.5	9.68	102.0
12H	31	0445	93.6–103.1	9.5	9.61	101.0
13H	31	0545	103.1–112.6	9.5	9.81	103.0
14H	31	0630	112.6–122.1	9.5	9.51	100.0
15H	31	0715	122.1–131.6	9.5	9.54	100.0
16H	31	0745	131.6–141.1	9.5	9.57	101.0
17H	31	0915	141.1–150.6	9.5	9.97	105.0
18H	31	1015	150.6–160.1	9.5	9.72	102.0
19H	31	1110	160.1–169.6	9.5	9.55	100.0
20H	31	1155	169.6–179.1	9.5	10.00	105.2
21H	31	1250	179.1–188.6	9.5	10.06	105.9
22H	31	1335	188.6–198.1	9.5	10.07	106.0
23H	31	1440	198.1–207.6	9.5	10.10	106.3
24H	31	1730	207.6–217.1	9.5	9.99	105.0
25X	31	1910	217.1–226.8	9.7	6.34	65.3
26X	31	2045	226.8–236.5	9.7	9.21	94.9

Table 1 (continued).

Core no.	Date (1990)	Time (UTC)	Depth (mbsf)	Cored (m)	Recovered (m)	Recovery (%)
130-803D- (Cont.)						
27X	31	2230	236.5–245.9	9.4	4.32	45.9
28X	31	2345	245.9–255.5	9.6	6.90	71.9
29X	Feb. 1	0045	255.5–265.1	9.6	7.46	77.7
30X	1	0145	265.1–274.7	9.6	6.00	62.5
31X	1	0245	274.7–284.3	9.6	5.81	60.5
32X	1	0345	284.3–294.1	9.8	7.98	81.4
33X	1	0430	294.1–303.3	9.2	7.85	85.3
34X	1	0515	303.3–313.0	9.7	9.54	98.3
35X	1	0555	313.0–322.7	9.7	9.01	92.9
36X	1	0645	322.7–332.3	9.6	9.16	95.4
37X	1	0740	332.3–342.0	9.7	9.63	99.3
38X	1	0810	342.0–351.6	9.6	8.44	87.9
39X	1	0855	351.6–361.3	9.7	9.06	93.4
40X	1	0955	361.3–371.0	9.7	7.51	77.4
41X	1	1045	371.0–380.7	9.7	5.50	56.7
42X	1	1135	380.7–390.4	9.7	7.05	72.7
43X	1	1225	390.4–400.0	9.6	7.28	75.8
44X	1	1320	400.0–409.7	9.7	8.28	85.3
45X	1	1430	409.7–419.3	9.6	9.18	95.6
46X	1	1530	419.3–429.0	9.7	8.39	86.5
47X	1	1630	429.0–438.6	9.6	7.20	75.0
48X	1	1730	438.6–447.8	9.2	6.01	65.3
49X	1	1830	447.8–457.5	9.7	6.03	62.1
50X	1	1930	457.5–467.2	9.7	6.17	63.6
51X	1	2030	467.2–476.9	9.7	4.60	47.4
52X	1	2145	476.9–486.6	9.7	4.52	46.6
53X	1	2245	486.6–496.3	9.7	5.66	58.3
54X	1	2345	496.3–506.0	9.7	6.63	68.3
55X	2	0045	506.0–515.6	9.6	6.37	66.3
56X	2	0145	515.6–525.3	9.7	9.10	93.8
57X	2	0230	525.3–534.6	9.3	5.66	60.8
58X	2	0345	534.6–544.3	9.7	1.26	13.0
59X	2	0430	544.3–554.0	9.7	3.90	40.2
60X	2	0535	554.0–563.7	9.7	2.50	25.8
61X	2	0645	563.7–573.4	9.7	0.80	8.3
62X	2	0800	573.4–583.0	9.6	0.40	4.2
63X	2	1215	583.0–588.7	5.7	0.37	6.5
64X	2	1505	588.7–598.4	9.7	0.55	5.7
65X	2	1715	598.4–601.9	3.5	0.48	13.7
66X	2	1940	601.9–612.0	10.1	0.36	3.6
67R	4	0645	612.0–621.8	9.8	2.52	24.7
68R	4	0810	621.8–631.4	9.6	4.95	51.5
69R	4	1140	631.4–641.1	9.7	3.91	40.3
70R	4	1555	641.1–650.8	9.7	3.10	31.9
71R	4	1910	650.8–656.0	5.2	3.13	60.2
Coring totals				656.0	494.96	75.5

during Cores 130-803B-3H through -7H, but the camera malfunctioned and no data were recovered.

Cores 130-803B-6H and -7H were taken using the new APC breakaway piston head (BPH), with 19.0 m of sediment cored and 14.20 m recovered (74.74% recovery; see Table 1). The BPH separated successfully on both runs.

While putting the APC core-barrel assembly into position for Core 130-803B-8H, the core barrel became stuck and could not be pulled out with an air tugger. Several attempts to free the core barrel were unsuccessful, and the drill pipe was finally tripped out of the hole to recover the core barrel. The bit cleared the seafloor at 0530 hr on 29 January 1990, ending Hole 803B.

Hole 803C

The ship was offset 20 m east of Hole 803B for further APC coring. We intended to run the drill pipe 19 mbsf to spud the hole, but the first two APC attempts were water cores. A recheck of the drill pipe revealed that one stand had been left out of the string. The additional stand was run in the hole, and

Hole 803C was spudded at 1130 hr, 29 January 1990; the hole was washed to 19.0 mbsf.

Cores 130-803C-1H through -23H were taken from 19.0 to 237.5 mbsf, with 218.5 m of sediment cored and 226.31 m recovered (103.6% recovery; see Table 1). Orientation surveys were taken on Cores 130-803C-1H through -23H. Directional surveys at 28.5 and 57.0 mbsf indicated 1° of vertical drift. After Core 130-803C-24H (247.0 mbsf) was fired, the core would not pull free, even with 100,000 lb of overpull. The new, "stronger" APC piston rod parted in the top thread, leaving the core barrel, with Core 130-803C-24H, in the hole. The drill pipe was pulled out of the hole to retrieve the core barrel, and it cleared the seafloor at 1445 hr on 30 January 1990, thus ending Hole 803C.

Hole 803D

The ship was offset 20 m east of Hole 803C, and Hole 803D was spudded at 1630 hr on 30 January 1990 in 3412.2 m of water. Cores 130-803D-1H through -24H were taken from 0 to 217.1 mbsf, with 217.1 m of sediment cored and 228.88 m recovered (105.43% recovery). Orientation surveys were taken on Cores 130-803D-3H through -24H.

Core 130-803D-24H did not fully stroke out, and the core barrel temporarily became stuck in moderately stiff nannofossil ooze. Attempts to drill over the core barrel proved unsuccessful. Repeated overpulls, up to 170,000 lb, finally freed the core barrel.

We ended APC coring at this point and began coring with the XCB. Cores 130-803D-25X through -66X were taken from 217.1 to 612.0 mbsf with 394.9 m of sediment cored and 248.47 m recovered (62.92% recovery). Various flapper and finger core catchers and XCB bits were tried in an effort to improve the XCB recovery of the stiff white nannofossil/chalk sediments. Good core recovery (62.79%) was obtained with six-tooth, hard-formation (sharp) carbide bits using two, hard-formation core catchers with soft springs. Recovery dropped to 15.69% below Core 130-803D-57X (534 mbsf) as a result of the core jamming in the bit. Poor circulation through the bit was suspected, and the bit seal was found to be severely cut (after sustaining 90 core barrel runs).

An FFF was dropped in Hole 803D so that we could core into basement with an RCB reentry in the same hole, rather than wash down a new RCB hole. The purpose in using the FFF was not only to save time but also to test the televiewer (TV) camera and coaxial cable, which would be required later at proposed Site OJP-5. The TV picture was fuzzy but usable on deck. However, the picture was lost at 140 meters below sea level (mbsl), despite repair attempts. Although the loss of the TV picture was critical, the FFF was equipped with four floats and a sonar target as a precaution, and through-the-drill-pipe slimline sonar was available as a reentry backup tool. The bottom hole assembly (BHA) was run in to 8 m above the sea floor, the Schlumberger logging line was rigged up, and the sonar was run through the drill pipe. The sonar acquired the FFF target, and reentry was successfully completed. This was the first known reentry of an FFF using the through-the-drill-pipe slimline sonar tool.

Cores 130-803D-67R through -71R were taken from 612.0 to 656.0 mbsf. Basalt was encountered at 630.4 mbsf, and a total of 9.59 m of hard rock was recovered. At this point, we had achieved our scientific objectives; therefore, we terminated coring and released the bit at the bottom of the hole. After a short trip to condition the hole, a viscous mud sweep was circulated to clean the hole. The seafloor was unconsolidated down to 55 mbsf, so the open-ended BHA was pulled up to only 109 mbsf for logging.

Downhole logs were run as follows:

Run No. 1 (NGT/DIT/HLDT/LSS/TLT). The log was run from a depth of 649.2 to 534.9 mbsf at a speed of 900 ft/hr. Because the HLDT/LSS tools were not functioning properly, the tool was run at a speed of 1800 ft/hr to 98.7 mbsf.

Run No. 2 (NGT/FMS/TLT). The connector head on the FMS tool flooded as the tool was run in the hole. The tool was pulled out of the hole and dried out, and a successful run was made from 609.8 to 98.7 mbsf. A repeat log was run from 191.7 to 98.7 mbsf.

Run No. 3 (NGT/ACT/GST/HLDT). The log was run from 610.5 to 464.8 mbsf at 600 ft/hr. Because the GST was not functioning properly, the log was run at 900 ft/hr from 464.8 to 98.7 mbsf.

Run No. 4 (NGT/BHC/TLT). Two logs, one from 605.6 to 98.7 mbsf and another from 606.8 to 101.1 mbsf, were run successfully.

When the logging program was completed, the pipe was pulled out of the hole and the BHA cleared the rotary table at 1730 hr, 6 February 1990, ending Hole 803D.

LITHOSTRATIGRAPHY

Introduction

Four holes were drilled at Site 803. Holes 803A and 803B were cored with the APC, and approximately 60 m of sediment was recovered from the top of the section in each. The recovery rate averaged 99.5% at these two holes. Hole 803C was cored with a combination of APC and XCB methods; sediments were recovered to 226 mbsf, with a recovery rate of 103.6%. The complete section was cored at Hole 803D with a combination of APC, XCB, and RCB methods, and sediments were recovered throughout the entire thickness of 626 m. The average recovery rate was 75.7%, but it gradually decreased downhole. The cored sequence is composed predominantly of nannofossil ooze and chalk, with variable abundances of foraminifers. Radiolarian abundances increase below 564 mbsf, and siliciclastic rocks dominate the basal 4.5 m of sediment. The recovered sediments range in age from Pleistocene to early Late Cretaceous and overlie basaltic rocks, which were recovered in Section 130-803D-68R-4 through Core 130-803D-71R. The basalts are described elsewhere in this chapter (see "Igneous Petrology" section, this chapter).

The sedimentary section at Site 803 has been divided into three lithologic units (Table 2 and Fig. 3). Unit I (0–563.7 mbsf) is composed of Pleistocene to upper Eocene nannofossil ooze and chalk to foraminifer nannofossil ooze and chalk and is divided into two subunits on the basis of degree of consolidation. Subunit IA is composed of ooze, whereas Subunit IB contains chalk; the ooze-chalk transition is located between 210 and 220 mbsf (near the base of Core 130-803D-24H), the level at which cores could no longer be split with a wire. Unit II is composed of approximately 58 m of nannofossil chalk with radiolarians, radiolarian nannofossil chalk, nannofossil radiolarite, and minor amounts of chert, and is late Eocene to middle Eocene in age. Unit III is composed of approximately 4.5 m of claystone, clayey siltstone, and minor radiolarite of latest Paleocene to early Late Cretaceous age; this unit is severely condensed and contains several major unconformities.

Description of Units

Unit I

Intervals: Hole 803A, Cores 130-803A-1H to -6H; Hole 803B, Cores 130-803B-1H to -7H; Hole 803C, Cores 130-803C-1H to -23H; Hole 803D, Cores 130-803D-1H to -60X
Age: Pleistocene–late Eocene
Depth: 0–563.7 mbsf

Table 2. Lithologic summary, Site 803.

Lithologic unit	Cores	Depth (mbsf)	Age	Lithology
IA	803A-1H to -6H 803B-1H to -7H 803C-1H to -23H 803D-1H to -24H	0–217.1	Pleistocene to middle Miocene	Nannofossil ooze to foraminifer nannofossil ooze
IB	803D-25 to -60X	217.1–563.7	middle Miocene to late Eocene	Nannofossil chalk to nannofossil chalk with foraminifers
II	803D-61X to -67R	563.7–621.8	late Eocene to middle Eocene	Nannofossil chalk with radiolarians to nannofossil radiolarite and chert
III	803D-68R-1 to -68R-3	621.8–626.3	middle Eocene to early Late Cretaceous	Claystone and clayey siltstone

Unit I is composed of nannofossil ooze and chalk to foraminifer nannofossil ooze and chalk and has been divided into two subunits. Subunit IA (0–217.1 mbsf) comprises the nannofossil ooze to foraminifer nannofossil ooze, whereas Subunit IB (217.1–563.7 mbsf) contains the nannofossil chalk to foraminifer nannofossil chalk.

Subunit IA

Intervals: Hole 803A, Cores 130-803A-1H to -6H; Hole 803B, Cores 130-803B-1H to -7H; Hole 803C, Cores 130-803C-1H to -23H; Hole 803D, Cores 130-803D-1H to -24H
Age: Pleistocene–middle Miocene
Depth: 0–217.1 mbsf

Subunit IA contains 217.1 m of nannofossil ooze, nannofossil ooze with foraminifers, and foraminifer nannofossil ooze. Foraminifer abundances decrease downhole through the first 30–60 m of Subunit IA, producing a lithologic transition from foraminifer nannofossil ooze to nannofossil ooze with foraminifers to nannofossil ooze. Foraminifer abundances remain low (<10%) through the remainder of Subunit IA, with a slight increase in Cores 130-803D-17H and -18H (upper Miocene sediments).

Dominant colors are various types of white (2.5Y N8/, 2.5Y 8/2, 5Y 8/1, 10YR 8/1, and 10YR 8/2) and light gray (2.5Y N7/, 5Y 7/1, and N7/). The uppermost 20 m, the Pleistocene section, also exhibits pale yellowish brown (10YR 6/3) to pale yellow (10YR 7/3) colors. Primary depositional sedimentary structures were not observed in Subunit IA. Bioturbation is ubiquitous, ranging in intensity from slight to heavy (Fig. 4). Faint color bands, one centimeter to several tens of centimeters thick in various shades of green, purple, and red, are common in most of Subunit IA (Fig. 5). Only Cores 130-803C-20H, -21H, and -23H, and Cores 130-803D-23H and -24H, in the lowermost portion of Subunit IA, do not contain these color bands.

Small faults with centimeter-scale offsets were observed in Sections 130-803B-6H-3 through -7H-2 (45–55 mbsf), 130-803C-9H-1 through -4 (95–101 mbsf), and 130-803D-16H-4 (136–138 mbsf) (Fig. 6). Angular discordances in color banding not attributed to coring disturbance were observed in Sections 130-803C-7H-4 through -6 (81–86 mbsf), 130-803C-14H-1 through -3 (142–147 mbsf), 130-803C-18H-6 through -19H-2 (188–193 mbsf), 130-803C-22H-3 through -6 (221–228 mbsf), and 130-803D-22H-2 through -7 (190–198 mbsf). These angular discordances are commonly overlain by an interval, one to several meters thick, that contains 5%–10% more foraminifers than the underlying sediments.

The only significant occurrence of a different lithology within Subunit IA is a thin (<1 cm thick) volcanic ash layer recovered in Sections 130-803C-18H-2, 77 cm, and 130-803D-21H-2, 61 cm (Figs. 7 and 8). In both holes, the ash layer is underlain by approximately 6 cm of very dark gray (5Y 3/1) nannofossil ooze with minor amounts of apatite and zeolites. This ash is a clear marker horizon in natural gamma-ray logging data obtained at Hole 803D (see "Logging" section, this chapter).

Subunit IA is predominantly composed of nannofossils and variable amounts of foraminifers (Fig. 9). On average, the calcareous biogenic constituents form more than 95% of these sediments. The dominance of carbonates in these sediments is also indicated by the results of shipboard carbonate analyses (Fig. 10) and X-ray diffraction (XRD) scans. Accessory biogenic components include radiolarians, silicoflagellates, sponge spicules, and diatoms, whereas quartz, feldspar, volcanic ash, and clay minerals are the common terrigenous components. Texturally, the sediments are predominantly silts and clayey silts. Shipboard grain-size determinations (Fig. 11 and Table 3) indicate that mean grain size generally decreases downhole through the first 100 m, reflecting the decrease in foraminifer abundance described previously. The mean grain size then increases by a factor of 2 over the interval from 100 to 150 mbsf, as foraminifers become more abundant in Cores 130-803D-17H and -18H (upper Miocene sediments). Grain size again decreases below 150 mbsf as foraminifer abundances decrease.

During visual description of Subunit IA, a qualitative transition from "soft" ooze to "stiff" ooze was noted at approximately 150 mbsf. This transition exists as a zone of change in grain size, physical properties (see "Physical Properties" section, this chapter), and log signatures (resistivity and velocity; see "Logging" section, this chapter) from 135 to 145 mbsf, and produces a major horizon on seismic reflection profiles in this area (see "Seismic Stratigraphy" section, this chapter).

Subunit IB

Intervals: Hole 803D, Cores 130-803D-25X to -60X
Age: middle Miocene–late Eocene
Depth: 217.1–563.7 mbsf

Subunit IB consists of 346.6 m of nannofossil chalk and nannofossil chalk with foraminifers and is distinguished from Subunit IA on the basis of the ooze-chalk transition. Sediment recovery was good (77% average) over most of the interval, but decreased drastically in the last three cores of Subunit IB (26% average; Fig. 3), in which minor amounts of chert were recovered. In these last three cores of Subunit IB, a marked decrease
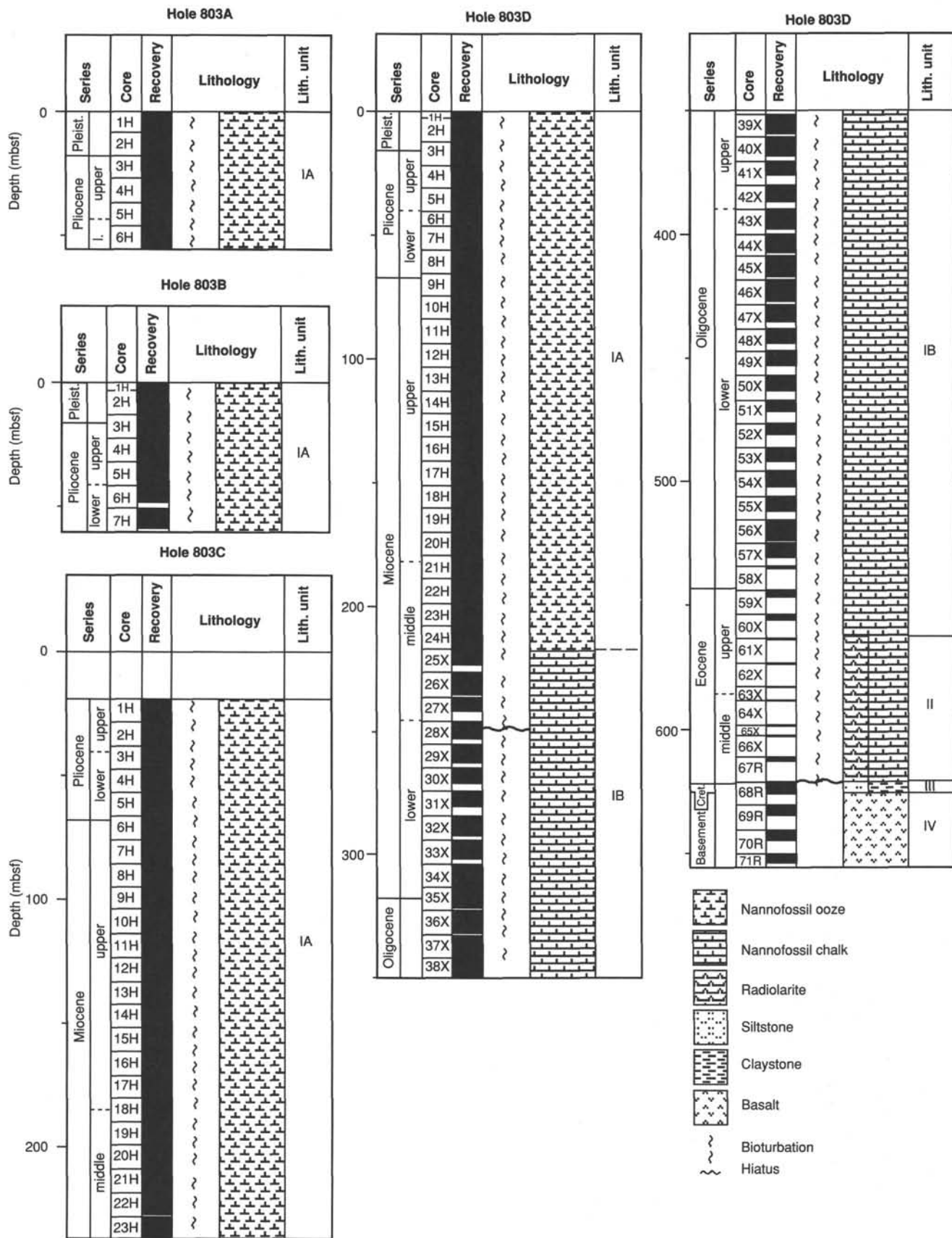
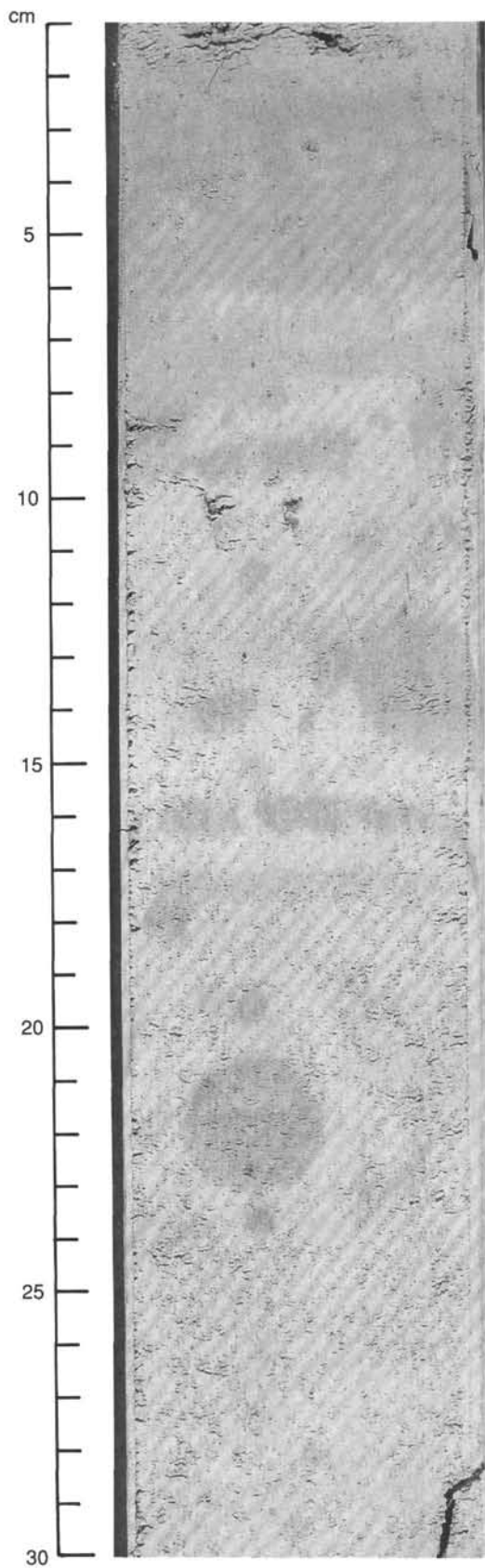Figure 3. Lithologic summary, Site 803.

Figure 4. Photograph of general nature of bioturbation in Subunit IA (Section 130-803C-3H-6, 1–30 cm).
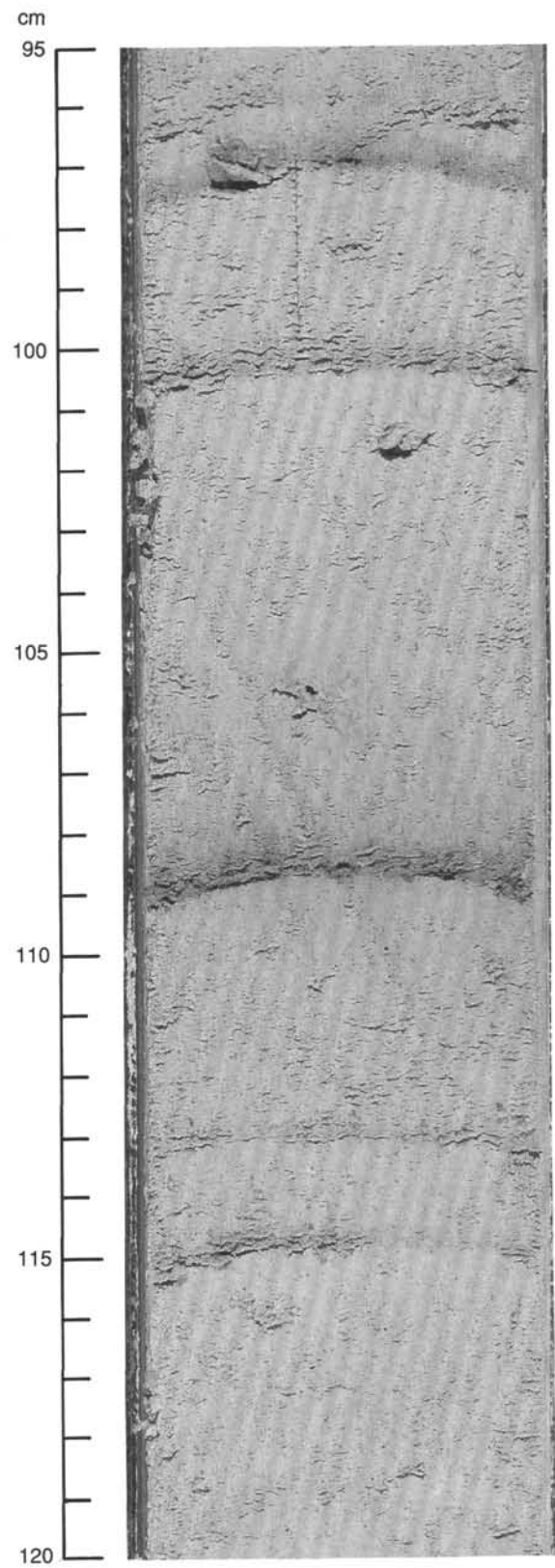

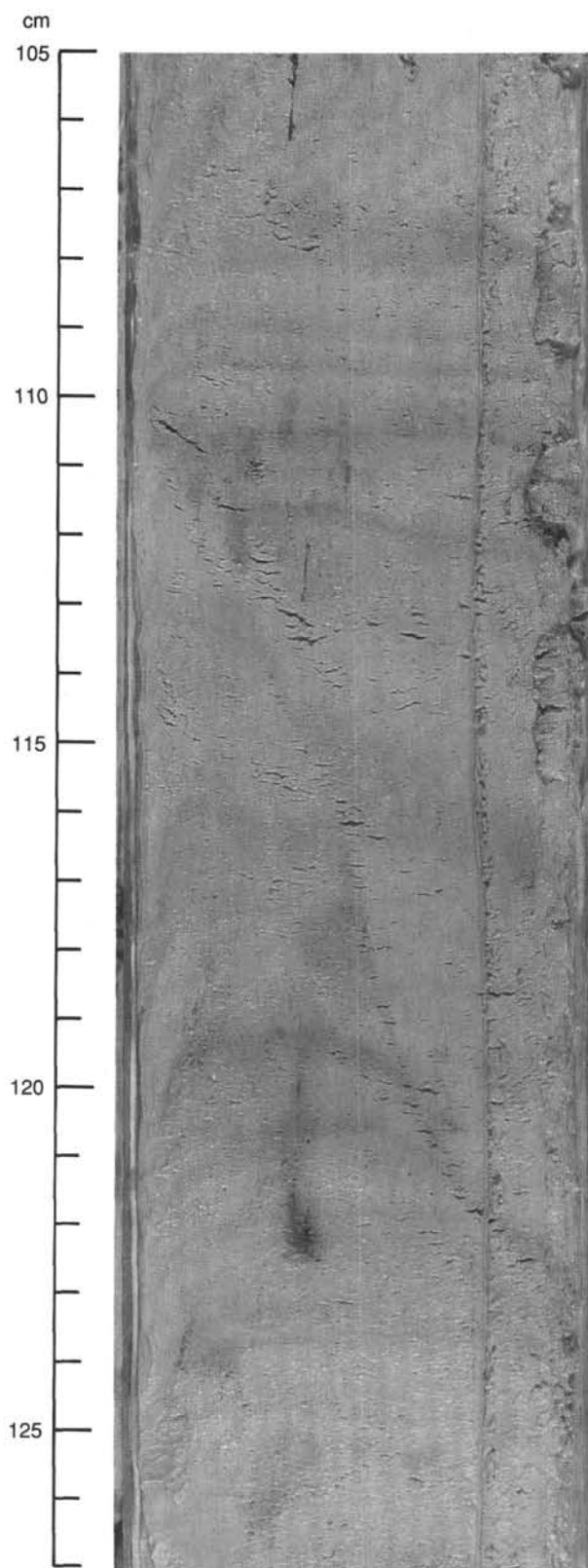Figure 5. Photograph of color banding in Subunit IA (Section 130-803D-4H-1, 95–120 cm).

Figure 6. Photograph of small fault offsetting color banding in Subunit IA (Section 130-803C-9H-1, 105–127 cm).
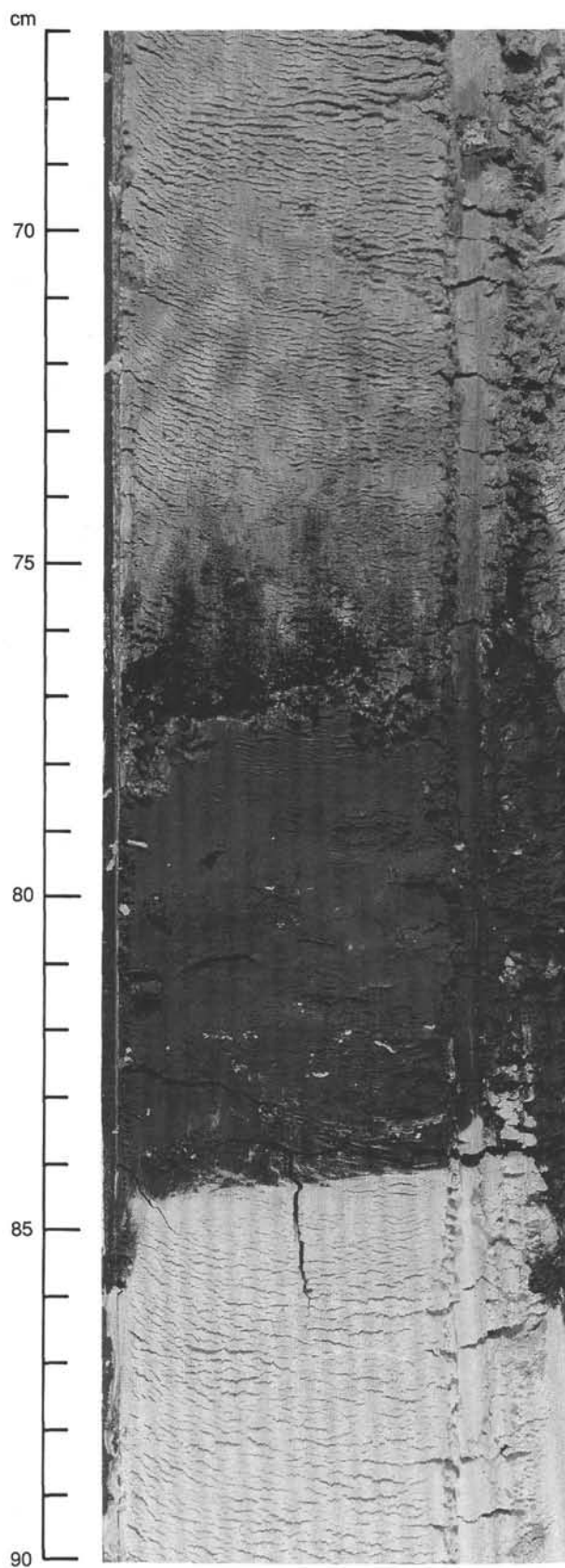

Figure 7. Photograph of ash layer in Subunit IA (Section 130-803C-18H-2, 67–90 cm).

Figure 8. Photomicrograph of smear slide of ash layer in Subunit IA. Field of view is approximately 1 mm wide; plane polarized light.
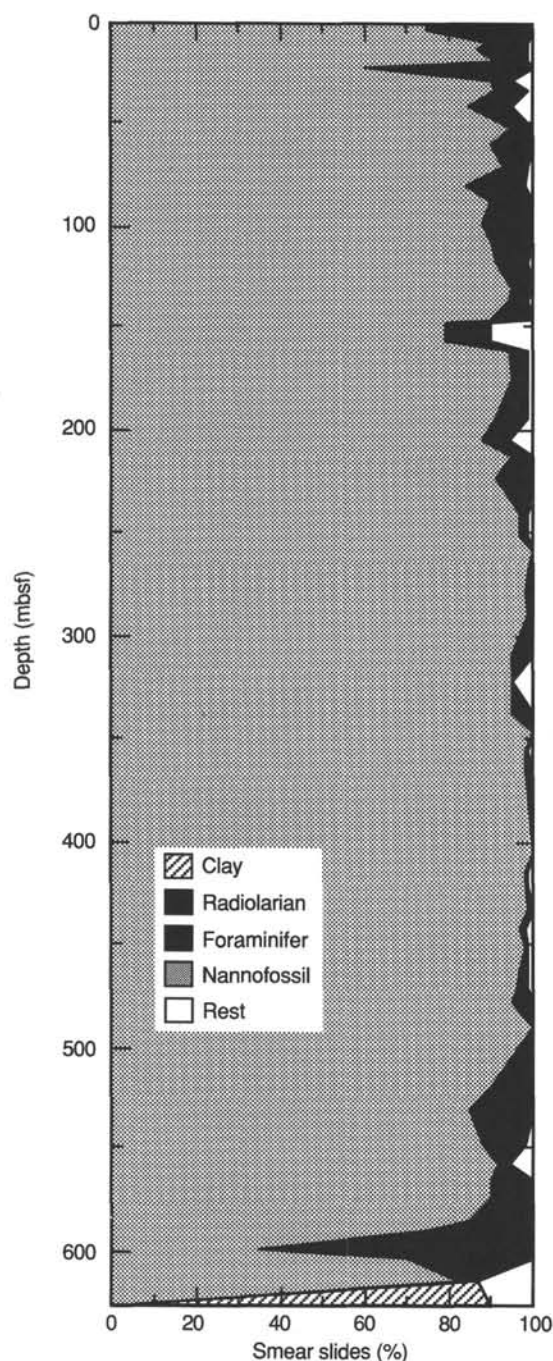
Figure 9. Composition of sediments at Hole 803D as compiled from smear slide data.

Figure 10. Calcium carbonate content of sediments at Hole 803D, as determined by shipboard analyses.

in pore-water silica concentration indicates the onset of silica reprecipitation (see "Inorganic Geochemistry" section, this chapter), and the irregular nature of velocity and density logs suggests interbedding of hard and soft sediment types below 520 mbsf (see "Logging" section, this chapter). All of these data suggest that well-cemented biosiliceous sediments first appear as thin beds near the base of Subunit IB, and that the presence of interbedded hard and soft sediment types reduced the coring effectiveness of the XCB.

The primary colors of Subunit IB are essentially the same as those of Subunit IA. Indicators of bioturbation are common to abundant throughout Subunit IB (Fig. 12) and include diffuse mottling, disseminated pyritic burrow linings, millimeter-scale simple burrows, and large, more complex and identifiable discrete trace fossils. Among the latter are several excellent examples of *Zoophycos* and *Chondrites* (Fig. 13). The faint color banding characteristic of Subunit IA is absent in Cores 130-803D-25X through -44X (217–409 mbsf), but is present in the next 100 m below (lower Oligocene sediments of Cores 130-803D-45X to -55X). The color bands become more abundant, intense, and distinct downhole. In intervals that contain both color bands and bioturbation features, the color bands are continuous across and through burrows.

As in Subunit IA, the composition of Subunit IB is dominated by biogenic carbonate, as demonstrated by smear-slide examination, shipboard carbonate analyses, and XRD scans (Figs. 9 and 10). Foraminifer abundances are low throughout most of Subunit IB and exceed 10% only in Cores 130-803D-57X through -59X (525–554 mbsf), which span the Eocene/Oligocene boundary. Radiolarians are the most common biogenic sili-
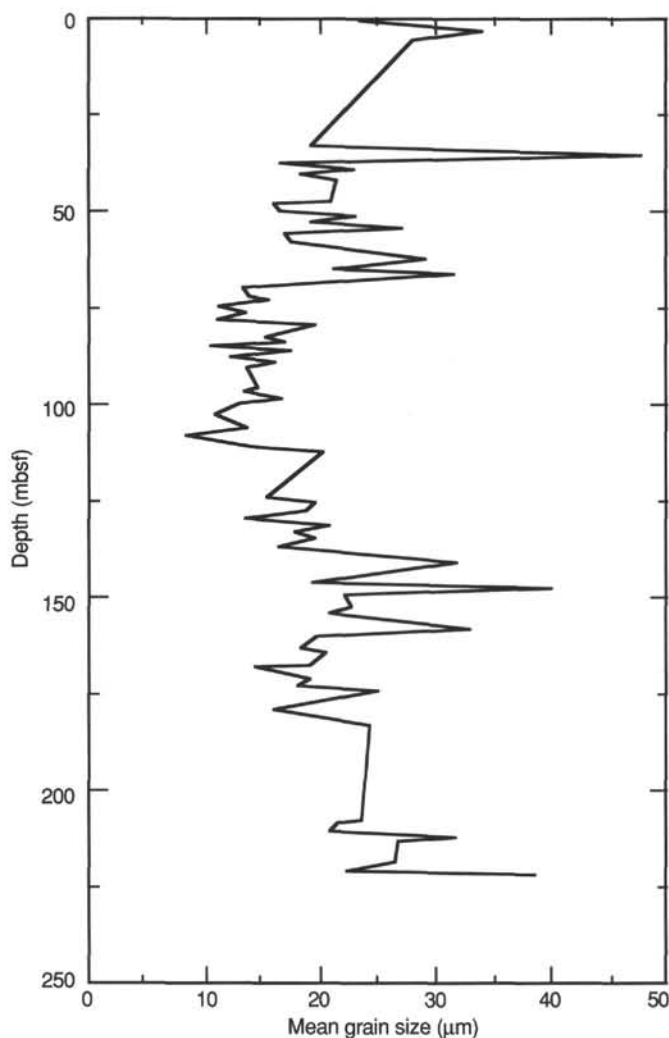
Figure 11. Mean grain size of sediments in Subunit IA.

Table 3. Grain size results, Hole 803D.

Core, section, interval (cm)	Depth (mbsf)	Mean grain size (μm)	Core, section, interval (cm)	Depth (mbsf)	Mean grain size (μm)
130-803D-			130-803D-(Cont.)		
1H-1, 123	1.2	23.2	13H-4, 102	108.6	12.1
1H-2, 38	1.9	34.0	13H-5, 108	110.2	13.9
2H-2, 37	4.4	27.5	13H-6, 110	111.7	20.0
5H-1, 106	32.1	19.0	15H-1, 113	123.2	15.3
5H-2, 131	33.8	47.3	15H-2, 112	124.7	19.2
5H-3, 106	35.1	30.0	15H-3, 112	126.2	18.6
5H-4, 110	36.6	16.6	15H-4, 113	127.7	16.1
5H-5, 111	38.1	22.6	15H-5, 107	129.2	13.4
5H-6, 112	39.6	18.3	15H-6, 107	130.7	20.5
5H-7, 36	40.4	21.2	16H-1, 106	132.7	17.7
7H-1, 36	46.5	20.7	16H-2, 111	134.2	19.4
7H-1, 111	47.2	15.8	16H-3, 112	135.7	17.8
7H-2, 110	48.7	16.2	16H-4, 31	136.4	16.2
7H-3, 113	50.2	22.9	16H-5, 111	138.7	23.3
7H-4, 111	51.7	18.9	16H-6, 112	140.2	31.7
7H-5, 111	53.2	26.9	17H-1, 111	142.2	26.3
7H-6, 110	54.7	16.8	17H-3, 109	145.2	19.2
8H-1, 112	56.7	17.4	17H-4, 105	146.7	39.9
8H-2, 110	58.2	22.3	17H-5, 112	148.2	22.2
8H-3, 110	59.7	25.1	17H-6, 102	149.6	22.1
8H-4, 111	61.2	28.8	18H-1, 110	151.7	22.6
8H-5, 111	62.7	26.5	18H-2, 115	153.2	20.8
8H-6, 110	64.2	20.9	18H-3, 110	154.7	22.3
8H-7, 35	64.9	31.5	18H-4, 110	156.2	28.8
9H-1, 111	66.2	21.2	18H-5, 111	157.7	32.9
9H-2, 110	67.7	15.0	18H-6, 110	159.2	28.0
9H-3, 109	69.2	12.9	18H-7, 30	159.9	19.4
9H-4, 106	70.7	13.6	19H-1, 110	161.2	19.2
9H-5, 114	72.2	15.0	19H-2, 111	162.7	18.2
9H-6, 111	73.7	11.2	19H-3, 115	164.2	20.5
10H-1, 99	75.6	13.4	19H-5, 110	167.2	18.7
10H-2, 108	77.2	11.0	19H-5, 110	167.2	14.1
10H-3, 108	78.7	19.3	19H-6, 110	168.7	14.8
10H-5, 109	81.7	14.9	20H-1, 111	170.7	19.2
10H-6, 109	83.2	16.7	20H-2, 110	172.2	18.0
10H-7, 36	84.0	10.4	20H-3, 110	173.7	25.1
11H-1, 110	85.2	17.0	20H-5, 111	176.7	18.1
11H-2, 110	86.7	12.1	20H-7, 31	178.9	15.6
11H-3, 108	88.2	15.6	21H-3, 109	183.2	24.1
11H-4, 109	89.7	13.5	23H-7, 39	207.5	23.3
12H-1, 110	94.7	14.5	24H-1, 116	208.8	21.1
12H-2, 110	96.2	13.2	24H-2, 104	210.1	20.7
12H-3, 110	97.7	16.6	24H-3, 104	211.6	31.6
12H-4, 110	99.2	12.7	24H-4, 104	213.1	26.4
12H-5, 112	100.7	11.6	24H-6, 104	216.1	26.0
12H-6, 110	102.2	10.8	25H-1, 107	218.2	26.4
13H-2, 111	105.7	13.6	25H-3, 72	220.8	22.0
13H-3, 111	107.2	8.4	25H-4, 41	222.0	38.8

ceous component, but their abundance never exceeds 7% in smear slides; sponge spicules are present in trace amounts. The terrigenous component is dominated by quartz and clay minerals, as determined from XRD scans.

Unit II

Intervals: Hole 803D, Cores 130-803D-61X to -67R
Age: late Eocene–middle Eocene
Depth: 563.7–621.8 mbsf

Unit II consists of approximately 58 m of nannofossil chalk with radiolarians, radiolarian nannofossil chalk, nannofossil radiolarite, and minor amounts of chert. Radiolarian abundances generally increase downhole from Cores 130-803D-61X to -65X and decrease below that level (Fig. 9), although chert was recovered in Section 130-803D-67R-CC. The nannofossil radiolarite and the chert provide useful markers for correlating the lithostratigraphy to other shipboard measurements. The nannofossil radiolarite appears as a high-porosity, low-velocity zone in physical properties data (see "Physical Properties" and "Logging" sections, this chapter) and a low-density interval from 595 to 597 mbsf in logging data (see "Logging" section, this chapter). The chert appears as a thin resistive bed on the electrical resistivity log (see "Logging" section, this chapter), has high measured velocities (see "Physical Properties" section, this chapter),

and is identifiable as a major reflector on seismic profiles (see "Seismic Stratigraphy" section, this chapter).

These sediments are white (2.5Y 8/0, 10YR 8/1, and 10YR 8/2) to light brownish gray (10YR 7/3) in color and are slightly to heavily bioturbated. No physical sedimentary structures were observed in Unit II, although any structures present may have been obscured by the poor recovery and significant drilling disturbance of sediments from this interval.

Sediment compositions in Unit II are more variable than those in Unit I (Fig. 9) because of the wide range of nannofossil and radiolarian contents. Nannofossil abundances range from 35% to 90%, whereas radiolarian abundances range from 15% to 65%. Foraminifers and sponge spicules are present in trace amounts. The lower average carbonate content of Unit II and its increased variability are also expressed in shipboard carbonate analyses (Fig. 10). Terrigenous components in Unit II include clays and quartz; the diffractograms also indicate the increased abundance of opal in Cores 130-803D-63R through -66R. On the basis of smear-slide estimates, the sediments of Unit II are classified texturally as silts and sandy silts.
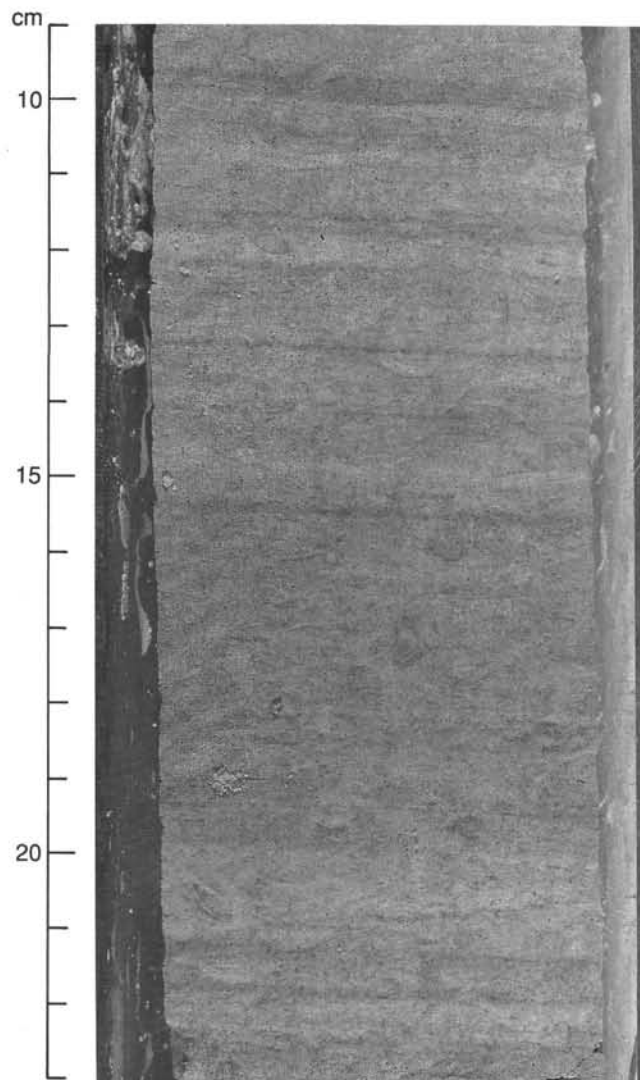
Figure 12. Photograph of general nature of bioturbation in Subunit IB (Section 130-803D-58X-CC, 9–23 cm).
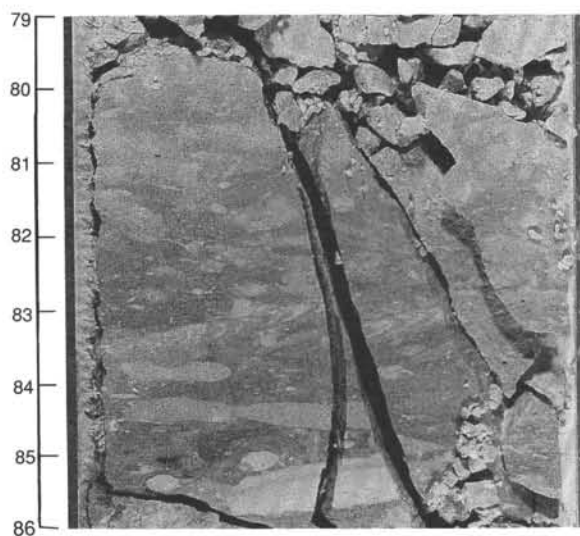

Figure 13. Photograph of bioturbation in Subunit IB, including well-developed *Zoophycos* trace fossils (Section 130-803D-55X-4, 79–86 cm).

Unit III

Intervals: Hole 803D, Sections 130-803D-68R-1 to -3
Age: middle Eocene–early Late Cretaceous
Depth: 621.8–626.3 mbsf

Unit III is composed of claystone and clayey siltstone, with minor radiolarian-rich intervals. We recovered 4.5 m of sediment from Unit III, but resistivity logs suggest that this lithology continues from 621.8 mbsf to basement at 632 mbsf (see "Logging" section, this chapter). Dominant colors are very dark brown (10YR 2/2), dark brown (10YR 3/3, 7.5YR 4/2, and 7.5YR 4/4), and brown (7.5YR 5/4), with minor intervals of dark yellowish brown (10YR 4/4). The radiolarian-rich sediments (radiolarian clayey siltstone to radiolarite) are dark yellowish brown, whereas the radiolarian-poor sediments exhibit more reddish colors. Sharp contacts separate intervals of different color in Sections 130-803D-68R-1 and -3 and may represent significant unconformities (Fig. 14). Bioturbation is common to abundant throughout most of Unit III, but distinct millimeter-scale lamination is present in parts of the Cretaceous interval (Sections 130-803D-68R-2 and -3; Fig. 15).

The siliciclastic sediments of Unit III are composed of 80% or more silica-rich grains and clays, with iron-oxide coatings common to abundant. Many of the silica-rich grains exhibit unusual internal heterogeneity in extinction under cross-polarized light, similar to the characteristics of chert. XRD scans identify quartz, plagioclase and potassium feldspar, illite, and mixed-layer clays as the dominant siliciclastic components. Nannofossil abundances in Unit III are low (20% or less), as indicated by smear-slide examination (Fig. 9), shipboard carbonate analyses (Fig. 10), and XRD scans. Radiolarians are abundant to dominant in the dark yellowish-brown intervals, but rare to absent in the remainder of Unit III (Fig. 16). Although Unit III directly overlies basaltic basement, these sediments are not metalliferous. This evidence suggests that a significant hiatus exists between the basal sediments and the underlying basalts. The limited thickness of Unit III and the available biostratigraphic data (see "Biostratigraphy" section, this chapter) indicate that significant hiatuses also exist within Unit III. Despite the presence of such hiatuses, shipboard biostratigraphic data indicate that a continuous Cretaceous/Tertiary boundary was recovered within Interval 130-803D-68R-1, 38–53 cm. The boundary lies near Section 130-803D-68R-1, 46.5 cm (Fig. 17).

Discussion

The depositional history of Site 803 began with a period of slow and discontinuous siliciclastic sedimentation, which extended from the Cretaceous into the Eocene. Since that time, Site 803 has been dominated by pelagic sedimentation, with evidence for significant variations in water-column productivity, dissolution, and/or sediment reworking. These environmental variations are recorded by changes in sediment composition, sediment grain size, and accumulation rates, and by the presence and extent of hiatuses.

Formation of the Ontong Java Plateau is interpreted to have begun during the middle Jurassic (approximately 160 Ma; Kroenke et al., 1986). Crust in the vicinity of Site 803 was probably erupted in Late Cretaceous time or earlier based on paleontological information and on an $^{40}Ar/^{39}Ar$ date (113 Ma) on a basalt sample from nearby DSDP Site 289 (see "Background and Objectives" section, this chapter). Initial sedimentation at Site 803 was dominated by siliciclastic rocks, as observed in lithologic Unit III. The presence of radiolarians, the extent and nature of bioturbation, and the preservation of laminated intervals in Unit III all indicate that it was deposited under marine conditions.

Stratigraphic control within Unit III is limited at present, but the available data indicate that Unit III ranges from early Late
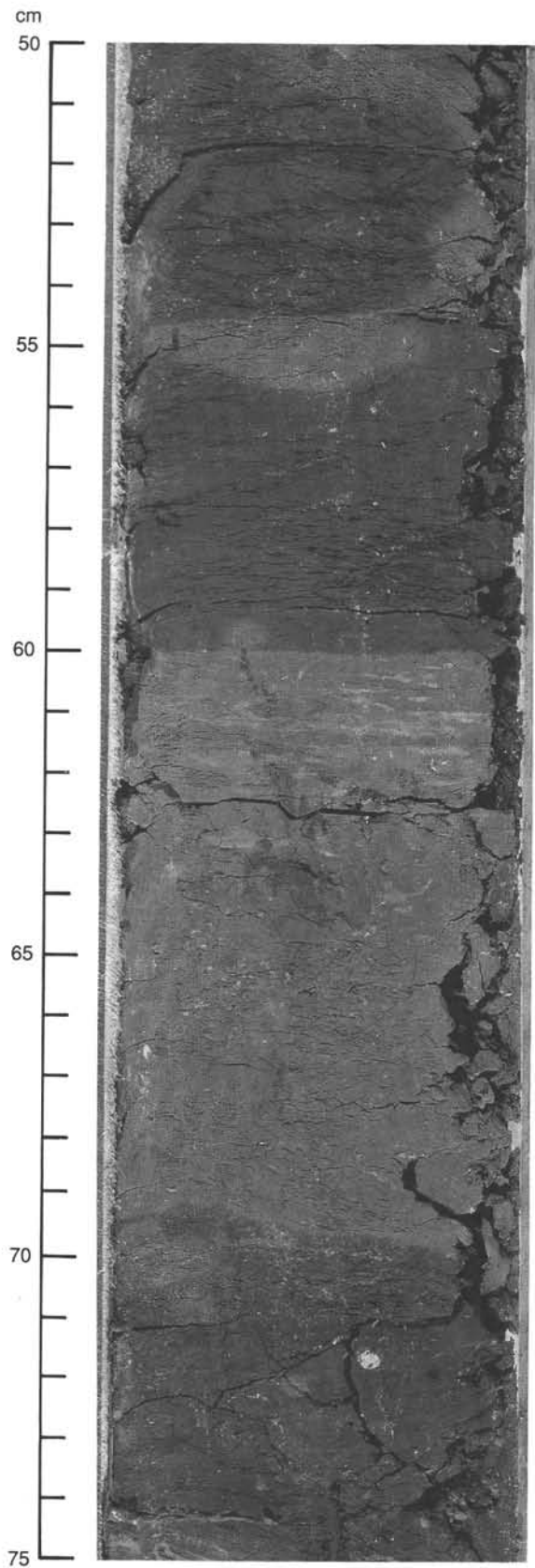
Figure 14. Photograph of sharp color contacts in Unit III (Section 130-803D-68R-1, 50–75 cm).
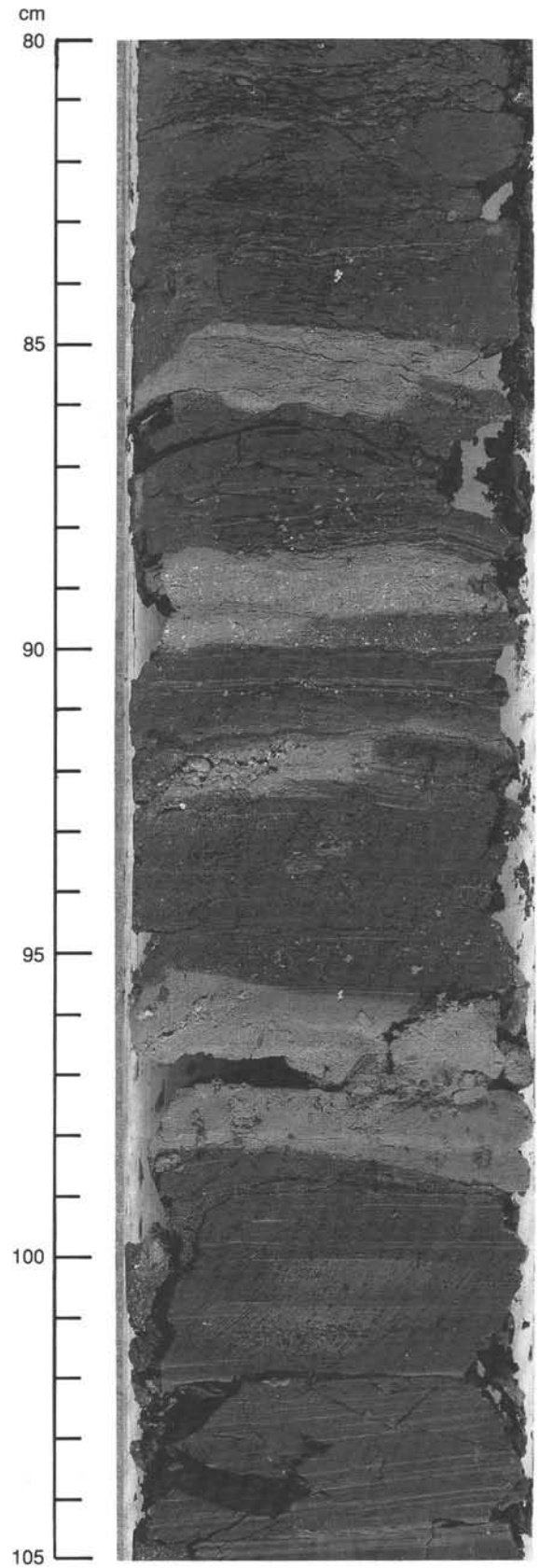

Figure 15. Photograph of bioturbated and laminated intervals in Unit III (Section 130-803D-68R-3, 80–105 cm). The contacts between the bioturbated and laminated intervals are sharp.
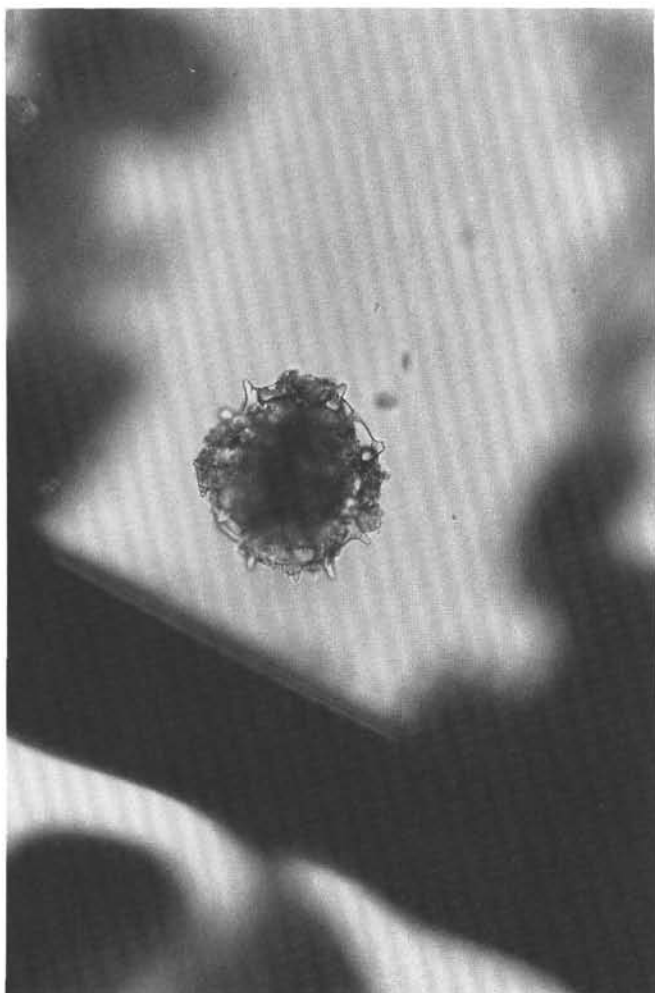
Figure 16. Photomicrograph of radiolarian from Unit III; note the extent of recrystallization exhibited. Field of view is approximately 0.5 mm wide.
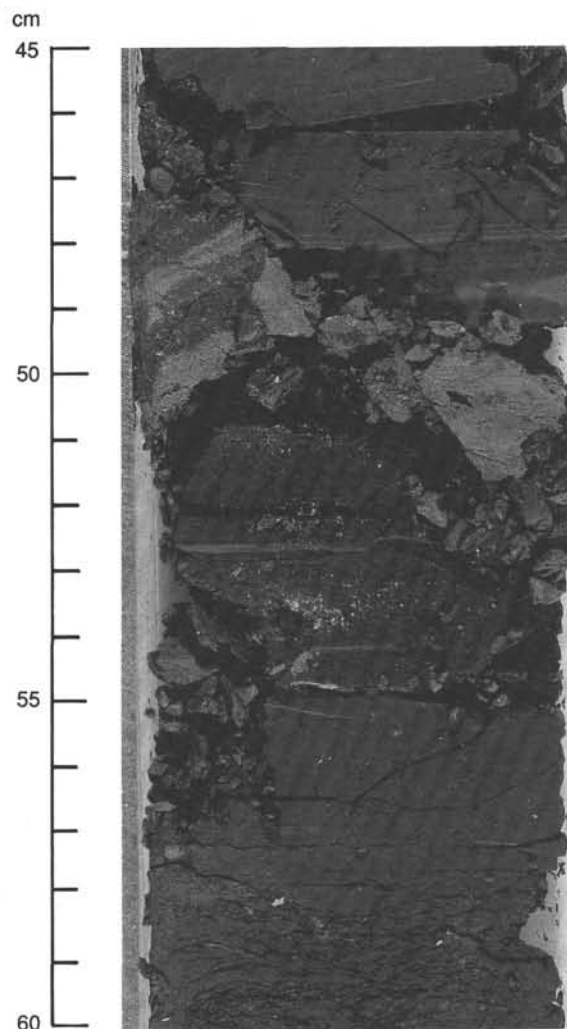

Figure 17. Photograph of interval in Unit III that contains the Cretaceous/Tertiary boundary (Section 130-803D-68R-1, 45–60 cm). Shipboard biostratigraphic analysis places the boundary at Section 130-803D-68R-1, 46.5 cm.

Cretaceous to middle Eocene in age. As Unit III is only 4.5 m thick, extremely slow sedimentation rates and/or major hiatuses clearly are indicated. The absence of metalliferous sediments directly overlying basalt suggests a hiatus of unknown origin and duration. Shipboard biostratigraphic studies have identified a hiatus that encompasses most of the Paleocene and part of the Eocene, which is located near the top of Unit III (see "Biostratigraphy" section, this chapter). Additional unconformities may be located at the sharp color contacts described previously.

The siliciclastic component in Unit III includes a significant number of silica-rich grains, with characteristics similar to chert. The largest of these grains are sand-sized and spherical and appear to be altered radiolarians (Fig. 16). The presence of the silica-rich grains indicates that at least a portion of the siliciclastic component was derived from a chert source, although the location of such a source (autochthonous vs. allochthonous) is unknown. Biogenic carbonate is rare to absent in Unit III, indicating deposition near or below the carbonate compensation depth (CCD). The removal of carbonate by dissolution probably was one important mechanism in maintaining the low sedimentation rates in Unit III. Additional periods of erosion and/or nondeposition within Unit III also are evident, although the reasons for such hiatuses are unknown at this time.

Conditions favorable for the deposition of biogenic pelagic sediments were initiated by Eocene time, as recorded in the mixed biosiliceous-calcareous sediments of lithologic Unit II. The increased carbonate content of Unit II indicates deposition above the CCD, at least episodically throughout the Eocene. Radiolarians are common to abundant throughout Unit II and are present at the base of Unit I, indicating conditions favorable for the supply and preservation of silica. Similar conditions were found for Eocene sediments at Site 289 and were interpreted as a signal of enhanced productivity (Andrews, Packham, et al., 1975). The Eocene record at Site 289 also was interrupted by several intervals of erosion and/or nondeposition.

Pelagic carbonate deposition has dominated Site 803 from the late Eocene to the Quaternary. Deposition in the Oligocene appears to have been rather continuous and little affected by major changes in carbonate preservation or removal. A major episode of dissolution/erosion produced a hiatus in the early to middle Miocene (15–21 Ma; see "Biostratigraphy" section, this chapter). This hiatus can be correlated with extensive unconformities in other areas (Keller and Barron, 1983). Such exten-

sive gaps in the marine record presumably reflect climatic and/or tectonic events that caused major changes in oceanic circulation and chemistry. Conditions favoring pelagic sedimentation were reestablished by middle Miocene time and have generally been maintained since then.

Microfaulted, dipping, and contorted color bands were observed in Subunit IA, and these disturbed intervals were often overlain by beds of homogeneous nannofossil ooze enriched in foraminifers. These features may record sediment mass movements of various types, including slumps and debris flows. Mass wasting processes have previously been reported from the flanks of the Ontong Java Plateau (Berger and Johnson, 1976; Berger et al., 1977), and seismic reflection profiles provide abundant evidence for sediment faulting and slumping near Site 803 (see "Seismic Stratigraphy" section, this chapter). Berger and Johnson (1976) suggest that sediment failure may be produced by undercutting of downslope support by dissolution, by seismic activity, or by both.

Deposition at Site 289 was interpreted to be continuous from the Oligocene to the Quaternary, based on both nannofossil and foraminifer zonations (Andrews, Packham, et al., 1975). Foraminifers were reported as abundant throughout this interval. In contrast, the equivalent record at Site 803 is interrupted by a major unconformity, and foraminifers are rare, except in lowermost Oligocene, upper Miocene, and upper Pliocene/Pleistocene sediments. In detail, foraminifers become more abundant moving upcore through the upper Pliocene-to-Pleistocene section at Site 803. These data suggest differences in the histories of productivity, preservation, and/or winnowing at Sites 289 and 803, resulting, at least in part, from the deeper location of Site 803. Subtle variations of productivity/preservation conditions at Site 803 also may be recorded by the color banding common in Unit I. The origin of this color banding is not known, but a working hypothesis focuses on diagenetic enhancement of subtle primary compositional differences (especially organic carbon content) by preferential redox reactions of iron and manganese. Shore-based studies will examine the nature and origin of these variations, to help interpret the chemical and physical history of sedimentation on the Ontong Java Plateau from the Oligocene to the Pleistocene.

BIOSTRATIGRAPHY

Introduction

The sediments recovered at Site 803 yielded a continuous stratigraphic record from the present back to the middle Eocene (0–46 Ma), with the exception of one distinct hiatus across the middle/lower Miocene boundary (approximately 15.5–21.3 Ma). These Holocene to Eocene sediments are chiefly of biogenic origin. The five major microfossil groups that make up the bulk of the material (calcareous nannofossils, planktonic and benthic foraminifers, diatoms, and radiolarians) occur in varying proportions and show variable states of preservation.

In contrast to the upper section of the drilled sequence, hiatuses of substantial duration characterize the lowermost part of the sediment section, as follows:

1. The Paleocene/Eocene boundary, the entire lower Eocene, and the lower half of the middle Eocene are missing. The middle Eocene is underlain by a mere 1-cm-thick sediment layer of late Paleocene age (about 58 Ma). This hiatus is estimated to span over some 12 m.y.

2. Almost all of the Paleocene is missing. The uppermost Paleocene is underlain by basal Paleocene sediments that presumably were deposited shortly (probably <0.5 m.y) after the Cretaceous/Tertiary boundary, implying a Paleocene hiatus representing about 8 m.y.

3. The Cretaceous is poorly represented. Less than 5 m of condensed(?) and virtually carbonate-free sediments rest on the volcanic basement. Occurrences of radiolarians in a few discrete layers in these deep-sea clays suggest an early Cenomanian age within a meter of the basement. These few meters of nearly nonfossiliferous sediments thus represent a time interval spanning at least 30 m.y. (approximately 67–97 Ma); presumably several substantial hiatuses are present.

Considering the fact that the time interval from 45 Ma to roughly 100 Ma is represented by <5 m of sediment, it appears all the more remarkable that the Cretaceous/Tertiary (K/T) boundary is preserved intact in this section.

Detailed information on biostratigraphic assignments, abundance, and preservation of the different microfossil groups is presented below. A generalized picture of the biostratigraphy is shown in Figure 18.

Calcareous Nannofossils

Hole 803A

Pleistocene

Pelagic oozes in Hole 803A contain well to moderately preserved, diverse assemblages of nannofossils. The youngest assemblage observed from this hole belongs to Zone NN20 and is present in Sample 130-803A-1H-3, 0–1 cm, in which *Gephyrocapsa caribbeanica* and *Gephyrocapsa oceanica* occur together with abundant small *Gephyrocapsa*. Rare *Helicosphaera inversa* is also found in this sample. A single reworked specimen of the Cretaceous species *Watznaueria barnesae* was recognized. Samples 130-803A-1H-CC and -2H-CC are assigned to Zone NN19 based on the presence of abundant *Pseudoemiliania lacunosa*, common to abundant Pleistocene gephyrocapsids, and the absence of the Pliocene discoasters. Both *Helicosphaera sellii* and *Calcidiscus macintyrei* are present in Sample 130-803A-2H-CC, placing this sample in the very basal Pleistocene or the very topmost Pliocene.

Pliocene

Sample 130-803A-3H-CC contains *Discoaster brouweri* and is assigned to Zone NN18. The Pliocene/Pleistocene boundary falls approximately midway between the successive last occurrences (LOs) of *D. brouweri* and *C. macintyrei* and lies, therefore, between Samples 130-803A-2H-CC and -3H-CC. The former sample also contains the uppermost observed presence of *Coccolithus pelagicus*, which is a typical cool-water species in the present oceans. Specimens of the genus *Gephyrocapsa* were not observed in or below Sample 130-803A-3H-CC. *Discoaster pentaradiatus*, the LO of which defines the NN17/NN18 zonal boundary, occurs in and below Sample 130-803A-4H-CC, placing this sample in Zone NN17. A single specimen of *Discoaster surculus* was recognized, which was considered reworked. Sample 130-803A-5H-CC contains comparatively diversified discoasters such as *D. asymmetricus, D. brouweri, D. challengeri, D. pentaradiatus, D. surculus, D. tamalis, D. triradiatus,* and *D. variabilis.* This sample was assigned to Zone NN16. We recognized a few sphenoliths; therefore, this sample was placed in the lowermost part of Zone NN16 (between the LOs of *Sphenolithus* spp. and *Reticulofenestra pseudoumbilica*).

The first downhole observation of common *Reticulofenestra pseudoumbilica* was made in Sample 130-803A-6H-1, 75 cm, marking the top of lower Pliocene Zone NN15. The bottom of Hole 803A contains a typical lower Pliocene assemblage, with abundant placoliths (*Calcidiscus leptoporus, R. pseudoumbilica,* small morphotypes of *Reticulofenestra*) and sphenoliths, and a varied asterolith association. *Discoaster asymmetricus*
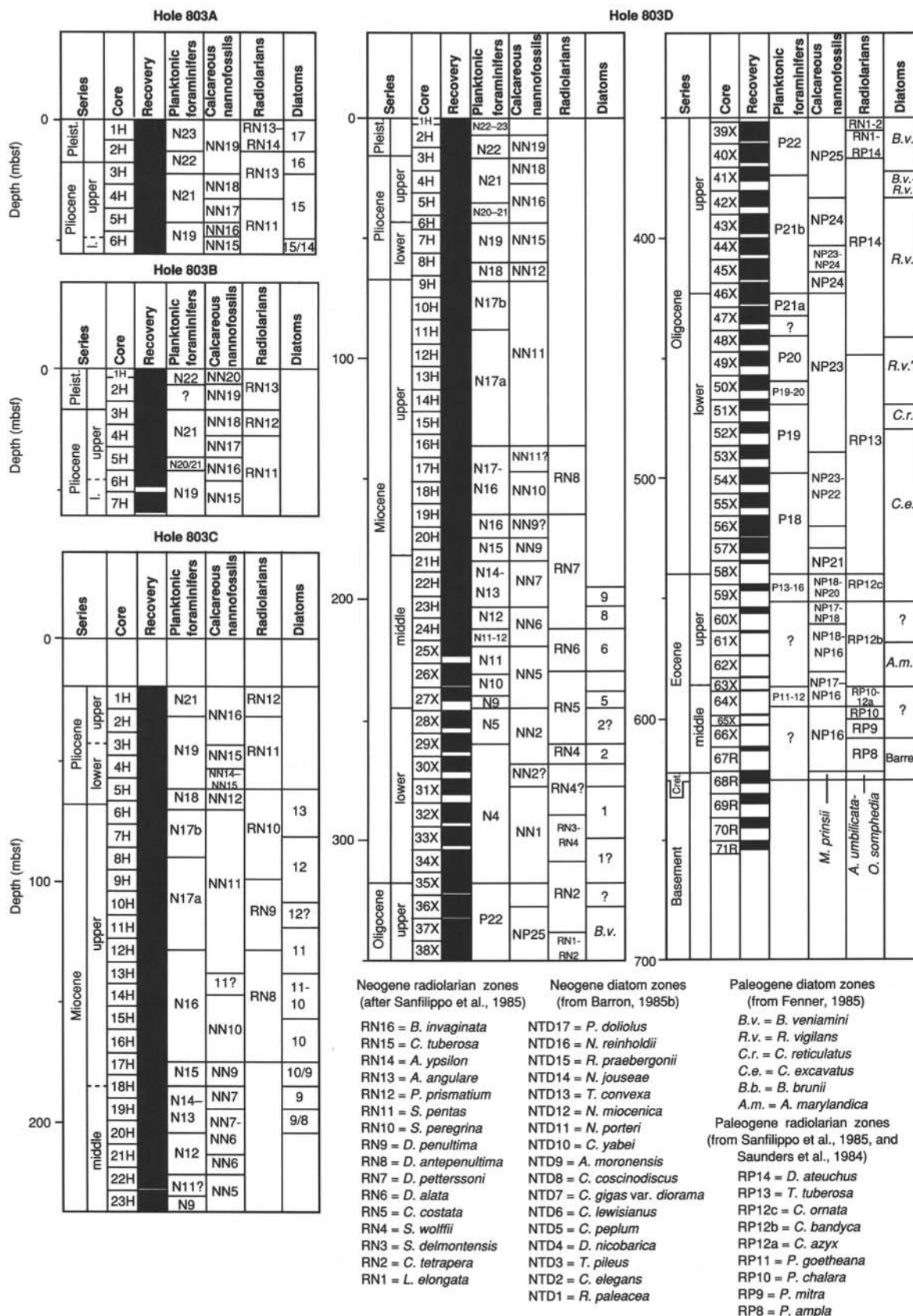
Figure 18. Biostratigraphic hole summaries, Site 803. RN = radiolarian Neogene zone, NTD = Neogene tropical diatom zone, RP = radiolarian Paleogene zone, and NN = nannofossil Neogene zone.

Neogene radiolarian zones (after Sanfilippo et al., 1985)

RN16 = B. invaginata
RN15 = C. tuberosa
RN14 = A. ypsilon
RN13 = A. angulare
RN12 = P. prismatium
RN11 = S. pentas
RN10 = S. peregrina
RN9 = D. penultima
RN8 = D. antepenultima
RN7 = D. petterssoni
RN6 = D. alata
RN5 = C. costata
RN4 = S. wolffii
RN3 = S. delmontensis
RN2 = C. tetrapera
RN1 = L. elongata

Neogene diatom zones (from Barron, 1985b)

NTD17 = P. doliolus
NTD16 = N. reinholdii
NTD15 = R. praebergonii
NTD14 = N. jouseae
NTD13 = T. convexa
NTD12 = N. miocenica
NTD11 = N. porteri
NTD10 = C. yabei
NTD9 = A. moronensis
NTD8 = C. coscinodiscus
NTD7 = C. gigas var. diorama
NTD6 = C. lewisianus
NTD5 = C. peplum
NTD4 = D. nicobarica
NTD3 = T. pileus
NTD2 = C. elegans
NTD1 = R. paleacea

Paleogene diatom zones (from Fenner, 1985)

B.v. = B. veniamini
R.v. = R. vigilans
C.r. = C. reticulatus
C.e. = C. excavatus
B.b. = B. brunii
A.m. = A. marylandica

Paleogene radiolarian zones (from Sanfilippo et al., 1985, and Saunders et al., 1984)

RP14 = D. ateuchus
RP13 = T. tuberosa
RP12c = C. ornata
RP12b = C. bandyca
RP12a = C. azyx
RP11 = P. goetheana
RP10 = P. chalara
RP9 = P. mitra
RP8 = P. ampla

and *Ceratolithus rugosus* are present, but *Amaurolithus* spp. were not observed. Core 130-803A-6H, hence, can be referred to the NN15–NN13 zonal interval.

Hole 803B

Pleistocene

An upper Pleistocene assemblage with abundant gephyrocapsids characterizes Sample 130-803B-1H-CC. The absence of both *Emiliania huxleyi* and *Pseudoemiliania lacunosa* places this sample in Zone NN20. *Helicosphaera inversa* also occurs in this sample. The LO of *P. lacunosa* was observed between Samples 130-803B-1H-CC and -2H-1, 70 cm. Sample 130-803B-2H-CC contains some specimens of *Gephyrocapsa* that have distal shield sizes in excess of 6 μm; this sample is accordingly referred to the interval between the LOs of large *Gephyrocapsa* and *Helicosphaera sellii*. *Calcidiscus macintyrei* disappears between Samples 130-830B-3H-2, 10 cm, and -3H-2, 145 cm, placing the latter layer in the basal Pleistocene.

Pliocene

The last appearances of *Discoaster brouweri* and *Discoaster triradiatus* were observed between the 10- and 82-cm levels in Section 130-803B-3H-4. As the Pliocene/Pleistocene boundary roughly falls midway between the successive LOs of *D. brouweri* and *C. macintyrei*, this boundary is placed in Section 130-803B-3H-3, which agrees with magnetostratigraphic information obtained from this hole (with the termination of the Olduvai Subchron at 130-803B-3H-3, 10 cm; see "Paleomagnetics" section, this chapter). *Coccolithus pelagicus* was observed only below the Pliocene/Pleistocene boundary, in agreement with the observation from Hole 803A.

The LO of *Discoaster pentaradiatus* was observed between Samples 130-803B-4H-2, 103 cm, and -4H-3, 5 cm. Rare *Discoaster surculus* and *Discoaster tamalis* in Sample 130-803B-4H-CC, therefore, indicate a position well within the upper Pliocene Zone NN16. Sample 130-803B-5H-CC is also assigned to Zone NN16, but it belongs to the lower half of that zone because of the presence of *Discoaster variabilis*. Indeed, rare sphenoliths in Sample 130-803B-5H-CC suggest a position at basal Zone NN16.

Sample 130-803B-6H-CC contains common *Reticulofenestra pseudoumbilica*, abundant sphenoliths, and few *Ceratolithus rugosus*, indicating a position somewhere between the top of Zone NN15 and the bottom of Zone NN13. Further subdivision in that interval was not possible because of the absence of critical marker species (i.e., *Discoaster asymmetricus* and *Amaurolithus* spp.). Sample 130-803B-7H-CC, at the bottom of this hole, is assigned to Zone NN12 because of the presence of *Ceratolithus acutus* in an otherwise typical lower Pliocene low-latitude assemblage, with abundant sphenoliths and small placoliths (particularly *Reticulofenestra* <5 μm and *Dictyococcites productus*). Both *Ceratolithus rugosus* and *Discoaster quinqueramus* are absent in Sample 130-803B-7H-CC. The absence of *Reticulofenestra pseudoumbilica*, however, must be a result of ecological exclusion, and these unfavorable conditions must have ended during Zone NN13 time (see Hole 803A).

Hole 803C

Pliocene

Hole 803C was washed down to 19 mbsf, but from there on it shows an apparently continuous upper Pliocene through middle Miocene sequence. The occurrences of *Discoaster pentaradiatus* together with *D. surculus* indicate Zone NN16 for Samples 130-803C-1H-CC and -2H-CC. The latter sample contains rare *Discoaster tamalis*. The occurrences of *Reticulofenestra pseudoum-*

bilica and *Sphenolithus abies* in Sample 130-803C-3H-CC shows that this sample belongs to Zone NN15. Sample 130-803C-4H-CC contains *Amaurolithus tricorniculatus* and *Discoaster asymmetricus* and is accordingly assigned to Zone NN14. The absence of *Discoaster asymmetricus* and *Ceratolithus rugosus* and the presence of *Ceratolithus acutus* in Sample 130-803C-5H-CC places this sample in Zone NN12.

Miocene

Section 130-803C-6H-2 contains the LO of *Triquetrorhabdulus rugosus* and the first occurrence (FO) of *Ceratolithus acutus*, whereas the LO of *Discoaster quinqueramus* was observed in Section 130-803C-6H-4. This latter section, therefore, is assigned to Zone NN11, and the top of this zone approximately indicates the position of the Miocene/Pliocene boundary. The characteristic central knob in *Discoaster quinqueramus* is not so well developed in the oldest and youngest associations of this species, often making precise determinations of its entry and exit levels difficult. Sample 130-803C-6H-CC contains abundant specimens of *Coccolithus pelagicus* relative to other samples from Hole 803C.

Amaurolithus spp. are consistently rare in the lower Pliocene and upper Miocene sediments, and primary morphological characters are typically masked by substantial calcite overgrowth. Representatives of this group could be followed down to Sample 130-803C-11H, 5 cm, but not deeper; the deepest species observed is *Amaurolithus tricorniculatus*.

The LO of *Discoaster neohamatus* was observed in Section 130-803C-11H-6, and shorter rayed variants of *Discoaster quinqueramus* (*Discoaster berggrenii*) become progressively more common below that section. It was difficult to determine the NN10/NN11 zonal boundary precisely; well-developed *Discoaster quinqueramus* and *Discoaster berggrenii* were observed in Sample 130-803C-12H-CC, whereas intermediate morphotypes between these two knob-possessing species and their knob-lacking ancestor species *Discoaster bellus* occur abundantly in Sample 130-803C-13H-CC. Sample 130-803C-14H-CC clearly belongs to Zone NN10 because the above-mentioned five-rayed, knob-possessing morphotypes as well as *Discoaster hamatus* are absent. Therefore, the uncertainty in placing the NN10/NN11 zonal boundary encompasses the length of two full cores.

The NN9/NN10 zonal boundary (LO of *Discoaster hamatus*) occurs in Section 130-803C-17H-2. The nominate species is rare in the uppermost 3–4 m of its range, and some samples contain triradiate morphovariants of the five-rayed *Discoaster hamatus*. A shift in dominance between *Discoaster hamatus* and the six-rayed *Discoaster neohamatus*, an event that probably is biochronologically useful once properly evaluated, occurs in the upper part of Section 130-803C-17H-4. *Catinaster calyculus* disappears between Samples 130-803C-17H-4, 100 cm, and -17H-4, 150 cm, whereas the FO of *Discoaster neohamatus* occurs between Samples 130-803C-17H-5, 125 cm, and -17H-6, 75 cm.

Discoaster hamatus has its FO (defining the NN8/NN9 boundary) in Section 130-803C-18H-5. Overgrown specimens of *Catinaster coalitus* were observed in rare numbers throughout Section 130-803C-18H-6, and the NN7/NN8 zonal boundary is placed between that sample and Sample 130-803C-18H-CC. The middle/upper Miocene boundary is defined as falling within Zone NN8 and thus can be placed in the lower part of Core 130-803C-18H.

The middle Miocene assemblages contain abundant *Dictyococcites perplexus* and small reticulofenestrids. The *Triquetrorhabdulus* assemblage increases in diversity and the distinct, large *Coccolithus miopelagicus* has its LO in Sample 130-803C-18H-CC. Calcite overgrowth on discoasters prevents accurate identification of *Discoaster kugleri*, the FO of which defines the

NN6/NN7 boundary. The successive LOs of *Coronocyclus nitescens* and *Cyclicargolithus floridanus* can be used to subdivide the NN6–NN7 zonal interval. Neither of these events falls chronologically near the NN6/NN7 boundary, although the former species event is closer (0.6 m.y. older than the NN6/NN7 boundary estimate).

The LOs of *Cyclicargolithus floridanus* and *Sphenolithus heteromorphus* were both observed between Samples 130-803C-22H-3, 15 cm, and -22H-3, 50 cm. The latter species event defines the NN5/NN6 zonal boundary. Large-sized (>7 μm) *Reticulofenestra pseudoumbilica* appear within upper Zone NN5. This event was observed in Core 130-803C-22H. Sample 130-803C-23H-CC, which ends Hole 803C, still is within Zone NN5 because the ratio of the *Discoaster deflandrei* group/total number of discoasters is <30% (see Rio et al., 1990).

Hole 803D

Middle and Lower Miocene

Only core-catcher samples were investigated in the upper 24 cores of Hole 803D (i.e., in the Pleistocene to middle Miocene interval). The results from these core catchers are similar to the results obtained from Holes 803A through 803C, results that are summarized in Figure 18.

The NN5/NN6 boundary falls in Section 130-803D-25X-2, and a stable Zone NN5 assemblage is maintained throughout Sample 130-803D-27X-CC. This assemblage is composed mainly of abundant *Cyclicargolithus floridanus* and reticulofenestrids, common *Sphenolithus heteromorphus*, *Sphenolithus moriformis*, and *Coccolithus pelagicus*, few to rare discoasters, *Coccolithus miopelagicus*, *Coronocyclus nitescens*, *Helicosphaera granulata*, and *Triquetrorhabdulus rugosus*. The ratio of the *Discoaster deflandrei* group/total number of discoasters is <30% in Sample 130-803D-27X-CC, suggesting placement within Zone NN5 (i.e., younger than about 16 Ma) for this sample (see Rio et al., 1990).

A major change in taxonomic composition that is of biostratigraphic importance occurs between Samples 130-803D-27X-CC and -28X-1, 140 cm. The middle Miocene NN5 assemblage of the former sample is replaced by a typical early Miocene assemblage belonging to the NN2 *Discoaster druggii* Zone in the latter sample. The biostratigraphically most critical components in the older Zone NN2 assemblage include *Sphenolithus belemnos*, *Discoaster druggii*, and *Triquetrorhabdulus carinatus*. The co-occurrences of these taxa indicate an age ranging between 19.5 and 20.0 Ma for upper Core 130-803D-28X, and the presence of a hiatus between the bottom of Core 130-803D-27X and the top of Core 130-803D-28X. This hiatus, therefore, has a minimum duration of approximately 3.4 m.y.

Sphenolithus belemnos has its FO in the core break separating Core 130-803D-28X from the next underlying core. A prominent feature of the lower Miocene is that this part of the stratigraphic column still provides, at least in terms of nannofossil biostratigraphy, few reliable species events. The NN1/NN2 zonal boundary is difficult to recognize because of inconsistent occurrences and poor preservation (severe overgrowth disguising primary characters) of *Discoaster druggii*. Nonetheless, some potentially useful biostratigraphic events were observed: in Core 130-803D-29X, the LO of *Ericsonia obruta;* in Section 130-803D-31X-1, the LO of large-sized (>11 μm) *Cyclicargolithus* spp.; and in Core 130-803D-34X, the LO of abundant to dominant *Triquetrorhabdulus carinatus*. None of these events are directly correlated to magnetostratigraphy.

Oligocene

The distinct acme interval of *Sphenolithus delphix*, lasting from shortly above the LO of *Sphenolithus ciperoensis* to the Oligocene/Miocene boundary in the equatorial Indian Ocean (Rio et al., 1990) was not observed. Neither *Helicosphaera recta* (which defines the NP25/NN1 boundary) nor *Dictyococcites bisectus* was observed in the Miocene to Oligocene transitional interval, implying that the next deeper tie point was provided by the LO of *Sphenolithus ciperoensis* at the core break separating the bottom of Core 130-803D-39X from the top of Core 130-803D-40X.

Sphenolith species events that are critical for several Oligocene zonal boundary definitions were generally rare in Hole 803D. *Sphenolithus distentus* was observed (looking downhole) from Core 130-803D-42X, thus indicating Zone NP24. Sample 130-803D-45X-CC was also assigned to Zone NP24 because of the presence of rare *Sphenolithus ciperoensis*.

The sequence ranging from Samples 130-803D-46X-CC to -52X-CC is characterized by the absence of *Sphenolithus ciperoensis* and *Reticulofenestra umbilica*, and this section belongs to Zone NP23. *Sphenolithus pseudoradians* was observed in Sample 130-803D-48X-CC. Samples 130-803D-53X-CC through -55X-CC contain forms similar to *Reticulofenestra hillae;* therefore, these samples tentatively were placed in the NP23/NP22 zonal interval. Sample 130-803D-56X-CC contains *Ericsonia formosa* together with the first downhole occurrence of typical, large *Reticulofenestra hillae*. Thus, this sample is assigned to Zone NP21; typical *Reticulofenestra umbilica*, however, was not observed in Sample 130-803D-56X-CC. Sample 130-803D-58X-CC still belongs to Oligocene Zone NP21, with common *Bramlettius serraculoides*, *Dictyococcites bisectus/Dictyococcites hesslandii*, *Ericsonia formosa*, *Reticulofenestra umbilica*, *Reticulofenestra hillae*, and abundant *Cyclicargolithus floridanus*.

Eocene

The bottom of Core 130-803D-59X contains an upper Eocene assemblage, with *Discoaster saipanensis*, *Discoaster barbadiensis*, and *Cribrocentrum reticulatum*. Of these, only *Discoaster saipanensis* remains present at the top of this core, suggesting that the sample is located shortly below the Eocene/Oligocene boundary.

Preservation becomes progressively poorer (both dissolution and overgrowth) downhole throughout the Eocene sequence, and placolith fragments are common. Martini's (1971) zonal scheme does not work well in open-ocean, low-latitude sediments in the upper half of the Eocene. The composition of the Eocene assemblages, however, is generally stable in Hole 803D. *Calcidiscus protoannulus* has its LO in Core 130-803D-62X and *Chiasmolithus grandis* has its LO in the next deeper core. The latter event marks the middle/upper Eocene boundary. The *Dictyococcites bisectus/Dictyococcites hesslandii* complex has been a common to abundant member of the lower Oligocene and Eocene assemblages; the FO of this taxonomic category was observed in Core 130-803D-65X. The FO of *Reticulofenestra umbilica* (>14 μm) falls in the core break below Core 130-803D-66X. Core 130-803D-67X, however, contains well-developed, large *Coccolithus eopelagicus* and/or *Chiasmolithus gigas*. Rare occurrences, in combination with preservation problems, prevented identification of the central area structure of these similarly constructed morphotypes, and hence they could not be distinguished. If specimens of *Nannotetrina* spp. were present, they could not be recognized, even at the generic level, because of severe calcite overgrowth. Nevertheless, it is important to note that Sample 130-803D-67X-CC belongs to the middle Eocene interval between the FOs of *Chiasmolithus gigas* and *Reticulofenestra umbilica*.

Paleocene

Sample 130-803D-68R-1, at 0.1 and 0.9 cm, contains an assemblage characteristic of the uppermost Paleocene that in-

cludes common *Discoaster multiradiatus,* few *Discoaster nobilis,* abundant *Fasciculithus tympaniformis* (and other late Paleocene fasciculith morphotypes), and rare *Ellipsolithus macellus.* These samples are assigned to Zone NN9. The next sample from only 1 cm further downcore is barren except for a single, poorly preserved specimen that probably belongs to the Cretaceous genus *Micula.* See the "Lithostratigraphy" section of this chapter for a description of the major change in sediment lithology occurring between Cores 130-803D-67R and -68R.

Cretaceous/Tertiary Boundary

The sediments in Hole 803D are barren of calcareous nannofossils below Sample 130-803D-68R-1, 73 cm. From this sample and upward to Sample 130-803D-68R-1, 3 cm, the poorly preserved and low-diversity assemblages (presumably preservational artifact) are predominantly of uppermost Cretaceous origin. About 40 smear slides were examined from this interval to obtain adequate representation of the different sediment types. The stratigraphic distribution of selected species in this upper part of Section 130-803D-68R-1 is illustrated in Table 4.

The dissolution-resistant genus *Micula* is a major component throughout the pertinent interval, with the consistent presence of *Micula prinsii.* This conspicuous species has its FO shortly before the K/T boundary and disappears together with other Cretaceous taxa at the boundary. At Shatsky Rise Site 577, the FO of *Micula prinsii* can be calculated to 65.5–66.6 Ma, combining data from Monechi (1985) and Bleil (1985). This evolutionary event consequently occurred only shortly before the K/T boundary (66.4 Ma; Berggren et al., 1985a) in the western Pacific Ocean.

Monechi (1985) used the FO and subsequent rapid increase in abundance of the calcareous dinoflagellate *Thoracosphaera* spp. for recognition of the K/T boundary, an event that coincides precisely with the iridium spike at DSDP Site 577 (Wright

et al., 1985). Monechi's criterion for recognition of the K/T boundary is adopted here, partly because *Thoracosphaera* (fragments, mostly) is one of the few taxonomic categories that is preserved in the strongly dissolved sediments encountered in Section 130-803D-68R-1.

Pure upper Maestrichtian assemblages (with *Micula prinsii*) were observed between in Sample 130-803D-68R-1, between 53 and 73 cm. Fragments of *Thoracosphaera* spp. appear in Sample 130-803D-68R-1, 46.5 cm, become abundant in the next higher Sample 130-803D-68R-1, 38 cm, and remain abundant above that sample (Table 4). *Markalius astroporus* is present in Sample 130-803D-68R-1, 29.5 cm. This sample also contains another basal Danian marker, namely *Biantholithus sparsus.* The FO of the former species was observed about 20 cm above the K/T boundary at Site 577 (Monechi, 1985).

If using the data and definitions described above, the conclusion is reached that the K/T boundary is preserved intact in Sample 130-803D-68R-1, between 38 and 53 cm, and that this boundary lies near Sample 130-803D-68R-1, 46.5 cm. It follows that the Cretaceous calcareous nannofossils occurring above the boundary must be considered to be reworked.

Planktonic Foraminifers

The discussion of planktonic foraminifers that follows is a composite summary of the zones recognized at Site 803 and their diagnostic taxa. Problems regarding dissolution and missing marker species also are discussed. Figure 18 summarizes the planktonic foraminifer zonation of the four holes drilled at Site 803 and their correlation with those of the calcareous nannofossils, diatoms, and radiolarians. Hole 803D represents the complete sequence drilled at this site; therefore, it is used as the reference hole.

We found that planktonic foraminifers were abundant from the surface to well within middle Miocene Zone N10 (Sections

Table 4. Range chart of calcareous nannofossil species across the Cretaceous/Tertiary boundary interval (Section 130-803D-68R-1).

Species	0.1	0.9	5	10	15	25	26	30	38	47	53	59	60	61	63	68	73
upper Paleocene:																	
C. pelagicus	X	X								K/T							
D. mohleri	X	X								L							
D. multiradiatus	X	X								A							
D. nobilis	X	X								Y							
E. macellus	X	X								E							
F. tympaniformis	X	X								R							
S. primus	X	X															
lower Paleocene:																	
B. sparsus								X									
Thoracosphaera			X	X	X	X	X	X	X	X							
M. astroporus								X									
Cretaceous:																	
A. cymbiformis											X	X		X			
C. aculeus					X					X		X			X		X
C. ehrenbergii					X							X					
C. margerelii										X					X	X	X
L. quadratus				X	X												
Micrantholithus			X		X												
M. decussata			X	X	X	X			X			X	X	X	X	X	X
M. murus			X	X	X	X		X		X	X	X	X	X	X	X	X
M. prinsii					X					X	X	X	X	X	X	X	X
P. cretacea										X		X	X				
Q. trifidium		X															
W. barnesae	X	X	X	X	X	X	X	X	X	X	X	X	X	X	X	X	X

Note: The importance of the thoracosphaerids for recognition of the boundary is discussed in the text.

130-803D-1H-CC to -25X-CC). The sediments become distinctly more chalky from Sections 130-803D-25X-CC to -26X-CC (about 230 mbsf). Preservation in this upper part of the section at Site 803 ranges from moderate to good. Selective dissolution of planktonic foraminifer tests is responsible for the absence of some taxa, including several marker species, and for the breakage of tests. Estimates of foraminifer fragmentation range between 20% and 50% for this interval. Although *Globigerinoides sacculifer* is one of the most abundant species, its test often appears thin and fragile, as do the tests of *Orbulina universa*.

Foraminifer abundance, in general, decreases from "abundant" to "few" and "common" in the lower middle Miocene through Oligocene interval (Samples 130-803D-26X-CC to -58X-CC). Preservation is generally moderate, although slightly poorer preservation is noted in the lowermost Miocene (*Globorotalia kugleri* Zone N4) through upper Oligocene (*Globigerina ciperoensis* Zone P22) interval (130-803D-32X-CC to -40X-CC). Foraminifers are very rare in the upper to middle Eocene interval (130-803D-59X-CC to -66X-CC), and the assemblages contain only solution-resistant taxa.

The Pliocene/Pleistocene boundary is difficult to locate based on the planktonic foraminifers recovered at Site 803. According to Berggren et al. (1985b), the FO of *Globorotalia truncatulinoides* is in the uppermost Pliocene and marks the boundary between Zones N21 and N22 (base of the *Globorotalia truncatulinoides* Zone). Other workers use the FO of *G. truncatulinoides* to mark the Pliocene/Pleistocene boundary (e.g., Bolli and Saunders, 1985; Kennett and Srinivasan, 1983). The LO of *Globigerinoides fistulosus* would serve as a good marker of the Pliocene/Pleistocene boundary according to Berggren et al. (1985b), but we did not record the co-occurrence of *G. truncatulinoides* and *G. fistulosus* in core-catcher samples examined from Site 803.

Globigerinoides fistulosus is a good upper Pliocene (uppermost N19 and N21) marker species at Site 803. Its presence most likely represents the lower *Globorotalia tosaensis* Zone and the upper part of the *Globorotalia miocenica* Zone (1.9–2.9 Ma according to Berggren et al., 1985b). *Globorotalia miocenica* does not occur in the Pacific (Berggren et al., 1985b), but *G. tosaensis* does occur consistently throughout much of the upper Pliocene section. The presence of *Sphaeroidinellopsis* spp. in the absence of *Globorotalia margaritae* also marks the upper Pliocene *G. miocenica* Zone (uppermost N19).

The LO of *Globorotalia margaritae* marks the top of lower Pliocene Zone N19. However, the nominate taxon was not observed in the lower part of the zone, perhaps because of dissolution effects. Other diagnostic taxa of this zone include *Sphaeroidinella dehiscens* s.l., *Sphaeroidinellopsis paenedehiscens*, *S. seminulina*, *Globoquadrina altispira*, *Globorotalia tumida*, *G. plesiotumida*, *G. menardii*, *G. multicamerata*, *Globigerinoides extremus*, *Pulleniatina primalis*, and *Globigerina venezuelana*. *Pulleniatina spectabilis* is present in the lower part of the zone. *Globigerina nepenthes* is noticeably absent or found only in very small numbers, which again is attributed to dissolution. The FO of *S. dehiscens* s.l. marks the top of Zone N18.

The Miocene/Pliocene boundary (N17/N18) is marked by the FO of *Globorotalia tumida* and the LO of *Globoquadrina dehiscens*. The upper Miocene *Neogloboquadrina dutertrei* s.l. Zone (N17) is characterized by *Globigerinoides* spp., *Neogloboquadrina acostaensis*, *Globoquadrina dehiscens*, *G. altispira*, *Sphaeroidinellopsis seminulina*, *Globorotalia plesiotumida*, *G. merotumida*, the *G. menardii* group, and *G. lenguaensis*. *Pulleniatina primalis* is present in the uppermost part of this zone and can be used to subdivide N17 (e.g., Kennett and Srinivasan, 1983).

The FO of *Globorotalia plesiotumida* marks the top of the upper Miocene *Neogloboquadrina acostaensis* Zone (N16). The

differentiation of *G. plesiotumida* and *G. merotumida* is obscured by numerous transitional forms. As a result, the position of the N16/N17 boundary is rather tenuous at Site 803. The *N. acostaensis* Zone has a similar fauna to that of the overlying *N. dutertrei* s.l. Zone. The lower upper Miocene *Globorotalia menardii* Zone (N15) is characterized by the absence of *Neogloboquadrina acostaensis* (FO at the base of Zone N16) and the absence of *Globorotalia siakensis* (LO at the top of Zone N14).

The upper middle Miocene *Globorotalia mayeri* Zone (N14) is characterized by *Globorotalia siakensis* (= *G. mayeri*), *Sphaeroidinellopsis* spp., *Globoquadrina dehiscens*, *G. altispira*, and *Neogloboquadrina continuosa*. Numerous *G. siakensis* and species of *Globigerina* replace species of *Globigerinoides* as the dominant taxa of the sediment assemblages. This may be a preservational or paleoecological signal, or a combination of both. The FO of *Globigerina nepenthes* defines the top of Zone N13, but this taxon is very rare in material from Site 803. Therefore, the recognition of the N13/N14 boundary is not certain based on shipboard results.

The *Globorotalia fohsi* lineage defines several zones within the middle Miocene (N10–N12): *G. fohsi robusta*, *G. fohsi lobata*, and *G. fohsi fohsi* are characteristic of Zone N12; *G. fohsi praefohsi* and *G. peripheroacuta* are diagnostic of Zone N11; and the presence of *G. peripheroacuta* in the absence of *G. fohsi praefohsi* distinguishes Zone N10. Other diagnostic taxa of Zones N10–N12 include *Globorotalia siakensis*, the *G. archeomenardii-praemenardii* plexus, *Globoquadrina altispira*, *G. dehiscens*, *Catapsydrax parvulus*, and *Neogloboquadrina continuosa*.

The FO of *Globorotalia peripheroacuta* and the LO of *Globigerinoides sicanus* define the top of middle Miocene *Globorotalia peripheroronda* Zone N9. However, the *Praeorbulina-Orbulina* lineage is poorly represented in the Site 803 material, probably the consequence of dissolution. As a result, it is difficult to differentiate the lowermost zones of the middle Miocene (N8 and N9).

A significant stratigraphic break between Sections 130-803D-27X-CC and -28X-CC separates sediments of lower middle Miocene Zone N9 from sediments of the lower Miocene *Catapsydrax dissimilis* Zone (N5). The lower part of Zone N5 is indicated by the presence of *Globoquadrina binaiensis*. Therefore, sediment, representing approximately 4–6 m.y. of time, is missing in the disconformity. The diagnostic taxa of Zone N5 include *Catapsydrax dissimilis*, *C. stainforthi*, *Globoquadrina binaiensis*, *G. dehiscens*, *Globorotalia siakensis*, and *Globigerinoides primordius*. *Globorotalia kugleri* Zone N4 is characterized by *G. kugleri* s.s., *G. siakensis*, *Catapsydrax dissimilis*, *Globoquadrina dehiscens*, *G. binaiensis*, and *Globigerina sellii*. *Globorotalia peripheroronda* is present in the upper part of the zone.

The Oligocene/Miocene boundary (P22/N4) is based on the FO of *Globorotalia kugleri* s.s. (see "Explanatory Notes" chapter, this volume). Upper Oligocene *Globigerina ciperoensis* Zone P22 is distinguished by the absence of both *G. kugleri* s.s. and *Globorotalia opima opima* in the Site 803 material. The nominate taxon, as well as *Globigerina angulisuturalis* and *Globigerinoides primordius*, are absent, probably a result of selective dissolution. Species present include *Globorotalia opima nana*, *Catapsydrax dissimilis*, *C. unicavus*, and *Globigerina venezuelana*. *Globorotalia kugleri* s.l. and *G. siakensis* are present in the upper part of the zone.

The LO of *Globorotalia opima opima* defines the top of the mid-Oligocene *G. opima opima* Zone (P21). The assemblage is very similar to that of the overlying *Globigerina ciperoensis* Zone. Furthermore, *G. opima opima* is present consistently throughout the zone. Subzones P21a and P21b could not be differentiated during shipboard work because of the absence of

Chiloguembelina cubensis, the LO of which would normally be used to recognize the top of Subzone P21a (lower Oligocene/ upper Oligocene boundary). Its absence is probably related to selective dissolution. The FO of *Globigerina angulisuturalis* defines the top of Zone P20; however, because this taxon was not observed in material from Site 803, the differentiation of Zone P20 and the lower part of Zone P21 is not precise. The LO of *Globigerina angiporoides* in the absence of *Globigerina ampliapertura* does, however, serve as a proxy for Zone P20 at this site.

The FO of *Globigerina opima opima* is used to identify the top of the lower Oligocene *Globigerina ampliapertura* Zone. The LO of *G. ampliapertura* defines the top of Zone P19. These two datums occur within 0.1 m.y. of each other, according to Berggren et al. (1985a). In addition to the nominate taxon, *Globorotalia opima nana, Catapsydrax dissimilis,* and *C. unicavus* also are present within Zone P19. *Globigerina angiporoides* is present sporadically. Specimens transitional between *G. ampliapertura* and *Globorotalia increbescens* are present in the lower part of the zone.

The top of the lower Oligocene *Cassigerinella chipolensi-Pseudohastigerina micra* Zone P18 is defined by the LO of *Pseudohastigerina.* Preservation is good throughout this zone at Site 803, and this is perhaps why *P. micra* and *Chiloguembelina cubensis* are present throughout the zone. *Globigerina ampliapertura, Catapsydrax dissimilis,* and *Globigerina eocaena* also are present.

The Eocene/Oligocene boundary could not be identified at Site 803 based on planktonic foraminifers. Foraminifer preservation is generally poor and abundance is low throughout the middle and upper Eocene interval (Sections 130-803D-58X-CC to -67R-CC). Diversity is very low and only solution-resistant forms are found. A general late middle Eocene–late Eocene age (P13–P16) is suggested by the presence of *Catapsydrax dissimilis, Globigerina eocaena,* and *G. tripartita* in Section 130-803D-59X-CC. A general middle Eocene age (P11–P12) is assigned to Section 130-803D-64X-CC based on the presence of *Acarinina broedermanni, Globorotalia* cf. *bolivariana* (Toumarkine and Luterbacher, 1985), and *Globigerina senni.*

Basal Tertiary and Cretaceous sediments of Core 130-803D-68R represent a highly condensed interval, including an apparently complete K/T boundary sequence in the upper part of Section 130-803D-68R-1, according to the calcareous nannofossil data. No foraminifer samples were taken in the boundary interval for shipboard analysis. Below the K/T boundary interval, planktonic foraminifers are absent. Deep-water, agglutinated benthic foraminifers are present in very low abundances. The agglutinated taxa *Trochamminoides proteus* and *T. irregularis* from Sample 130-803D-68R-1, 110–112 cm, indicate a Maestrichtian-Paleocene age according to the range data of Kaminski et al. (1986). Agglutinated taxa are present in Sample 130-803D-68R-3, 143–145 cm, but they are not age diagnostic based on shipboard analysis.

Benthic Foraminifers

Core-catcher samples from Hole 803D were examined for benthic foraminifers. Benthic specimens are present in all of the Quaternary through middle Eocene core-catcher samples from Sections 130-803D-1H-CC through -67R-CC. Near the base of the hole, Samples 130-803D-68R-1, 110–112 cm, and -68R-3, 143–145 cm, contain agglutinated foraminifers of mid-Cretaceous to Late Cretaceous age, based on nannofossil and radiolarian data.

Benthic foraminifers generally are well preserved in all of these samples and vary in abundance relative to planktonic specimens according to the amount of dissolution affecting the planktonic components. Intervals of strong dissolution with a high concentration of radiolarians contain greater than the 1%–

2% benthic foraminifers, relative to the total foraminifer fauna, that would be expected for a deep-water site lying above the foraminifer lysocline. These intervals are represented mainly in Samples 130-803D-13H-CC and -14H-CC (upper Miocene), 130-803D-28X-CC through -42X-CC (lower Miocene through upper Oligocene), 130-803D-44X-CC through -55X-CC (lower Oligocene), and 130-803D-59X-CC through -67X-CC (lower upper Eocene through middle Eocene). Because the benthic assemblages from this site are consistently of lower bathyal to abyssal biofacies, as detailed below, water-mass changes rather than tectonic movements are indicated by the preservational state and relative proportions of the microfossil components of the pelagic ooze and chalk comprising the stratigraphic section.

The lowest Eocene sample, Sample 130-803D-67R-CC, of middle Eocene age, is a radiolarian ooze that contains a few rare specimens of calcareous benthic foraminifers, including the species *Alabamina dissonata,* which ranges from the upper Paleocene through the upper Eocene. In contrast to the good preservation of benthic specimens throughout the younger section, most of the specimens in this sample are broken and etched; no planktonic foraminifers are present. This sample was deposited below the middle Eocene CCD.

Listed in Table 5 are the most frequent species present in sand fraction (>63 μm) samples representative of the various time-stratigraphic units. Their percent frequencies among the benthic fauna are given, as well as the names of some less frequent members of the assemblages. The basic trend of these data indicates an upper Eocene through lower Oligocene species assemblage, an upper Oligocene through lower Miocene transitional assemblage, followed by a middle Miocene through Quaternary modern assemblage, all of deep-water origin (Woodruff, 1985; Thomas, 1990).

Diatoms

Neogene

Diatoms were examined in three (Holes 803A, 803C, and 803D) out of the four holes drilled at Site 803. As with planktonic foraminifers, the discussion of diatoms is also a composite summary of the diatom zones recognized in the Quaternary-Pliocene (Hole 803A), early Pliocene–late Miocene (Hole 803C), and middle Miocene–Oligocene (Hole 803D). Assignment of Site 803 samples to the low-latitude diatom zonation is summarized in Figure 18.

Diatoms are abundant to common (few) above 236.5 mbsf (Samples 130-803A-1H-CC to 130-803D-25X-CC), whereas large fluctuations in their abundance are seen below that level. In general, preservation is moderate to good, although poorer preservation is noted in the lower middle Miocene (Sample 130-803D-26X-CC) and upper Oligocene (Samples 130-803D-36X-CC through -39X-CC).

The sequence is complete from the Quaternary NTD 17 (for Neogene Tropical Diatom zone; Barron, 1985) *Pseudoeunotia doliolus* Zone (Sample 130-803A-1H-CC) through the lower middle Miocene NTD 5 *Cestodiscus peplum* Zone (Sample 130-803D-27X-CC), and from approximately early Miocene Sample 130-803D-29X-CC to -53X-CC. The diatom data suggest a hiatus in the early Miocene of approximately 4–6 m.y.

Two diatom zones, NTD 4 *Denticulopsis nicobarica* and NTD 3 *Triceratium pileus,* are completely missing at Site 803. This hiatus would correspond, in part, to Hiatus NH2 and Hiatus NH1b of Keller and Barron (1983), lumped together. This conclusion also is supported by nannofossil and planktonic foraminifer evidence.

The uppermost core-catcher sample (130-803A-1H-CC) is assigned to the NTD 17 *P. doliolus* zone. The Pliocene/Pleistocene boundary is difficult to locate, as diatom abundance is low and the valves are not well preserved.

Table 5. Benthic foraminifers as a percentage of total foraminifers.

Age and sample data	Species name	Sample (%)
Quaternary (N22) Sample 130-803D-1H-CC B = 3% N = 312 T = 9,984	Pseudoparrella exigua	15%
	Nuttallides umbonifera	11%
	Pullenia bulloides	9%
	Globocassidulina subglobosa	7%
	Cassidulina sp.	6%
	Oridorsalis umbonatus	6%
	Alabaminella weddellensis	5%
	(Others: Cassidelina complanata, Uvigerina bradyana, Fontbotia wuellerstorfi)	
early Pliocene (N18) Sample 130-803D-8H-CC B = 1% N = 208 T = 1,664	Nuttallides umbonifera	7%
	Globocassidulina subglobosa	6%
	Cibicidoides mundulus	6%
	Melonis affinis	6%
	Pleurostomella acuminata	6%
	(Others: Sigmoilina edwardsi, Uvigerina proboscidea, Favocassidulina favus)	
late Miocene (N17) Sample 130-803D-12H-CC B = <1% N = 161 T = 644	Globocassidulina subglobosa	11%
	Oridorsalis umbonatus	6%
	Nuttallides umbonifera	6%
	Pullenia bulloides	6%
	Sigmoilina edwardsi	6%
	Eggerella bradyi	6%
	Pleurostomella subnodosa	6%
	Siphouvigerina sp.	6%
	(Others: Fontbotia wuellerstorfi)	
middle Miocene (N11) Sample 130-803D-24H-CC B = <1% N = 154 T = 1,232	Oridorsalis umbonatus	16%
	Melonis affinis	10%
	Globocassidulina subglobosa	8%
	Nuttallides umbonifera	8%
	Cibicidoides sp.	7%
	(Others: Parrelloides bradyi, Gyroidinoides neosoldanii)	
early Miocene (N4) Sample 130-803D-31X-CC B = 4% N = 229 T = 458	Nuttallides umbonifera	19%
	Oridorsalis umbonatus	14%
	Linaresia pseudogrosserugosa	9%
	Globocassidulina subglobosa	7%
	Globocassidulina sp.	6%
	(Others: Parrelloides bradyi, Gyroidinoides zealandicus, Bolivinopsis cubensis)	
late Oligocene (P21–P22) Sample 130-803D-38X-CC B = 16% N = 280 T = 1,120	Oridorsalis umbonatus	16%
	Cassidulina subglobosa	11%
	Pseudoparrella aff. exigua	8%
	Nuttallides umbonifera	7%
	Pullenia bulloides	6%
	Gyroidinoides zealandicus	6%
	(Others: Anomalinoides spissiformis, Parrelloides bradyi, Bolivinopsis cubensis)	
early Oligocene (P18) Sample 130-803D-58X-CC B = <1% N = 143 T = 143	Oridorsalis umbonatus	13%
	Nonion havanense	10%
	Dorothia chapapotensis	10%
	Pullenia bulloides	8%
	Cibicidoides praemundulus	7%
	(Others: Cibicidoides grimsdalei, Anomalinoides spissiformis)	
late Eocene (P13–P16) Sample 130-803D-59X-1, 3–5 cm B = 82% N = 73 T = 73	Cibicidoides praemundulus	22%
	Oridorsalis umbonatus	19%
	Cibicidoides grimsdalei	10%
	Nonion havanense	7%
	Anomalinoides spissiformis	7%
	Gyroidinoides lamarckianus	7%
	(Others: Dorothia chapapotensis, Alabamina dissonata, no Nuttallides truempyi)	
late Eocene (P13–P16) Sample 130-803D-60X-CC B = 85% N = 449 T = 449	Oridorsalis umbonatus	20%
	Cibicidoides grimsdalei	18%
	Nuttallides truempyi	8%
	Globocassidulina subglobosa	6%
	Cibicidoides sp.	6%
	Gyroidinoides sp.	6%
	(Others: Alabamina dissonata, Anomalinoides spissiformis, Nonion havanense, Buliminella grata)	

Notes: B = the percentage of representation of benthic specimens relative to total foraminifer content; N = the number of specimens counted for the percent frequency data; and T = the total number of benthic specimens in each approximately 20-cm³ core-catcher sample, calculated from the sample split used for the census data.

The late Pliocene NTD 15 *Rhizosolenia praebergonii* Zone is found in Samples 130-803A-3H-CC, -4H-CC, and -5H-CC. The FO of *R. praebergonii*, the presence of *Thalassiosira convexa* var. *aspinosa*, and the LO of *Actinocyclus ellipticus* f. *lanceolatus* are in the lower late Pliocene samples (NTD 15/NTD 14 *Nitzschia jouseae* boundary: Sample 130-803A-6H-CC).

We could not resolve the subzones of NTD 13 *Thalassiosira convexa* defined by Burckle (1972). However, the LO of *Nitzschia miocenica*, the presence of *N. cylindrica* and members of the *T. convexa* group, and the FO of *Thalassiosira oestrupii* are contained in Samples 130-803C-5H-CC and -6H-CC assigned to this zone. The Miocene marker *Thalassiosira miocenica* was not observed. The NTD 12 *Nitzschia miocenica* Zone is rather large and expands possibly over at least three cores (Samples 130-803C-7H-CC through -9H-CC). Sample 130-803-10H-CC may represent the base of the NTD 12 Zone, slightly above the LO of *Nitzschia porteri*. The short overlap in the ranges of *N. miocenica* and *N. porteri* is seen in Sample 130-803C-11H-CC. This sample and Samples 130-803C-12H-CC and -13H-CC tentatively are assigned to the NTD 11 *N. porteri* Zone. The presence of *N. porteri* and *N. cylindrica* and the absence of *N. marina* leads us to do so. However, *Thalassiosira burckliana* was not observed.

The presence of *Coscinodiscus yabei* and the restricted range of *C. vetustissimus* var. *javanicus* fall within the NTD 10 *C. yabei* Zone (Samples 130-803C-15H-CC through -17H-CC). *Coscinodiscus nodulifer* var. *cyclopus* is present in this zone.

Sample 130-803C-17H-CC may represent the NTD 10/NTD 9 (*Actinocyclus moronensis*) boundary. The ranges of this species and *C. vetustissimus* var. *javanicus* overlap here. The species *Denticulopsis hustedtii* is missing. The late/middle Miocene boundary occurs within the NTD 9 Zone. The NTD 8 *Craspedodiscus cosinodiscus* Zone is contained in Sample 130-803D-23H-CC. At Site 803, the zone is characterized by the presence of *C. coscinodiscus* and *Synedra jouseana*, the LOs of *Denticulopsis punctata* f. *hustedtii* and *Actinocylcus ingens*, and the absence of *Hemidiscus cuneiformis*. The NTD 7 *Coscinodiscus gigas* var. *diorama* Zone may be compressed into the NTD 6 Zone, as only fragments of this species are recorded in the same sample (130-803D-24H-CC) in which the LOs of *Coscinodiscus lewisianus* and *Cestodiscus pulchellus* were observed. The NTD 6 *C. lewisianus* Zone extends from Samples 130-803D-24H-CC through -25X-CC. The occurrence of *Cestodiscus peplum* (NTD 5) is limited to Sample 130-803D-27X-CC.

As mentioned above, Zones NTD 4 and NTD 3 are missing. The LO of *Craspedodiscus elegans* in Sample 130-803D-29X-CC assigns this sample to the NTD 2 Zone. However, low diatom abundances and poor preservation prevents precise dating of this sample. The characteristic diatom *Thalassiosira fraga* is missing. The presence of *Rosiella paleacea* and the few to common abundances of *Synedra jouseana*, *Coscinodiscus lewisianus* var. *rhomboides*, *C. marginatus*, and *C. oligocenicus* would assign Samples 130-803D-31X-CC through -34X-CC to the NTD 1 *R. paleacea* Zone.

The poor preservation of Sample 130-803D-35X-CC does not allow dating of this sample. The *Rocella gelida* Zone may be removed or compressed (?) at Site 803. The Oligocene/Miocene boundary cannot be identified. Samples 130-803D-36X-CC through -40X-CC are assigned to the *Borgorovia veniamini* Zone. The interval of the *Rocella vigilans* Zone (Samples 130-803D-42X-CC to -47X-CC) is moderately to well preserved at Site 803. *R. vigilans* is the most consistently present species throughout the zone. *Cestodiscus reticulatus* is present in Sample 130-803D-51X-CC. The LO of *Coscinodiscus excavatus* is in Sample 130-803D-52X-CC, and its FO is in Sample 130-803D-59X-CC. We could not recognize the late Eocene *Baxteriopsis brunii* Zone proposed by Fenner (1984) in Hole 803D, and the

Eocene/Oligocene boundary could not be identified. Samples 130-803D-62X-CC and -63X-CC are tentatively assigned to the *Asterolampra marylandica* Zone. This assignment, however, is uncertain and is based mainly on the FO of *A. marylandica* in Sample 130-803D-63X-CC and the presence of *Triceratium inconspicuum* var. *inconspicuum* in Sample 130-803D-62X-CC. Diatoms are rare in Samples 130-803D-64X-CC to -66X-CC. *A. marylandica* is absent, and no other biostratigraphic marker species could be found in these samples. Sample 130-803D-67X-CC is barren.

Cretaceous

The 19 samples of Core 130-803D-68R used for radiolarian studies (see "Radiolarians" section, this chapter) were also used for diatom analysis. They contain no diatoms.

Radiolarians

Radiolarians were observed in all of the recovered core-catcher samples of Cenozoic age. Their preservational states generally deteriorate with increasing depth throughout the Neogene. They generally are well preserved in the Pleistocene to middle Miocene nannoplankton/foraminifer oozes. Moderate to poorly preserved radiolarians are present in the underlying middle Miocene–lower Miocene oozes and chalks. Chalky sediments, sometimes silicified, recovered from the Oligocene and the Eocene contain poorly preserved radiolarians. Zonal assignments were possible for all the Cenozoic samples, although in some cases more than one zone could not be differentiated. In the radiolarian record, sequential zones from the Pleistocene to the middle Eocene were found, and no significant hiatus was recognized above the middle Eocene at this site. A major hiatus occurs in the lowermost Tertiary. Cretaceous radiolarians were found in the sediment layers overlying the basement. Several samples yielded useful stratigraphic information. Figure 18 summarizes the radiolarian zonation of Holes 803A, 803B, 803C, and 803D as well as their correlation with the zones of other taxa.

Neogene

The following core-catcher samples, ranging from the seafloor to 361.3 mbsf in depth, were determined to be of Neogene age: 130-803A-1H-CC through -6H-CC; 130-803B-1H-CC through -7H-CC; 130-803C-1H-CC through -15H-CC; and 130-803D-16H-CC through -39X-CC. The upper Miocene sediments (i.e., the *Didymocyrtis antepenultima* Zone) were the thickest unit observed at this site.

Pleistocene

The two uppermost core-catcher samples from Hole 803B (130-803B-1H-CC and -2H-CC) can be assigned to the *Anthocyrtidium angulare* Zone of the lowermost Quaternary. The presence of *Lamprocyrtis neoheteroporos* and *Theocorythium trachelium* and the absence of *Collosphaera tuberosa* suggests that these samples are in the *A. angulare* Zone. Thus, it is apparent that the Holocene and upper Pleistocene sections are condensed (or missing) in the top several meters.

Pliocene

Samples 130-803B-3H-CC and 130-803C-1H-CC are placed in the uppermost Pliocene radiolarian zone (the *Pterocanium prismatium* Zone). The *Spongaster pentas* Zone is found in Samples 130-803B-4H-CC through -7H-CC and 130-803C-2H-CC through -4H-CC. Age-diagnostic taxa (and their FOs and LOs) found in these samples are *Spongaster tetras* (FO), *Spongaster berminghami* (LO), *S. pentas* (FO), *Stichocorys peregrina* (LO), and *Didymocyrtis penultima* (LO). The *S. peregrina* Zone begins from Sample 130-803C-5H-CC and extends into Sample

130-803C-8H-CC. Diagnostic taxa found in these samples are *S. peregrina, D. penultima, S. berminghami,* and *Solenosphaera omnitubus* (LO). As the *S. peregrina* Zone ranges from the lower Pliocene to the upper Miocene, the Miocene/Pliocene boundary lies between Cores 130-803C-5H and -8H.

Upper Miocene

Samples 130-803C-9H-CC through -11H-CC are assigned to the *Didymocyrtis penultima* Zone. The FO of *S. omnitubus* and the LOs of *Didymocyrtis antepenultima* and *Stichocorys delmontensis* are found in these samples. Samples 130-803C-12H-CC through -15H-CC and Samples 130-803D-16H-CC through -18H-CC are placed in the *D. antepenultima* Zone. In this zone, we recognized the following six datum levels: the LOs of *Dictyocoryne ontogenesis, Diartus hughesi, Didymocyrtis laticonus,* and *Diartus petterssoni;* and the FOs of *D. antepenultima* and *S. berminghami.*

Reworked middle Eocene specimens were recognized in three core-catcher samples: 130-803C-10H-CC (*Podocyrtis phyxis* [F = few]), 130-803C-11H-CC (*P. phyxis* [C = common]), and 130-803C-12H-CC (*Theocotyle cryptocephala* [F]). Species belonging to younger ages (e.g., Pliocene) were encountered in Sample 130-803C-14H-CC: *S. tetras* (F), *S. pentas* (R), and *D. penultima* (R). Pliocene specimens of *Anthocyrtidium prolatum* (F) and *S. pentas* (F) were also found in Sample 130-803D-17H-CC. Both of these are considered to be downcore contaminations during coring procedures.

Middle Miocene

Samples 130-803D-19H-CC through -23H-CC were assigned to the *D. petterssoni* Zone of the uppermost middle Miocene. In these samples, the FOs of following species were found: *Dictyocoryne ontogenesis, Diartus hughesi,* and *Diartus petterssoni.* Sample 130-803D-24H-CC lies in the upper part of the *Dorcadospyris alata* Zone; this zone continues to the next sample (130-803D-25X-CC). In these samples, the FOs of *D. laticonus* and *S. delmontensis* and the LOs of *Lithopera renzae* and *Lithopera neotera* are located.

Lower Miocene

The uppermost part of the *Calocycletta costata* Zone begins at Sample 130-803D-26X-CC; the same zone continues to Sample 130-803D-27X-CC, and the lower part of the zone is in Sample 130-803D-28X-CC. The LOs of *Didymocyrtis mammifera, Dorcadospyris dentata, Dorcadospyris forcipata, Liriospyris parkerae, Cyrtocapsella japonica,* and *Calocycletta caepa* were found in these samples. Datum levels of the FOs in the zone are *D. dentata* and *L. parkerae.* Samples 130-803D-29X-CC through -31X-CC are located in the *Stichocorys wolffii* Zone.

Samples 130-803D-32X-CC and -33X-CC cannot be differentiated between the *S. wolffii* and *Stichocorys delmontensis* Zones because of the lack of key species. Nevertheless, either of the zones would give no problem in terms of continuity in sedimentation. Sample 130-803D-34X-CC contains a radiolarian assemblage corresponding to the top of the *Cyrtocapsella tetrapera* Zone. Samples 130-803D-35X-CC and -36X-CC are also placed in the *C. tetrapera* Zone. Samples 130-803D-37X-CC and -38X-CC can be assigned to either the *C. tetrapera* or the *Lychnocanoma elongata* Zones, as they cannot be differentiated. Sample 130-803D-39X-CC belongs in the lower part of the *L. elongata* to the upper part of *Dorcadospyris ateuchus* Zones.

Paleogene

Paleogene sediments recovered from Hole 803D, composed of nannofossil chalks to foraminifer nannofossil chalks, generally contain poorly preserved radiolarians. Zonal assignments were usually possible. With increasing age and depth, the chalks

increased in degree of consolidation, and they were best treated with calgon, hydrogen peroxide, and ultrasonic disaggregation after boiling in a hydrochloric acid solution (see "Explanatory Notes" chapter, this volume).

Oligocene

Samples 130-803D-40X-CC through -48X-CC can be placed in the *D. ateuchus* Zone of the Oligocene. Diagnostic taxa in these samples include *Lithocyclia angusta, D. ateuchus,* and *Theocyrtis annosa.* Samples 130-803D-49X-CC through -58X-CC are placed in the *Theocyrtis tuberosa* Zone of the lower Oligocene. These samples usually include *Tristylospyris triceros, L. angusta,* and *Artophormis gracilis.* In the lower part of this zone, *Lithocyclia crux* and *Centrobotrys gravida* were present.

Upper Eocene

Sample 130-803D-59X-CC can be assigned to the *Cryptoprora ornata* Zone (Saunders et al., 1984, equivalent to the uppermost part of the *Thyrsocyrtis bromia* Zone of Sanfilippo et al., 1985) of the upper Eocene. This sample contains *T. triceros, Artophormis balbadensis, Calocyclas turris, C. ornata,* the *Sethochytris babylonis* group, *Dictyoprora mongolfieri, Dictyoprora pirum, Dictyoprora armadillo, Lophocyrtis jacchia,* and *Lychnocanoma amphitrite.* The *Calocyclas bandyca* Zone (Saunders et al., 1984; equivalent to the middle part of the *Thyrsocyrtis bromia* Zone of Sanfilippo et al., 1985) of the upper Eocene is placed in Samples 130-803D-60X-CC through -63X-CC, based on the presence of *T. bromia, C. turris, C. bandyca, C. ornata,* and *Cryptoprora azyx.*

Middle Eocene

Sample 130-803D-64X-CC tentatively is assigned from the *Podocyrtis chalara* to the *Cryptoprora azyx* Zones (Saunders et al., 1984, equivalent to the basal part of the *Thyrsocyrtis bromia* Zone of Sanfilippo et al., 1985), which cannot be differentiated. The diagnostic taxa present in this sample include *Eusyringium fistuligerum, Lithocyclia ocellus, Thyrsocyrtis triacantha, Thyrsocyrtis rhizodon, Dictyoprora mongolfieri,* and *Podocyrtis papalis.* Sample 130-803D-65X-CC is placed in the lower part of the *P. chalara* Zone as it contains *E. fistuligerum, Podocyrtis trachodes,* and *P. chalara.* Sample 130-803D-66X-CC, which contains *P. mitra* together with several other middle Eocene species, is placed in the *Podocyrtis mitra* Zone. Sample 130-803D-67X-CC is assigned to the *Podocyrtis ampla* Zone based on the presence of *P. mitra, Podocyrtis sinuosa, D. mongolfieri, Theocotylissa ficus,* and *Pterocodon lex.*

Cretaceous

We examined 19 samples from Core 130-803D-68R for radiolarians. Among them only three samples yielded useful, but poorly preserved, radiolarians for stratigraphic information. They can be found in Sample 130-803D-68R-3 at intervals of 86–87, 89–90, and 96–98 cm, all of which are light brown (10YR 4/4) soft sediments. Among these three samples, Sample 130-803D-68R-3, 89–90 cm, presents the best preservation as well as a large number (> 100 specimens/slide) of specimens. The sample can be assigned with reasonable confidence to the interval from the upper *Acaeniotyle umbilicata* Zone to the lower *Abesacapsula sophedia* Zone, which corresponds with the upper Albian to the lower Cenomanian (~ 103–95 m.y.) (Sanfilippo and Riedel, 1985). Three key species found in the sample include *Thanarla veneta* (A = abundant), *Thanarla elegantissima* (C = common), and *Pseudodictyomitra pseudomacrocephala* (A). Although most of the specimens are casts of silica filled all the way to the center of the specimens, and therefore their preservational states are defined as "poor," their original shapes (and thus outlines) as well as surface ornamentations are preserved,

which made the species identification possible. One sample lower in the section (130-803D-86R-3, 96–89 cm) yielded fewer radiolarians of poorer preservation. *Thanarla elegantissima* (R = rare) and *P. pseudomacrocephala* (F = few) in this sample present the same age bracket as the above sample. Furthermore, Sample 130-803D-68R-3, 86–87 cm, contained *P. pseudomacrocephala*? (R), but the species identification is tentative because of the very poor preservation. It may be possible that this sample also belongs to the same age as the above-mentioned two samples. There are several other nassellarian species preserved in all of the above three samples. However, it is not possible to provide further information because of the poor preservation.

PALEOMAGNETISM

Introduction

Pass-through magnetometer measurements were taken on all APC split-core archive sections recovered from Holes 803A, 803B, 803C, and 803D and on all XCB cores recovered from Hole 803D. Pass-through magnetometer measurements were also taken on RCB sediment split-core archive sections recovered from Hole 803D. Rotary coring of basalt at Hole 803D resulted in the recovery of continuous pieces 25–75 cm in length that could be unambiguously oriented with respect to the top, separated by smaller pieces with questionable orientations. To address this problem, a different measuring technique was adopted. A single, continuous segment of basalt was chosen from each section of the split-core archives and measured with the pass-through magnetometer.

Pass-through magnetometer measurements were taken at 1-, 3-, 5- and 10-cm intervals, depending on the interval of interest. The natural remanent magnetization was measured for all cores and the magnetization after treatment at 15 mT for most cores. On critical intervals, demagnetizations were carried out at 5, 10, and 15 mT. Pass-through magnetic susceptibility measurements were also taken on all unsplit core sections recovered at Site 803. These measurements were done at 3-, 5-, and 10-cm increments.

The multishot core orientation device failed at Hole 803A when difficulties in drilling resulted in the loss of a camera. This left only one operational camera for orientation. Orientations were attempted on Hole 803B but judged unreliable by the drilling crew. Orientations were recorded on Cores 130-803C-3H, -4H, and -5H of Hole 803C and below Core 130-803D-6H in Hole 803D.

Results

One of the most conspicuous characteristics of the pass-through magnetometer measurements of APC cores was an anomalously high magnetic intensity recorded for the top of the first section of each core. This high intensity gradually decreased downcore to a value similar to that of the remainder of the core at 50–100 cm within the first section. This effect was not entirely surprising as it corresponded roughly with the zone of physical disruption ("draw-in") caused by the hydraulic coring process. What was surprising, however, was that this effect sometimes extended beyond any visible signs of disruption, suggesting that the drilling disturbance in APC cores can be quite subtle. Therefore, the directional results from the first meter of recovery in each core were interpreted with caution. Alternating field (AF) demagnetization generally produced little change in direction in the Pliocene-Pleistocene cores. Occasionally, however, large changes were noted and were most probably the result of the removal of a present-day viscous magnetization.

Despite minor problems with core disturbance, the pass-through magnetometer measurements of APC cores yielded correlatable reversal boundaries at each hole for Pliocene-Pleistocene sediments. The magnetic intensity decreased before some

reversal boundaries and slowly increased afterward with transitional directional behavior recorded during the reversal (Fig. 19). This high-resolution record deteriorated rapidly below approximately 46 mbsf in each core, marked with a rapid decrease in intensity to very low levels (1×10^{-7} to 5×10^{-8} emu/cm^3) (Fig. 20).

Intensities for much of the Miocene sediments were at these low levels; therefore, AF demagnetization was halted. In the Oligocene sediments, intensities increased to interpretable values and AF demagnetization was resumed. Although the Oligocene

sediments were cored with the XCB, the pass-through magnetometer measurements yielded intervals of constant inclination that can be tentatively interpreted as a magnetostratigraphy. The single Cretaceous RCB core yielded fairly strong intensities, and we think that at least one reversal boundary present in the section contains the Cretaceous/Tertiary boundary (Section 130-803D-68R-1). The RCB basalt pieces also yielded results that are interpretable in terms of polarity.

Pass-through magnetic susceptibility measurements yielded high-resolution data for Pliocene-Pleistocene cores that allowed
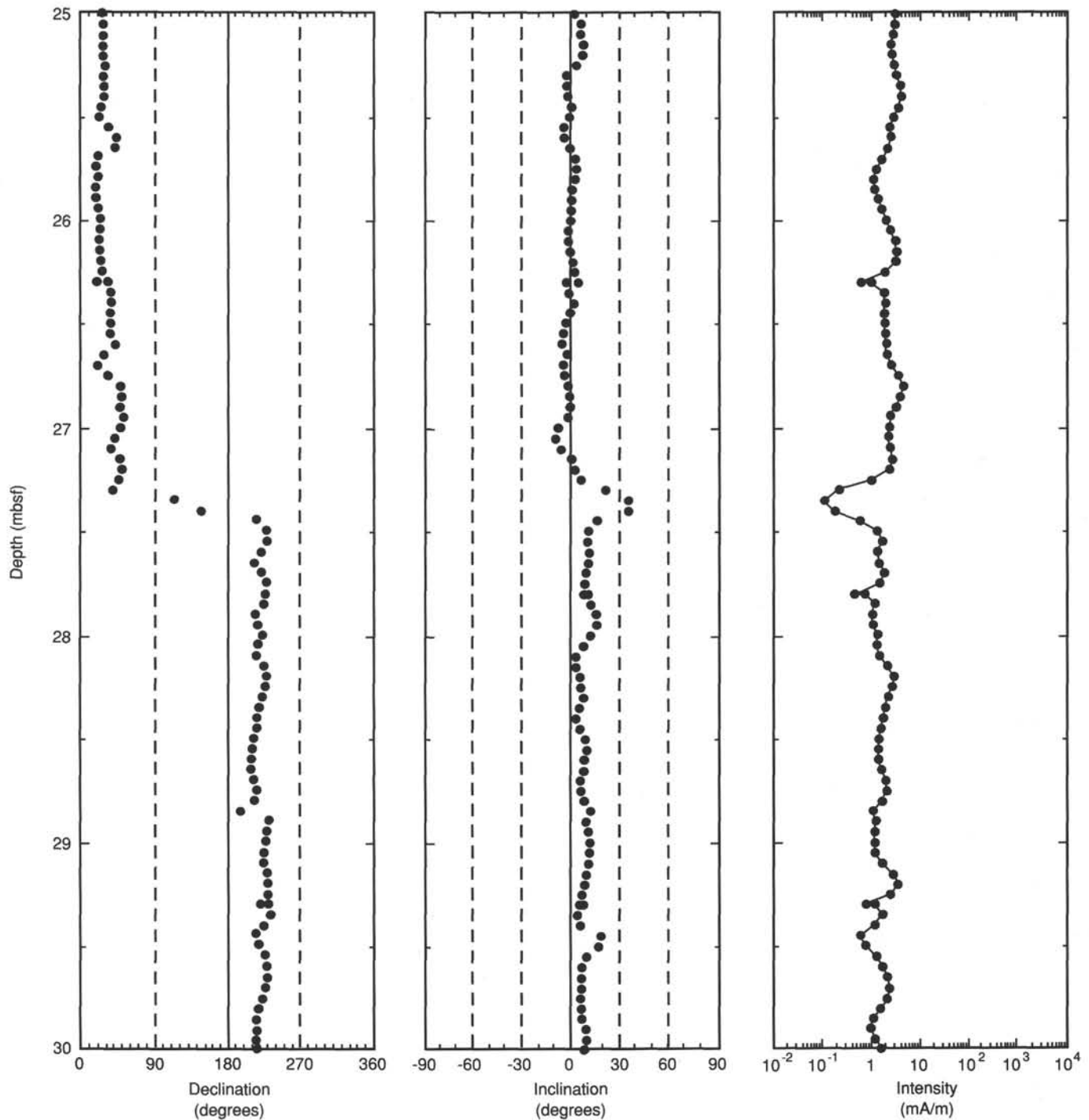
Figure 19. Reversal boundary between the Matuyama and Gauss chrons (2.47 Ma) observed at 27.4 mbsf in Core 130-803B-4H.
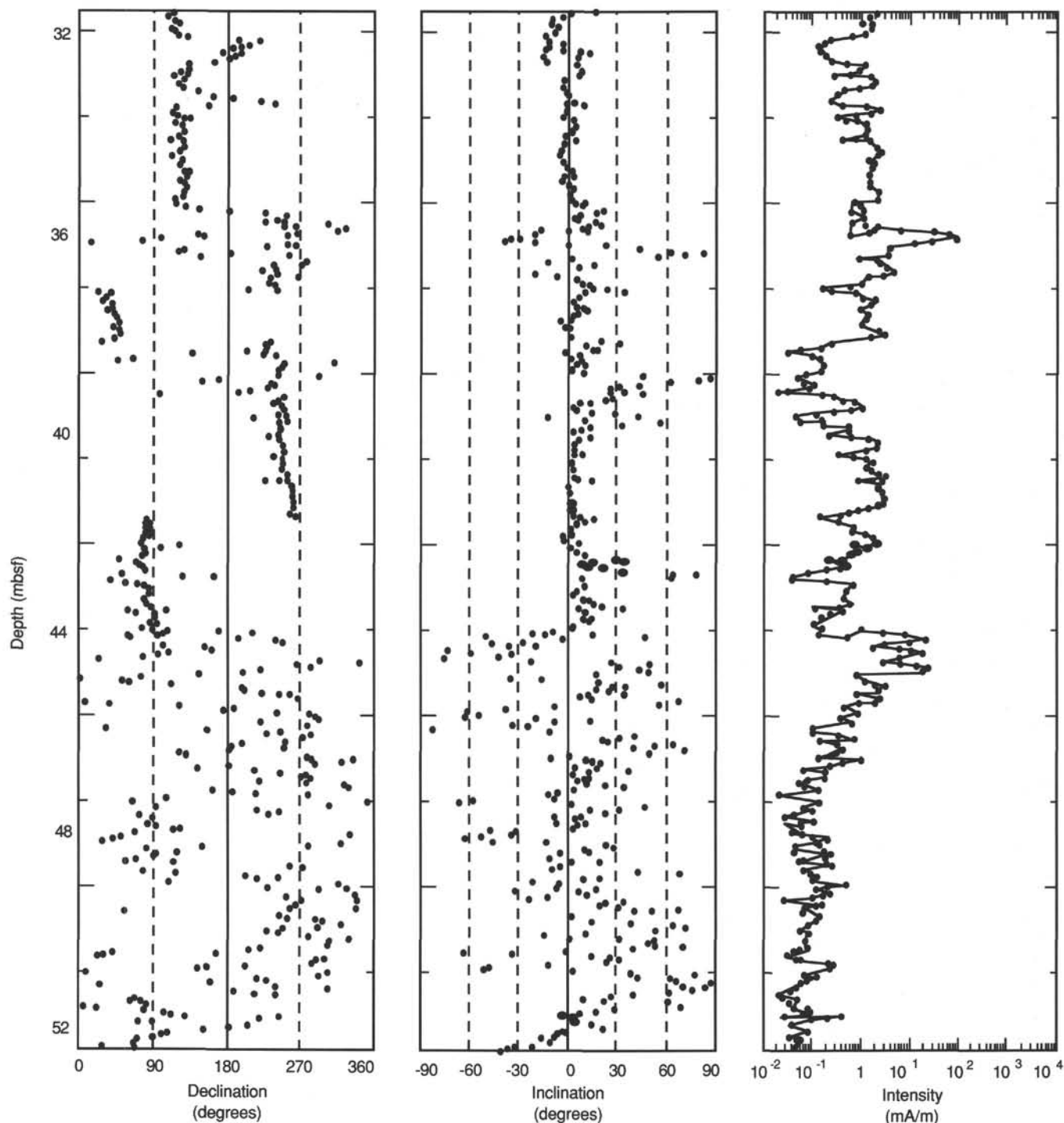
Figure 20. Rapid decrease in intensity below 46 mbsf in Hole 803A displayed in pass-through magnetometer measurements after demagnetization at 15 mT.

detailed correlations. Susceptibility measurements mirrored the magnetic intensity values, however, and became extremely low to negative in the Miocene sediments, clearly influenced by the diamagnetic calcite content. Severe drift problems with the M.S.1 susceptibility meter were suspected during measurements on Hole 803D. These suspicions were confirmed by measurements on a MnO_2 standard. Such behavior was monitored carefully, but some intervals in the data base are clearly dominated by this unusually high drift.

Correlation Between Holes 803A, 803B, 803C, and 803D: A Pliocene-Pleistocene Magnetostratigraphy

Site 803 is situated at 2°N; therefore, we could not use paleomagnetic inclinations for polarity determinations. As orientations were unavailable for many of the Pliocene-Pleistocene cores, a relative polarity scheme based on magnetic declination was developed to produce a composite magnetostratigraphy, in-

dependent of paleontological determinations. The first polarity in a given core was assigned polarity "A" and the second, polarity "B". In addition to these polarities, several possible short polarity events were also identified. Although some of these events may be true polarity zones or magnetic excursions of short duration (<50 ka), many are artifacts caused by the local reduction in intensity, remagnetization in zones of increased dissolution of magnetite, or local sediment disruption caused by coring processes. All such possible events have been omitted from the current analysis and will be examined further in shore-based studies. The magnetostratigraphic approach adopted for this site resulted in a stacked sequence of relative polarity determinations that is easily correlated to the geomagnetic time scale (Fig. 21).

Multishot Orientation Error

After we completed the Pliocene-Pleistocene magnetostratigraphy based on relative polarities, orientation data for Holes 803C and 803D were available. Unfortunately, these orientations resulted in declinations 75°–90° from expected. The drilling crew was notified, and they examined the coring assembly. The T-bar assembly that holds the camera to the pressure-case bottom plug was found to have rotated approximately 90° counterclockwise (when looking down the core barrel). When this correction was applied to Cores 130-803C-2H and -3H from Hole 803C and Cores 130-803D-3H through -5H from Hole 803D, the declinations were near 0° and 180°, suggesting polarities identical to the relative polarity interpretation.

Pliocene-Pleistocene Sedimentation Rates

The relative polarity magnetostratigraphy allows us to calculate the sedimentation rates for the Pliocene-Pleistocene interval in each hole (Fig. 22). These rates average 1 cm/k.y. for the interval from the base of the Olduvai Subchron (1.88 Ma) to the present and 1.5 cm/k.y. for the interval from the top of the Gilbert reversed polarity chron (3.40 Ma) to the base of the Olduvai. Fluctuations during the Pleistocene, suggested by using the boundaries of the Jaramillo Subchron as calibration points, are seen in the records from both Holes 803B and 803D. Sedimentation rates in the interval between the base of the Mammoth Subchron (3.18 Ma) and the top of the Gilbert may be slightly lower than 1.5 cm/k.y.

Preliminary Oligocene Magnetostratigraphy and Paleolatitude

Below the point at which multishot orientations were no longer available, polarity determinations could only be made on the basis of the sign of the inclination. Paleoinclinations for Site 803 during the Miocene can be expected to be low, reflecting the near-equatorial latitudinal position of the site during this time interval. Discrimination of the sign of such low inclinations was not possible, given the weak intensity of the cores. Both the intensity and the absolute value of the inclination increased sufficiently in the Oligocene cores of Hole 803D to allow the tentative recognition of intervals in which inclination was consistent in sign and magnitude after 15-mT demagnetization (Fig. 23). Assuming that the Ontong Java Plateau moved with the Pacific Plate over the interval from the Oligocene to the present (an assumption at variance with the results from DSDP Site 289; Hammond et al., 1975), normal polarity can be assigned to negative inclinations, from which the Oligocene magnetostratigraphy follows (Fig. 24). Paleontological dates are consistent with this magnetostratigraphy.

Age was determined as a function of stratigraphic depth from this magnetostratigraphy (Fig. 25). Sedimentation rates averaged 3.1 cm/k.y. during the early Oligocene, between Anoma-

lies 13 and 12, but they slowed later in the Oligocene to an average of 1.57 cm/k.y. between Anomalies 11 and 7.

Inclinations from the cores for which polarity information could be determined (Cores 130-803D-36X to -41X and Cores 130-803D-45X to -50X) are distributed by frequency, as shown in Figure 26. The distribution is biased toward low positive inclinations, reflecting the dominantly reversed polarity over these intervals and possibly also some unremoved viscous remanence. The mode of the inclination distribution occurs at 9°. If this represents the primary magnetization, the paleolatitude was 4.5°. Which hemisphere this represents cannot be directly determined, but if the Ontong Java Plateau has remained coherent with the Pacific Plate, then this paleolatitude was in the Southern Hemisphere, giving a total displacement for this site on the plateau of about 7° northward since the Oligocene. This is consistent to within 2° with the Pacific apparent polar wander path (Gordon, 1983; Sager, 1987). It appears that the paleomagnetic results from DSDP Site 289, which showed no paleolatitude shift until approximately 30 Ma, may have been biased in some fashion.

Cretaceous/Tertiary Boundary and Basement Polarity

Volume magnetic susceptibility measurements on the single Cretaceous RCB sediment core recovered at Hole 803D (Core 130-803D-68R) revealed values 10–40 times greater ($k = 100$–400×10^{-6} cgs) than the values recorded on the previous 622 m of sediment. In Section 130-803D-68R-1, two peaks in susceptibility occur (Fig. 27). Based on nannofossil ages, the Cretaceous/Tertiary boundary is thought to be present in the Interval 130-803D-68R-1, 38–53 cm. The first peak in susceptibility at 45 cm may correlate with the boundary since the Cretaceous-Tertiary boundary often exhibits high magnetic susceptibility values due to the presence of magnetic spherules. However, the high background magnetic susceptibility must also be explained as well as the additional peak in Section 130-803D-68R-1, 95 cm. A more definitive interpretation of these data awaits the results from discrete sampling.

Pass-through magnetometer measurements revealed a polarity transition at Section 130-803D-68R-1, 70 cm, as denoted by an 180° shift in declination in an unbroken portion of the core. The polarity record, however, cannot be unambiguously determined from the pass-through measurements because of the relative rotations between other portions of the cores and possible viscous overprinting. A polarity determination will be conducted as part of a shore-based study.

The measurement of discrete continuous segments of basalt from each section was successful in determining the dominant basement polarity. All pieces measured displayed clear negative inclinations indicative of normal polarity, as the Ontong Java Plateau was in the Southern Hemisphere in the Cretaceous.

Discussion

Given the low to intermediate sedimentation rates, the detail seen in the Pliocene through Pleistocene magnetostratigraphy is surprising. The magnetostratigraphic record is remarkably complete. The calculated 50% decrease in sedimentation rate before the base of the Olduvai Subchron (1.88 Ma) may record increased carbonate dissolution in the Pleistocene. Comparison of these records with those expected from shallower sites should provide further clues to the nature of this substantial change in carbonate sedimentation at the onset of the Pleistocene. The drilling of sites at different depths will also provide constraints on the origin of the transition from high-resolution magnetostratigraphic data to low-intensity signals observed at 46 mbsf at this site. This phenomenon may be either a result of the dissolution of magnetite with depth or the lack of an initial magnetite input relative to the carbonate accumulation.
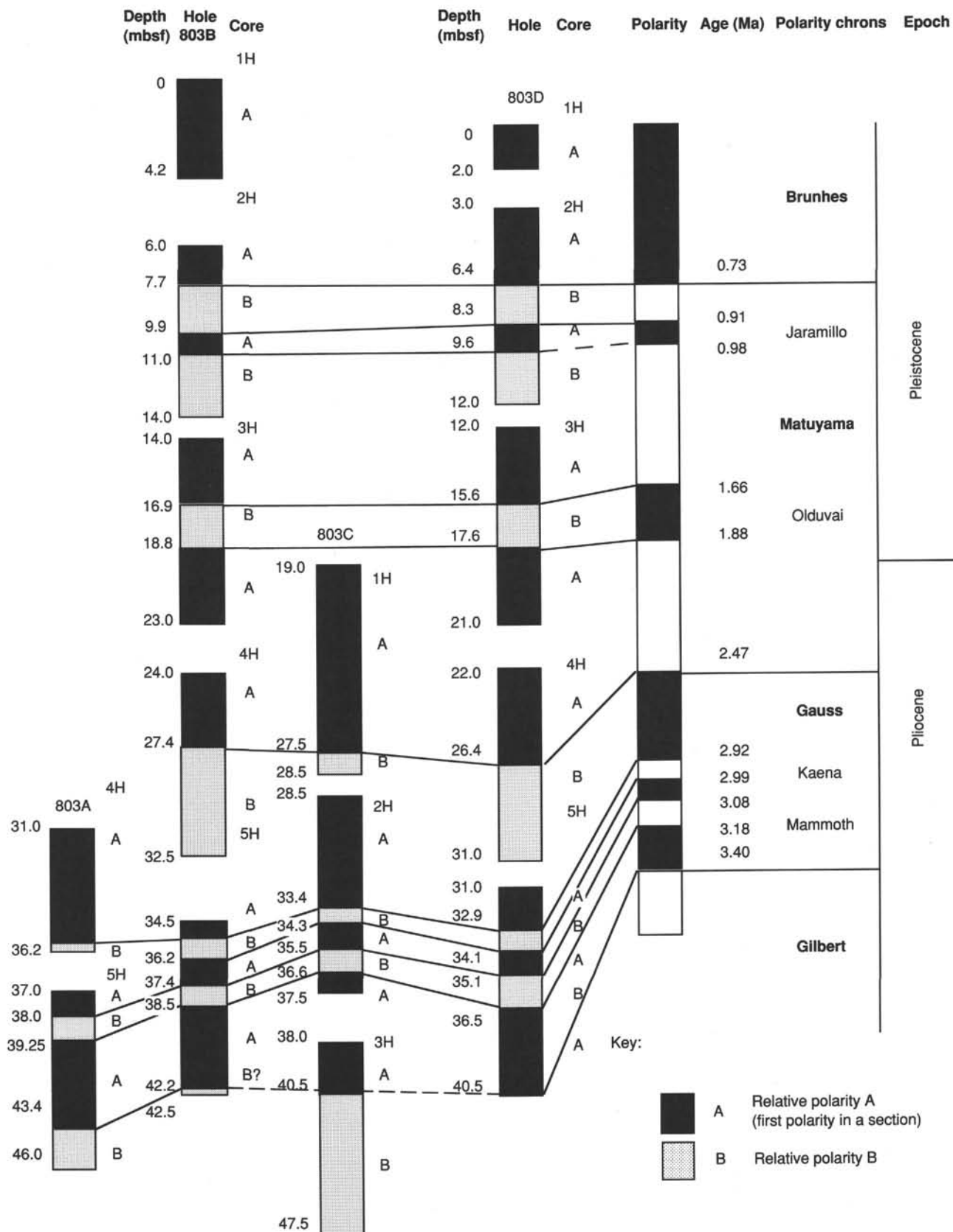
Figure 21. Preliminary Pliocene-Pleistocene magnetostratigraphy for Site 803 based on stacked sequences of relative polarities within individual sites. The first polarity in a core is labeled "A" and the second, "B". Possible short polarity intervals have been excluded in this analysis. No cores are oriented and inclination cannot be used for polarity determinations. The magnetostratigraphic column is based upon stacked cores containing relative polarity information.
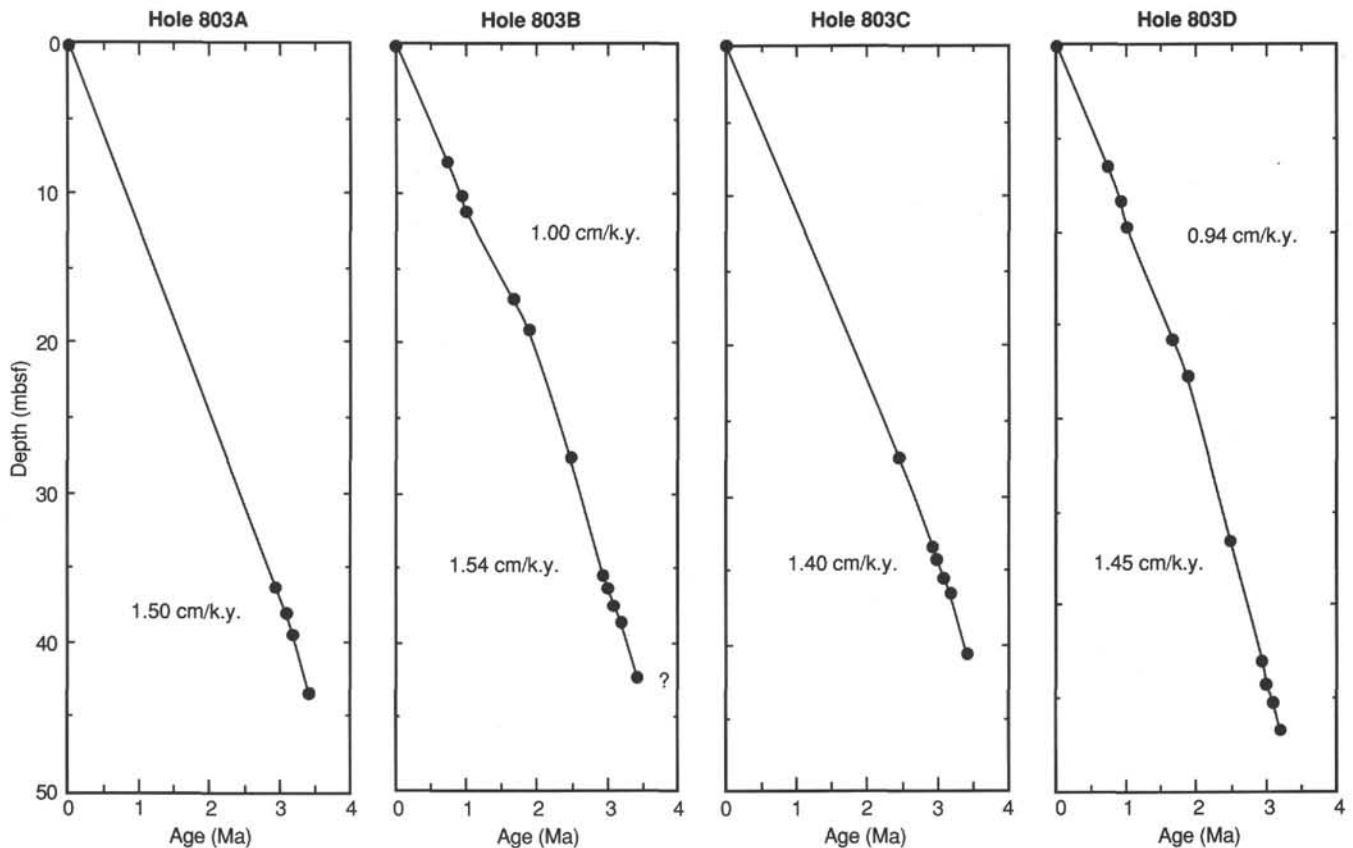
Figure 22. Sedimentation rates, Site 803.

SEDIMENTATION RATES

Over 200 age/depth indicators were gathered from the middle Eocene through Holocene sediments of Holes 803A through 803D. The majority of these indicators represent microfossil events because magnetostratigraphic data were obtained only from the Pliocene/Pleistocene intervals. All these age/depth indicators are listed as a function of increasing age in Table 6, and they are portrayed graphically in Figures 28 through 32. Sedimentations rates from the Eocene-Holocene interval have been calculated for all four holes and are presented in Table 7, and the rates from Holes 803C and 803D are shown graphically in Figure 33.

One Neogene hiatus was recognized between Samples 130-803D-27X-CC and -28X-1, 140 cm. The recovery rate for Core 130-803D-27X was 45.9%, implying that the hiatus falls somewhere between 241.5 and 247.3 mbsf. by making a downhole extrapolation of the sedimentation rate that was derived from the LO of *Discoaster hamatus* and the FO of *Globorotalia peripheroacuta* (Table 7), an age estimate of 15.4 Ma was obtained for the younger side of the Miocene hiatus. Hole 803C ended precisely at the young side of the hiatus.

Another Miocene hiatus was recognized at the core break between Cores 130-803D-28X and -29X at 255.5 mbsf. A minimum sedimentation rate of 17.8 m/m.y. was obtained in Core 130-803D-28X, which separates the two hiatuses. Thus, the old side of the upper hiatus is estimated to be about 19.5 Ma, whereas the young side of the lower hiatus is placed at 20.0 Ma. The old side of the lower hiatus is placed at 21.8 Ma, at the LO level of *Globorotalia kugleri*.

The age-depth relationships of two late Oligocene and one Oligocene/Miocene boundary marker (Fig. 30) suggest that a large portion of the late Oligocene (23.7–28.2 Ma) is somewhat condensed. The rates in the adjacent intervals are similar, which probably points to a similar surface-water productivity input across the entire late Oligocene–earliest Miocene interval and signifies that the condensation was caused by processes operating at depth.

Less than 5 m of sediments were preserved from the time interval between 45 (oldest middle Eocene sediments recovered) and about 100 Ma (Cretaceous sediment/basement contact). The age/depth relationships from the pertinent core (130-803D-68R) are not presented graphically.

INORGANIC GEOCHEMISTRY

We collected 24 interstitial water samples from Hole 803D at depths ranging from 8.5 to 623.2 mbsf (Table 8). The majority of the samples are from the nannofossil ooze and chalk of lithologic Unit I (see "Lithostratigraphy" section, this chapter); the lowermost sample is from the basal siliciclastic sediments of Unit III, 3 m above contact with basalt. Chemical gradients in the interstitial waters at this site are influenced by the biogenic-rich, organic-carbon-poor character of the sediments and by alteration reactions in the underlying basalt by means of diffusion through the sediment column.

Chlorinity increases by approximately 10% with depth (Fig. 34), as does salinity, measured refractively as total dissolved solids (Table 8). Sodium concentrations measured by flame emission spectrophotometry (Table 8) and those estimated by charge balance calculations agree to within <1.5% and are approximately constant with increasing depth. Alkalinity increases slightly to 3.9 mM by 166 mbsf in Core 130-803D-19H, then decreases to 2.4 mM at 509 mbsf in Core 130-803D-55X, with a sharp decrease to 0.36 mM at 623 mbsf in Core 130-803D-68R (Fig. 34).
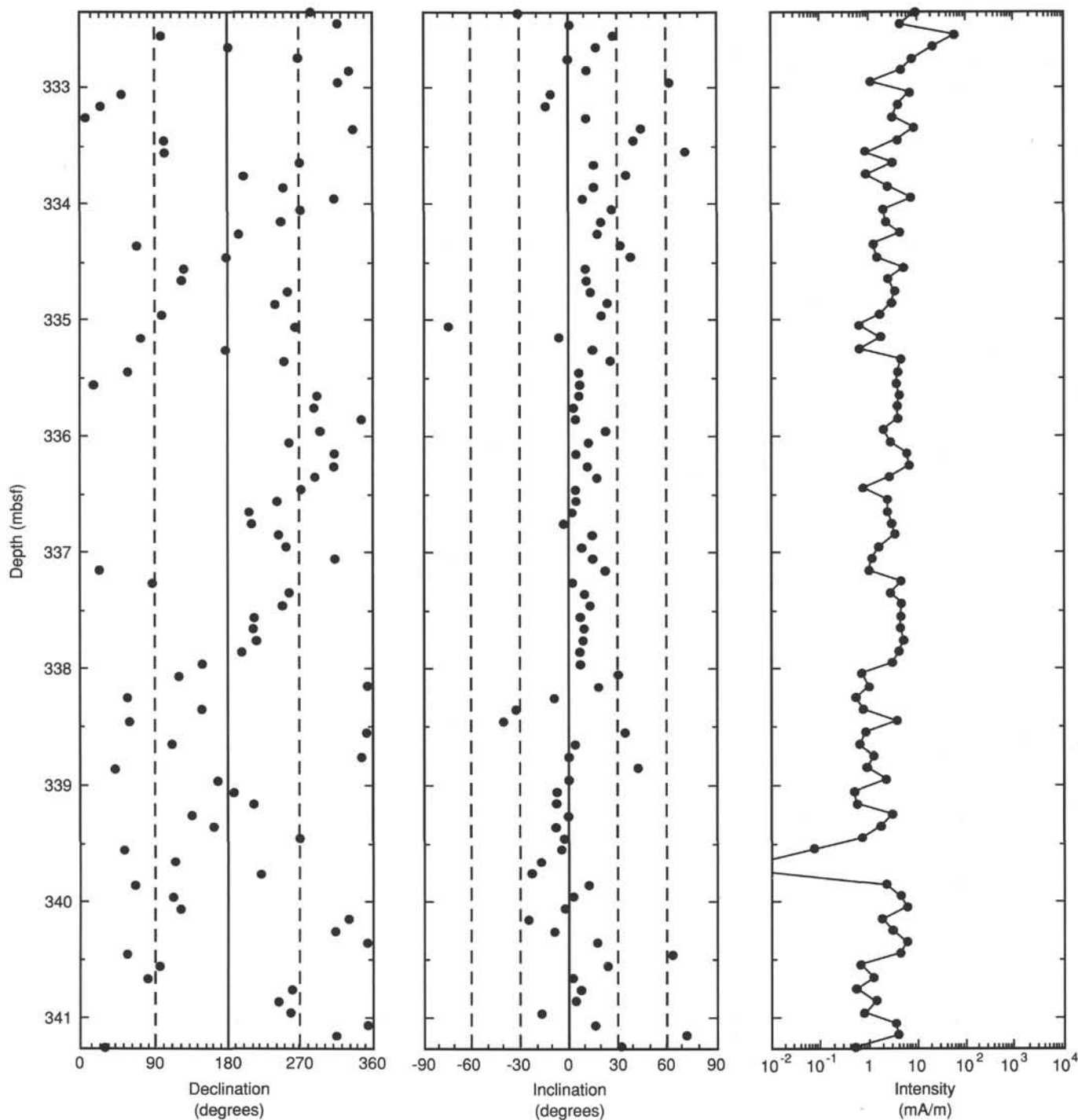
Figure 23. Declination, inclination, and intensity in Core 130-803D-37X, showing intervals of consistent low positive (335–338 mbsf) and low negative (338.7–339.5 mbsf) inclinations, together with intervals of scattered inclinations.

Sulfate concentrations decrease by approximately 20% to 195 mbsf and are essentially constant below that depth (Fig. 34). The extent of SO_4^{2-} depletion is limited, presumably because of the relatively low organic carbon content of these sediments. This interpretation is supported by the profiles of the labile nutrients, as well as by the limited alkalinity increase. Phosphate concentrations are below the detection limit of 1–2 μM in all samples analyzed (Table 8). Ammonia concentrations are generally low (from 10 to 110 μM), increasing from the surface to 195

mbsf and then decreasing slightly or remaining constant with increasing depth (Fig. 34).

Dissolved silica concentrations increase downcore from 470 μM at 8.5 mbsf to over 1200 μM at 546 mbsf, and then decrease sharply to 600 μM in the lowermost sample at 623 mbsf (Fig. 34). The increase in dissolved Si concentration with depth is consistent with continuous dissolution of biogenic silica; the dissolved Si decrease in the deepest interstitial water sample suggests precipitation and agrees with the discovery of chert in the

133
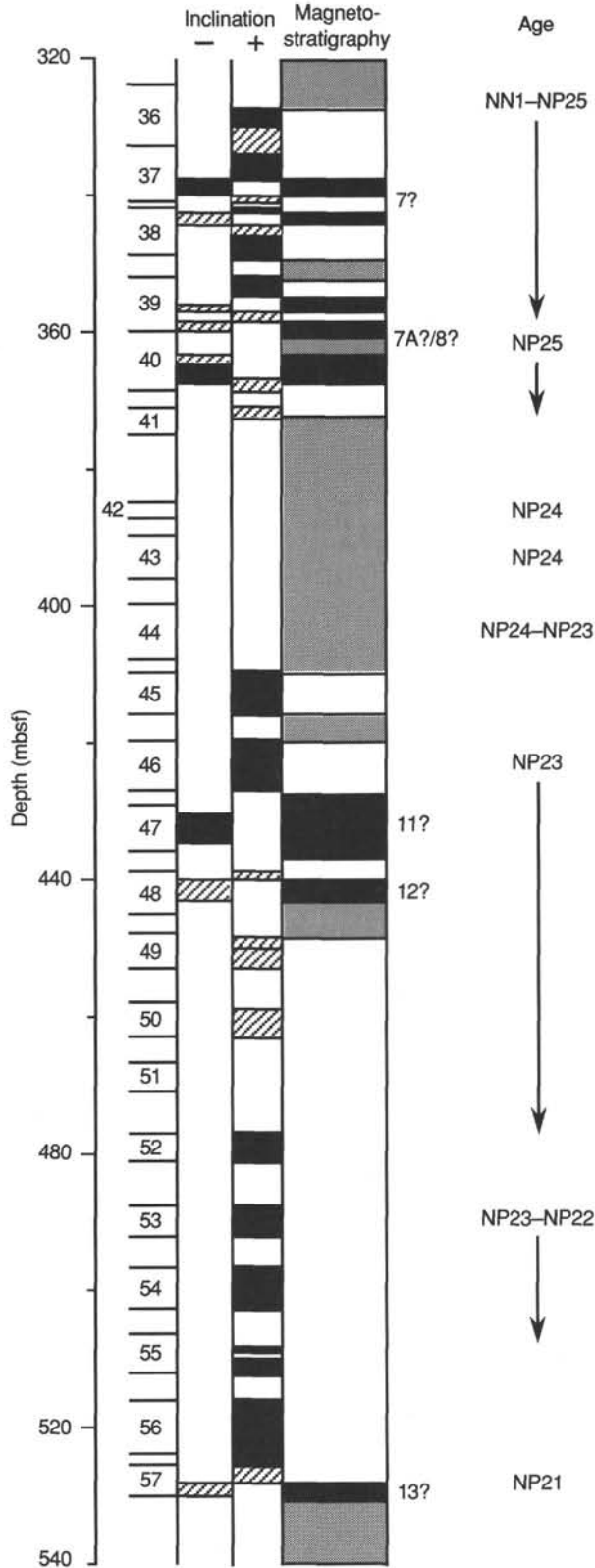
Figure 24. Record of intervals of consistent low positive and low negative inclinations, and corresponding magnetostratigraphy. Black sections of inclination column indicate confident polarity; hatched regions are probable, but uncertain; white sections are unknown. Black sections of magnetostratigraphy are normally polarized, white reversed, and hatched unknown.
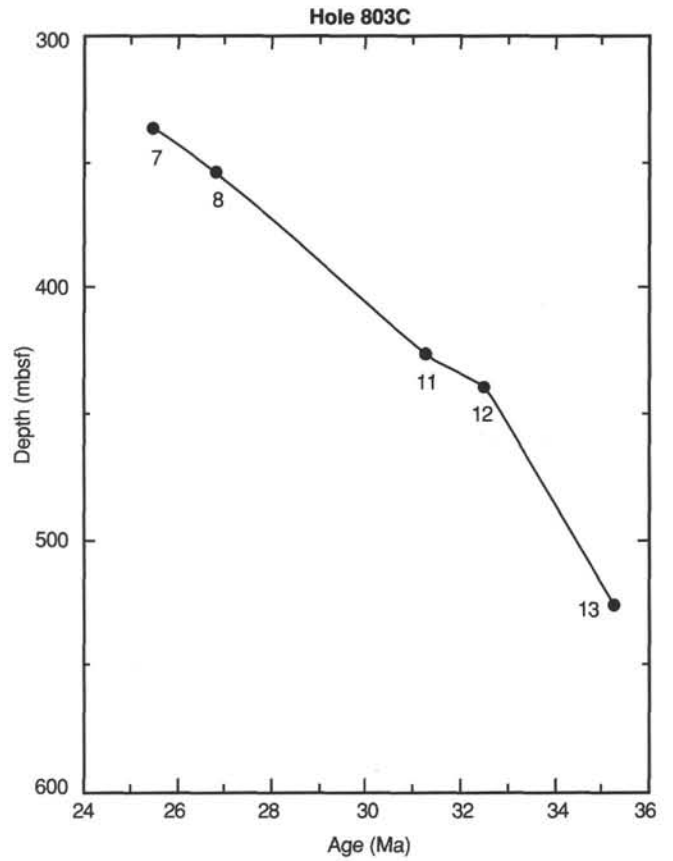
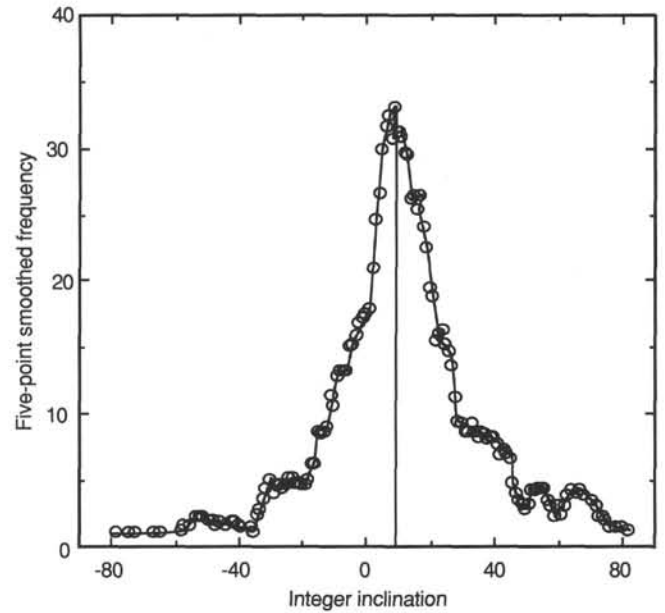Figure 25. Age vs. depth for the Oligocene. Chron numbers are indicated.

Figure 26. Frequency plot of inclination, smoothed over five integral divisions. The mode of the inclination at +9° is indicated.
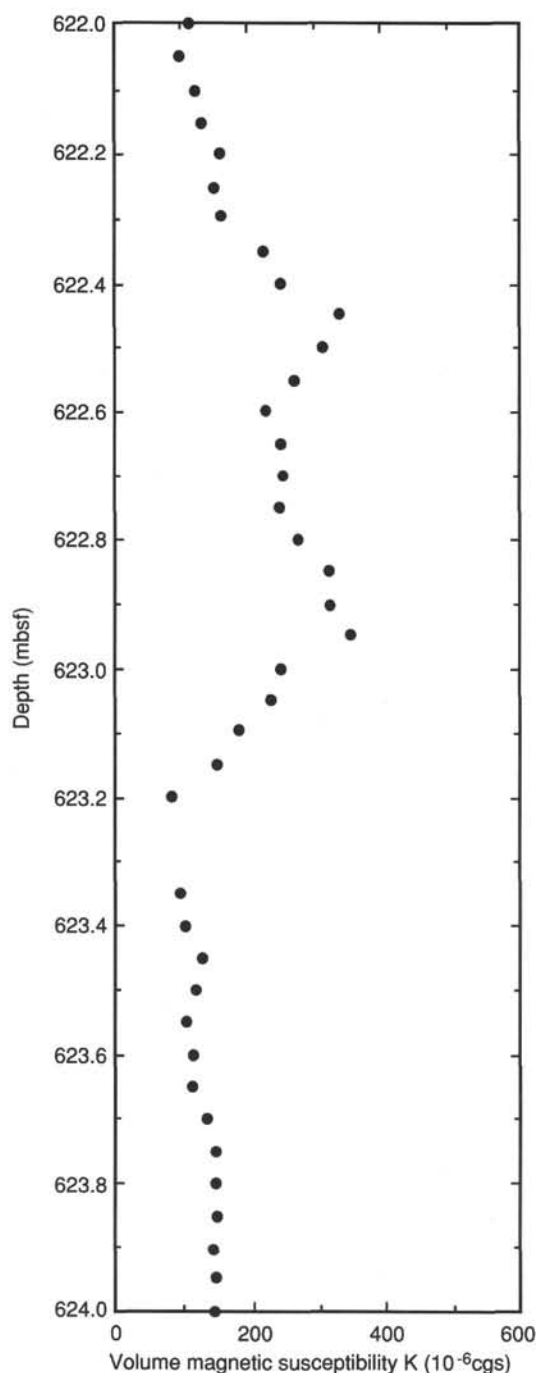
Figure 27. Volume magnetic susceptibility measurements from Section 130-803D-68X-1, which is thought to contain the Cretaceous/Tertiary boundary on the basis of nannofossil analyses.

lowermost sediments (see "Lithostratigraphy" section, this chapter). Manganese concentrations are below the detection limit ($<2-3$ μM) in samples from 8.5 to 546 mbsf, showing no enrichment with the increase in dissolved Si (Table 8). The elevated Mn concentration of 37 μM at 623 mbsf suggests the presence of a source in the sediments of Unit III or in the underlying basalt.

Calcium concentrations increase with depth, with an average gradient of 8 mM/100 m, and magnesium concentrations decrease with depth, with an average gradient of 4 mM/100 m (Fig. 34). Ca and Mg concentrations are correlated linearly (R^2

Table 6. Bio- and magnetostratigraphic events determined at Site 803.

Event	Depth (mbsf)	Age (Ma)
Hole 803A:		
FO *E. huxleyi* (N)	0.0–3.0	0.27
LO *P. lacunosa* (N)	3.0–8.0	0.46
LO *G. tosaensis* (F)	8.0–17.5	0.60
LO *N. reinholdii* (D)	8.0–17.5	0.65
LO *C. macintyrei* (N)	8.0–17.5	1.45
LO *R. praebergonii* var. *robusta* (D)	17.5–27.0	1.55
FO *P. doliolus* (D)	17.5–27.0	1.80
LO *D. brouweri* (N)	17.5–27.0	1.89
FO *G. truncatulinoides* (F)	17.5–27.0	1.90
LO *D. surculus* (N)	27.0–36.5	2.45
LO *G. multicamerata* (F)	17.5–27.0	2.90
LO *G. altispira* (F)	27.0–36.5	2.90
Kaena (T)	36.2–36.2	2.92
LO *Sphaeroidinellopsis* spp. (F)	36.5–46.0	3.00
FO *R. praebergonii* (D)	46.0–55.5	3.00
FO *Sphaeroidinella dehiscens* (F)	46.0–55.5	3.00
Mammoth (O)	39.25–39.25	3.18
LO *R. pseudoumbilica* (N)	46.0–46.8	3.56
Gauss (O)	43.4–43.4	3.40
Hole 803B:		
LO *P. lacunosa* (N)	4.3–5.0	0.46
LO *G. tosaensis* (F)	0.0–4.3	0.60
Brunhes (O)	7.7–7.7	0.73
Jaramillo (T)	9.9–9.9	0.91
Jaramillo (O)	12.2–12.2	0.98
LO *C. macintyrei* (N)	15.4–16.8	1.45
Olduvai (T)	16.9–16.9	1.66
Olduvai (O)	18.8–18.8	1.88
LO *D. brouweri* (N)	18.4–19.1	1.89
LO *D. pentaradiatus* (N)	25.8–26.4	2.35
Gauss (T)	27.4–27.4	2.47
LO *G. multicamerata* (F)	23.3–32.8	2.90
LO *G. altispira* (F)	32.8–42.3	2.90
Kaena (T)	35.4–35.4	2.92
Kaena (O)	36.2–36.2	2.99
LO *Sphaeroidinellopsis* spp. (F)	42.3–51.8	3.00
Mammoth (T)	37.4–37.4	3.08
Mammoth (O)	38.5–38.5	3.18
Gauss (O)	42.2–42.2	3.40
LO *R. pseudoumbilica* (N)	42.3–51.8	3.56
LO *C. acutus* (N)	51.8–61.3	4.60
Hole 803C:		
LO *P. prismatium* (R)	28.5–38.0	2.43
Gauss (T)	27.5–27.5	2.47
LO *S. peregrina* (R)	28.5–38.0	2.63
LO *D. tamalis* (N)	28.5–38.0	2.65
LO *G. altispira* (F)	28.5–38.0	2.90
Kaena (T)	33.4–33.4	2.92
Kaena (O)	34.3–34.3	2.99
LO *Sphaeroidinellopsis* spp. (F)	38.0–47.5	3.00
Mammoth (T)	35.5–35.5	3.08
Mammoth (O)	36.6–36.6	3.18
LO *P. fistula* (R)	38.0–47.5	3.27
LO *L. audax* (R)	38.0–47.5	3.34
Gauss (O)	40.5–40.5	3.40
LO *P. primalis* (F)	38.0–47.5	3.50
LO *P. doliolum* (R)	38.0–47.5	3.54
LO *R. pseudoumbilica* (N)	38.0–47.5	3.56
LO *S. pentas* (R)	38.0–47.5	3.78
FO *A. ypsilon* (R)	38.0–47.5	3.78
LO *S. berminghami* (R)	47.5–57.0	3.86
FO *S. pentas* (R)	57.0–66.5	4.25
LO *C. acutus* (N)	57.0–66.5	4.60
LO *S. omnitobus* (R)	57.0–66.5	4.75
LO *T. rugosus* (N)	67.4–68.6	4.90
LO *D. quinqueramus* (N)	68.6–71.6	5.00
LO *S. corona* (R)	66.5–76.0	5.05
FO *Sphaeroidinella dehiscens* s.l. (F)	57.0–66.5	5.10
FO *G. tumida* (F)	66.5–76.0	5.20
FO *P. spectabilis* (F)	66.5–76.0	5.20
LO *G. dehiscens* (F)	66.5–76.0	5.30
LO *A. tritubus* (R)	76.0–85.5	5.35

Table 6 (continued).

Event	Depth (mbsf)	Age (Ma)
Hole 803C: (Cont.)		
LO *N. miocenica* (D)	66.5–76.0	5.60
FO *P. primalis* (F)	85.5–95.0	5.80
FO *T. convexa* var. *aspinosa* (D)	85.5–95.0	6.10
LO *C. caepa* (R)	95.0–104.5	6.40
FO *S. omnitobus* (R)	114.0–123.5	6.40
LO *N. porteri* (D)	114.0–123.5	6.70
FO *Amaurolithus* spp. (N)	115.6–118.6	6.70
FO *N. miocenica* (D)	123.5–133.0	6.80
LO *D. hughesi* (R)	123.5–133.0	7.15
LO *N. porteri* (D)	114.0–123.5	7.20
FO *N. miocenica* (D)	123.5–133.0	7.30
LO *T. ontogenesis* (R)	123.5–133.0	7.45
LO *C. yabei* (R)	161.5–171.0	7.50
FO *D. quinqueramus/berggrenii* (N)	133.0–142.5	7.50
FO *A. tritubus* (R)	133.0–142.5	7.74
LO *D. laticonus* (R)	133.0–142.5	8.15
LO *B. miralestensis* (R)	142.5–152.0	8.15
LO *D. petterssoni* (R)	152.0–161.5	8.15
LO *C. vetustissimus* var. *javanicus* (D)	152.0–161.5	8.50
LO *C. yabei* (D)	161.5–171.0	8.60
LO *D. hamatus* (N)	172.7–174.0	8.70
LO *Catinaster* spp. (N)	176.0–177.0	8.80
LO *A. moronensis* (D)	171.0–180.5	8.90
FO *D. neohamatus* (N)	178.3–179.3	9.00
FO *N. acostaensis* (F)	171.0–180.5	10.20
LO *G. siakensis* (F)	180.5–190.0	10.40
FO *D. hamatus* (N)	187.0–188.5	10.50
LO *C. vetustissimus* var. *javanicus* (D)	152.0–161.5	10.70
LO *C. coscinodiscus* (D)	180.5–190.0	10.70
FO *C. coalitus* (N)	189.5–190.0	11.10
LO *A. moronensis* (D)	171.0–180.5	11.30
LO *G. fohsi lobata* (F)	199.5–209.0	11.50
LO *C. coscinodiscus* (D)	180.5–190.0	12.20
FO *G. fohsi lobata* (F)	218.5–228.0	13.10
LO *S. heteromorphus* (N)	218.0–221.5	13.60
FO *G. praefohsi* (F)	228.0–237.5	13.90
LO *G. peripheroronda* (F)	228.0–237.5	14.60
FO *G. peripheroacuta* (F)	228.0–237.5	14.90
LO *Praeorbulina sicana* (F)	228.0–237.5	14.90
Hole 803D:		
LO *P. lacunosa* (N)	2.5–12.0	0.46
Brunhes (O)	6.4–6.4	0.73
Jaramillo (T)	8.3–8.3	0.91
Jaramillo (O)	9.6–9.6	0.98
LO *C. macintyrei*	12.0–21.5	1.45
Olduvai (T)	15.6–15.6	1.66
Olduvai (O)	17.6–17.6	1.88
LO *D. brouweri* (N)	12.0–21.5	1.89
FO *G. truncatulinoides* (F)	12.0–21.5	1.90
LO *D. pentaradiatus* (N)	21.5–31.0	2.35
Gauss (T)	26.4–26.4	2.47
LO *D. tamalis* (N)	21.5–31.0	2.65
LO *G. multicamerata* (F)	21.5–31.0	2.90
LO *G. altispira* (F)	31.0–40.5	2.90
Kaena (T)	32.9–32.9	2.92
Kaena (O)	34.1–34.1	2.99
LO *Sphaeroidinellopsis* (F)	31.0–40.5	3.00
FO *Sphaeroidinella dehiscens* (F)	40.5–46.1	3.00
Mammoth (T)	35.1–35.1	3.08
FO *G. tosaensis* (F)	31.0–40.5	3.10
Mammoth (O)	36.5–36.5	3.18
LO *Sphenolithus* spp. (N)	31.0–40.5	3.45
LO *R. pseudoumbilica* (N)	40.5–46.1	3.56
LO *C. acutus* (N)	55.6–65.1	4.60
LO *D. quinqueramus* (N)	65.1–74.6	5.00
FO *G. tumida* (F)	65.1–74.6	5.20
FO *P. spectabilis* (F)	65.1–74.6	5.20
LO *G. dehiscens* (F)	74.6–84.1	5.30
FO *P. primalis* (F)	84.1–93.6	5.80
FO *Amaurolithus* spp. (N)	112.2–122.1	6.70
FO *G. plesiotumida* (F)	160.1–169.6	7.10
FO *D. quinqueramus* (N)	131.6–141.1	7.50
FO *S. berminghami* (R)	160.1–169.6	7.95

Table 6 (continued).

Event	Depth (mbsf)	Age (Ma)
Hole 803D: (Cont.)		
LO *S. wolffii* (R)	225.5–265.1	8.15
LO *D. hamatus* (N)	169.6–179.1	8.70
FO *D. hughesi* (R)	169.6–179.1	8.75
LO *C. japonica* (R)	179.1–188.6	10.15
FO *N. acostaensis* (F)	169.6–179.1	10.20
LO *G. siakensis* (F)	179.1–188.6	10.40
FO *D. hamatus* (N)	179.1–188.6	10.50
LO *C. coscinodiscus* (D)	198.1–207.6	10.70
LO *D. punctata* f. *hustedtii* (D)	198.1–207.6	10.70
LO *L. thomburgi* (R)	188.6–198.1	11.00
FO *C. coalitus* (N)	179.1–188.6	11.10
FO *H. cuneiformis* (D)	198.1–207.6	11.20
LO *G. fohsi lobata* (F)	198.1–207.6	11.50
LO *C. cornuta* (R)	198.1–207.6	11.75
LO *C. coscinodiscus* (D)	198.1–207.6	12.20
LO *D. punctata* f. *hustedtii* (D)	198.1–207.6	12.20
FO *H. cuneiformis* (D)	198.1–207.6	12.50
LO *C. nitescens* (N)	198.1–207.6	12.80
LO *C. lewisianus* (D)	217.1–226.8	12.90
FO *G. fohsi lobata* (F)	207.6–217.1	13.10
LO *C. floridanus* (N)	207.6–217.1	13.10
LO *C. lewisianus* (D)	217.1–226.8	13.50
LO *S. heteromorphus* (N)	217.1–226.8	13.60
FO *G. praefohsi* (F)	226.8–236.5	13.90
LO *G. peripheroronda* (F)	226.8–236.5	14.60
FO *G. peripheroacuta* (F)	237.3–241.0	14.90
LO *P. sicana* (F)	236.5–245.9	14.90
LO *A. californicus* (D)	245.9–255.5	15.00
FO *C. peplum* (D)	245.9–255.5	16.40
LO *C. stainforthi* (F)	245.9–255.5	17.40
LO *C. dissimilis* (F)	245.9–255.5	17.60
LO *S. wolffii* (R)	225.5–265.1	8.15
FO *S. heteromorphus* (N)	245.9–247.3	18.60
LO *C. elegans* (R)	245.9–255.5	18.70
LO *S. belemnos* (N)	245.9–247.3	18.80
LO *T. carinatus* (N)	245.9–247.3	19.50
LO *B. veniamini* (D)	255.5–265.1	19.90
FO *S. belemnos* (N)	255.5–255.7	20.00
LO *G. kugleri* (F)	255.5–265.1	21.80
LO *C. lewisianus* var. *rhomboides* (D)	255.5–265.1	22.50
FO *R. paleacea* (D)	313.0–322.7	22.70
FO *G. kugleri* (F)	313.0–322.7	23.70
LO *S. ciperoensis* (N)	322.7–332.3	25.20
LO *G. opima* (F)	342.0–351.6	28.20
LO *G. ampliapertura* (F)	457.5–467.2	32.80
LO *R. umbilica* (N)	486.6–496.3	33.80
LO *Pseudohastigerina* (F)	515.6–525.3	34.00
LO *E. formosa* (N)	515.6–525.3	34.90
LO *D. saipanensis* (N)	544.3–544.3	36.70
LO *D. barbadiensis* (N)	544.3–554.0	37.00
LO *C. reticulatum* (N)	544.3–554.0	37.70
LO *C. grandis* (N)	583.0–588.7	40.00
LO *D. bisectus/D. hesslandii* (N)	601.9–612.0	42.90
FO *R. umbilica* (N)	612.0–612.2	44.40

Notes: The depth uncertainty predominantly represents sampling intervals used. References for the age estimates are presented in the Explanatory Notes. N = nannofossil, F = foraminifer, D = diatom, R = radiolarian, FO = first occurrence, and LO = last occurrence. Magnetostratigraphic reversal boundaries followed by designation (T) or (O) refer to "termination" or "onset," respectively.

= 0.97) with a ΔCa/ΔMg ratio of approximately -2. The linear correlation is indicative of the conservative nature of these profiles, with Ca and Mg gradients controlled by reactions in the underlying basalt and diffusion between this boundary and overlying seawater (McDuff and Gieskes, 1976; McDuff, 1981). These gradients are larger than those observed at shallower Sites 288 and 289 (Leg 30) from the Ontong Java Plateau (Elderfield et al., 1982), presumably a result of the difference in sediment thickness between these sites (McDuff, 1981; for sedimentation
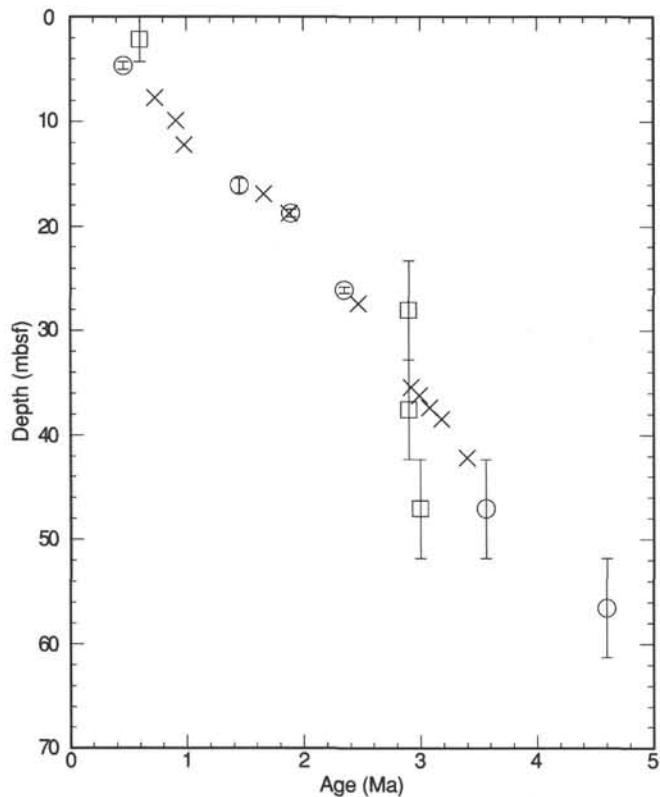
Figure 28. Age/depth relationships of bio- and magnetostratigraphic markers in Hole 803B. Error bars show sample interval uncertainties. Circle = nannofossils, square = foraminifers, and x = magnetostratigraphic reversal boundary.
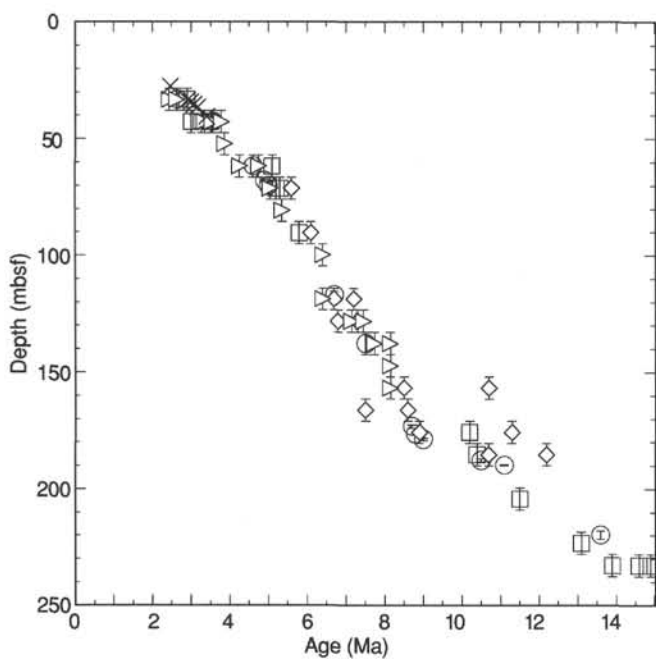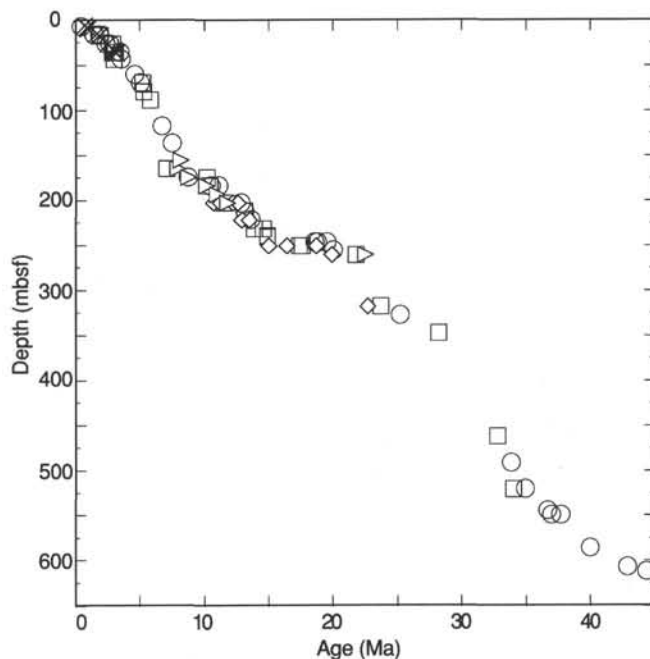

Figure 30. Age/depth relationships of bio- and magnetostratigraphic markers in Hole 803D. Symbol size approximates maximum sample interval uncertainties. Symbols are as in Figure 29.
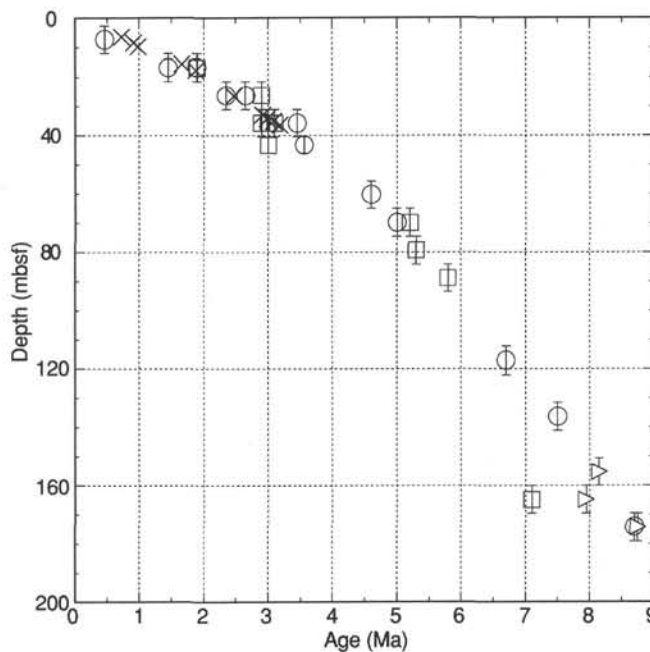

Figure 29. Age/depth relationships of bio- and magnetostratigraphic markers in Hole 803C. Error bars show sample interval uncertainties. Circle = nannofossil, square = foraminifers, diamond = diatom, triangle = radiolarian, and × = magnetostratigraphic reversal boundary.

Figure 31. Age/depth relationships of bio- and magnetostratigraphic markers in Hole 803D in the late Miocene through Holocene time interval. Error bars show sample interval uncertainties. Symbols are as in Figure 29.

Figure 32. Age/depth relationships of bio- and magnetostratigraphic markers in Hole 803D in the early late Miocene through early Miocene time interval. Error bars show sample interval uncertainties. Symbols are as in Figure 29.

Figure 33. Sedimentation rate history, Site 803.

Table 7. Estimated sedimentation rates from the Holocene through the middle Eocene interval, Site 803, and the control points determining those rates.

Control point	Depth (mbsf)	Age (Ma)	Rate (m/m.y.)
Hole 803A:			
Top section	0.00	0.00	
Mammoth (O)	39.25	3.18	12.3
Gauss (O)	43.40	3.40	18.9
Terminal depth	55.50	4.04	
Hole 803B:			
Top section	0.00	0.00	
Olduvai (O)	18.80	1.88	10.0
Gauss (O)	42.20	3.40	15.4
Terminal depth	61.30	4.64	
Hole 803C:			
Top section (top Core 1H)	19.00	1.86	
Gauss (T)	27.50	2.47	
Gauss (O)	40.50	3.40	14.0
LO *D. quinqueramus* (N)	69.90	5.00	18.4
LO *D. hamatus* (N)	173.40	8.70	28.0
LO *S. heteromorphus* (N)	220.25	13.60	9.6
Terminal depth	237.50	15.40	
Hole 803D:			
Top section	0.00	0.00	
Olduvai (O)	17.60	1.88	9.4
Mammoth (O)	36.50	3.18	14.5
LO *D. quinqueramus* (N)	69.85	5.00	18.3
LO *D. hamatus* (N)	174.35	8.70	28.2
FO *G. peripheroacuta* (F)	239.15	14.90	10.5
Young side hiatus	244.40	15.40	
Old side hiatus	244.40	19.50	
LO *T. carinatus* (N)	246.60	19.50	
FO *S. belemnos* (N)	255.50	20.00	17.8
Young side hiatus	255.50	20.00	
Old side hiatus	255.50	21.80	
LO *G. kugleri* (F)	260.30	21.80	30.3
FO *G. kugleri* (F)	317.85	23.70	30.3
LO *G. opima* (F)	346.80	28.20	6.4
LO *E. formosus* (N)	519.95	34.90	25.8
LO *C. grandis* (N)	585.90	40.00	12.9
FO *D. hesslandii* (N)	606.70	42.90	7.2
130-803D-67R-CC	621.80	45.01	

Notes: Age estimates for terminal depths of the different holes were obtained through linear extrapolation from the nearest shallower control point, using the sedimentation rates at that point. The Paleocene and Cretaceous sediments overlying the volcanic basement in Core 130-803D-68R are discussed in the "Biostratigraphy" section of this chapter. N = nannofossil, F = foraminifer, FO = first occurrence, and LO = last occurrence. Magnetostratigraphic reversal boundaries followed by the designation "T" or "O" refer to "termination" and "onset," respectively. See "Explanatory Notes" chapter (this volume) for a discussion of Leg 130 sedimentation rate philosophy.

Strontium concentrations increase with depth to a broad plateau (850–960 μM) below 150 m; they decrease slightly below 509 mbsf to 830 μM in the sample at 623 mbsf (Fig. 34). The gradient and broad maximum are typical of Sr profiles controlled by the release of Sr to interstitial water during recrystallization of biogenic calcite to inorganic calcite (e.g., Gieskes, 1981). Maximum Sr concentrations at this site are higher than those at Sites 288 and 289 (Leg 30) from the Ontong Java Plateau (Elderfield et al., 1982).

Lithium concentrations decrease from 21 μM near the surface to a minimum of 15 μM from 138 to 166 mbsf and then increase downcore with depth to ~35 μM in the deepest samples,

rates at these sites, see Andrews, Packham, et al., 1975, in particular the chapter on Site 288; and the "Sedimentation Rates" section of this chapter). There is no nonconservative behavior apparent in the Mg gradient from reaction with the thin (<1 cm) volcanic ash layer found at Section 130-803D-21H-2, 61 cm.

Table 8. Interstitial water geochemical data, Hole 803D.

Core, section, interval (cm)	Depth (mbsf)	pH	Alk. (mM)	Sal. (g/kg)	Cl⁻ (mM)	Na (mM)	SO₄²⁻ (mM)	PO₄³⁻ (μM)	NH₄⁺ (μM)	SiO₂ (μM)	Mn (μM)	Ca²⁺ (mM)	Mg²⁺ (mM)	Sr (μM)	Li (μM)	K (mM)	Rb (μM)
130-803D-																	
2H-4, 145–150	8.45	7.6	3.59	35.0	554	471	29.4	LD	12	472	LD	10.9	52.1	175	20.8	11.6	1.80
3H-4, 145–150	17.95	7.9	3.23	35.0	561	475	27.5	LD	24	543	LD	11.5	51.6	263	19.6	11.9	1.86
4H-4, 145–150	27.45	7.3	3.44	35.0	562	480	26.9	LD	29	543	LD	12.3	51.5	338	18.8	11.3	1.80
5H-4, 145–150	36.95	7.4	3.42	35.5	562	480	26.6	LD	39	575	LD	12.9	50.8	399	18.8	10.9	1.68
6H-4, 145–150	46.45	7.4	3.60	35.5	561	479	26.8	LD	43	615	LD	13.1	50.7	448	18.6	11.3	1.76
7H-4, 145–150	52.05	7.5	3.56	35.5	562	487	26.0	LD	51	652	LD	13.6	50.0	503	18.3	11.3	1.83
10H-4, 145–150	80.55	7.6	3.60	35.0	562	482	24.2	LD	68	723	LD	14.7	48.9	643	17.0	10.8	1.81
13H-4, 145–150	109.05	7.6	3.76	35.5	565	479	24.0	LD	87	763	LD	16.4	47.1	747	15.7	10.4	1.69
16H-4, 145–150	137.55	7.6	3.78	36.0	565	479	23.1	LD	96	853	LD	18.0	45.9	806	15.4	10.5	1.79
19H-4, 145–150	166.05	7.2	3.88	35.2	566	479	23.6	LD	99	838	LD	20.0	45.5	864	15.4	10.1	1.65
22H-4, 145–150	194.55	7.6	3.65	35.5	569	479	22.9	LD	114	903	LD	21.5	43.8	868	16.9	10.0	1.58
25X-3, 145–150	221.55	7.5	3.45	35.5	568	482	22.9	LD	105	861	LD	22.8	43.3	868	17.4	9.53	1.49
28X-3, 145–150	250.35	7.1	3.69	36.0	576	479	22.8	LD	105	907	LD	24.5	42.1	887	18.5	9.39	1.48
31X-2, 145–150	277.65	ND	ND	36.0	576	481	23.5	LD	ND	936	LD	26.7	41.3	921	18.6	9.03	ND
34X-4, 145–150	309.25	7.6	3.15	36.0	581	484	23.1	LD	ND	943	LD	28.6	40.5	953	17.7	8.91	1.40
37X-5, 140–150	339.70	7.6	2.89	39.0	586	483	23.7	LD	ND	959	LD	30.0	40.0	959	20.1	8.72	ND
40X-2, 140–150	364.20	7.6	2.68	36.5	584	490	22.9	LD	111	1016	LD	30.5	38.0	933	22.2	8.92	1.32
43X-3, 140–150	394.80	7.6	2.74	38.5	588	482	22.8	LD	ND	1018	LD	31.5	41.0	922	22.3	8.27	1.30
46X-4, 140–150	425.20	7.6	2.46	36.5	593	482	23.2	LD	111	1068	LD	35.3	37.4	931	22.3	8.13	1.28
49X-3, 140–150	452.20	ND	ND	35.5	593	492	24.1	ND	ND	1001	LD	35.3	38.5	884	26.3	8.28	ND
52X-1, 140–150	478.30	ND	ND	ND	594	487	23.2	ND	ND	1148	LD	38.5	36.3	920	28.2	7.93	ND
55X-2, 140–150	508.90	7.6	2.44	37.0	589	479	23.3	ND	97	1193	LD	40.4	35.0	932	29.0	7.40	1.08
59X-1, 140–150	545.70	ND	ND	38.0	596	484	22.5	ND	96	1264	LD	44.1	33.5	902	36.4	7.11	1.01
68R-1, 138–150	623.18	7.1	0.36	41.0	608	476	23.5	ND	98	594	37	61.7	26.4	830	34.5	4.31	0.47

Note: Alk. = alkalinity, Sal. = salinity, LD = concentrations lower than detection limit, and ND = not determined.

values greater than seawater concentrations (Fig. 34). There is no Li enrichment with the increase in dissolved silica, despite previous reports that biogenic silica dissolution is an important source of Li for interstitial waters (e.g., Gieskes, 1981). Potassium and rubidium concentrations both decrease with depth (Fig. 34) and are linearly correlated with the Ca increase with depth, suggesting that the decreases are related to uptake in low-temperature basalt alteration reactions.

CARBON GEOCHEMISTRY

Shipboard carbon geochemical analyses of samples from Site 803 included routine determinations of volatile hydrocarbons in sediments, inorganic carbon measurements on 481 samples, and 21 Rock-Eval analyses. The NCS elemental analyzer was inoperable during the time that we drilled Site 803; consequently, no shipboard nitrogen and sulphur data are available for this site. The methods used for these analyses are outlined in the "Explanatory Notes" chapter (this volume). Background and detailed descriptions are given by Emeis and Kvenvolden (1986). For safety considerations, hydrocarbon gases were routinely monitored by using the headspace technique. No volatile hydrocarbons were detected in the sediments of Site 803.

Inorganic carbon concentrations (see "Explanatory Notes" chapter, this volume) were determined on physical property samples. All data are summarized in Table 9 (microfiche, back pocket), and the carbonate values for Hole 803D are plotted vs. depth in Figure 10 (see "Lithostratigraphy" section, this volume). Unit I is characterized by very high carbonate concentrations ranging from 80% to 95%. Two ash layers, one at 146 and one at 181 mbsf (Sections 130-803D-17H-4 and -21H-2, respectively; Miocene), have low carbonate contents (≤10%; Fig. 10). In the opal-rich sediments of lithologic Unit II (middle and upper Eocene; Fig. 10), carbonate values range from 20% to 90% (Table 9). The Mesozoic sediments of Unit III have very low amounts of carbonate (<1%; Fig. 10 and Table 9).

Because the NCS analyzer was inoperable during Site 803, the contents of total organic carbon (TOC) in the sediments were estimated by means of the Rock-Eval pyrolysis technique (Espitalié et al., 1977). However, the measured amount of TOC in the sediments collected at Site 803 was always less than 0.05% (i.e., below the detection limit of the shipboard Rock-Eval pyrolysis). Because the TOC measurements made with the Rock-Eval pyrolysis are generally lower than those measured with the NCS analyzer (see "Site Summary" section, "Site 798" chapter, in Ingle, Suehiro, et al., 1990), the organic carbon contents will have to be verified independently by shore-based analyses.

PHYSICAL PROPERTIES

An intensive physical properties program was conducted at Site 803. Whole-round analyses consisted of measurements on the multisensor track (MST; see "Explanatory Notes" chapter, this volume) and needle-probe thermal conductivity. Split cores were used for vane shear, electrical resistivity, and velocity measurements and samples were taken for index properties analyses. This effort resulted in data that correlated well with the downhole logging data ("Logging" section, this chapter) and contributed to the construction of synthetic seismograms ("Seismic Stratigraphy" section, this chapter).

Multisensor Track

All sections of the four holes drilled at Site 803 were run through the MST. The GRAPE data for the upper 240 m in Holes 803C and 803D are presented in Figure 35. GRAPE data provide a good estimate of sediment bulk density and can be used as a means of making correlations between holes. The bars on Figure 35 denote the interval of the first section of each core, and the GRAPE profiles indicate that this section is often disturbed. Deeper sections also are affected in many of the cores, as demonstrated by the gradual increase of bulk density over several meters beneath many core breaks. This apparent disturbance problem is discussed further in the section on vane shear strength.

Despite the overprint of low-density spikes and the gradual rebound to undisturbed values on the profiles, other significant trends in the GRAPE data were observed. For example, the profiles show a trend of increasing GRAPE density from the seafloor to 100 mbsf. At this depth the profile changes character,
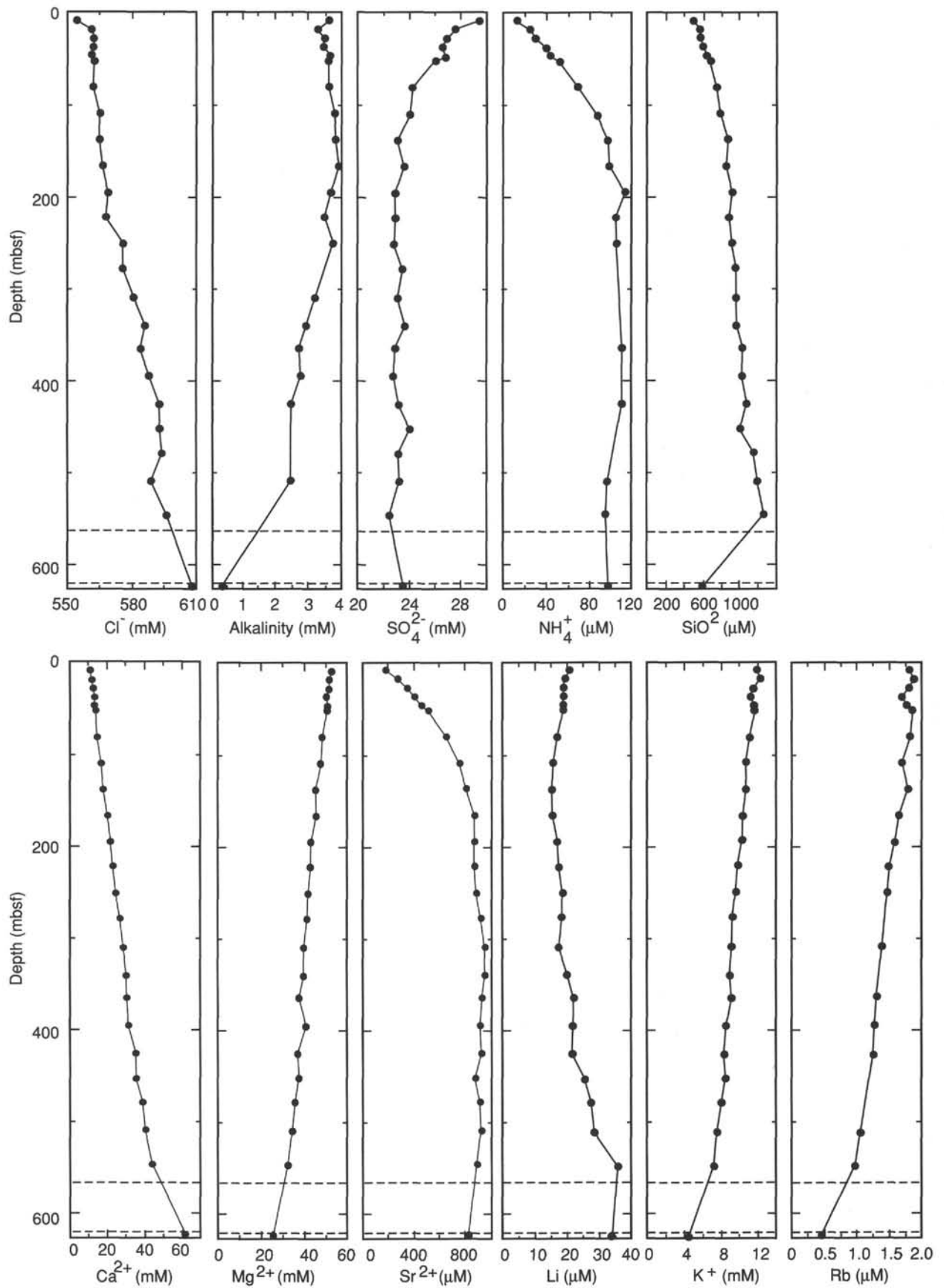
Figure 34. Interstitial water geochemical data vs. depth, Hole 803D. The two horizontal dashed lines represent depth boundaries between lithologic Units I, II, and III; the depth at the base of the plots is that of the contact of Unit III with basalt.
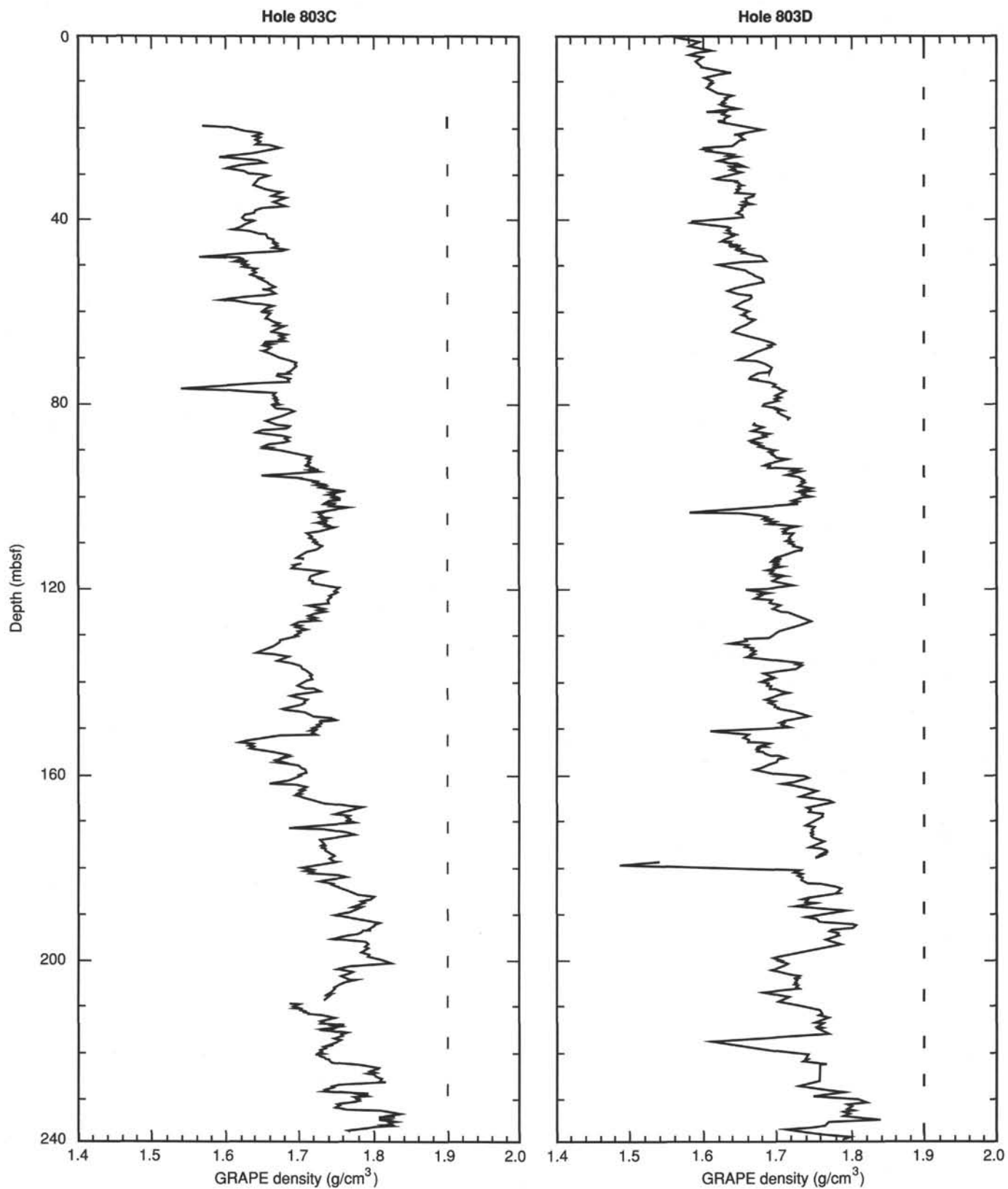
Figure 35. GRAPE bulk-density profiles in the upper 240 m of Holes 803C and 803D. Low-density spikes are the result of coring disturbance. Bars denote the depth interval of the first section of each core.

with average density decreasing to a depth near 160 mbsf. These trends appear to alternate downhole and may be related to alternations in calcium carbonate content, as discussed below with respect to the discrete index properties measurements. The quality of the GRAPE data deteriorates in XCB cores.

The MST also includes magnetic susceptibility and P-wave velocity sensors. The magnetic susceptibility data also provide a means of making correlations between holes and is discussed further in the "Paleomagnetism" section (this chapter). The P-wave velocity data have not been processed yet.

Thermal Conductivity

Thermal conductivity was measured in three sections per core in each hole at Site 803; values are given in Table 10. Profiles of thermal conductivity (W/m · K) with depth in Holes 803C and 803D are presented in Figure 36. Problems were encountered with calibrating the probes as well as with malfunctioning probes; thus, the data show considerable scatter. The thermal conductivity value is a mean calculated by averaging the thermal conductivities measured on the third, fourth, and fifth sections of each core (see "Explanatory Notes" chapter, this volume). In general, thermal conductivity values increase downhole, corresponding to decreasing porosity. This crude relationship is shown in Figure 37, which presents a plot of thermal conductivity vs. porosity.

Vane Shear Strength

Undrained shear strength was measured using a motorized minivane in split core sections (see the procedures outlined in the "Explanatory Notes" chapter, this volume). Vane measurements were made in APC cores and in competent biscuits of XCB cores until the sediment became too stiff. In many cases, progressive cracking of the sediment occurred during the test, thus negating the assumption that a cylinder of sediment is uniformly sheared about the axis of the vane. Where failure was dominated by cracking, the post-peak values could not be interpreted as residual strengths (Pyle, 1984).

Drilling-induced disturbance in the cores has a considerable effect on the peak shear strength values. As discussed previously with respect to the GRAPE data, the upper section(s) of many of the piston cores are disturbed. This is evident in the GRAPE profiles from core-length cycles consisting of a low-density spike followed by a gradual increase in the upper few sections to "undisturbed" values (recognizing that disturbance occurs during the coring process). It might be expected that the peak strength values obtained in the upper sections of those disturbed cores would be lower than those obtained in the deeper sections of each core. Examination of the peak strength data on a core-by-core basis, however, indicates that, in some cases, the first section has a peak strength higher than that measured for deeper sections in the core. Figure 38 shows peak shear strength vs. section number for Hole 803D. In most cases, the first section has a higher shear strength than the second and third sections, with the strength values increasing again in the last three to four sections of each core.

It is possible the soil skeleton in the upper section is compressed, resulting in an increase of the friction component of the shear strength. Thus, shear strength is actually increased despite disturbance. This conclusion, however, seems at odds with the GRAPE data, which show a low-density spike in the upper section(s) of most cores. Examination of the upper section on each core shows water and soupy mud between the sediment and liner. It appears that water trapped between the piston and the sediment surface has been forced between the core and the liner, while also resulting in some compression of the sediment in the upper sections. The water between the liner and sediment explains the low GRAPE density values; compression of the

Table 10. Thermal conductivity data, Site 803.

Depth (mbsf)	Thermal conductivity (W/m · K)
Hole 803A:	
7.8	1.09
17.2	1.16
26.6	1.14
45.7	1.09
55.2	1.07
Hole 803B:	
22.4	1.10
31.8	1.16
41.4	1.06
52.4	1.32
61.8	1.12
71.4	1.12
79.4	1.25
90.4	1.22
99.9	1.33
109.4	1.40
120.4	1.43
128.4	1.37
137.9	1.39
147.4	1.41
156.9	1.27
166.4	1.22
175.9	1.48
185.4	1.46
194.9	1.42
213.9	1.46
223.4	1.36
232.9	1.41
Hole 803C:	
6.6	1.09
15.4	1.14
26.4	1.21
34.4	1.28
45.4	1.21
51.0	1.38
60.4	1.42
70.0	1.30
79.5	1.34
89.0	1.30
98.5	1.35
108.0	1.30
117.5	1.33
127.0	1.28
136.5	1.43
174.5	1.33
193.5	1.30
212.5	1.45

sediment explains the higher vane shear strength values measured.

Profiles of undrained shear strength for Holes 803B, 803C, and 803D are presented in Figure 39. Residual strengths were obtained where cracking did not dominate failure. Both peak and residual values are given in Table 11 (microfiche, back pocket). Measurements in Holes 803C and 803D were performed until the sediment was judged to be too stiff, near 240 mbsf. The low shear strengths observed for these sediments, relative to other marine sediments, reflect their lack of cohesion and the associated susceptibility to coring disturbance (Lee, 1982). Shear strengths are slightly higher in the ooze from approximately 15 to 60 mbsf, corresponding to a larger mean grain size caused by an increase in foraminifer content (see "Lithostratigraphy" section, this chapter). This relationship of higher shear strength with increased preservation of foraminifers has also been shown in vane shear strength data from box cores obtained on the Ontong Java Plateau (Berger and Johnson, 1976).
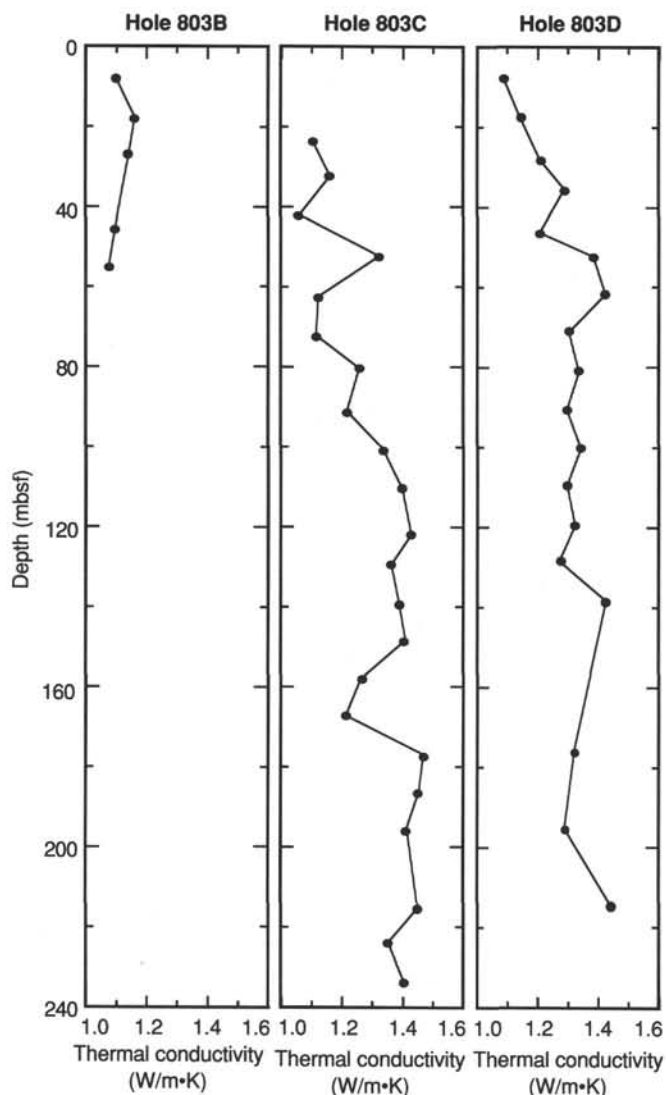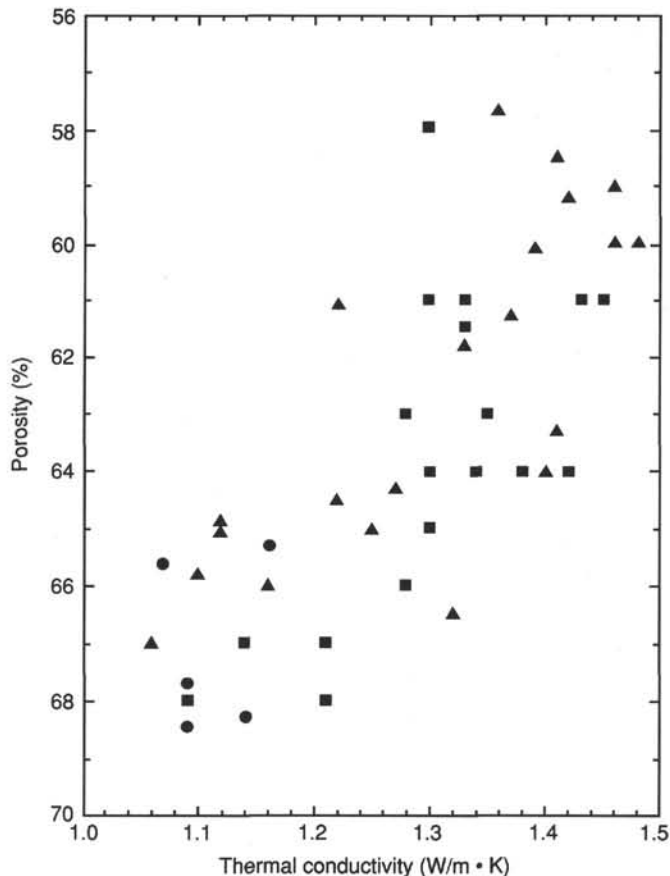
Figure 36. Thermal conductivity vs. depth, Holes 803B, 803C, and 803D.

Figure 37. Thermal conductivity vs. porosity, Site 803. Dot = Hole 803B, triangle = Hole 803C, and square = Hole 803D.

Peak shear strengths increase just below 150 mbsf, indicating the onset of lithification. The transition zone between ooze and chalk has been defined as 210–220 mbsf (see "Lithostratigraphy" section, this chapter). The observed change in shear strength could be caused by either chemical (the onset of cementation) or mechanical (the interaction of granular particles and higher friction effects after reaching a critical porosity) effects.

Formation Factor

Electrical resistivity measurements were made in Holes 803A, 803B, and 803C using a four-electrode arrangement in split cores (see the procedures outlined in the "Explanatory Notes" chapter, this volume). The probe system malfunctioned during measurements in Hole 803D, giving unstable readings of resistivity. This problem was caused by a leak in the epoxy holding the probes. Because of the high-resolution velocity measurements and the extensive index properties sampling program, time was not available to fix the probes and measurements were stopped at this point. Furthermore, analyses of the data showed variation that could not be correlated between holes but seemed, instead, to be operator dependent. In light of these problems,

and the fact that good downhole resistivity logs were obtained (see "Logging" section, this chapter), the electrical resistivity data obtained from the probe measurements are not presented.

Velocity

Compressional wave (P-wave) velocities were measured on split cores in two directions to give vertical (parallel to core axis) and horizontal (perpendicular to core axis) velocity and attenuation. Measurements were performed with the Dalhousie sediment velocimeter (DSV; see "Explanatory Notes" chapter, this volume) at a sample frequency of two per section in APC cores. The system used with this apparatus provides storage of waveforms to allow for subsequent attenuation analysis. This will be performed as a shore-based project. The Hamilton Frame apparatus was used to measure velocity in lithified sediment. In general, the lithified sediment at Site 803 withstood the processes of XCB and RCB coring quite well; thus, Hamilton Frame measurements could generally be conducted at a rate of one per section, with velocities measured in both the vertical and horizontal directions. Waveform data from the Hamilton Frame were also captured by the DSV oscilloscope, allowing the possibility of future analysis for attenuation.

Profiles of vertical and horizontal P-wave velocity with depth for Holes 803C and 803D are shown in Figure 40. Table 12 (microfiche, back pocket) presents the velocity data for all Site 803 holes. Velocities remain close to 1550 m/s in the upper 150 m of sediment at Site 803, with some slight variations caused by changes in the carbonate content and grain size. Detailed examination of these trends must await shore-based investigation of
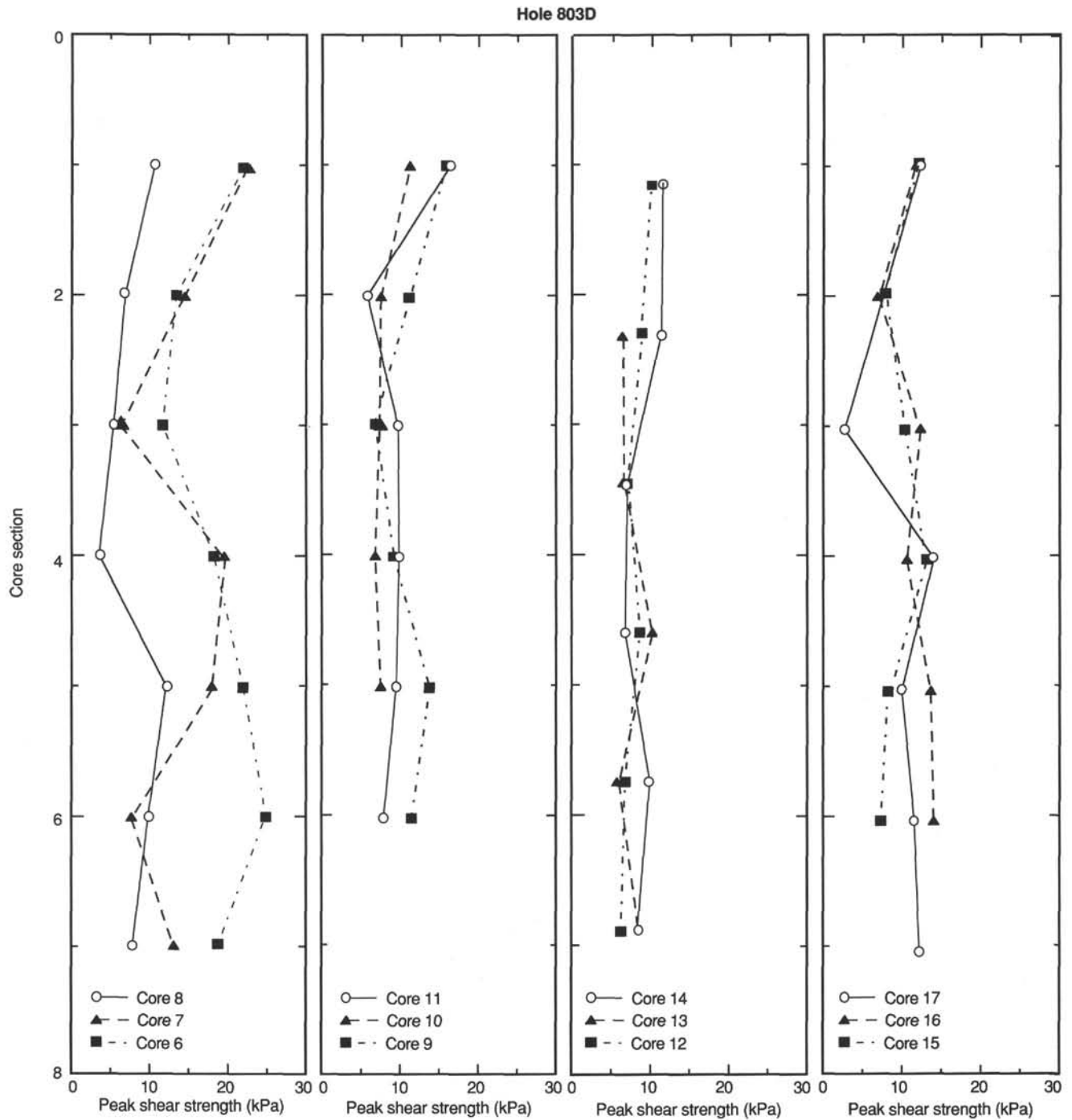
Hole 803D

Figure 38. Vane shear strength vs. section number for Cores 130-803D-6H through -17X.

grain size, carbonate content, crystallinity, and isotopes. In many cases, the relationship between carbonate content, grain size, and velocity is not clear.

Velocities increased near 175 mbsf, indicating the onset of lithification. Although the transition between ooze and chalk has been defined at 210–220 mbsf, velocity is a sensitive indicator of increases in rigidity of the sediment framework. The depth of increase of *P*-wave velocity corresponds to the increase in vane shear strength. Variations in velocity over the next 100 m probably reflect changes in the degree of cementation. Near the

bottom of Hole 803D, several intervals of radiolarites occur. These highly siliceous layers result in velocities much lower (ca. 1500 m/s) than the surrounding carbonate sequences, which have velocities greater than 2000 m/s. The last measurement in Hole 803D was obtained on basalt, thus the sudden increase in velocity to 4300 m/s.

Laboratory velocity data are compared with log sonic velocity data in the "Logging" section of this chapter. Laboratory velocities were expected to be lower than log velocities because of the removal of overburden and coring disturbance, and this re-
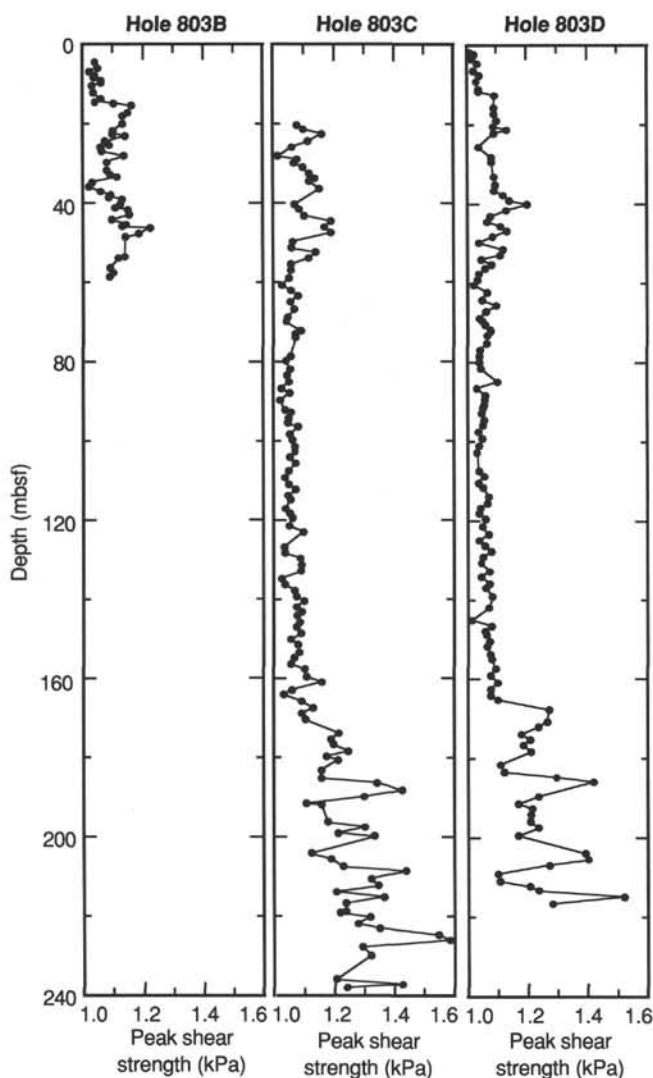
Figure 39. Laboratory vane peak shear strength vs. depth, Site 803.

lationship was seen. Most of the trends in the laboratory data are echoed in the log data, however, lending credibility to both data sets.

Index Properties

The index properties calculated from the weight and volume data for Site 803 samples are wet-bulk density, grain density, water content (based on dry weight), porosity, and dry-bulk density (see "Explanatory Notes" chapter, this volume). These data are presented in Table 13 (microfiche, back pocket).

Because of the high calcite content of these sediments (generally >85%; see Fig. 10), the grain density is generally constant with depth, with values near 2.7 g/cm³. The bulk density of calcareous sediment is affected by the grain shape, level of dissolution, grain size, stress history, and overburden pressure (Lee, 1982). A preliminary comparison of bulk-density profiles with calcium carbonate content data indicates a strong relationship. In fact, the bulk-density profiles closely mimic the carbonate profiles for most of the Site 803 sediments.

Laboratory bulk-density profiles were compared with log bulk-density results (see "Logging" section, this chapter). These data show a closer relationship than the laboratory and logging

velocity data, and correlation between the two data sets is exceptionally good.

Bulk-density data for Holes 803C and 803D are shown vs. depth in Figure 41. Porosity and water content are presented in Figures 42 and 43, respectively. In the upper 20 m of the sediment column, there are rapid changes in index properties, associated with consolidation of young sediment. Over this interval, bulk density increases from 1.45 g/cm³ near the seafloor to 1.55 g/cm³ at 20 mbsf, whereas water content decreases from 110% to 75% over the same interval. Between 20 and 110 mbsf, the gradients are not as strong, with bulk density increasing gradually from values of 1.55 g/cm³ at 20 mbsf to 1.65 gcm³ at 110 mbsf.

Near 110 mbsf, there is a change in the profile from the trend usually associated with a normally consolidating sediment sequence. Over the interval of approximately 110–155 mbsf, bulk density decreases slightly. This phenomenon is associated with a major dissolution event (see "Biostratigraphy" section, this chapter) and corresponds to a decrease in carbonate content over this interval. The relationship between density and dissolution has previously been documented for carbonates from the equatorial Pacific (Mayer et al., 1986). From 155 to 210 mbsf, a steady increase in bulk density corresponds to an increase in carbonate content, the two curves again showing similar trends. One interesting anomaly in this interval is an ash layer, measured in both Holes 803C and 803D. Bulk densities in the ash layer drop to near 1.5 g/cm³, whereas porosity jumps to 75% and water content to 110%. Bulk densities decrease again over the interval from 195 to 210 mbsf, again corresponding to a decrease in carbonate content.

Bulk density begins to increase rapidly with increasing depth near 210 mbsf, from approximately 1.6 to 1.85 g/cm³ at 255 mbsf. Porosity decreases from 62% to 50% and water content decreases from 53% to 40% over this interval. This corresponds to the zone of increasing cementation. Bulk density increases gradually (from 1.85 to 1.95 g/cm³) down to 560 mbsf, with some variation caused by the slight changes in carbonate content. Porosity and water content show corresponding decreases over this interval.

Changes in sediment type between 595 to 640 mbsf result in extremes in index properties over this interval. A radiolarite, measured at 598 mbsf, has a bulk-density value of 1.46 g/cm³. Water content and porosity increase sharply at this depth, and grain density is 2.24 g/cm³. These results agree with those of equatorial Pacific sediments that have high radiolarian contents (Mayer et al., 1986). The remaining measurements, except for the last one in Hole 803D, were on lithified red clay. The final measurement in Hole 803D, at 632 mbsf, is on a basalt, yielding a bulk density of 2.71 g/cm³, a grain density of 2.82 g/cm³, and a porosity of 2.4%.

If compaction of the sediment in the upper section of core is occurring, as suggested by the vane shear data, a decrease in discrete sample porosities would also be expected in this section. Examination of the index properties data on a core-by-core basis shows this to be true for many cores. The first section of each of those cores has a lower porosity, with the next few sections having higher porosities, below which the porosity returns to the general trend of the sediment interval containing that particular core.

Summary

The intensive physical properties program conducted at Site 803 has resulted in a suite of data that correlates well with the log data and that can be used with confidence in the construction of synthetic seismograms. This chapter describes the major trends in the physical properties data. Detailed investigation of
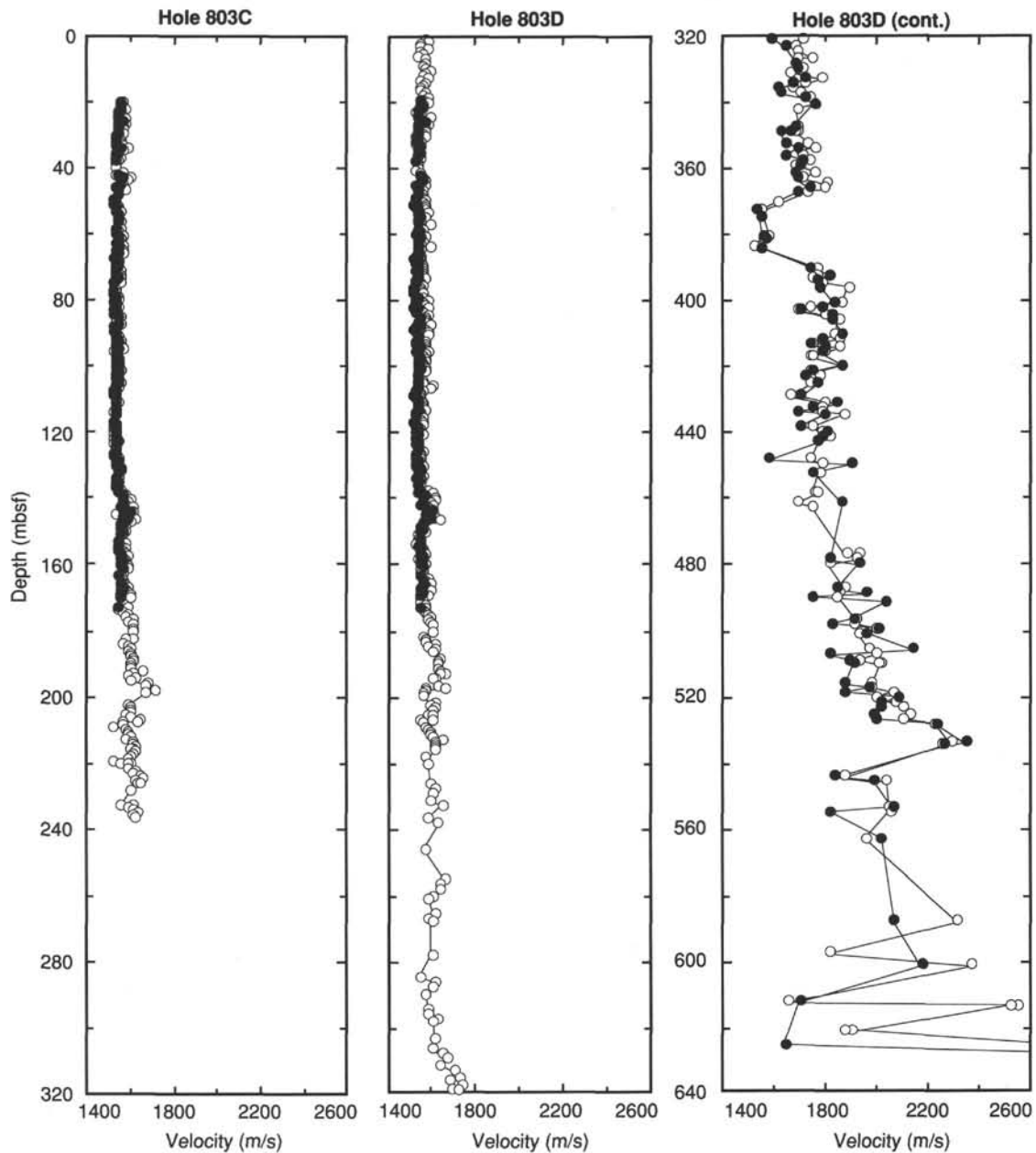
Figure 40. Laboratory compressional wave velocity (m/s) vs. depth in Holes 803C (0–320 mbsf) and 803D (0–640 mbsf). Filled circles = vertical measurements (parallel to core axis); open circles = horizontal measurements (perpendicular to core axis).

the physical causes of these trends, and their relationship to paleoceanographic events, will be conducted on shore.

Coring disturbance in the upper sections of many cores is clearly evidenced by the GRAPE and vane shear strength data. Despite the influence of this disturbance on the profiles of the various physical properties measured, correlation of physical properties trends between holes and with trends in calcium carbonate and grain size is possible.

IGNEOUS PETROLOGY

Introduction

Tholeiitic basalts were encountered in Hole 803D at a depth of 631.0 mbsf below brown Albian clay in Section 130-803D-

68R-4. Note that this depth does not correspond to the curated depth of 626.3 mbsf but refers to the depth at which the drillers "felt" basement. Coring of basalt continued until drilling was stopped at 656.0 mbsf in Core 130-803D-71R; recovery averaged 38% (Fig. 44). The rocks mainly consist of successive pillow lavas. They are predominantly nonvesicular, hypocrystalline, fine-grained, aphyric to very sparsely plagioclase-, clinopyroxene-, or olivine-phyric; rare, large phenocrysts of plagioclase and clinopyroxene as large as 0.5–1.0 cm across were observed in three instances (Sections 130-803D-69R-1, Piece 9; -70R-3, Piece 6; and -71R-1, Piece 2). Alteration ranges from severe to moderate within pillow interiors, where the development of smectite and other secondary minerals typically gives a mottled brown and gray, or blotchy reddish brown and gray appearance. Pillow rims
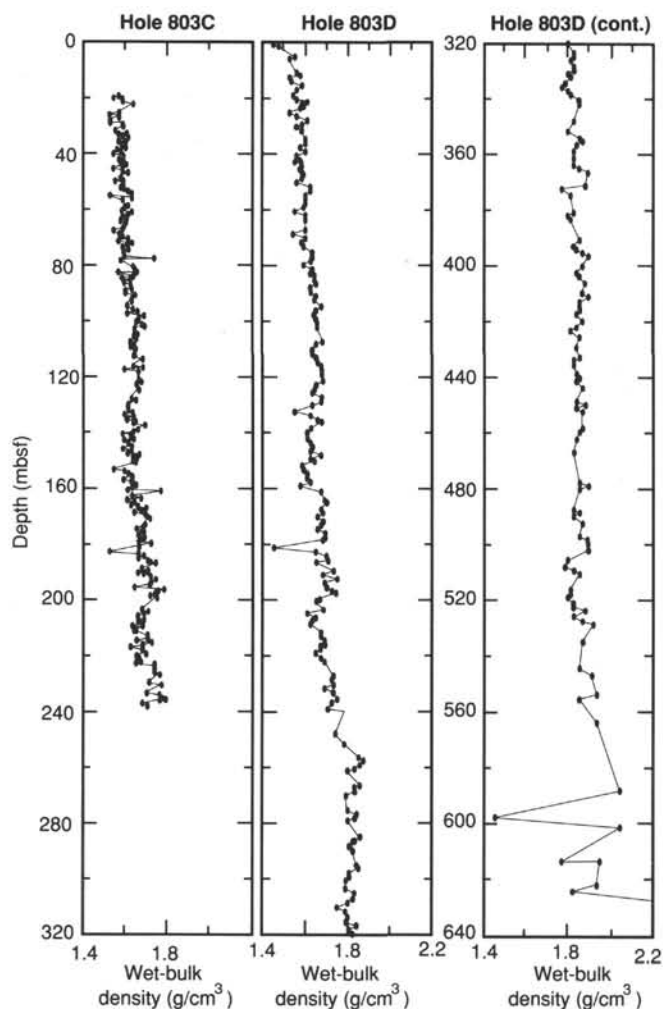
Figure 41. Laboratory bulk density (g/cm³) vs. depth in Holes 803C (0–320 mbsf) and 803D (0–640 mbsf).

Figure 42. Laboratory porosity (%) vs. depth in Holes 803C (0–320 mbsf) and 803D (0–640 mbsf).

tend to be much less altered, and although most glass is at least partially devitrified, small amounts of fresh glass are present on many rims.

In general, alteration decreases slightly going downward in the hole. The most altered interval is Section 130-803D-68R-4, directly below the sediment contact. At the contact, the basalt is capped by a flat, ~2-cm-thick hydrothermal(?) layer consisting of several alternating bands of calcite and a bright green clay mineral, probably celadonite. Fractures and calcite-filled veins (0.5–5 mm thick) are fairly numerous throughout the basalt section and mainly appear to represent remnants of cooling cracks in individual pillows; basalt alteration tends to be more intense near such veins.

Several thin (< 20 cm thick) interpillow limestones are present. Of these, several are best described as breccias, as they contain variable proportions of bright to dark green lapilli-size clasts (celadonite?), which appear to be completely altered fragments of spalled-off basaltic glass. Microfossils in these limestones, although present, have been recrystallized beyond specific recognition, probably by baking during emplacement of the overlying lava.

The entire basalt section at Site 803 roughly corresponds to a single stratigraphic "subunit" at Site 807, given that three of the subunits at Site 807 are thicker than the entire basement interval cored at Site 803. Although the basalts are similar macroscopically throughout the recovered section, the cores were divided

into nine subdivisions (as opposed to "subunits" at Site 807) on the basis of intercalated limestones or breccias, which suggest a passage of time greater than that for a single eruption. These subdivisions are numbered 1 through 9 below. The distribution of these subdivisions relative to core recovered is shown in Figure 44.

Following ODP guidelines, it was possible to divide the cores on an even finer scale (e.g., 9a, 9b, etc.) according to the presence of glassy or chilled pillow tops or changes in phenocryst type or abundance. Several of these secondary subdivisions probably represent individual pillows. This classification does not necessarily imply that all of the secondary subdivisions within a given primary subdivision reflect the same eruption; only that definitive macroscopic evidence to the contrary was lacking in the recovered portion of the core. Indeed, chemical data indicate that some of the secondary subdivisions comprising individual primary subdivisions are derived from different magmas. Detailed visual core descriptions with subdivision and secondary subdivision boundaries are appended at the end of this chapter.

Subdivision Thickness, Designation, and Alteration Summary

Subdivision 1: 150 cm thick (Sections 130-803D-68R-4, 7 cm, to -69R-1, 110 cm); aphyric, very fine-grained, nonvesicular basalt; highly to intensely altered.
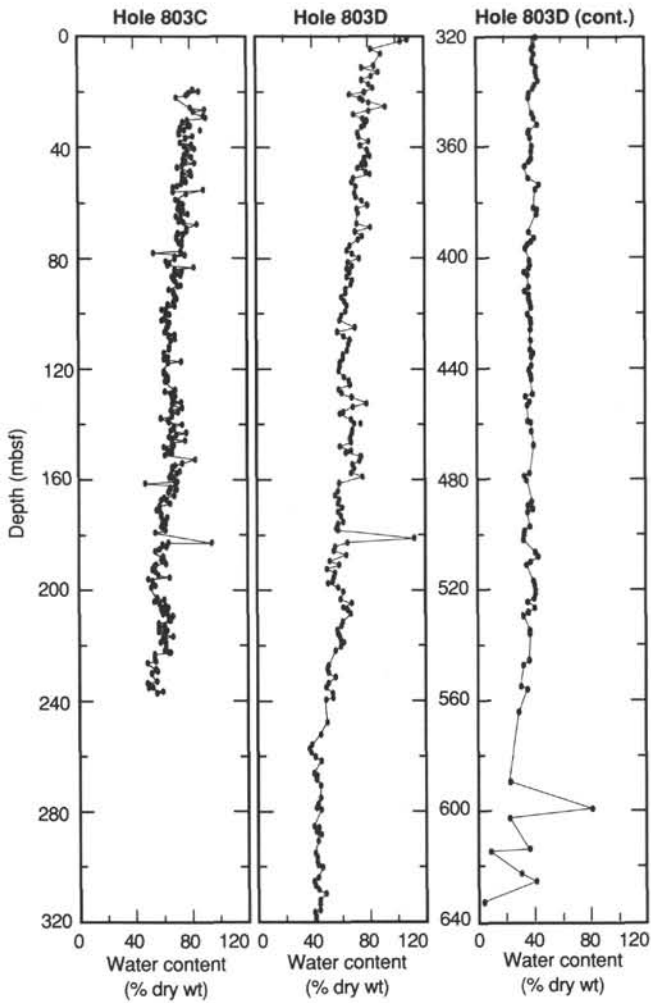
Figure 43. Laboratory water content (% dry wt) vs. depth in Holes 803C (0–320 mbsf) and 803D (0–640 mbsf).

Subdivision 2: 53 cm thick (Sections 130-803D-69R-1, 120 cm, to -69R-2, 40 cm); aphyric, very fine-grained, nonvesicular basalt with glassy pillow rims; alteration high overall but less than Subdivision 1.

Subdivision 3: 40 cm thick (Sections 130-803D-69R-2, 50 cm, to -69R-2, 90 cm); aphyric, fine-grained, nonvesicular basalt with glassy pillow rim; highly altered.

Subdivision 4: 90 cm thick (Cores 130-803D-69R-2, 110 cm, to -69R-3, 50 cm); aphyric, fine-grained, nonvesicular basalt with glassy pillow rims to sparsely plagioclase-olivine(?) phyric basalt; highly to moderately altered interiors, fairly fresh rims.

Subdivision 5: 193 cm thick (Sections 130-803D-69R-3, 70 cm, to -70R-1, 90 cm); aphyric to sparsely plagioclase phyric to sparsely clinopyroxene (?) phyric, nonvesicular basalt; alteration varies from moderate to high in interiors with fresher pillow rims.

Subdivision 6: 18 cm thick (Sections 130-803D-70R-1, 100–120 cm); aphyric, very fine-grained, nonvesicular basalt; very highly to moderately altered, decreasing toward pillow rim.

Subdivision 7: 23 cm thick (Sections 130-803D-70R-1, 130 cm, to -70R-2, 10 cm); aphyric, very fine-grained, nonvesicular basalt; very highly to moderately altered, decreasing toward pillow rims.

Subdivision 8: 88 cm thick (Sections 130-803D-70R-2, 20–110 cm); aphyric, very fine-grained basalt; moderately to very
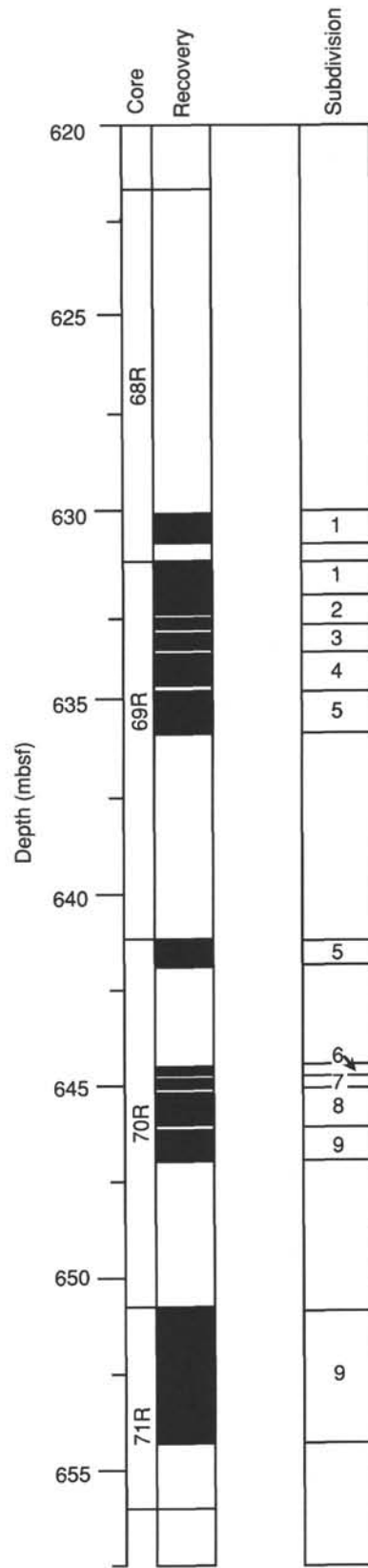

Figure 44. Basalt recovery at Site 803, showing proportion of material recovered (in black) and division into nine main subdivisions.

highly altered near veins and fractures; one calcite-filled amygdule (~1 mm) near bottom.

Subdivision 9: 454 cm thick (Sections 130-803D-70R-2, 140 cm, to -71R-3, 80 cm); aphyric to sparsely clinopyroxene-plagioclase phyric basalt; rare subhedral phenocrysts of plagioclase up to 8 mm across in 9b (Section 130-803D-71R-1, Piece 2); 9b also contains rare, 1-4-mm-thick, calcite-filled amygdules at top and bottom; highly to moderately altered with patches of less altered massive material.

Note that the "curated" recovery is 11.09 m whereas the actual amount of basement recovery was 9.59 m. This discrepancy results from "curated" recovery figure including the spacers that separate the pieces of basalt.

Petrography

Thin-section examination of pillow interiors from several subdivisions confirmed their fine-grained, typically aphyric, hypocrystalline nature (see attached thin-section descriptions at the end of this book in Section 5). Phenocrysts observed include rare subhedral (<0.5 mm across) pseudomorphs of olivine in Section 130-803D-68R-4, 45-47 cm, and rare, fairly fresh, 3-5 mm thick, subhedral to anhedral, compositionally zoned clinopyroxene in Sample 130-803D-70R-3, 60-62 cm; the clinopyroxene is notable for numerous, fresh inclusions of basaltic glass up to 0.05 mm across. A large, fairly fresh (1 cm thick) subhedral plagioclase crystal occurs in Sample 130-803D-69R-1, 87-90 cm. Once-glassy groundmasses are generally altered to dark, cryptocrystalline material, probably smectite; plagioclase laths, sometimes skeletal, also are somewhat altered, and groundmass clinopyroxene grains often are partially replaced by brownish to reddish clays. Despite alteration, textures are well preserved; they are mainly intersertal (hyalophitic) and are subordinately intergranular or subophitic. The most noteworthy petrographic aspect of these rocks, however, is the scarcity of phenocryst phases.

Shipboard Chemical Analyses

Major and trace elements were determined by X-ray fluorescence spectrometry (see "Explanatory Notes" chapter, this volume) on 13 specimens from pillow interiors representing most of the subdivisions; water loss on ignition (LOI) was determined gravimetrically on the same samples. Data are presented in Table 14. The basalts are all fairly evolved (Mg-number = 35-53), mildly quartz- to olivine-normative tholeiites. They possess MORB-like Ti/Zr (111-116 vs. ~100 for normal MORB) and Zr/Y (2.9-3.5 vs. ~3.0 for normal MORB) ratios, but rather high Sr (145-197 vs. 100-120 ppm for normal MORB), CaO (11.07-13.66 wt%), and K_2O (0.30-1.44 wt%) concentrations. Zr/Nb ratios are distinctly low compared with normal MORB (15-17 vs. ~30 or more), as are TiO_2, Zr, and Y abundances for the level of differentiation indicated by Mg-number (Figs. 45 and 46).

In general, the major elements and compatible trace elements do not display simple interelement relationships, suggesting that the rocks may represent more than one liquid line of descent or parental magma. For example, Fe_2O_3 and MgO do not define a single trend; nor do Ni and Cr vary coherently with Mg-number (Fig. 46). The incompatible elements Nb, Zr, Y, and Ti display very limited overall variations in abundance, and ratios between them remain almost constant within analytical uncertainties. Rubidium and potassium, and to a lesser extent phosphorus, exhibit significantly greater ranges and define rough positive correlations with water LOI (Fig. 47), indicating that some of the measured variation is a result of alteration by seawater. Loss on ignition is between 1.19 and 3.17 wt% for all but one sample; such values are typical of moderately altered lavas.

Preliminary Conclusions

Several different eruptions are represented in Hole 803D. All the basalts are moderately differentiated tholeiites, and they may have been derived from more than one parental magma. There is no evidence at this site for the thick, massive flood lavas postulated to compose the upper levels of basement over much of the plateau (e.g., Kroenke, 1972); instead, the thin, pillowed nature of the flows implies that their feeder vents were not very distant and eruption rates were low. This feature may be related to the location of this site on the flank of the plateau.

The rocks are distinct from normal MORB (see above), but also distinct from typical oceanic-island tholeiites. The latter are much more enriched in immobile incompatible elements (such as Zr, Nb, and Ti), have higher Zr/Y (generally >4), and much lower Zr/Nb ratios (commonly <12). The closest resemblance of the Site 803 lavas is to the few available basalts from other Pacific plateaus (see Fig. 45, for example); in particular, those from the Manihiki Plateau (Jackson et al., 1976) and the single flow of Ontong Java basalt recovered at Site 289 (Stoeser, 1975). They also are quite similar to lavas from the islands of Malaita and Santa Isabel (J. Mahoney, unpubl. data, 1989), which may represent an uplifted portion of the western edge of the Ontong Java Plateau (e.g., Kroenke, 1972), and to the Cretaceous sill and flow complex in the Nauru Basin to the east of the plateau (e.g., Floyd, 1986; Saunders, 1986). In conjunction with Nd and Sr isotopic studies, the above chemical characteristics have been interpreted to reflect mantle sources that are a combination of MORB and oceanic-island-type components (Mahoney, 1987; P. Castillo, pers. comm., 1990).

Significantly, as with the other Pacific plateau samples (Mahoney, 1987), the Site 803 basalts show no evidence of having interacted with continental crust, although several workers (e.g., Nur and Ben-Avraham, 1982) have proposed on the basis of seismic refraction data that the Ontong Java Plateau is a subsided continental fragment. Finally, we note that the poorly defined Cretaceous age of the lowermost sediments at Site 803 does not allow any firm conclusions regarding the duration of late-stage volcanism at this site vs. Site 289 or 807.

LOGGING

Logging Operations

An almost complete set of high-quality logging data was collected at Hole 803D despite abundant technical problems. The logging operations are summarized in Table 15; acronyms used are listed in Table 16. Four logging runs were made during the course of 32 hr, one each with a geophysical and a geochemical tool string, one with an electrical resistivity imaging tool (the formation microscanner or FMS), and one with a sonic velocity tool. Each of the tool strings also carried the natural gamma-ray tool so as to correlate depths between individual runs.

The first run employed a geophysical tool string that consisted of a sonic tool (LSS), a resistivity tool (DIT), a density tool (HLDT), and a natural gamma-ray tool (NGT). In addition, the string carried the Lamont temperature tool (TLT) at its base. The LSS malfunctioned when we had a minor problem passing the bit release at the end of the drill string; the malfunction not only made it impossible to record sound velocities, but also made it impossible to command the caliper on the density tool to open. The caliper is needed to push the HLDT sensors against the borehole wall and receive proper density readings of the formation. Because of the tool failures, good data were acquired only from the natural gamma-ray, resistivity, and temperature tools. The tool string was able to reach within 10 m of the base of the hole (653 mbsf) and thus was able to log the upper 20 m of basalt and the lowermost sedimentary section.

Table 14. Major element, trace element, and CIPW-normative compositions of basalts from Hole 803D analyzed on board ship.

Core, section	68R-4	69R-1	69R-1	69R-2	69R-3	69R-3	69R-4	70R-1	70R-2	70R-3	71R-1	71R-2	71R-3
Interval (cm)	38–41	6–8	88–90	135–137	48–50	83–85	28–30	62–64	32–34	61–62	129–131	86–88	37–39
Subdivision	1A	1B	1D	4A	4B	5A	5C	5D	8A	9B	9D	9F	9H
Major elements (wt%):													
SiO_2	48.94	49.46	48.67	50.25	49.11	49.43	50.86	50.02	49.32	50.02	49.57	49.89	49.71
TiO_2	1.44	1.31	1.31	1.32	1.31	1.31	1.47	1.34	1.38	1.31	1.27	1.33	1.26
Al_2O_3	16.62	14.96	15.19	15.00	14.87	15.29	16.70	15.07	15.72	15.24	14.77	15.19	14.26
[a]Fe_2O_3	12.88	12.05	12.89	10.70	12.58	12.04	9.68	11.51	11.56	10.16	11.74	10.70	11.84
MnO	0.15	0.17	0.19	0.17	0.18	0.16	0.11	0.17	0.16	0.18	0.20	0.17	0.24
MgO	3.94	5.87	5.39	6.95	5.59	5.58	5.29	6.54	6.41	6.57	6.93	6.06	7.12
CaO	11.63	12.76	13.62	12.69	12.47	12.84	11.17	12.24	11.11	12.92	12.82	12.93	12.49
Na_2O	2.19	1.92	1.89	1.92	1.78	1.97	2.18	2.01	2.27	1.97	1.84	2.05	1.89
K_2O	1.04	0.36	0.45	0.31	0.61	0.64	1.44	0.66	0.84	0.31	0.35	0.42	0.42
P_2O_5	0.21	0.11	0.12	0.11	0.13	0.13	0.37	0.13	0.15	0.12	0.11	0.12	0.10
Total	99.02	98.97	99.70	99.42	98.61	99.37	99.26	99.67	98.90	98.99	99.59	98.85	99.30
LOI	3.17	1.62	2.83	1.19	1.72	2.31	8.49	1.66	2.41	1.63	1.34	1.59	1.76
N	2	1	4	1	2	2	4	2	2	2	4	2	2
[b]CIPW norms:													
Quartz	0.48	1.57		1.76	1.63	0.61	1.72	0.60		1.84	0.67	1.42	0.64
Orthoclase	6.25	2.17	2.70	1.86	3.67	3.85	8.65	3.96	5.07	1.84	2.11	2.54	2.50
Albite	18.86	16.57	16.22	16.47	15.38	16.89	18.72	17.17	19.59	16.96	15.77	17.69	16.21
Anorthite	33.13	31.75	32.02	31.83	31.56	31.49	31.98	30.52	30.81	32.49	31.41	31.61	29.68
Diopside	20.58	26.62	29.73	25.70	25.75	26.91	18.19	24.85	20.19	26.39	26.61	27.23	26.89
Hypersthene	14.83	16.08	13.29	17.42	16.61	15.00	15.15	17.72	16.46	15.60	18.36	14.50	19.04
Olivine			0.66						2.50				
Apatite	0.47	0.25	0.27	0.24	0.29	0.28	0.81	0.29	0.33	0.26	0.25	0.27	0.22
Ilmenite	2.79	2.54	2.52	2.55	2.54	2.53	2.83	2.57	2.68	2.54	2.44	2.58	2.43
Magnetite	2.62	2.45	2.60	2.16	2.57	2.44	1.96	2.32	2.35	2.06	2.37	2.17	2.40
Mg#	35.01	46.09	42.29	53.21	43.80	44.87	49.02	49.89	49.32	53.06	50.81	49.79	51.17
Trace elements (ppm):													
Nb	4.8	5.0	4.4	4.4	4.7	4.7	5.2	4.4	4.6	4.8	4.5	4.2	4.7
Zr	83.0	73.9	72.8	73.4	75.3	75.6	85.5	75.4	79.1	75.4	71.3	73.1	77.5
Y	26.9	21.5	22.0	20.8	23.1	23.5	29.3	23.8	24.2	23.5	23.0	22.5	24.0
Sr	196.6	157.8	159.0	154.0	160.6	163.0	187.5	162.2	168.1	158.0	144.6	148.1	154.5
Rb	22.7	8.7	8.1	4.8	13.3	13.3	18.1	12.7	13.8	2.5	6.1	6.8	6.7
Zn	219.9	111.2	116.5	99.3	129.8	102.5	72.7	110.8	88.0	77.1	89.1	89.4	100.3
Cu	70.1	87.1	92.1	59.1	124.6	59.1	71.2	55.4	83.5	135.1	37.9	37.9	53.9
Ni	182.8	134.2	108.9	119.8	90.0	93.4	91.1	105.3	95.5	135.2	103.8	107.2	115.6
Cr	284.0	239.4	232.8	231.9	237.7	238.4	255.1	230.9	247.5	233.0	224.0	227.5	260.4
V	294.5	298.6	298.7	278.3	268.3	288.1	251.2	252.1	272.9	258.0	265.4	270.5	278.1

Notes: CIPW-normative after Johanssen, 1931, for example. LOI = loss on ignition, N = number of analyses.
[a] All Fe expressed as Fe_2O_3.
[b] Fe_2O_3/FeO set at 0.15 and Mg# = (atomic) $100 Mg/Mg + Fe^{2+}$.

The formation microscanner (FMS) was used in the second logging run. The FMS can be used to image bedding and fractures downhole. About halfway to the seafloor, a connector flooded and shorted the tool out. The FMS was brought back on deck, the pressure casings were opened, the tool was dried, and the run was repeated. By the time the tool string passed to a lower part of the hole, it encountered a bridge at 610 mbsf. Thus, no further logging data were acquired from the basement or lower sedimentary section. The main logging run collected FMS, natural gamma-ray, and temperature data (TLT) to the drill pipe. The uppermost section of the hole was washed out to such an extent that the caliper arms of the FMS lost contact with the borehole wall and no usable data were collected over this interval. The tools were lowered to 192 mbsf, repeating measurements in the upper, soft sedimentary section to ascertain the reliability of the FMS data in these unconsolidated sediments.

The third run consisted of the geochemical tool string, modified to include the HLDT. The tool configuration was, from the top down, NGT (natural gamma-ray), HLDT (density), ACT (aluminum), GST (eight-element, fast-capture, neutron activation spectroscopy). Although the entire tool string checked out correctly on deck, when the GST was calibrated at the mud line the spectra were out of tolerance and could not be deconvolved into elemental data. The run was continued to collect density data and aluminum percentages in the section. The interval from 610.5 mbsf to the pipe at 98.7 mbsf was logged on the main logging pass and the section from 311.1 to 98.7 mbsf was logged again.

The fourth logging run consisted of the NGT (natural gamma-ray), a mechanical caliper to help center the tool, the BHC (borehole-compensated sonic tool), and the TLT (temperature). The BHC sonic tool was used because the backup LSS malfunctioned on deck. The main logging pass recorded data from 605.6 to 98.7 mbsf. A section from 606.8 to 101.1 mbsf was logged a second time to check the reproducibility of the BHC in this soft formation. After this run, the sonic string was pulled out of the hole and logging was concluded.

The logs show that the hole was in good condition below 250 mbsf, but the hole had widened considerably above this depth. Above 200 mbsf, the hole was significantly wider than the maximum opening of the density tool caliper. Hence, above this depth the log density measurements average about 1.4 g/cm^3, compared with core measurements of about 1.6 g/cm^3 (see Fig.
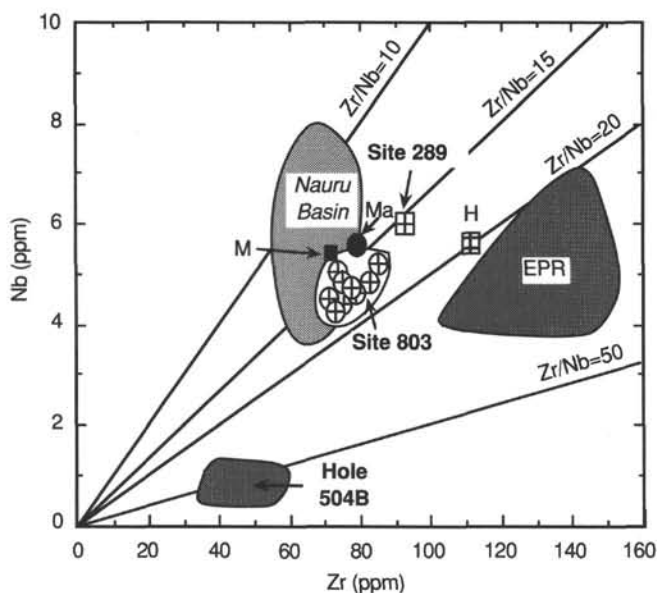
Figure 45. Plot of Zr vs. Nb for Site 803 tholeiites. For comparison, fields are shown for the East Pacific Rise (EPR; Humphries et al., 1980), Hole 504B on the Costa Rica Rift (Kempton et al., 1985), and the Nauru Basin (Floyd, 1986; Saunders, 1986). Averages for Manihiki Plateau lavas ("M"; Jackson et al., 1976) and Malaita basement basalts ("Ma"; J. Mahoney, unpubl. data, 1989) are also plotted, as are data for the single basalt flows recovered at Site 289 (Stoeser, 1975) and on Hess Rise ("H"; Seifert et al., 1981).

48). Below this depth, core and log measurements are in better agreement. Density measurements from the logs above 200 mbsf are suspect.

The original logs were recorded in depth increments of feet below rig floor. Each logging tool combination contained a natural gamma-ray detector (NGT) that recorded a prominent spike produced by the thick ash layer seen at 181.3 mbsf in the core (see "Lithostratigraphy" section, this chapter). All logging depths were converted to meters and adjusted to align the gamma-ray peaks at 181.3 mbsf.

Log Stratigraphic Units

Well-log data defined the extent of sediment types that were poorly recovered at Site 803. Perhaps of greater importance, the logs illustrated the nature of transitions in the sedimentary column, such as ooze to chalk, which could not be recorded in great detail from core observations or measurements. These transitions strongly influence the seismic character of the site.

Rather than describe the behavior of the well logging data in terms of the rock stratigraphic units recognized in the recovered core, the data have been subdivided into log stratigraphic units based solely on internal consistencies of the logging profiles. Log stratigraphic units do not necessarily coincide with lithologic units. The units (described as A, B, C, etc., to distinguish them from lithologic Units I, II, III) are described in Table 17. All of the logs, with the log stratigraphic units defined, are displayed in Figures 49 through 52. Correlations between density, electrical resistivity, and compressional wave velocity are fairly consistent (i.e., they all exhibit changes and inflections near the same depths).

Gamma-ray activity is somewhat independent of the other properties and has different trends. This difference may be a result of the extremely low signal seen in the gamma-ray logs and the portion of the sediments that produce the signal. Normal

gamma-ray counts from continental margin carbonates are in the tens of API units; shale counts are about 100. Whatever component is producing the gamma radiation in the Site 803 sediments (probably windblown clay or volcanic ash) is very dilute.

Although the concentration variations may be enough to produce the regular changes that are found in the gamma-ray log, they are not enough to effect such other properties as density seriously, as these are a sum of all components of the sediments. Aluminum, another log associated with clay content in these sediments, is plotted along with the "noncarbonate content" ($100 - \%CaCO_3$) from core samples (Fig. 50). Visually, there appears to be correlation between the two signals. Temperature logs (Fig. 51) show an increase from 1.6°C at the mud line to near 7.0°C at the bottom of the hole.

Logging Unit A extends from the top of the logged interval (106 mbsf) to approximately 199 mbsf. It includes the ash layer depth tie point at 181.3 mbsf (labeled "Ash" in Fig. 49). Logging Unit A is defined by generally increasing compressional wave velocity (1.65–1.85 km/s) and gamma-ray activity (3.5–5.0 API). Unexpected (from core descriptions) features of logging Unit A are the two zones of increased electrical resistivity (132.2–144.9 and 182.9–199.2 mbsf). These intervals of increased resistivity correlate with small but significant increases in compressional wave velocity at the same depths. No marked reduction in porosity was observed in core samples from these intervals (see "Physical Properties" section, this chapter).

Gradients in bulk density, electrical resistivity, and gamma-ray activity characterize logging Unit B. Wet-bulk density increases from 1.60 to 1.85 g/cm³ in the depth range from 199 to 259 mbsf. Resistivity also increases, with a local maximum at approximately 259 mbsf. Gamma-ray activity continues to increase from about 150 mbsf, in logging Unit A, to a local maximum within logging Unit B at 248 mbsf, and drops sharply in the bottom 11 m of the unit. Logging Unit B also increases in overall compressional wave velocity (1.85 km/s at 200.3 mbsf and 2.11 km/s at 259.4 mbsf), but the increase is more discontinuous over the interval, with several local maxima and minima. The velocity fluctuations, coupled with density variations, are the source of strong reflectors seen in the seismic section (see "Seismic Stratigraphy" section, this chapter).

Between 259 and 521 mbsf in Hole 803D (logging Unit C), there is a gradual increase in velocity (2.11–2.28 km/s), almost constant density (1.85 g/cm³), and two broad minima in gamma-ray activity and electrical resistivity. The resistivity and gamma-ray minima are approximately coincident at around 320 and 470 mbsf. A slight velocity minimum appears to correlate with the shallower of the two resistivity and gamma-ray minima. In general, this section of the sediment column behaves as might be expected of normally compacting carbonate sediments.

Logging Unit D (521–596 mbsf) is again a depth interval of increased gradients and irregular log response. Bulk density increases from 1.85 to 2.07 g/cm³ by 583 mbsf. Compressional wave velocity increases over the same depth range (2.28–2.62 km/s) with a peak at 583 mbsf. Resistivity also increases with depth over the interval. All three of these properties do not increase smoothly, but rather show local maxima and minima that are seen in the seismic record as the strong reflectors near the bottom of the sedimentary column (see "Seismic Stratigraphy" section, this chapter).

The short interval between 596 and 601 mbsf is singled out as an individual unit (logging Unit E) because of the extreme drop in velocity and electrical resistivity occurring over these 5 m. Logging Unit E corresponds to the recovery of a nannofossil radiolarite with an equally anomalous low laboratory velocity (see "Lithostratigraphy" and "Physical Properties" sections, this chapter).
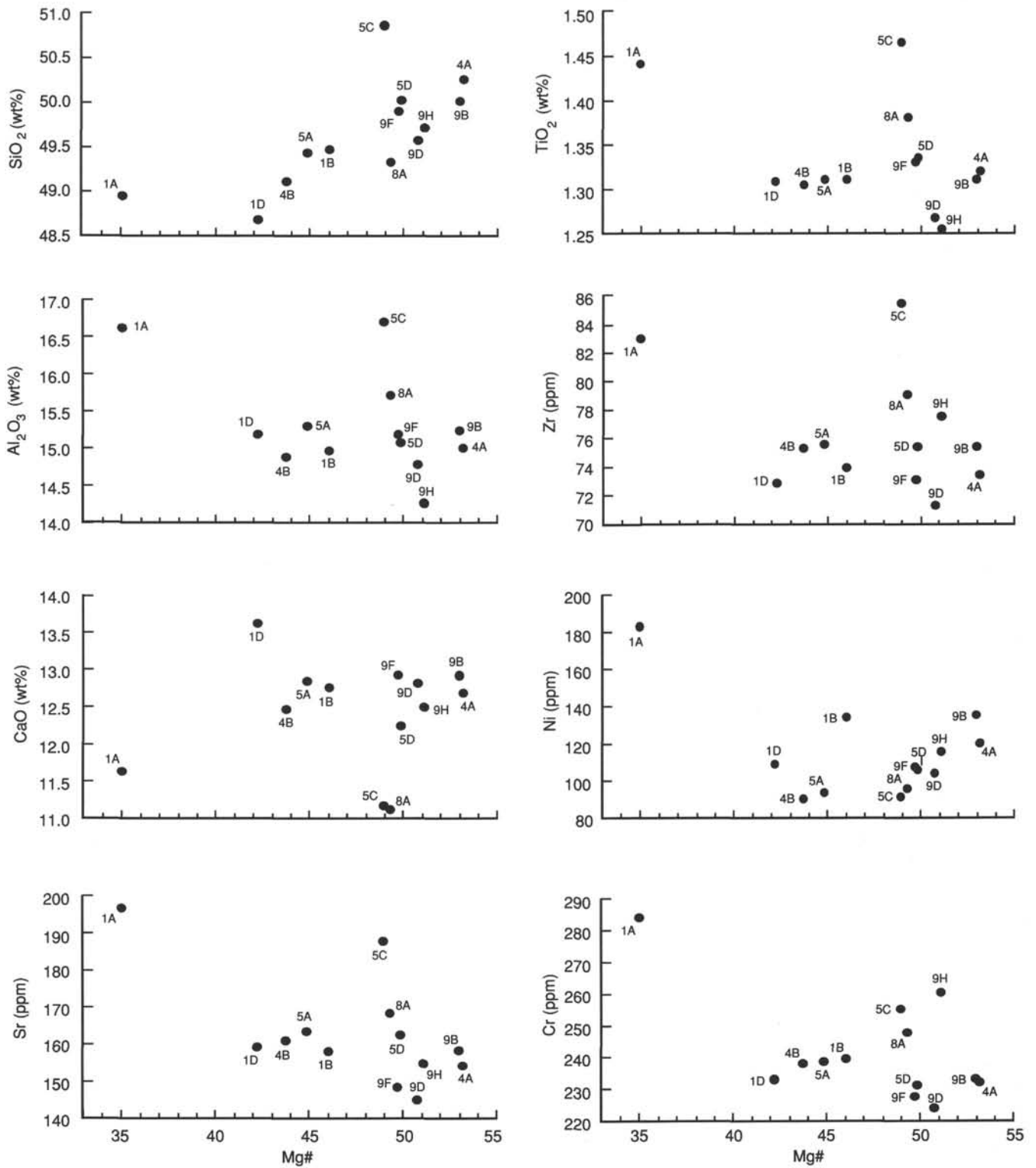
Figure 46. Variation of selected major and trace elements vs. Mg-number for Site 803 basalts. Numbers and letters next to points indicate subdivisions and secondary subdivisions, respectively.

The remaining sedimentary unit, logging Unit F, extends from 601 mbsf to basement at approximately 630.4 mbsf. It is defined solely by electrical logs (Fig. 52) as no other logs could be taken over this interval. Resisting the urge to break the bottom 30 m of the hole into three logging units, we note that there is a minimum in resistivity at 615 mbsf and a rather strong maximum at 618–620 mbsf. The minimum may be associated with another silica-rich interval; the maximum appears to coincide with a continuous chert layer partially recovered in the core (see "Lithostratigraphy" section, this chapter).
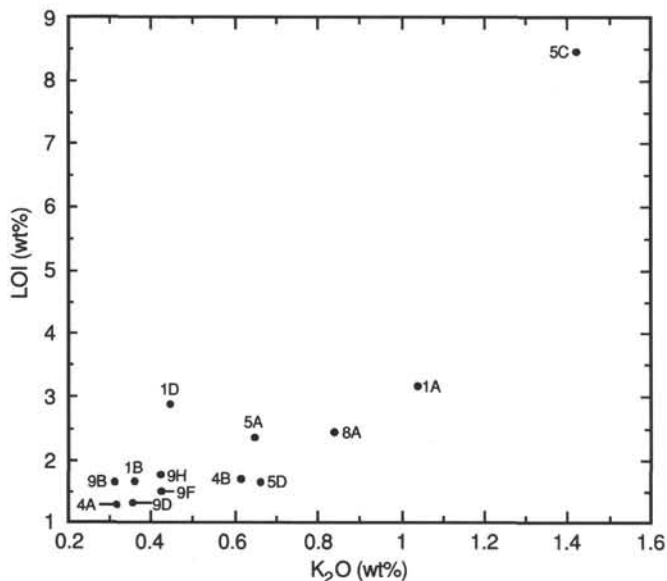
Figure 47. K_2O vs. weight loss on ignition (LOI) for Site 803 tholeiites. Numbers and letters next to points indicate subdivisions and secondary subdivisions, respectively.

Basement appears in the resistivity logs at a depth of 631.4 mbsf. It is characterized by resistivities in the range from 10 to 1000 ohmm, typical of weathered oceanic pillow basalts.

Correlation with Lithostratigraphy

Although the log stratigraphic unit boundaries do not coincide with the lithostratigraphic unit boundaries, there are some correlations. The two lithostratigraphic unit boundaries (IA/IB and IB/II) that fall within the intervals of comprehensive logging coverage (Fig. 49) are located in log stratigraphic units defined by strong property gradients. Thus, the ooze-to-chalk transition at 217.1 mbsf described from the recovered core is seen as a true transition zone in the logs (logging Unit B), extending over 60 m. The transition also has an irregular character, suggestive of hard and soft intervals, as the oozes above grade into the chalks below. Logging Unit D, containing the Subunit IB/Unit II boundary, appears to be another zone of enhanced gradients caused by diagenetic change; in this case, the onset of precipitation of authigenic silica as opal-CT cement and/or chert.

In at least three instances, the logs add detail of structure and sediment distribution where core recovery was low near the base of the hole. Poor core recovery began with Core 130-803D-57X, coinciding with the top of logging Unit D (521 mbsf). Nodular chert first appeared in the cores at this level. Chert formation and enhanced grain cementation in general are probably responsible for the local high-velocity layers within logging Unit D at 521–541, 546–558, and the generally higher velocity values below 564 mbsf (where the break is made between lithostratigraphic Subunit IB and Unit II). Similarly, the chert horizon in Unit F (partially recovered in Core 130-803D-67X) is defined by a zone of high resistivity about 2 m thick. Core 130-803D-65X recovered only a few centimeters of radiolarite, but the logs indicate that there may be an interval of radiolarite that is nearly 5 m thick (logging Unit E).

Finally, the fairly constant electrical resistivity log data between 621.8 mbsf and basement at 631.4 mbsf implies that lithologic Unit III is uniform. The recovered 5 m of the section are representative of a 10-m-thick unit.

Comparison with Laboratory Data

Compressional wave velocity and bulk density data recorded *in situ* during well logging at Hole 803D are directly comparable with laboratory measurements of the same properties made on

Table 15. Diary of logging operations, Hole 803D.

Local day	Local time	Cumulative hours	[a]Depth (mbsf)	
2/5/90	5:10			Last core on deck
2/5/90	13:45	0.0		RIH with Quad Combo (NGT/DIT/HLDT/LSS/TLT)
2/5/90	15:09	1.4		At mud line
2/5/90	16:49	3.1	649.2	On bottom of hole, 9 m above total drilled section
2/5/90	17:15	3.5		Main log pass; only NGT/DIT/TLT functioning; up at 900 ft/hr
2/5/90	17:41	3.9	534.9	Change speed to 1800 ft/hr as HLDT not functioning
2/5/90	18:30	4.7	98.7	Tool in pipe at 3516 mbrf (11,539 ft); POOH
2/5/90	20:00	6.2		Tool string on deck
2/5/90	21:15	7.5		RIH with NGT/FMS/TLT; connector head flooded at 6000 ft
2/6/90	0:53	11.1		RIH with NGT/FMS/TLT
2/6/90	2:47	13.0	609.8	At bottom of hole; hole bridged
2/6/90	2:59	13.2		Up log of FMS
2/6/90	4:59	15.2	98.7	Enter pipe; end main FMS log
2/6/90	5:20	15.6	191.7	Repeat uplog from 11,850 ft to pipe at 11,539 ft
2/6/90	5:48	16.0	98.7	POOH with FMS
2/6/90	7:50	18.1		RIH with geochemical string (NGT/ACT/GST/HLDT)
2/6/90	9:30	19.7		Pause at mud line; GST has spectra out of tolerance
2/6/90	10:30	20.7		Decide to go down with nonfunctioning GST
2/6/90	11:02	21.3	610.5	Start log up; 600 ft/hr (NGT/ACT/HLDT)
2/6/90	11:49	22.1	464.8	GST not coming up; change logging speed to 900 ft/hr
2/6/90	13:10	23.4	98.7	Into pipe
2/6/90	13:25	23.7	311.1	Start repeat section logging up
2/6/90	14:15	24.5	98.7	Back into pipe; POOH
2/6/90	16:23	26.6		RIH for second attempt at sonic run (NGT/BHC/TLT)
2/6/90	17:54	28.1	605.6	Hit bottom of hole at 13,214 ft
2/6/90	18:03	28.3		Start up log
2/6/90	18:45	29.0	98.7	End up log
2/6/90	19:09	29.4	606.8	Start repeat of sonic run from 13,216 ft
2/6/90	19:50	30.1	101.1	End repeat sonic run 11,557 ft; POOH
2/6/90	22:00	32.3		Rigged down from logging runs.

[a] Based on correlation of ash layer observed at 181.3 m in core to NGT spike at 11,810 ft in quad combo; 11,816 ft in FMS main; 11,824 ft in geochemical string; 11,822 ft in sonic main; 11,820 ft in sonic repeat.

Table 16. Acronyms used in well logging.

Acronym	Definition or meaning
ACT	Aluminum clay tool
API	American Petroleum Institute standard units of gamma activity calibrated to test pit in Houston, TX
BHC	Borehole compensated sonic tool
DIT	Phasor dual induction tool
fbrf	Feet below rig floor
FMS	Formation microscanner
GST	Geochemical spectral tool
HLDT	High-temperature lithodensity tool
LSS	Long-spaced sonic logging tool
mbrf	Meters below rig floor
mbsf	Meters below sea floor
NGT	Natural gamma tool
POOH	Pull out of hole
RIH	Run into hole
SDT	Long-spaced sonic digital tool
TLT	LDGO temperature logging tool

Table 17. Log-stratigraphic units defined at Hole 803D.

Logging unit	Depth range	Description
A	<199	Velocity gradient (1.65–1.85 km/s) Resistivity relatively constant (0.7 ohmm)
B	199–259	Gradients in density (1.60–1.85 g/cm^3) Resistivity (0.7–0.8 ohmm) Velocity (1.85–2.11 km/s)
C	259–521	Velocity gradient (2.11–2.28 km/s) Resistivity varies (0.8–1.0 ohmm) Density varies between (1.8–1.9 g/cm^3)
D	521–596	Density gradient (1.9–2.1 g/cm^3) Velocity increase (2.28–2.62 km/s) Resistivity increase (1.0–1.6 ohmm)
E	596–601	Velocity and resistivity minima (1.79 km/s, 0.7 ohmm)
F	601–630.4	Variable resistivity No sonic, density
Basement	630.4	

discrete sections of recovered core. Plots of superimposed logging and laboratory data vs. depth are presented in Figure 48. The laboratory data are uncorrected for ocean-bottom temperature and pressure. The corrected laboratory data (to *in-situ* conditions) will have slightly higher velocities and densities. Comparison of the laboratory and logging data allow both logging specialists and the physical properties specialists to evaluate the effects of hole conditions and core disturbance on their data.

Laboratory wet-bulk density values agree well with density logs below 200 mbsf. Above this level the density log is shifted toward unrealistically low values (<1.40 g/cm^3). Based on the comparison of the two sets of data, the density logs are unreliable above 200 mbsf. The compressional wave velocity logs can be used to edit both logging and shipboard sample results. Within the upper 250 mbsf at Hole 803D, there are several relative maxima and minima in both data sets. Excursions that are seen in the results of both experiments have been retained. Low-velocity intervals in the well logs from 121.1 to 126.1, 187.8 to 188.7, 223.7 to 227.6, and 243.1 to 247.7 mbsf have been discounted. For similar reasons, the low velocities measured in five laboratory samples between 370 and 390 mbsf are attributed to core disturbance rather than to an *in-situ* occurrence. On a positive note, many local maxima and minima that might have been suspect in either individual laboratory or logging data are confirmed as real events by the data comparison (e.g., a local velocity maximum between 138 and 147 mbsf and an extreme velocity minimum between 596.9 and 600.8 mbsf).
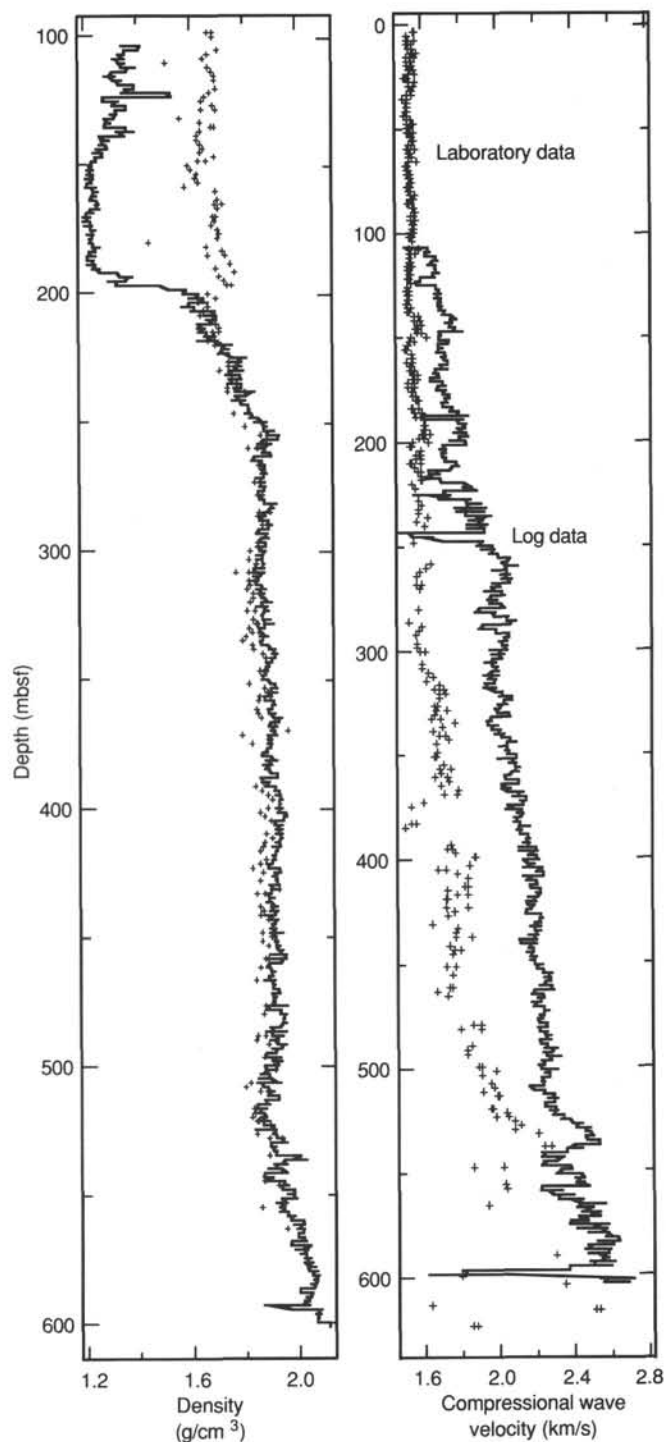

Figure 48. Logging and laboratory velocity and density data, Hole 803D. Laboratory data at STP.

Velocity-Resistivity Relationship

Compressional wave velocity is plotted vs. electrical resistivity in Figure 53. The figure illustrates this relationship as well as that of velocity to porosity in the sediment column as diagenesis takes place. We have used a 1-m running average value of the logs in Figure 53 to reduce the number of points and to clarify the diagram. The different log-stratigraphic units have been identified in the plot. Electrical resistivity is used because it is
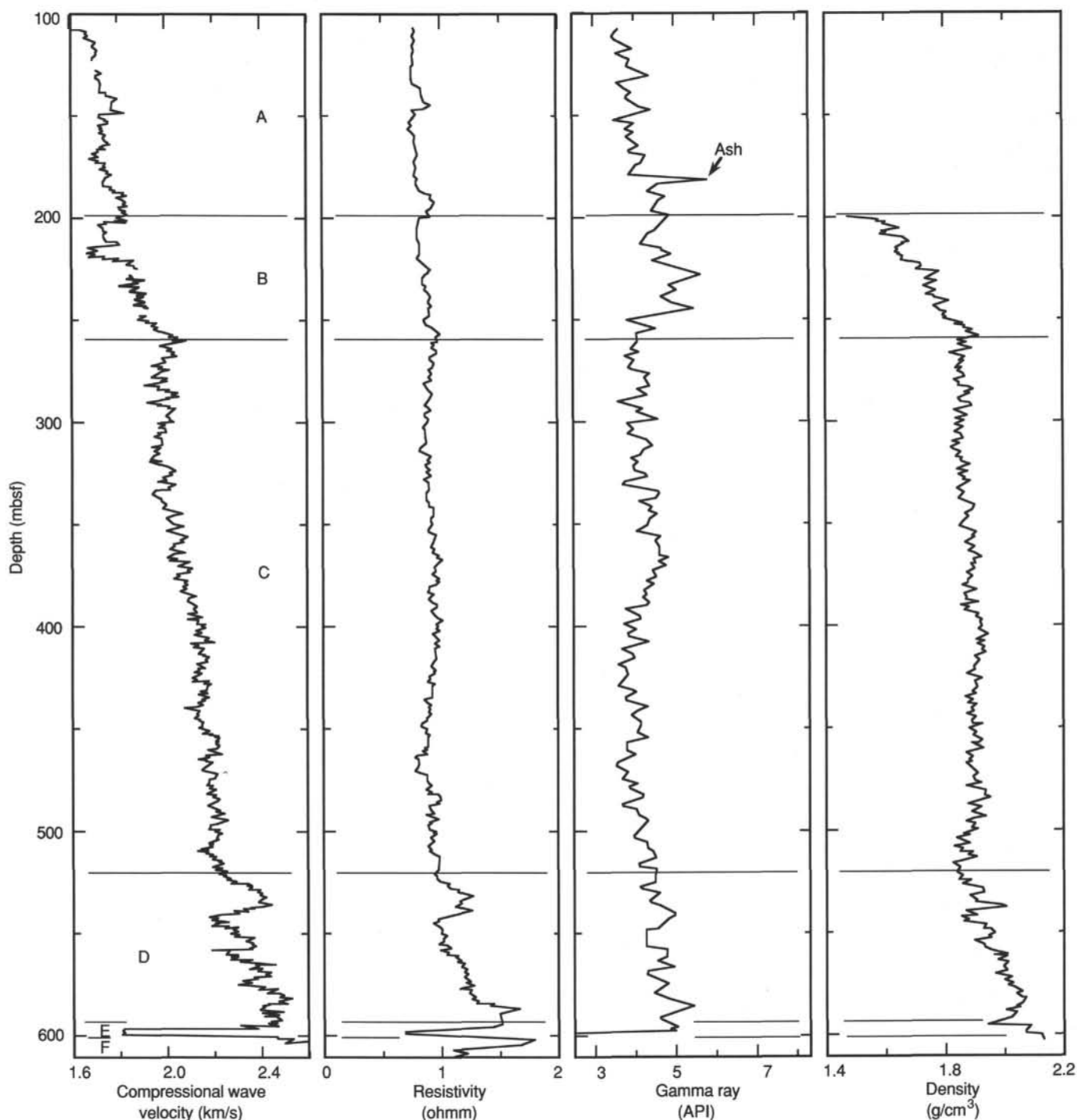
Figure 49. Well logging data, Hole 803D. Logging units A–D are shown for reference.

an analog of porosity in these sediments. The different units occupy overlapping fields that tend toward lower porosities (higher resistivities) and increasing velocities with depth. The velocity-resistivity relationship illustrates the change from a regime where there is a substantial change in velocity (1.55–2.40 km/s) with very little change in resistivity (0.7–1.0 ohmm, logging Units A, B, and C) to one in which there is a much smaller change in velocity 2.40–2.60 km/s) over a wider range of resistivity (1.0–1.8 ohmm, logging Units D and F). The rapid rise in velocity with little change in resistivity represents the effects of increasing cementation on sediment grains in the upper part of the column. The harder sediments follow a normal porosity-velocity relationship.

The formation microscanner images are presented on microfiche at the back of this volume (see back pocket).

SEISMIC STRATIGRAPHY

Introduction

The seismic character of the Ontong Java Plateau in the vicinity of Site 803 is transitional between the "layer cake" stratigraphy of the thick section at the top of the plateau and the more
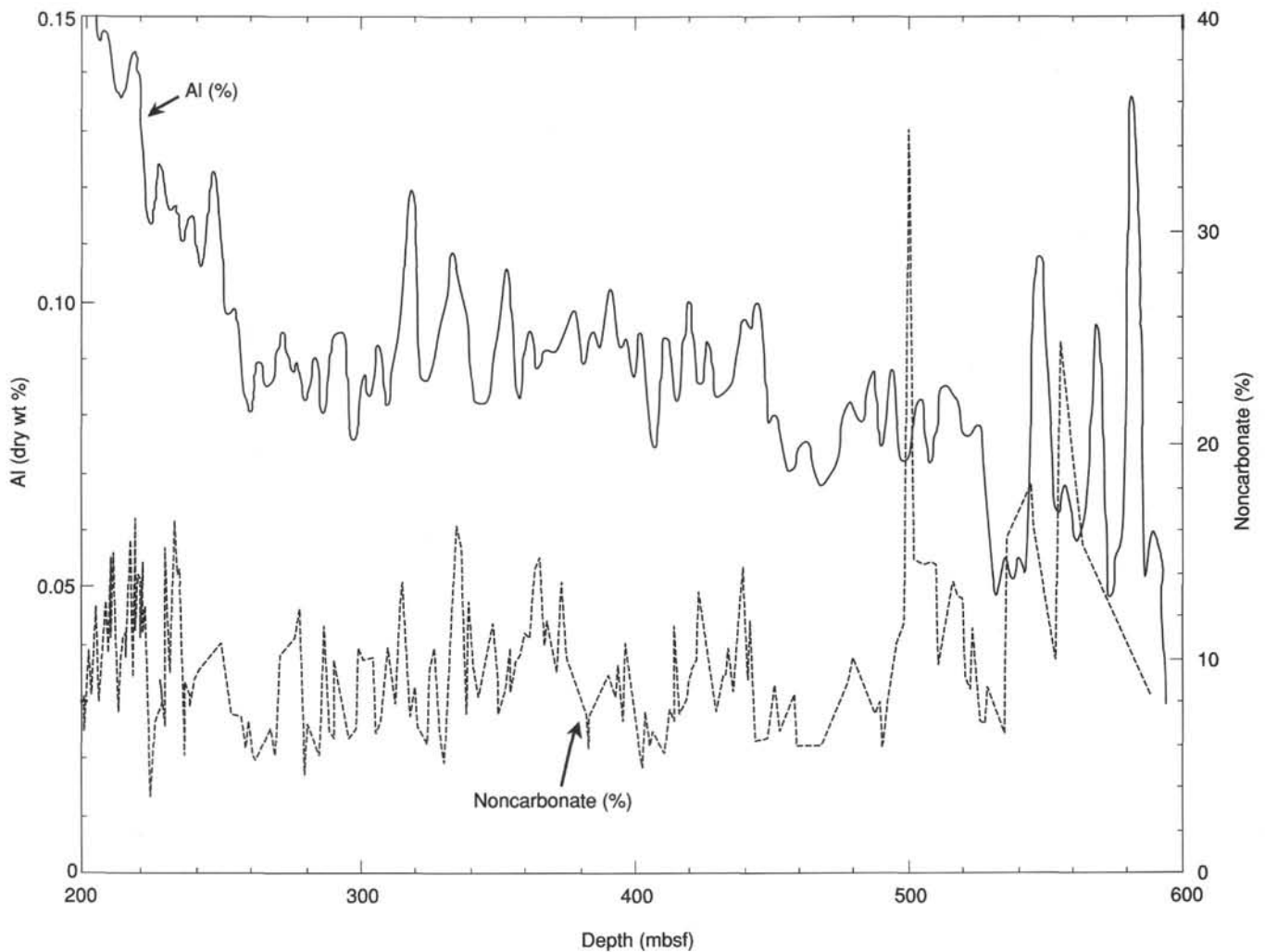
Figure 50. Aluminum log (solid line) and noncarbonate fraction (dashed line), Hole 803D. The noncarbonate fraction is calculated as 100 − %CaCO₃, where the CaCO₃ value is taken from the "Carbon Geochemistry" section, this chapter.

variable seismic signature of the thinned flanks (see Mayer et al., this volume). Site 803 lies within a depth range that is characterized by numerous examples of mid-section reverberations (MSRs); some of these reverberant layers have a rough, basementlike acoustic character that disrupts the overlying section whereas others are more flat-lying and do not seem to affect the sediments above. The former may be basalt sills and the latter may represent local, diagenetically enhanced features (see Mayer et al., this volume). Site 803 lies approximately 1.6 km west of a small MSR (Fig. 54). This feature, however, appears to have little influence on the seismic stratigraphy at the drill site.

Slumping and sediment remobilization are ubiquitous on the plateau, and several small zones of apparently displaced sediments were found in the cores recovered at Site 803. The seismic record at Site 803, however, shows little evidence of major mass movement events. Seismically, the section is well stratified and, at 0.65 s thick, is approximately 40% thinner than the section at Sites 289/586 (on the top of the plateau; Andrews, Packham, et al., 1975). In this section, we will look at the origin of some of the major reflectors at Site 803 and thus gain insight into the nature of this thinning. In combining these results with those from the other Ontong Java Plateau sites, we hope to lay the groundwork for future studies that will use the seismic record to extract a detailed record of the tectonic and paleoceanographic history of the Ontong Java Plateau.

Seismic Modeling

Although the seismic record often has the appearance of a geologic cross-section and can easily be interpreted in terms of structural relationships, two problems make the direct stratigraphic use of the seismic record a difficult task. First, the seismic section presents events as a function of traveltime and not depth. Second, the limited bandwidth of seismic systems prevents resolution on the scale of the true geologic variability; instead, seismic reflections are commonly interference composites resulting from the complex interaction of the true geologic structure and the outgoing pulse of the seismic system (Mayer, 1979). Both of these problems are particularly serious in the pelagic carbonate sequences of the Ontong Java Plateau where low sedimentation rates and the subtle physical response of the sediment to paleoceanographic change result in a seismic section that is composed of numerous closely spaced reflectors. Interference must clearly play a role in producing the seismic record here and, given the closely-spaced nature of the reflectors, an inaccurate traveltime-to-depth conversion would easily result in the miscorrelation of a reflector with a geologic event.

To convert a seismic section into a depth section (and thus to know where in the borehole record to look for the cause of a particular seismic event), we must accurately determine the true sonic velocity structure of the sediment column. At Site 803, we
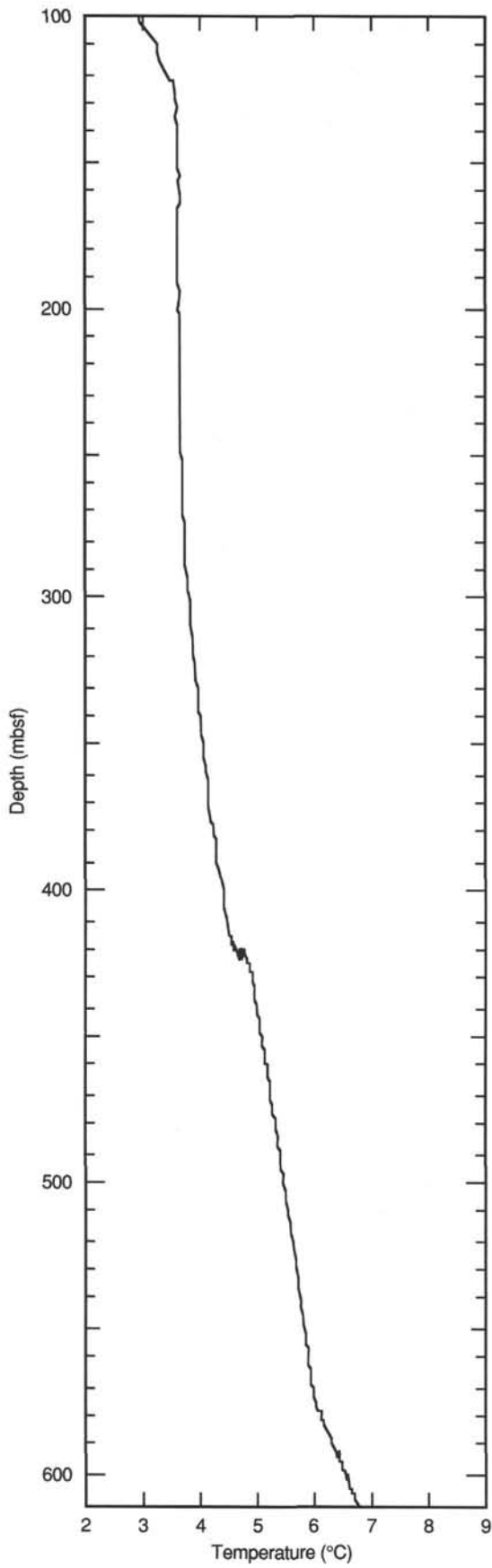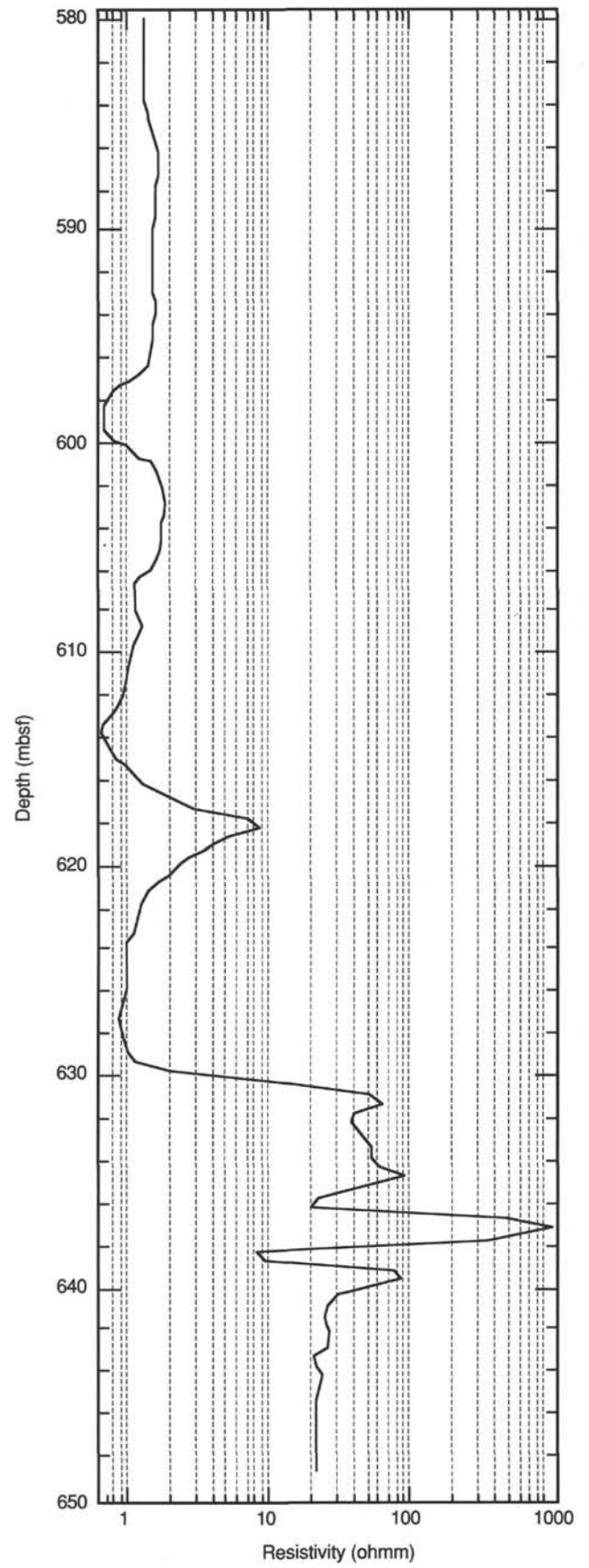
Figure 51. Temperature log, Hole 803D.

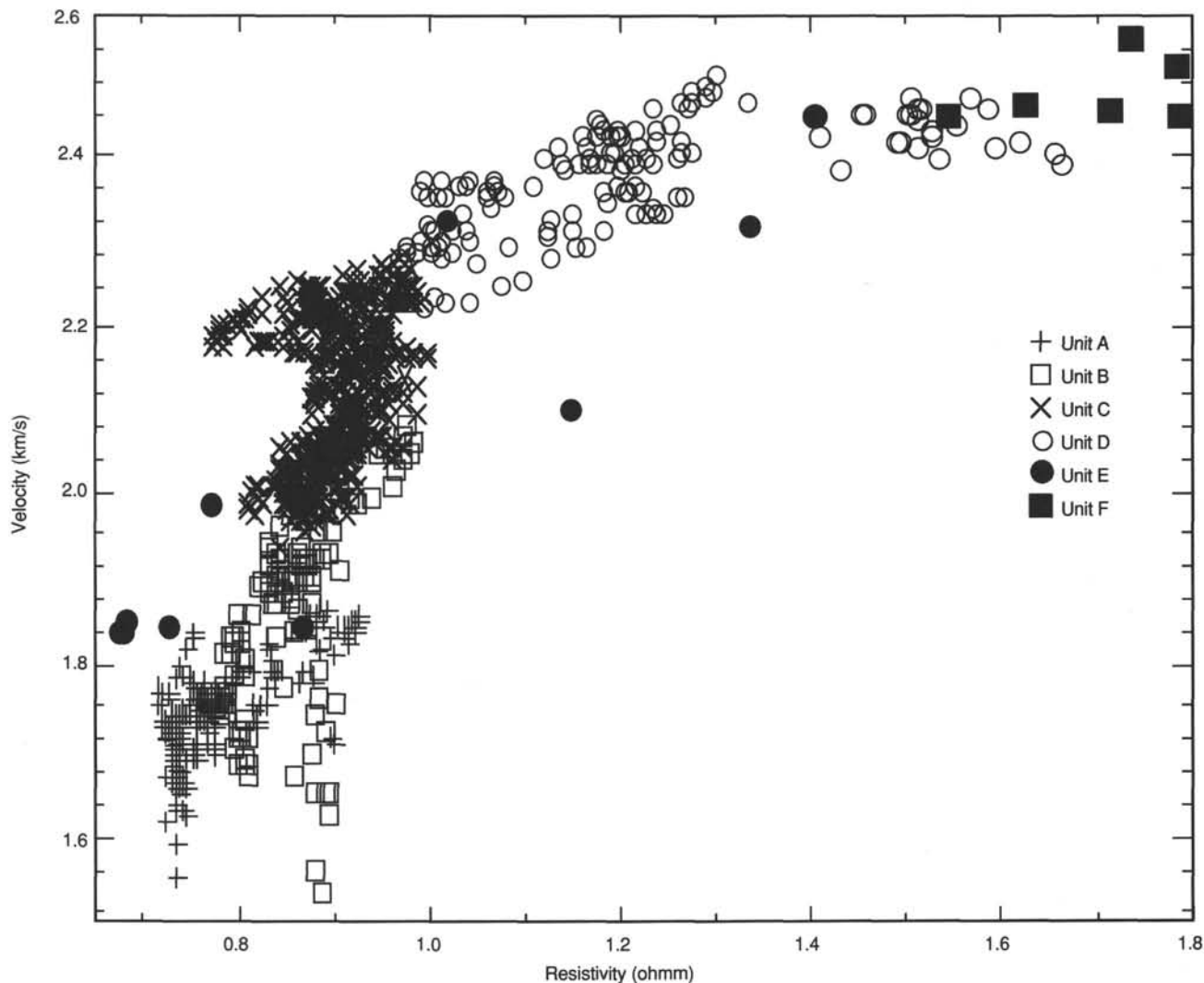Figure 52. Resistivity log from the lower part of Hole 803D.

Figure 53. Cross-plot of velocity and resistivity logging data, Hole 803D. Key on figure denotes logging units.

have several sources of data available to us for this purpose. The most accurate source of velocity data is downhole logging that provides an *in-situ* measure of sonic velocity. A successful sonic log was collected in Hole 803D that provided us with high-quality, *in-situ* velocity data for the interval from about 100 to 605 mbsf; the sample interval for this data is approximately 15 cm (60-cm sensor spacing; see "Logging" section, this chapter). To fill the gap in the upper part of the section, laboratory velocity data collected with the Dalhousie digital sediment velocimeter (DSV; see "Physical Properties" section, this chapter) were corrected to *in-situ* values and merged with the logging data (Fig. 55); the sample interval for the laboratory data was approximately 60 cm.

The adjustment of laboratory velocity measurements to *in-situ* values is a complicated task involving corrections for porosity rebound, temperature, and pressure. A carbonate-specific rebound relationship was used to correct the measured porosity for the effect of the removal of overburden, a velocity-porosity relationship was established to correct the velocity, and, finally, standard equations for the change of sound speed as a function of pressure and temperature were used to calculate *in-situ* velocity (the same procedure was applied for the adjustment of labo-

ratory density values). Failure to make these adjustments can lead to errors in the traveltime-to-depth conversion of as much as 15%. Details of these corrections can be found in Mayer et al. (1985). Once *in-situ* velocities are calculated, seismic traveltimes can be converted to depth.

The veracity of the traveltime-to-depth conversion can be evaluated through the generation of synthetic seismograms and the comparison of the synthetic seismogram to the actual seismic record collected over the site. Synthetic seismograms were generated using the corrected laboratory velocity and density data merged with the log velocity and density data. These data were resampled at a 1-ms sample interval (approximately 75 cm) and then used to calculate acoustic impedance (the product of velocity and density) and reflection coefficients (the rate of change of the acoustic impedance; Fig. 56). In principle, the reflection coefficient profile represents what a seismic profile would look like if we had a source of infinite bandwidth (perfect resolution). The reflection coefficient profile is convolved with the water-gun seismic source signature measured on the site survey cruise (Fig. 57) to generate a synthetic seismogram. The model assumes plane waves, no multiples, and no attenuation; details of the model are described in Mayer et al. (1985).
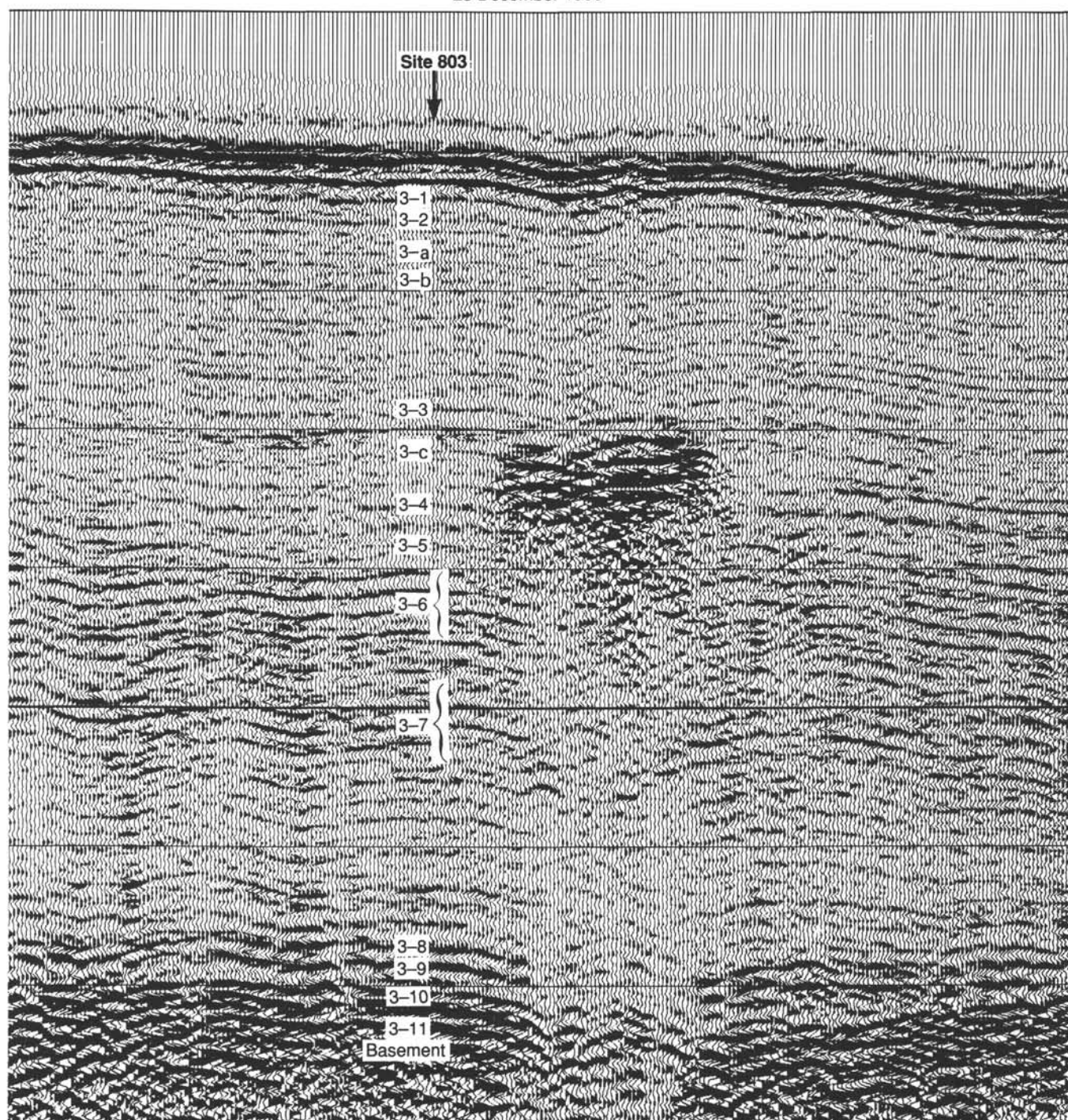
23 December 1988

Figure 54. Seismic record collected on the ROUNDABOUT Cruise 11 site survey over Site 803 using the 80-in.^{3} water gun, 70–250 Hz bandpass filter. For details of reflectors (e.g., 3-1, 3-2, 3-a), see Table 18.

Results

A comparison of the synthetic seismogram (filtered with the same filter parameters as the field record) with the seismic profile collected at Site 803 reveals an excellent match between the two (Fig. 58). The seismic data presented here was that collected on the site survey cruise aboard the *Thomas Washington* (see Mayer et al., this volume). There is almost a one-to-one correspondence between reflectors, with the larger reflectors clearly identifiable on both the synthetic seismogram and the field record. Deeper in the section, the synthetic seismogram shows a few smaller events that do not appear on the field record. This is probably caused by the lack of attenuation in the model and thus the preservation of low-amplitude, high-frequency events
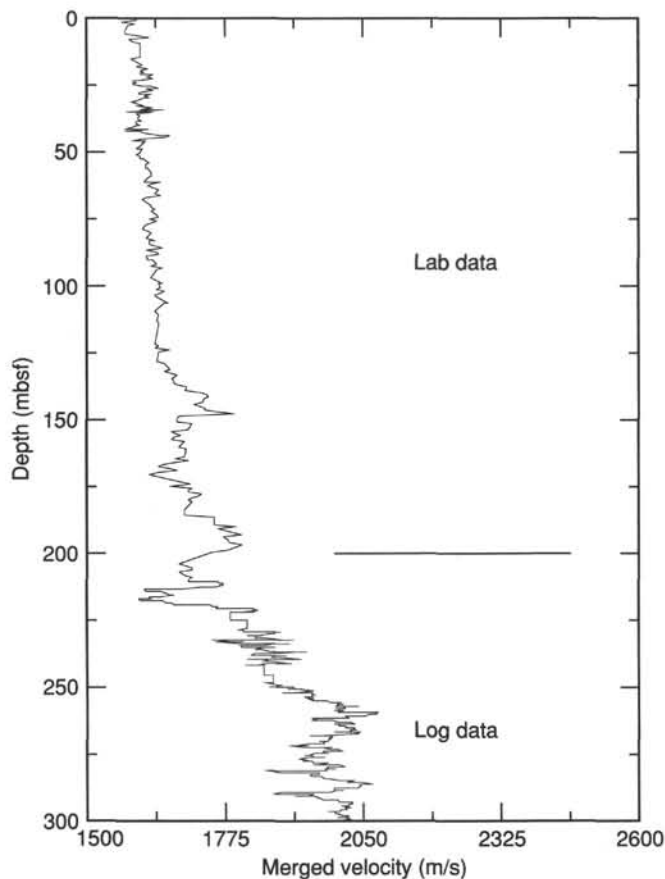
Figure 55. Merged laboratory and log velocity profile. Laboratory values are from 0 to 200 mbsf, log values from 200 to 605 mbsf.

at depth. Nonetheless, the correlation between the field record and the synthetic seismogram indicates that the traveltime-to-depth conversion is fairly accurate (close examination reveals that the model-determined velocities are about 1.2% too high).

Two sets of synthetics were generated, one including the physical properties measured on the few centimeter-thick ash layers found at 181 mbsf and one without these ash values. Although the approximately 1-cm-thick ash layer is probably too thin to be resolved on the field seismic record, the strongly contrasting physical properties associated with it and the interpolation process involved in generating the synthetic make it a clearly distinguishable event on the synthetic seismogram and thus provides a good tie point between the synthetic seismogram and the drilling results.

Given an acceptable traveltime-to-depth conversion, we can now look at the origin of some of the reflectors at Site 803. We emphasize that these are preliminary results that will undoubtedly be modified after more careful analysis.

We were able to identify 11 major reflectors or reflector packages (3-1 through 3-11) on the field record at Site 803 (Fig. 54). These reflectors were selected based on their amplitude and lateral coherency within the immediate area of Site 803. No effort has been made to select reflectors that appear to be regionally correlatable (see Mayer et al., this volume). In addition, three reflectors (a–c) that are large-amplitude events on the synthetic record but are less well defined on the field record (at least at the exact location of Site 803) have been identified. Reflectors were not picked in the upper 30 ms of the seismic record because of the disrupting effect of the outgoing pulse. The depths (in both traveltime and mbsf) as well as the ages (based on the bio-

stratigraphy of Site 803; see "Biostratigraphy" section, this chapter) of these reflectors are presented in Table 18.

Although a detailed understanding of the origin and paleoceanographic significance of these events must await careful shore-based studies, we can use the preliminary physical properties, lithologic, and biostratigraphic data to speculate on the cause of the reflectors. Associated with each major reflector is a change in acoustic impedance. Occasionally, a large reflector can result from the constructive interference of several small impedance contrasts, or a large impedance contrast does not show up as a reflector because of destructive interference (e.g., the impedance contrast at 77 mbsf [95 ms] that does not appear on either the field record or the synthetic). For the most part, however, the major reflectors are associated with a significant change in acoustic impedance (Fig. 56).

The youngest reflectors identified (3-1 and 3-2) are associated with small but rapid increases in bulk density that correspond to carbonate content maxima (Fig. 59) and, in the case of 3-1, a large increase in mean grain size (Fig. 59). No grain size measurements were made over the interval of 3-2. In contrast, the 3-a and 3-b events are the result of density shifts related to carbonate and grain size minima. The association of high carbonate content and large grain size (Reflectors 3-1 and 3-2) probably indicates increased preservation that results from the greater abundance of whole foraminifer tests. The decrease in grain size and carbonate minima associated with Reflectors 3-a and 3-b, on the other hand, probably represent periods of enhanced dissolution.

At 153 mbsf, Reflector 3-3 has yet a different signal with a low carbonate content and a grain size maximum. There is also a sharp increase in velocity at this depth, in opposition to the normal association of increasing velocity with increasing carbonate content and indicative of the dominant role that grain size variations can have in controlling the physical properties of sediments. This association of physical properties may indicate the removal of nannofossils by current winnowing. Reflector 3-c, like its letter-named counterparts, shows a dissolution signal characterized by low carbonate content, small mean grain size, and low velocity. On the synthetic seismogram that includes the ash layer, the ash occurs a few meters above Reflector 3-c. The level of the ash layer precisely corresponds to the top of the MSR (Fig. 54) and may indicate that volcanism was associated with the emplacement of the MSR. This association may also place an age constraint on the MSR.

Reflector 3-4 is at a velocity, density, and carbonate minimum; grain size data is ambiguous with the reflector lying in a transitional position between a small change from fairly coarse to fine-grained sediments. The signal appears to be one of dissolution. The sedimentologists place the ooze-chalk transition several meters below Reflector 3-4 (see "Lithostratigraphy" section, this chapter). This transition is clearly seen in the sharp change in slope of both the velocity and density curves (Fig. 56). Reflector 3-5, at about 240 mbsf, presents more of a mystery. Although it lies several meters below a large change in carbonate content, the reflector appears to be more related to the rapid changes in velocity in this part of the section. Carbonate data is spotty and no grain size information is available for this interval, so it is difficult to speculate on the origin of these velocity changes. It is possible, however, that these are the result of high-frequency changes in the degree of cementation.

Reflector 3-5 lies at the top of a major hiatus (see "Biostratigraphy" section, this chapter); the large contrast in age across this stratigraphic break may result in a rather sharp jump in the state of induration of the sediment and thus the velocity and density structure (Fig. 56). Early cementation has a large effect on the rigidity of the sediment; rigidity is the dominant parameter in determining the sonic velocity of a material. Thus, small
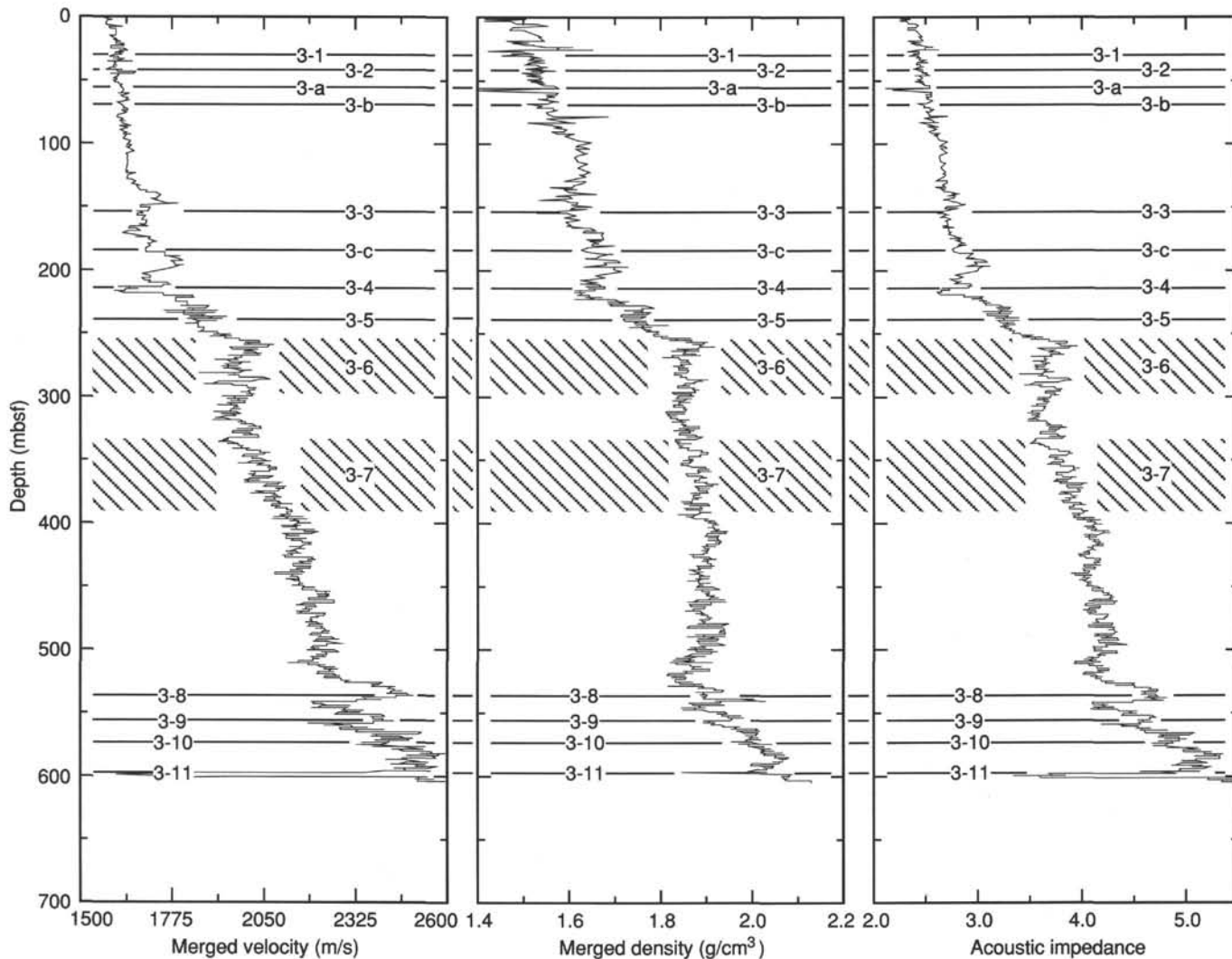
Figure 56. Velocity, density, acoustic impedance, and reflectivity data used for generating Site 803 synthetic seismogram. For details of reflectors (e.g., 3-1, 3-2, 3-a), see text.
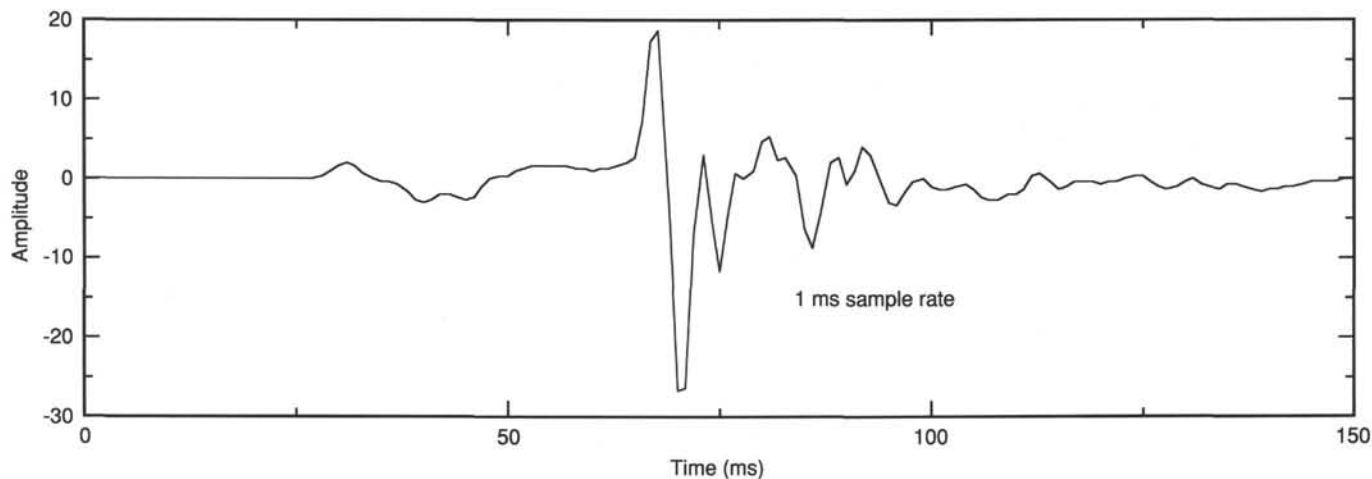

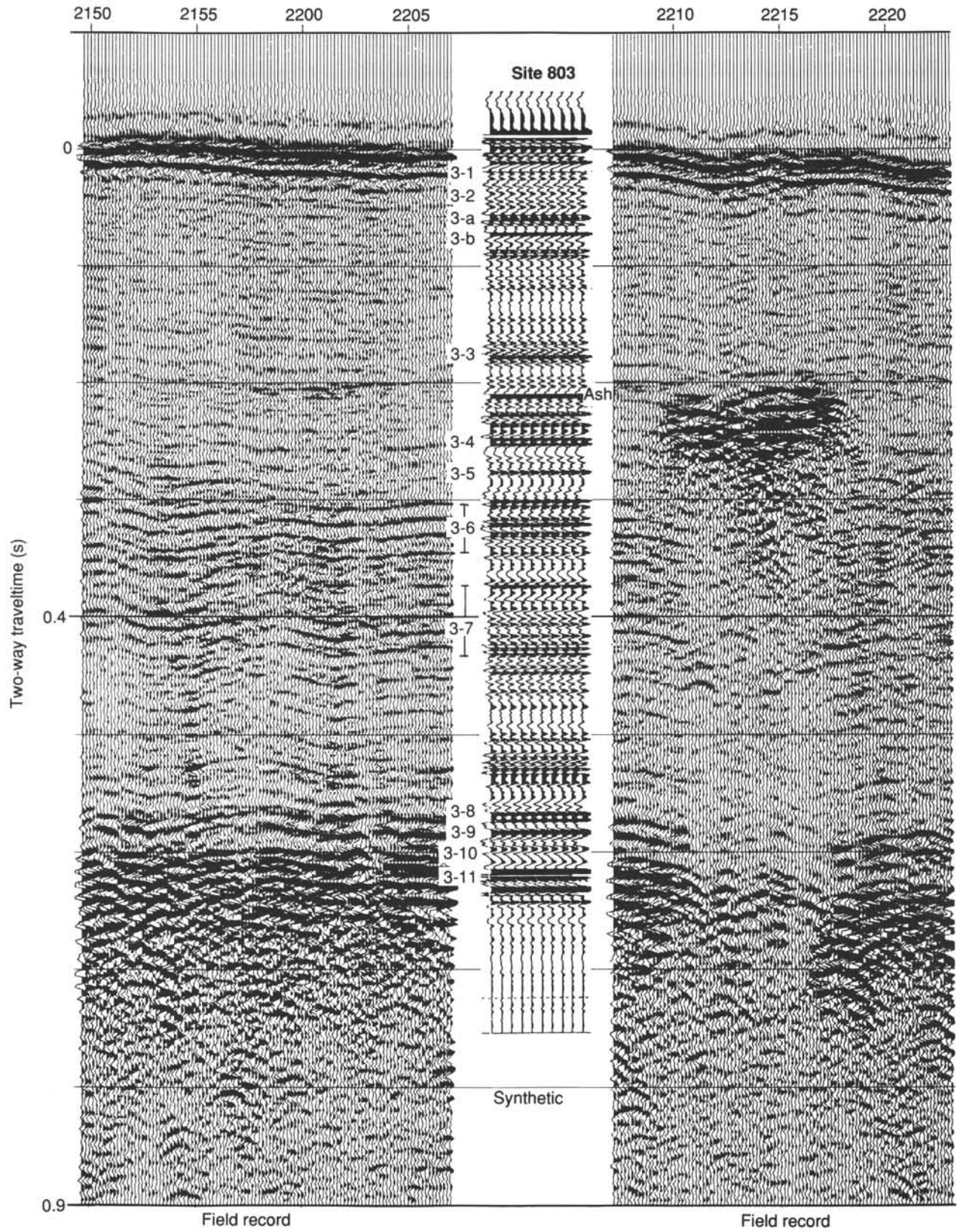Figure 57. *Thomas Washington* 80-in.[3] water-gun, farfield source signature.

Figure 58. Comparison of synthetic seismogram and field record, Site 803.

Table 18. Summary of traveltimes, depths, and ages for Site 803 reflectors.

Reflector	Two-way seismic (s)	Traveltime synthetic (s)	Depth Seismic (mbsf)	Synthetic (mbsf)	Age (Ma)
3-1	0.036	0.037	29	30	2.58
3-2	0.051	0.052	41	42	3.3–3.4
3-3	0.188	0.190	153	156	8.0–8.1
3-4	0.256	0.250	212	215	12.3–12.5
3-5	0.282	0.288	234	240	14.5–14.83
3-6	0.300–0.345	0.305–0.350	254–296	255–297	21.5–23.02
3-7	0.385–0.440	0.385–0.440	335–392	335–392	24.3–27.25
3-8	0.569	0.572	534	538	36.5–37.00
3-9	0.585	0.589	552	558	38.00
3-10	0.605	0.605	576	576	39.00
3-11	0.620	0.622	595	598	40.83
3-a		0.072		57	4.3
3-b		0.087		70.6	5.03
3-c		0.222		183	9.72

Notes: Depths and traveltimes to seismic events are picked on both the synthetic seismograph (synthetic) and the field record (seismic). Ages are from sedimentation rate curves (see "Sedimentation Rates" section, this chapter).

cyclic variations in the degree of cementation can result in a velocity structure much like that observed near Reflector 3-5.

Reflectors 3-6 and 3-7 are the two reverberant reflector packages in the lower part of the section at Site 803. Although the synthetic seismogram allows for the identification of individual reflectors within these packages, such detail is beyond the scope of this report and will be deferred to shore-based study. These reverberant packages occur within a zone of fairly high, but strongly fluctuating carbonate values (Fig. 59) that result in a highly variable density and, in particular, velocity structure. Carbonate content, velocity, and density all increase together, but a full understanding of the oceanographic processes responsible for this signal will have to await more detailed study.

The deepest reflectors (3-8 to 3-11) are the result of large decreases in velocity and density that accompany decreases in carbonate content and the appearance of significant amounts of biogenous silica. Biogenic silica typically results in decreased densities and velocities because of the low grain density of the siliceous tests (2.1 g/cm^3) and the ability of siliceous tests to maintain an open structure despite substantial overburden. This is borne out by the changes in the log resistivity (a porosity proxy) that correlate with these low-velocity zones (see "Logging" section, this chapter). The relative roles of productivity
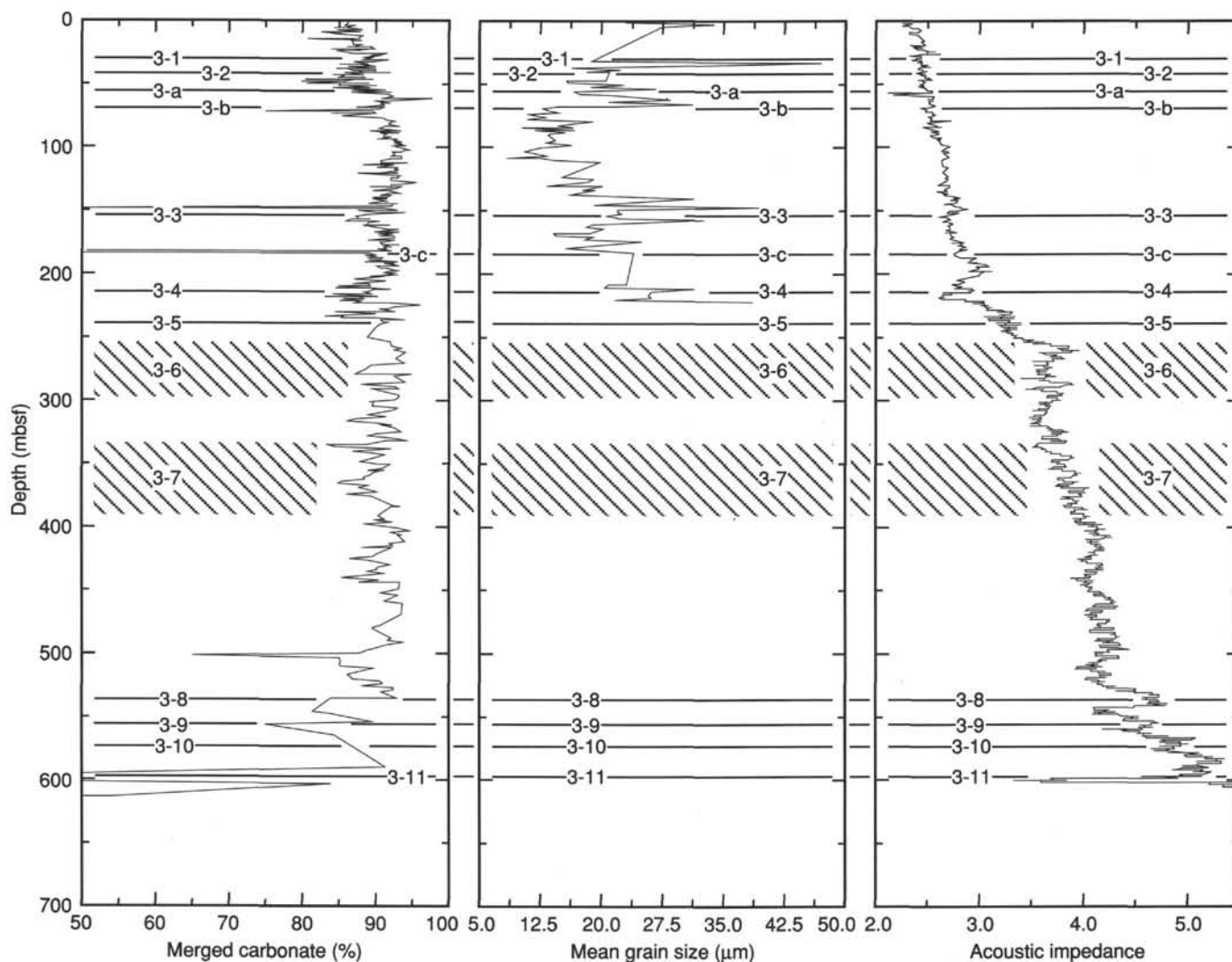

Figure 59. Carbonate content, grain size, and acoustic impedance vs. depth at Site 803. For details of reflectors (e.g., 3-1, 3-2, 3-a), see text.

and dissolution in determining the sedimentary composition of this interval must await further study. The density and velocity logs, and thus the seismic modeling, stopped short of a thin chert layer partially recovered and clearly identified on the logs, a 4.5-m-thick claystone, and finally basalt recovered at 626 mbsf. Extrapolating from existing data places basement at approximately 640 m/s below seafloor (Fig. 54).

Although the regional and global significance of the seismic events examined at Site 803 cannot be evaluated until more sites are drilled, it is interesting to speculate on the possible paleoceanographic significance of some of these events. Reflectors 3-1 and 3-2 are events that appear to be related to increases in carbonate preservation in the western equatorial Pacific. Reflector 3-1 at 2.58 Ma is within 10,000 yr of the time cited by Jansen and Sjoholm (1990) for the initiation of true Northern Hemisphere glaciation and the 3.3–3.4 Ma age for Reflector 3-2 corresponds to a time noted for increased North Atlantic Deep Water (NADW) and a shift in the benthic $\delta^{18}O$ record possibly related to increased Antarctic Bottom Water (AABW) activity (Backman, 1979; Prell, 1985).

In contrast, Reflectors 3-a and 3-b at 4.3 and 5.03 Ma, respectively, which indicate dissolution events in the Pacific, are associated with peaks in carbonate preservation in the Atlantic (Jansen and Sjoholm, 1990). The 5.03-Ma event may be related to the isolation of the Mediterranean (the Messinian interval). As noted before (Berger, 1970; Mayer et al., 1986), the chemistry, and thus the seismic response of sediments of the equatorial Pacific, appears closely linked with the history of Atlantic water masses. The winnowing indicated as the cause for Reflector 3-3 (8–8.1 Ma) may be a regional phenomenon as this is not a time of major paleoceanographic change. Reflector 3-c (9.72 Ma), apparently another dissolution event, is, on the other hand, coincident with a central Pacific-wide reflector that has been linked to global oceanographic events and, in particular, major changes in NADW circulation as is Reflector 3-4 (12.3–12.5 Ma; Mayer et al., 1986).

Reflector 3-5 (15.8 Ma) lies at the end of a major hiatus at Site 803 (see "Biostratigraphy" section, this chapter); this hiatus (in varying degrees of severity) is widespread (Keller and Barron, 1983) and also has been linked to major changes in ocean circulation and seismic events. Finally, the deepest reflectors, including Reflector 3-8 at the Eocene/Oligocene boundary, clearly represent major changes in productivity and dissolution at Site 803. Although it is likely that these too may correspond to regional if not global events, it is too early to speculate at this point.

SUMMARY AND CONCLUSIONS

Site 803 is situated on the equatorial northeastern margin of the Ontong Java Plateau in 3410 m of water at 2°26'N and 160°32'E. It was drilled as part of a Neogene depth transect to serve as a deep-water anchor site. The primary objective was to sample a section affected by substantial carbonate dissolution, yet sufficiently complete to provide a record of dissolution gradients, events, and cycles, that could be tied into a biostratigraphic framework. Other objectives were to provide Paleogene and Cretaceous sediments for paleoceanographic studies and to obtain basement rock that might shed light on the origin of the Ontong Java Plateau. The site was located on a *Thomas Washington* single-channel seismic (SCS) line acquired during the ROUNDABOUT Cruise 11 "DANCER" survey between proposed Sites OJP-4 and OJP-4B, upslope from a mid-section reflector (MSR).

Coring Results

Site 803 was occupied for 8.7 days. We cored 991.3 m of sediments: 552.4 m with the APC (103% recovery), 394.9 m with the XCB (63% recovery), and 7.0 m with the RCB (38% recovery). Also, we cored 25.6 m of basalt, recovering a total of 9.6 m in all (38% recovery). Total core recovery was 837.4 m. We drilled four holes as follows: Hole 803A with the APC from 0 to 55.5 mbsf; Hole 803B with the APC from 0 to 61.3 mbsf; Hole 803C with the APC from 19 to 237.5 mbsf; and Hole 803D with the APC from 0 to 217.1 mbsf, with the XCB from 217.1 to 612.0 mbsf, and with the RCB from 612.0 to 656.0 mbsf.

The recovered sediments range in age from Pleistocene to early Late Cretaceous; they were divided into three units. The uppermost unit, Unit I, takes up most of the section (0–563.7 mbsf); it ranges from late Eocene to Pleistocene in age and consists of nannofossil ooze and chalk to foraminifer nannofossil ooze and chalk. Unit II (563.7–621.8 mbsf) ranges from the middle to the late Eocene in age and consists of approximately 58 m of nannofossil chalk with radiolarians, radiolarian nannofossil chalk, nannofossil radiolarite, and minor amounts of chert. Unit III (621.8–626.3 mbsf) ranges from the early Late Cretaceous to the middle Eocene in age and is composed of claystone and clayey siltstone, with minor radiolarian-rich intervals. Resistivity logs suggest that this lithology continues from 621.8 mbsf to basement at 630.4 mbsf.

The record is continuous from the Pleistocene to the lower Miocene, where there is a significant stratigraphic break at 245.9 mbsf with a double hiatus within the period from 22 to 15 Ma, the first of three major stratigraphic breaks encountered above the Cretaceous/Tertiary (K/T) boundary. The other two stratigraphic breaks occur across the Paleocene/Eocene boundary (~45–~58 Ma) at 621.8 mbsf and in the Paleocene (~58–~66 Ma) immediately below. The section below the K/T boundary, which was penetrated at 622.25 mbsf, is condensed and, presumably, also contains several substantial hiatuses.

In Unit I, the ooze-chalk transition occurs between 210 and 220 mbsf and provides the basis for division into Subunits IA and IB. The logging data suggest that this transition extends over 60 m in the sedimentary column.

Subunit IA (0–217 mbsf) consists of nannofossil ooze, nannofossil ooze with foraminifers, and foraminifer nannofossil ooze. The foraminifer content is high in the Pleistocene and adjacent upper Pliocene ooze and decreases downhole through the first 30 to 60 mbsf, so that most of the subunit is nannofossil ooze. There is a slight increase in foraminifer content within the upper Miocene sediments, somewhat below the middle of the section. Bioturbation is ubiquitous. Colors are dominantly various types of white and light gray; the Pleistocene section also exhibits colors with a yellowish hue. Faint green, purple, and red color bands are common, except in the upper middle Miocene nannofossil ooze (ca. 14–10 Ma). These appear to have an origin analogous to "Liesegang" rings, which arise through diffusion along redox gradients that surround objects that contain reducing matter.

Sediment instability is indicated by microfaulted and discordant color banding at several levels in the section, especially in the lower Pliocene and uppermost Miocene ooze, but also within the upper and middle Miocene portions. One thin discrete ash layer is present in Unit I (at 181.2 mbsf in Hole 803D) that clearly ties the recovered section to the logging data.

Subunit IB (217–564 mbsf) consists of nannofossil chalk and nannofossil chalk with foraminifers. Its upper boundary is marked by a shift to higher velocity in the log data, with only one more low-velocity layer downhole between 240 and 250 mbsf. Subunit IB is much like the younger Subunit IA, except for the presence of lithification. Colors are.similar, as is intensity of bioturbation. Color banding appears in lower Oligocene sediments (around 420–520 mbsf). The bands become more abundant, intense, and distinct downhole in this interval. They are continuous across and through burrows.

Radiolarians are present in low proportions throughout the section and their abundance never exceeds 7% in smear slide analyses. Minor amounts of chert were recovered at 546.15 mbsf in lowermost Oligocene sediments. A marked decrease in pore-water silica near this level indicates the onset of silica precipitation. Chert formation and enhanced grain cementation in the upper Eocene chalk is probably responsible for the local high-velocity layers detected in the logs at 521–541 and 546–558 mbsf and below 564 mbsf.

Unit II (564–622 mbsf) consists of interbedded upper to middle Eocene nannofossil chalk with radiolarians, radiolarian nannofossil chalk, and nannofossil radiolarite. Drilling disturbance was significant in this unit. Minor amounts of chert were recovered. These sediment types produce distinctive records in the physical properties measurements, logging data, and seismic reflection profiles. Chert presumably is more abundant than coring reveals: it may appear as a thin bed with high values in the resistivity log and with high sound velocities; furthermore, it may be responsible for a major reflector on the seismic profiles at that depth.

Unit III (622–626 mbsf) is surprisingly thin for the age range (middle Eocene–early Late Cretaceous). It is composed of dark-colored claystone and siltstone, predominated by deep-sea siliciclastic sediments. Unit III also contains a complete Cretaceous/Tertiary boundary sequence as well as several major unconformities.

In Unit IV, nine basalt subdivisions were recognized based on the presence of intercalated limestones or breccias. The age, based on paleontology, is probably Cenomanian or older. The basalts are predominantly aphyric, fine-grained, and nonvesicular tholeiites. Shipboard XRF measurements indicate that the basalts are fairly evolved and, in terms of their Zr/Nb ratio (15–17), distinct from both normal mid-ocean-ridge basalt (Zr/Nb greater than 30) and typical oceanic-island tholeiites (Zr/Nb commonly less than 12). Slight compositional variations within the basalts indicate that they may have been derived from more than one parental magma.

Seismic Stratigraphy

Site 803 is characterized by a layer-cake seismic stratigraphy. The 14 reflectors that have been identified in the synthetic seismograms, generated from Site 803 physical property and logging data, almost exactly match those in the SCS survey profiles (see "Seismic Stratigraphy" section, this chapter). Reflectors 3-1 and 3-2 (at 2.6 and 3.3–3.4 Ma, respectively) appear to be related to fluctuations in carbonate preservation in the western equatorial Pacific and possibly linked to the initiation of Northern Hemisphere glaciation and the increased activity of North Atlantic Deep Water (NADW) (cf. Mayer et al., 1986). Reflectors 3-a and 3-b (at 4.3 and 5.0 Ma, respectively) are believed to be indicative of dissolution events.

The winnowing suggested to be the possible cause for Reflector 3-3 (at 8–8.1 Ma), as indicated by the high sand content at about 146 mbsf at Site 803, may be a regional phenomenon unrelated to a major paleoceanographic change. However, a similar winnowing event is indicated in DSDP Site 586 at about that time. Reflector 3-c (9.7 Ma) apparently coincides with a central Pacific-wide reflector that has been linked to global oceanographic events, in particular, to major changes in NADW production. The same is true for Reflector 3-4 (at 12.3–12.5 Ma; Mayer et al., 1986). Reflector 3-5 (at 15.1–15.5 Ma) coincides with a major hiatus, typical for this period of Antarctic cooling. Reflector packages 3-6 and 3-7 mark the late Oligocene to early Miocene transition period. They presumably arose in response to carbonate fluctuations produced as a consequence of climatic change when the Drake passage opened. The deepest reflectors, including 3-8 near the Eocene/Oligocene boundary, clearly represent major changes in depositional style and diagenesis at Site 803, especially in the accumulation of silica.

Sequence of Events

Widespread volcanism occurred in the region of the Ontong Java Plateau in Aptian-Albian time. At Site 803 on the flank of the plateau, the thin, pillowed nature of the flows implies that their feeder vents were not very distant and that eruption rates were low. The severe alteration of the uppermost lava flow of Unit IV coupled with the absence of metalliferous sediments directly overlying the basalt indicates the presence of a hiatus of unknown origin and duration.

The depositional history at Site 803 began in the early Late Cretaceous with slow and/or discontinuous siliciclastic sedimentation below the CCD. Sedimentation apparently was continuous across the K/T boundary. The fact that these sediments are preserved is remarkable and calls for an explanation. We propose early lithification as an answer. The presence of a major hiatus, occupying most of the Paleocene to early Eocene time, suggests erosional activity within or at the end of this period. The hiatus ended with the onset of pelagic sedimentation in the middle Eocene, suggesting a deepening of the CCD, as well as the return of conditions favorable for the production and preservation of biogenic silica (cf. Berger and Winterer, 1974; van Andel et al., 1975). Since the late Eocene, carbonate deposition has dominated in this location. Sedimentation rates, about 7 m/m.y. during the middle Eocene, doubled in the late Eocene, to 13 m/m.y. at 40 Ma.

Sedimentation at Site 803, continuous across the Eocene/Oligocene boundary, remained near 13 m/m.y. into the early Miocene. Paleomagnetic analyses of the Oligocene sediments have resulted in a tentative magnetostratigraphy spanning Chrons 11 through 7. Preliminary analyses indicate a paleolatitude of 4.5°S for Site 803 during the Oligocene, which, in turn, implies that the Ontong Java Plateau has been part of the Pacific Plate for the past 30 m.y. In the early Miocene, the one significant Neogene hiatus developed, involving the record between 22 and 15 Ma (NH2 of Keller and Barron, 1983). The sediments above the hiatus, of middle Miocene age, were deposited at rates near 10 m/m.y. The hiatus may be related to earthquake activity associated with a resurgence of transcurrent motion along nearby fracture zones caused by a change in Indo-Australia plate motion. This event, which took place about 16 Ma, resulted in renewed convergence along the Melanesian Subduction Zone (Manus–North Solomon–Vitiaz trenches) and a rejuvenation of volcanism along the Melanesian Arc (Kroenke, 1984).

In the late middle Miocene, ash was erupted from a not-too-distant source, a source that may also have been responsible for the emplacement of a nearby mid-section reflector. Although possibly related to incipient Solomon Island Arc volcanism, the ash more likely is the product of nearby tectonic volcanism, resulting from transtensive stress release, linked again to a resurgence of transcurrent motion along nearby fracture zones that was caused by still another change in Indo-Australian Plate motion. The latter event, occurring roughly ca. 10–12 Ma, also probably coincided with the formation of the new Solomon Island Subduction Zone (along the New Britain–San Cristobal trenches). In the late Miocene, sedimentation rates abruptly increased to between 25 and 30 m/m.y., with peak rates centered on ~7 Ma. In the Pliocene, sedimentation rates decreased to 15 m/m.y.; in the Pleistocene, they decreased still further to about 10 m/m.y. The magnetic stratigraphy shows that the decrease takes place at the base of the Olduvai Subchron (1.88 Ma).

Comparison of Site 803 with Sites 288, 289/586, and 462

Of the sites previously drilled on the Ontong Java Plateau, Sites 289/586 are the nearest to Site 803 and contain the most complete and well-studied sections. In comparing the sites, a few notable similarities were observed. The basement basalts at Site 803 are compositionally quite similar (at least in terms of Zr and Nb) to the basalt drilled at Site 289 as well as to the few analyzed basement lavas of Malaita (eastern Solomon Islands) and to the basalt flows and sills drilled at Site 462 in the Nauru Basin northeast of the Ontong Java Plateau.

Numerous hiatuses were encountered in the lower Paleogene and Upper Cretaceous sections drilled at DSDP Sites 288 and 289 on the Ontong Java Plateau that may well correlate with missing intervals at Site 803. These hiatuses may be associated with tectonic events that occurred around the region during Late Cretaceous and early Paleogene time. For example, hiatuses that occur deep in the section at Sites 288 and 289, and perhaps even at Site 807, may be related to the Campanian volcanic events recorded at Site 462 in the Nauru Basin (Moberly, Schlanger, et al., 1986). Early Paleogene hiatuses at all three sites may be related, in part, to the initiation of subduction along the Papuan–New Caledonia trenches and the end of seafloor spreading in the Tasman and Coral Sea basins (Kroenke, 1984).

With regard to Paleogene sediments, it appears that similar conditions, favorable for the supply and preservation of silica, existed in the Eocene at Sites 803 and 289. Such conditions are typical of the entire central Pacific (Berger, 1973; van Andel et al., 1975). Likewise, the Eocene record at both sites was interrupted by several intervals of erosion and/or nondeposition. The descriptions of the Neogene nannofossil oozes and chalks with their various subordinate components also are quite similar for these two sites. However, there are substantial differences in detail, especially with regard to sedimentation rates. These differences may be summarized as follows:

1. The basalts at Site 803 are pillow basalts that comprise many thin flows in contrast to the single massive flow drilled at Site 289.

2. In the sediments, no chert was observed in the Miocene at Site 803, and the amount of chert encountered deep in the hole was minor in contrast to the massive cherts encountered at Site 289 in the middle Eocene–Upper Cretaceous section.

3. A complete K/T transition sequence was found at Site 803 (albeit within a claystone-siltstone sequence) as opposed to the hiatus encountered at Site 289.

4. Significantly, and in contrast to Site 289, no stratigraphic break was observed at the Eocene/Oligocene boundary at Site 803.

5. On the other hand, sedimentation rates were higher at Sites 289/586 than at Site 803 because of the shallower depth of the former (2200 vs. 3400 m) and no Miocene hiatus was observed at Sites 289/586.

When comparing overall sedimentation rate patterns of Site 803 with those of Sites 289/586, one notes striking changes in the ratios for the Neogene sediments. This ratio ranges from 0.32 (for the lower Pliocene) to 0.77 (for the upper Miocene). Expressed inversely, the rates at Site 289 are higher by a factor of between 3 and 1.3. Some of this variation is quite probably a result of the changing intensity of winnowing on top of the plateau, but most of it must be ascribed to the changing intensity of dissolution below 3000 m depth.

REFERENCES

Andrews, J. E., Packham, G., et al., 1975. *Init. Repts. DSDP,* 30: Washington (U.S. Govt. Printing Office).

Backman, J., 1979. Pliocene biostratigraphy of DSDP Sites 111 and 116 from the North Atlantic Ocean and the age of the Northern Hemisphere Glaciation. *Stockholm Contrib. Geol.,* 32:115–137.

Barron, J. A., 1985. Miocene to Holocene planktonic diatoms. *In* Bolli, H. M., Saunders, J. B., and Perch-Nielsen, K. (Eds.), *Plankton Stratigraphy:* Cambridge (Cambridge Univ. Press), 763–809.

Berger, W. H., 1970. Biogenous deep-sea sediments: fractionation by deep-sea circulation. *Geol. Soc. Am. Bull.,* 81:1385–1401.

_____, 1973. Cenozoic sedimentation in the eastern tropical Pacific. *Geol. Soc. Am. Bull.,* 84:1941–1954.

Berger, W. H., and Johnson, T. C., 1976. Deep-sea carbonates: dissolution and mass wasting on Ontong Java Plateau. *Science,* 192:785–787.

Berger, W. H., Johnson, T. C., and Hamilton, E. L., 1977. Sedimentation on Ontong-Java Plateau: observations on a classic "carbonate monitor." *In* Anderson, N. R., and Malahoff, A. (Eds.), *The Fate of Fossil Fuel CO$_2$ in the Oceans:* New York (Plenum Press), 543–567.

Berger, W. H., and Mayer, L. A., 1978. Deep-sea carbonates: acoustic reflectors and lysocline fluctuations. *Geology,* 6:11–15.

Berger, W. H., and Winterer, E. L., 1974. Plate stratigraphy and the fluctuating carbonate line. *In* Hsü, K. J., and Jenkyns, H. C. (Eds.), *Pelagic Sediments on Land and Under the Sea.* Spec. Publ., Int. Assoc. Sedimentol., 1:11–48.

Berggren, W. A., Kent, D. V., and Flynn, J. J., 1985a. Jurassic to Paleogene: Part 2. Paleogene geochronology and chronostratigraphy. *In* Snelling, N. J. (Ed.), *The Chronology of the Geological Record.* Mem. Geol. Soc. (London), 10:141–195.

Berggren, W. A., Kent, D. V., and Van Couvering, J. A., 1985b. The Neogene: Part 2. Neogene geochronology and chronostratigraphy. *In* Snelling, N. J. (Ed.), *The Chronology of the Geological Record.* Mem. Geol. Soc. (London), 10:211–260.

Bleil, U., 1985. The magnetostratigraphy of northwest Pacific sediments, Deep Sea Drilling Project Leg 86. *In* Heath, G. R., Burckle, L. H., et al., *Init. Repts. DSDP,* 86: Washington (U.S. Govt. Printing Office), 441–458.

Bolli, H. M., and Saunders, J. B., 1985. Oligocene to Holocene low latitude planktic foraminifera. *In* Bolli, H. M., Saunders, J. B., and Perch-Nielsen, K. (Eds.), *Plankton Stratigraphy:* Cambridge (Cambridge Univ. Press), 155–262.

Burckle, L. H., 1972. Late Cenozoic planktonic diatom zones from the eastern equatorial Pacific. *Nova Hedwigia Beih.,* 39:217–246.

Elderfield, H., Gieskes, J. M., Baker, P. A., Oldfield, R. K., Hawkesworth, C. J., and Miller, R., 1982. ^{87}Sr/^{86}Sr and ^{18}O/^{16}O ratios, interstitial water chemistry and diagenesis in deep-sea carbonate sediments of the Ontong-Java Plateau. *Geochim. Cosmochim. Acta,* 46:2259–2268.

Emeis, K.-C., and Kvenvolden, K. A., 1986. Shipboard organic geochemistry on *JOIDES Resolution.* ODP Tech. Note, No. 7.

Espitalié, J., Laporte, J. L., Madec, M., Marquis, F., Leplat, P., Paulet, J., and Boutefeu, A., 1977. Method rapide de caracterisation des roches mère de leur potentiel petrolier et de leur degree d'evolution. *Rev. Inst. Fr. Pet.,* 32:23–42.

Fenner, J., 1984. Eocene-Oligocene planktic diatom stratigraphy in the low latitudes and the high southern latitudes. *Micropaleontology,* 30:319–342.

Floyd, P. A., 1986. Petrology and geochemistry of oceanic intraplate sheet-flow basalts, Nauru Basin, Deep Sea Drilling Project Leg 89. *In* Moberly, R., Schlanger, S. O., et al., *Init. Repts. DSDP,* 89: Washington (U.S. Govt. Printing Office), 471–497.

Gieskes, J. M., 1981. Deep-sea drilling interstitial water studies: implications for chemical alteration of the oceanic crust, Layers I and II. *In* Warme, J. E., Douglas, R. G., and Winterer, E. L. (Eds.), *The Deep Sea Drilling Project: A Decade of Progress.* Spec. Publ., Soc. Econ. Paleontol. Mineral., 32:149–167.

Gordon, R. G., 1983. Late Cretaceous apparent polar wander of the Pacific plate: evidence for a rapid shift of the Pacific hotspots with respect to the spin axis. *Geophys. Res. Lett.,* 10:709–712.

Hammond, S. R., Kroenke, L. W., and Theyer, F., 1975. Northward motion of the Ontong-Java Plateau between -110 and -30 m.y.: a paleomagnetic investigation of DSDP Site 289. *In* Andrews, J. E., Packham, G., et al., *Init. Repts. DSDP*, 30: Washington (U.S. Govt. Printing Office), 415–418.

Humphris, S. E., Thompson, R. N., Gibson, I. L., and Marriner, G. F., 1980. Comparison of geochemistry of basalts from the East Pacific Rise, OCP Ridge and Siqueiros Fracture Zone, Deep Sea Drilling Project, Leg 54. *In* Rosendahl, B. R., Hekinian, R., et al., *Init. Repts. DSDP*, 54: Washington (U.S. Govt. Printing Office), 635–649.

Hussong, D. M., Wipperman, L. K., and Kroenke, L. W., 1979. The crustal structure of the Ontong Java and Manihiki oceanic plateaus. *J. Geophys. Res.*, 84:6003–6010.

Ingle, J. C., Jr., Suehiro, K., von Breymann, M. T., et al., 1990. *Proc. ODP, Init. Repts.*, 128: College Station, TX (Ocean Drilling Program).

Jackson, E. D., Bargar, K. E., Fabbi, B. P., and Heropoulos, C., 1976. Petrology of the basaltic rocks drilled on Leg 33 of the Deep Sea Drilling Project. *In* Schlanger, S. O., Jackson, E. D., et al., *Init. Repts. DSDP*, 33: Washington (U.S. Govt. Printing Office), 571–630.

Jansen, E., and Sjoholm, J., 1990. Late Miocene–Pleistocene evolution of Northern Hemisphere and global glaciations. *Nature*.

Johanssen, A., 1931. *A Descriptive Petrography of the Igneous Rocks* (Vol. 1): Chicago (Univ. of Chicago Press).

Johnson, T. C., Hamilton, E. L., and Berger, W. H., 1977. Physical properties of calcareous ooze: control by dissolution at depth. *Mar. Geol.*, 24:259–277.

Kaminski, M. A., Gradstein, F. M., Berggren, W. A., Geroch, S., and Beckmann, J. P., 1986. Flysch-type agglutinated foraminiferal assemblages from Trinidad: taxonomy, stratigraphy and paleobathymetry. *Proc. Second Int. Workshop on Agglutinated Foraminifera*, Vienna.

Keller, G., and Barron, J. A., 1983. Paleoceanographic implications of Miocene deep sea hiatuses. *Geol. Soc. Am. Bull.*, 94:590–613.

Kempton, P. D., Autio, L. K., Rhodes, J. M., Holdaway, M. J., Dungan, M. A., and Johnson, J., 1985. Petrology of basalts from Hole 504B, Deep Sea Drilling Project, Leg 83. *In* Anderson, R. N., Honnorez, J., et al., *Init. Repts. DSDP*, 83: Washington (U.S. Govt. Printing Office), 129–164.

Kennett, J. P., and Srinivasan, M. S., 1983. *Neogene Planktonic Foraminifera: A Phylogenetic Atlas*: Stroudsburg, PA (Hutchinson Ross).

Kroenke, L. W., 1972. Geology of the Ontong Java Plateau. *Hawaii Inst. Geophys. Rep.*, HIG 72-5.

———, 1984. Cenozoic Tectonic Development of the Southwest Pacific. *U.N. ESCAP, COOP/SOPAC, Tech. Bull.*, No. 6.

Kroenke, L. W., Jouannic, C., and Woodward, P. (Comps.), 1983. Bathymetry of the Southwest Pacific: Chart 1 of the Geophysical Atlas of the Southwest Pacific, CCOP/SOPAC.

Kroenke, L. W., Resig, J., and Cooper, P. A., 1986. Tectonics of the southeastern Solomon Islands: formation of the Malaita Anticlinorium. *In* Vedder, J. G., Pound, K. S., and Boundy, S. Q. (Eds.), *Geology and Offshore Resources of Pacific Island Arcs, Central and Western Solomon Islands*. Circum-Pacific Counc. Energy Mineral Resourc., Earth Sci. Ser., 4:109–116.

Lee, H. J., 1982. Bulk density and shear strength of several deep-sea calcareous sediments. *In* Demars, K. R., and Chaney, R. C. (Eds.), *Geotechnical Properties, Behavior, and Performance of Calcareous Soils*. ASTM Spec. Tech. Publ., 777:54–78.

McDuff, R. E., 1981. Major cation gradients in DSDP interstitial waters: the role of diffusive exchange between seawater and upper ocean crust. *Geochim. Cosmochim. Acta*, 45:1705–1713.

McDuff, R. E., and Gieskes, J. M., 1976. Calcium and magnesium in DSDP interstitial waters: diffusion or reaction? *Earth Planet. Sci. Lett.*, 33:1–10.

Mahoney, J. J., 1987. An isotopic survey of Pacific oceanic plateaus: implications for their nature and origin. *In* Keating, B. H., Fryer, P., Batiza, R., and Boehlert, G. W. (Eds.), *Seamounts, Islands, and Atolls*. Am. Geophys. Union Monogr., 43:207–220.

Mammerickx, J., and Smith, S. M., 1985. *Bathymetry of the North Central Pacific*: Boulder, CO (Geological Society of America), Map and Chart Ser., No. MC-52.

Martini, E., 1971. Standard Tertiary and Quaternary calcareous nannoplankton zonation. *In* Farinacci, A. (Ed.), *Proceedings of the Second International Conference on Planktonic Microfossils, Roma*: Rome (Ed. Technoscienza), 2:739–785.

Mayer, L. A., 1979. The origin of fine scale acoustic stratigraphy in deep-sea carbonates. *J. Geophys. Res.*, 804:6177–6184.

Mayer, L. A., Shipley, T. S, Theyer, F., Wilkens, R. W., and Winterer, E. L., 1985. Seismic modeling and paleoceanography at Deep Sea Drilling Project Site 574. *In* Mayer, L. A., Theyer, F., Thomas, E., et al., *Init. Repts. DSDP*, 85: Washington, (U.S. Govt. Printing Office), 947–970.

Mayer, L. A., Shipley, T. H., and Winterer, E. L., 1986. Equatorial Pacific seismic reflectors as indicators of global oceanographic events. *Science*, 233:761–764.

Moberly, R., Schlanger, S. O., et al., 1986. *Init. Repts. DSDP*, 89: Washington (U.S. Govt. Printing Office), 213–235.

Monechi, S., 1985. Campanian to Pleistocene calcareous nannofossil stratigraphy from the northwest Pascific Ocean, Deep Sea Drilling Project Leg 86. *In* Heath, G. R., Burckle, L. H., et al. *Init. Repts. DSDP*, 86: Washington (U.S. Govt. Printing Office), 301–336.

Nur, A., and Ben-Avraham, Z., 1982. Oceanic plateaus, the fragmentation of continents, and mountain building. *J. Geophys. Res.*, 87: 3644–3661.

Prell, W. L., 1985. Pliocene stable isotope and carbonate stratigraphy (Holes 572C and 573A): paleoceanographic data bearing on the question of Pliocene glaciation. *In* Mayer, L., Theyer, F., Thomas, E., et al., *Init. Repts. DSDP*, 85: Washington (U.S. Govt. Printing Office), 723–734.

Pyle, M. R., 1984. Vane shear data on undrained residual strength. *J. Tech. Div. Am. Soc. Civ. Eng.*, 110:543–547.

Rio, D., Fornaciari, E., and Raffi, I., in press. Late Oligocene through early Pleistocene calcareous nannofossils from western equatorial Indian Ocean (ODP Leg 115). *In* Duncan, R. A., Backman, J., Peterson, L. C., et al., *Proc. ODP, Sci. Results*, 115: College Station, TX (Ocean Drilling Program).

Sager, W. W., 1987. Late Eocene and Maastrichtian paleomagnetic poles for the Pacific plate: implications for the validity of seamount paleomagnetic data. *Tectonophysics*, 144:301–314.

Sanfilippo, A., and Riedel, W. R., 1985. Cretaceous radiolaria. *In* Bolli, H. M., Saunders, J. B., and Perch-Nielsen, K. (Eds.), *Plankton Stratigraphy*: Cambridge (Cambridge Univ. Press), 573–630.

Sanfilippo, A., Westberg-Smith, M. J., and Riedel, W. R., 1985. Cenozoic radiolaria. *In* Bolli, H. M., Saunders, J. B., and Perch-Nielsen, K. (Eds.), *Plankton Stratigraphy*: Cambridge (Cambridge Univ. Press), 631–712.

Saunders, A. D., 1986. Geochemistry of basalts from the Nauru Basin, Deep Sea Drilling Project Legs 61 and 89: implications for the origin of oceanic flood basalts. *In* Moberly, R., Schlanger, S. O., et al., *Init. Repts. DSDP*, 89: Washington (U.S. Govt. Printing Office), 499–517.

Saunders, J. B., Bernoulli, D., Müller-Merz, E., Oberhänsli, H., Perch-Nielsen, K., Riedel, W. R., Sanfilippo, A., and Torrini, R., Jr., 1984. Stratigraphy of late middle Eocene to early Oligocene in the Bath Cliff section Barbados, West Indies. *Micropaleontology*, 30: 390–425.

Seifert, K. E., Vallier, T. L., Windom, K. E., and Morgan, S. R., 1981. Geochemistry and petrology of igneous rocks, Deep Sea Drilling Project Leg 62. *In* Thiede, J., Vallier, T. L., et al., *Init. Repts. DSDP*, 62: Washington (U.S. Govt. Printing Office), 945–954.

Stoeser, D. B., 1975. Igneous rocks from Leg 30 of the Deep Sea Drilling Project. *In* Andrews, J. E., Packham, G., et al., *Init. Repts. DSDP*, 30: Washington (U.S. Govt. Printing Office), 401–414.

Thomas, E., 1990. Late Cretaceous through Neogene deep-sea benthic foraminifers (Maud Rise, Weddell Sea, Antarctica). *In* Barker, P. F., Kennett, J. P., et al., *Proc. ODP, Sci. Results*, 113: College Station, TX (Ocean Drilling Program), 571–591.

Toumarkine, M., and Luterbacher, H., 1985. Paleocene and Eocene planktic foraminifera. *In* Bolli, H. M., Saunders, J. B., and Perch-Nielsen, K. (Eds.), *Plankton Stratigraphy*: Cambridge (Cambridge Univ. Press), 87–154.

van Andel, T. H., Heath, G. R., and Moore, T. C., Jr., 1975. Cenozoic history and paleoceanography of the central equatorial Pacific. *Mem. Geol. Soc. Am.*, 143:1–134.

Winterer, E. L., Riedel, W. R., et al., 1971. *Init. Repts. DSDP,* 7: Washington (U.S. Government Printing Office).
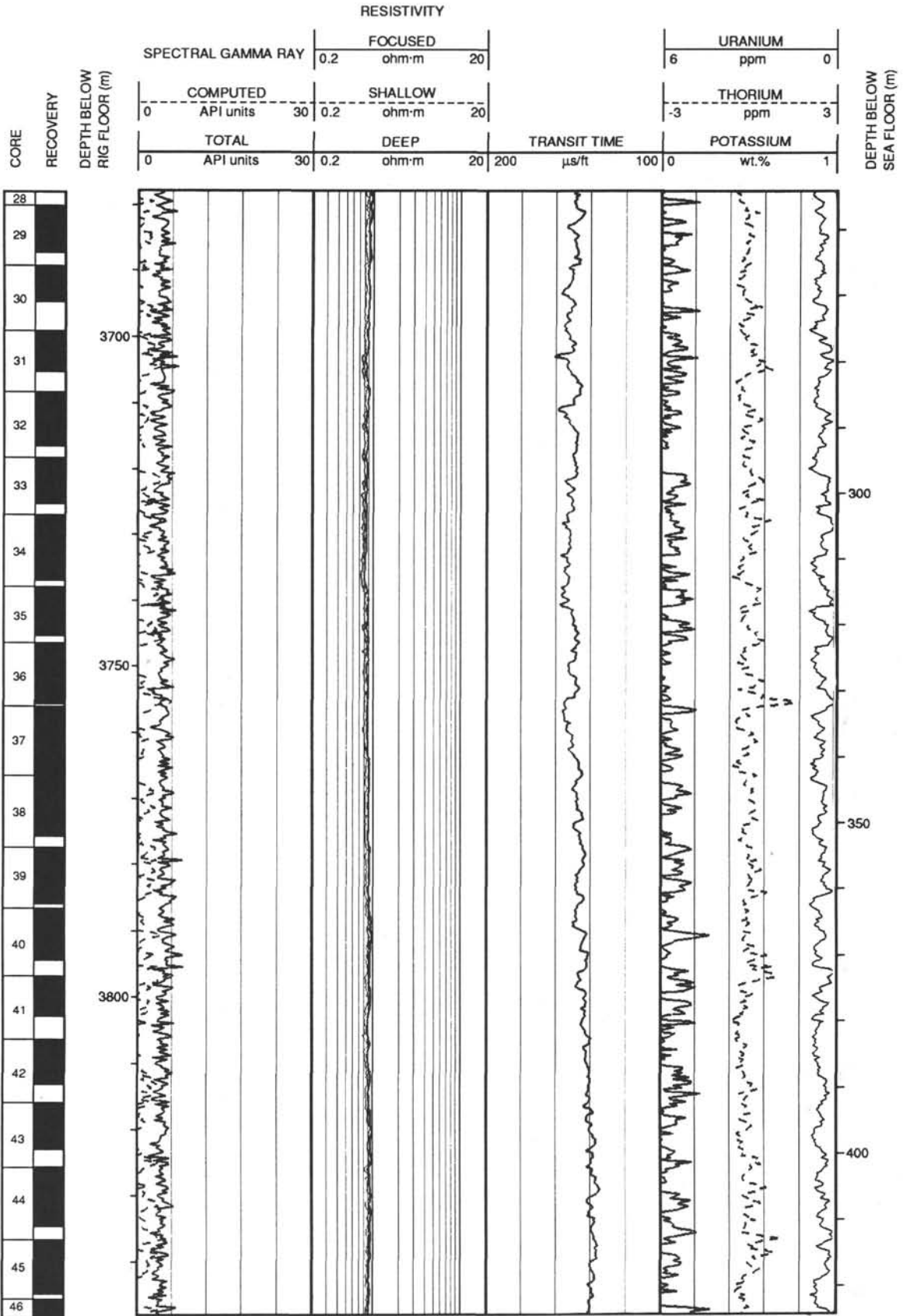
Woodruff, F., 1985. Changes in Miocene deep-sea benthic foraminiferal distribution in the Pacific Ocean: relationship to paleoceanography. *In* Kennett, J. P. (Ed.), *The Miocene Ocean: Paleoceanography and Biogeography.* Mem. Geol. Soc. Am., 163:131–175.

Wright, A. A., Bleil, U., Monechi, S., Michel, H. V., Shackleton, N. J., Simoneit, B.R.T., and Zachos, J. C., 1985. Summary of Cretaceous/Tertiary boundary studies, Deep Sea Drilling Project Site 577, Shatsky Rise. *In* Heath, G. R., Burckle, L. H., et al., *Init. Repts. DSDP,* 86: Washington (U.S. Govt. Printing Office), 799–804.

Ms 130A-105

NOTE: All core description forms ("barrel sheets") and core photographs have been printed on coated paper and bound as Section 5, near the back of the book, beginning on page 559.

Hole 803D: Resistivity-Sonic-Gamma Ray Log Summary
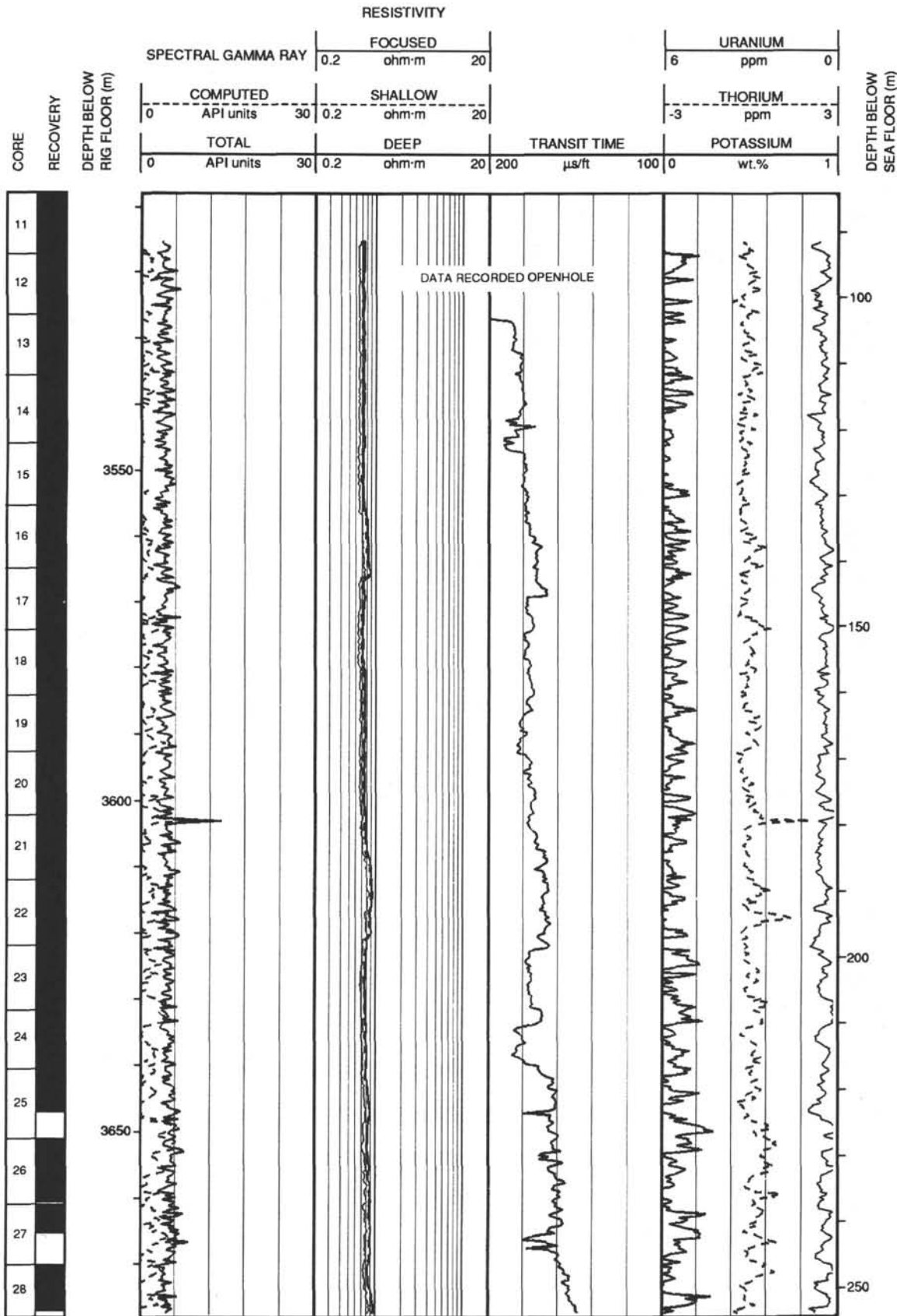
Hole 803D: Resistivity-Sonic-Gamma Ray Log Summary (continued)

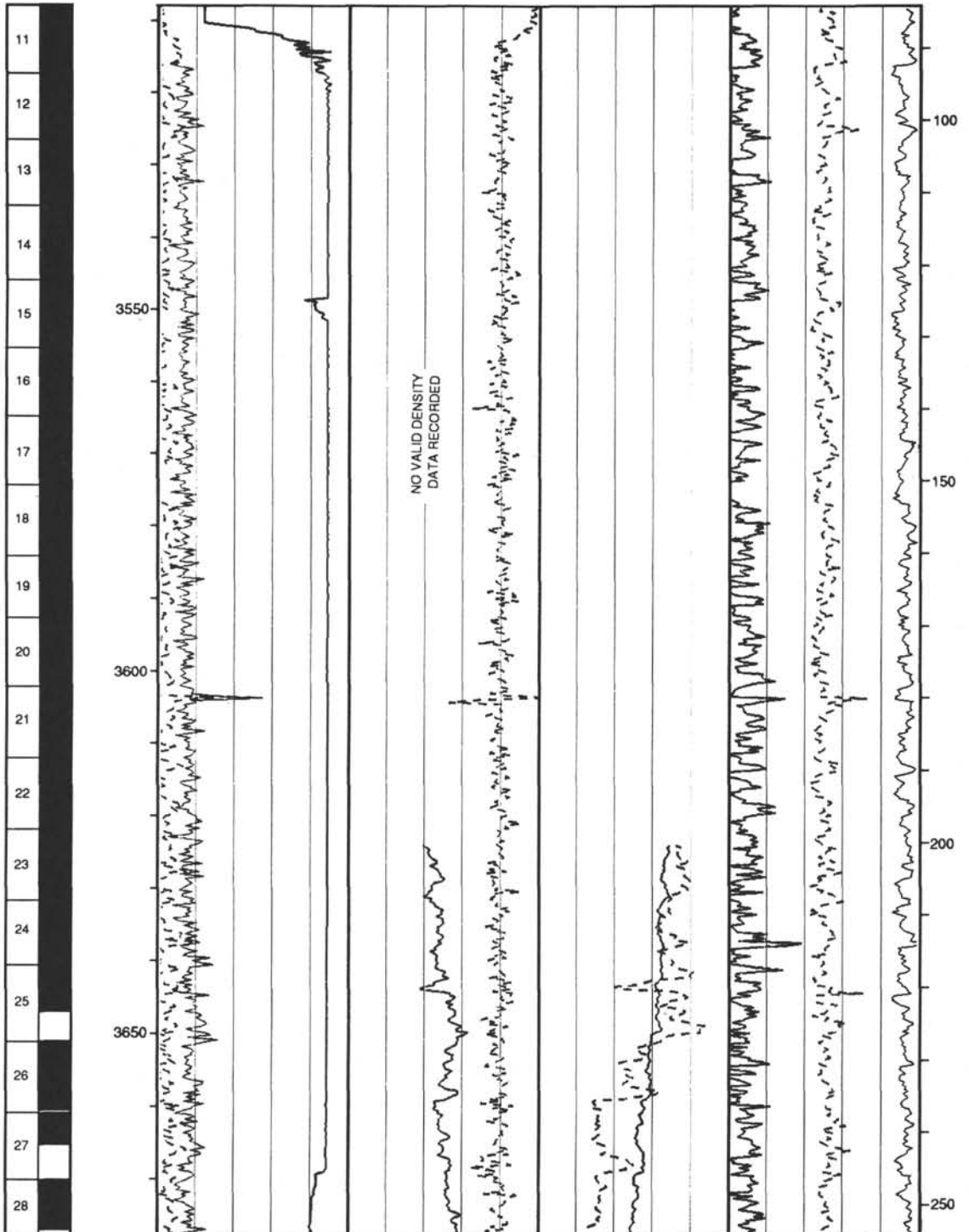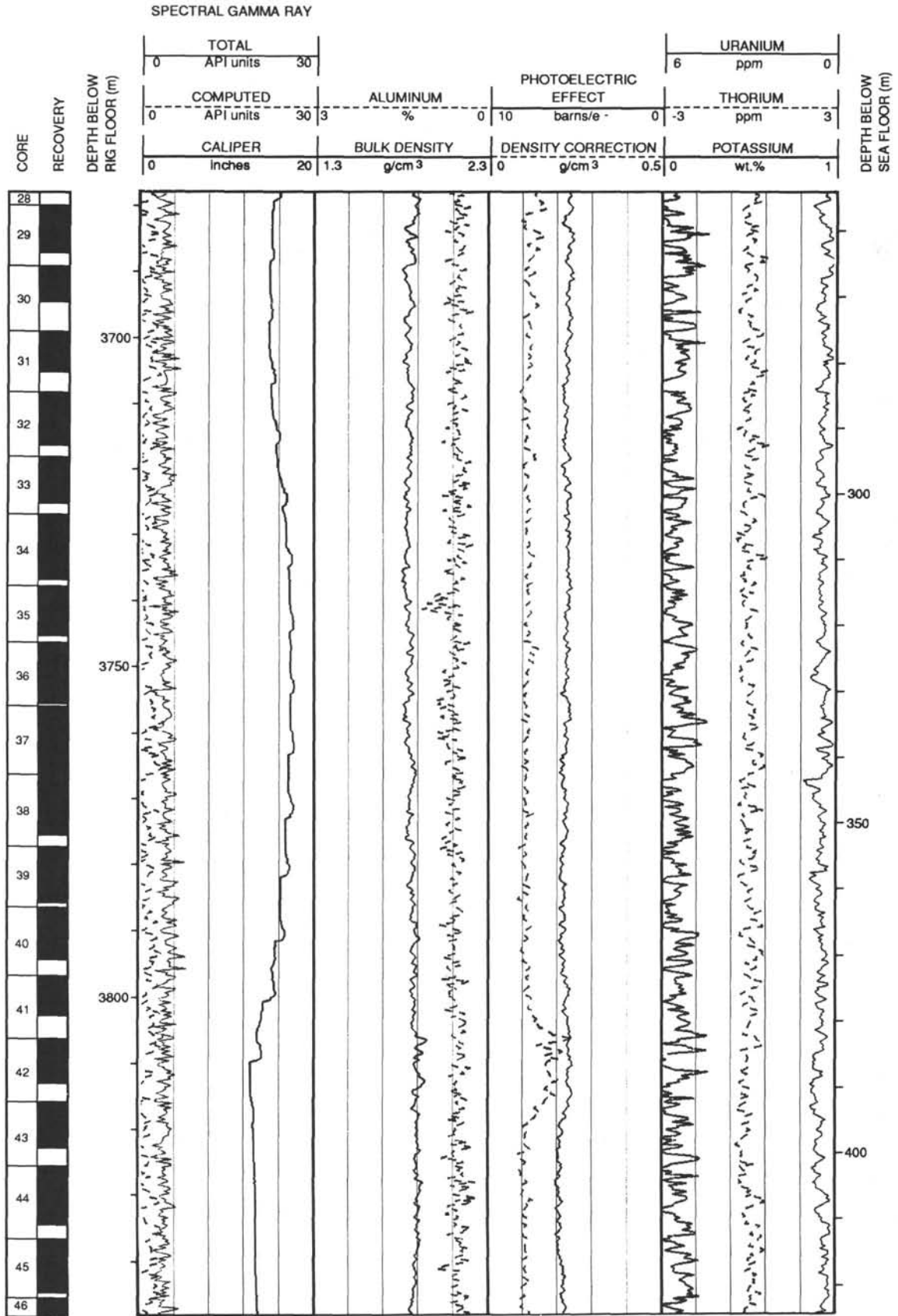Hole 803D: Resistivity-Sonic-Gamma Ray Log Summary (continued)

Hole 803D: Density-Gamma Ray-Aluminum Log Summary

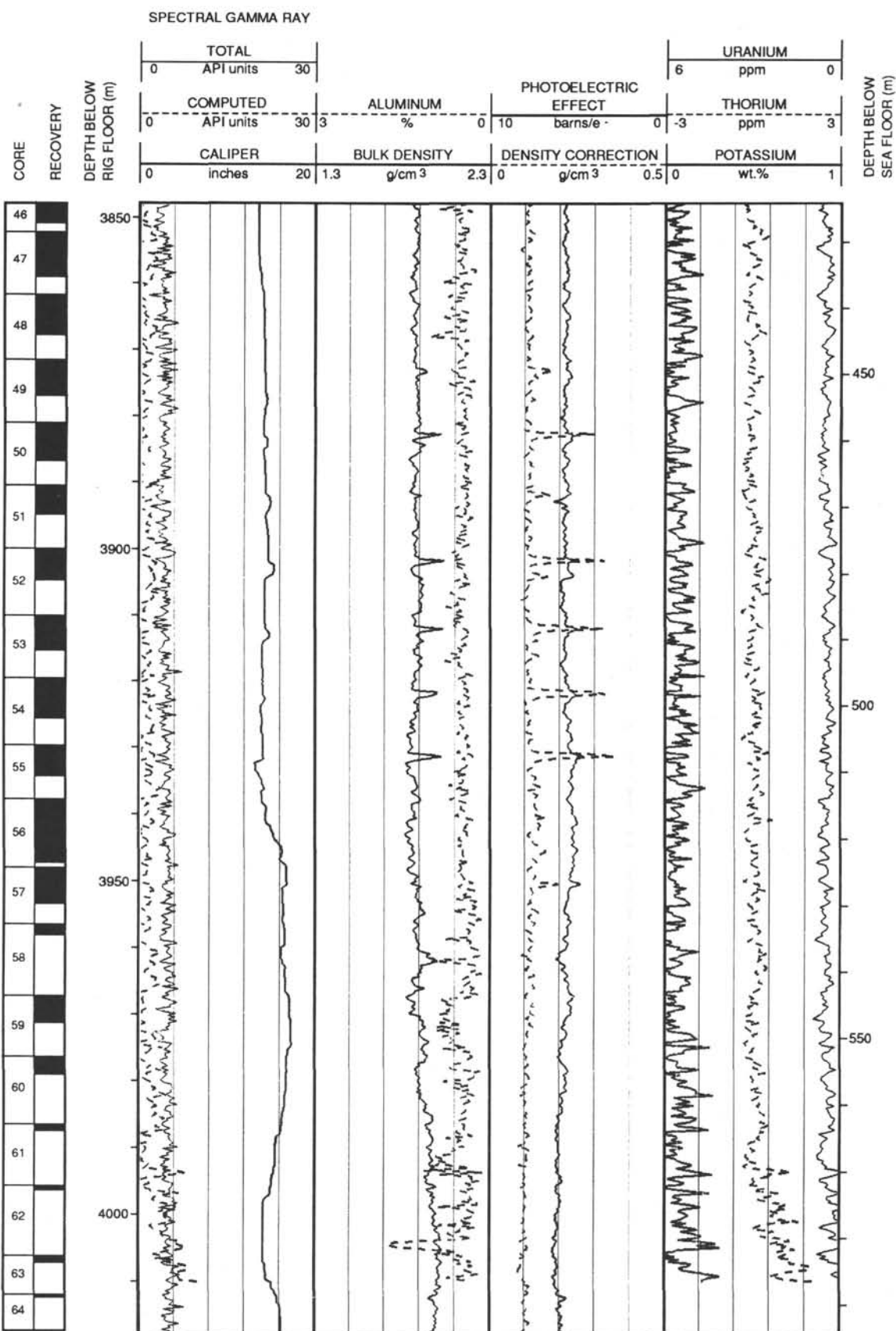## Hole 803D: Density-Gamma Ray-Aluminum Log Summary (continued)

Hole 803D: Density-Gamma Ray-Aluminum Log Summary (continued)

Hole 803D: Density-Gamma Ray-Aluminum Log Summary (continued)